Effect of numerical modelling assumptions on the simulated corneal response during Goldmann applanation tonometry

by

Natasha Botha

A dissertation submitted in partial fulfillment
of the requirements for the degree

Master of Engineering

in the

Department of Mechanical and Aeronautical Engineering
Faculty of Engineering, Built Environment and Information Technology

University of Pretoria
Pretoria
South Africa

January 27, 2014

"The eye encompasses the beauty of the whole world"
Leonardo da Vinci (1452-1519)

ABSTRACT

Title: Effect of numerical modelling assumptions on the simulated corneal response during Goldmann applanation tonometry

Author: Natasha Botha

Supervisor: Prof. Schalk Kok

Co-Supervisor: Ms. Helen. M. Inglis

Department: Department of Mechanical and Aeronautical Engineering

Degree: Master of Engineering

Keywords: finite element modelling, cornea, Goldmann applanation tonometry, intraocular pressure, fibre reinforced elastic model, modelling assumptions

It is widely known that Central Corneal Thickness (CCT) and Radius of Curvature (RoC) influence the estimated IntraOcular Pressure (IOP) obtained from Goldmann Applanation Tonometry (GAT). However, not much is known about the influence of corneal material properties, especially in a clinical setting.

Several numerical studies have been conducted in an attempt to quantify the influence of corneal material properties on the IOP. These studies agree that corneal material properties do influence the estimated IOP, which contradict the initial premise on which GAT was designed, namely that material properties do not influence the obtained GAT readings. Also, there is no consensus among these studies with respect to corneal material properties, thus a wide range of proposed properties exist.

A possible explanation for this range of available corneal properties is the numerical mod-

elling assumptions used, which seem to be quite different. Different sets of experimental inflation test data were used to calibrate the constitutive models and different limbal boundary conditions were applied to simulate the experimental setup as well as *in vivo* conditions during GAT simulations. Therefore the purpose of this study is to determine whether these modelling assumptions influence the obtained IOP and ultimately the overall conclusions.

A Finite Element (FE) model of the human cornea is developed, implementing a constitutive model to represent the complex corneal structure and two limbal boundary conditions. This model is then calibrated using two different sets of experimental inflation test data. During calibration of the fibre reinforced elastic constitutive model it is found that independent of the assumptions made regarding the material coefficients, that the numerical inflation data compare well with the experimental data for all cases.

Using this model a GAT simulation is conducted to estimate the IOP and the influence of the modelling assumptions, cornea geometry and material properties are then investigated. The results indicate that the modelling assumptions, cornea geometry and material properties do influence the estimated IOP. However, when assuming the cornea ground substance stiffness to be constant, it is found that the influence on IOP due to material properties is not as significant. A correction equation is also proposed to account for the corneal geometric properties by calibrating the numerical model for a numerically normal cornea. This is done by utilising the various data sets which are obtained during the calibration of the constitutive model with the experimental inflation test data.

It is concluded that using only inflation data to calibrate the constitutive model is not sufficient to uniquely describe the corneal material. This is evident as different material data sets are obtained, even though the experimental inflation data is matched well for a variety of considered cases. Each of these material data sets, in conjunction with geometric properties, yield different estimates for IOP during GAT simulations.

This study therefore recommends the use of additional experimental data, such as strip extensometry, along with inflation test data to adequately calibrate a numerical model. It should also be noted that when modelling GAT care should be taken when considering the choice of limbal boundary condition, experimental data for calibration and assumptions made with regards to material coefficients, as these choices could potentially influence the outcomes and conclusions of a study.

OPSOMMING

Titel: Effek van numeriese modelleerings aannames op die gesimuleerde kornea gedrag tydens Goldmann verplattings tonometrie

Outeur: Natasha Botha

Studieleier: Prof. Schalk Kok

Mede Studieleier: Ms. Helen. M. Inglis

Departement: Departement van Meganiese en Lugvaartkundige Ingenieurswese

Graad: Meesters in Ingenieurswese

Sleutelwoorde: eindige element analise, kornea, Goldmann verplattings tonometrie, interne okulêre druk, versterkte elastiese vesel model, modellerings aannames

'n Algemene waarneming is dat die sentrale kornea dikte en krommings radius 'n invloed het op die Interne Okulêre Druk (IOD) wat gemeet word deur middel van Goldmann Verplattings Tonometrie (GVT). Daar is egter nie veel inligting beskikbaar oor die invloed van kornea materiaaleienskappe nie, veral nie in 'n kliniese omgewing nie.

Verskeie numeriese studies is al gedoen in 'n poging om die invloed van kornea materiaaleienskappe op die IOD te kwantifiseer. Hierdie studies stem wel ooreen dat kornea materiaaleienskappe 'n invloed het op die bepaalde IOD. Hierdie waarneming is egter in teenstryd met die oorspronklike aanname dat GVT lesings nie beïnvloed word deur materiaaleienskappe nie. Daar is ook geen konsensus oor die bepaalde materiaaleienskappe nie, dus is daar 'n wye reeks van voorgestelde eienskappe.

'n Moontlike verduideliking vir die wye reeks waardes, is the numeriese modellerings aannames wat gemaak word, wat verskillend is vir elke studie. Verskillende stelle eksperimentele inflasie data was gebruik om die materiaal model te kalibreer, asook verskillende limbus randvoorwaardes om die eksperimentele opstelling en *in vivo* kondisies tydens GVT simulasies voor te stel. Die doel van hierdie studie was dus om te bepaal of hierdie modellerings aannames 'n invloed het op die bepaalde IOD en die uiteindelike bevindinge.

'n Eindige Element (EE) model van 'n menslike kornea, insluitende die implementasie van 'n materiaal model om die komplekse kornea struktuur te verteenwoordig en twee randvoorwaardes vir die limbus, word ontwikkel. Hierdie model word dan gekalibreer deur gebruik te maak van twee beskikbare stelle eksperimentele inflasie toets data. Tydens die kalibrasie proses van die versterkte elastiese vesel model, word waargeneem dat onafhanklik van die aannames wat gemaak word ten opsigte van materiaal koëffisiënte, dat die numeriese inflasie toets resultate goed vergelyk met die eksperimentele data.

Die IOD word bepaal deur middel van 'n GVT simulasie deur gebruik te maak van die EE model. Die invloed van die modellerings aannames, kornea geometrie en materiaaleienskappe op die bepaalde IOD word dan ondersoek. Die resultate dui aan dat die modellerings aannames, kornea geometrie en materiaaleienskappe wel 'n invloed het op die bepaalde IOD. Nieteenstaande, sodra die kornea stroma elastisiteit as konstant beskou word, is dit bevind dat die invloed van materiaaleienskappe, op die bepaalde IOD, nie beduidend is nie. 'n Korreksie vergelyking, wat die geometriese eienskappe van die kornea in ag neem, word dan voorgestel deur die numeriese model te kalibreer vir 'n numeriese normale kornea. Dit word gedoen deur gebruik te maak van die verskeie data stelle wat verkry is tydens die numeriese kalibrasie van die materiaal model met die eksperimentele inflasie toets data.

'n Belangrike gevolgtrekking van die studie is dat die inflasie toets data nie genoegsaam is om die kornea materiaal te karakteriseer nie. Die gevolgtrekking is voor die hand liggend, aangesien verskeie stelle verskillende materiaaleienskappe verkry word, terwyl die numeriese resultaat van elke geval baie goed vergelyk met die eksperimentele inflasie data. Gevolglik het elke stel materiaaleienskappe, tesame met 'n verandering in geometrie, 'n verskillende waarde vir die bepaalde IOD verkry tydens die GVT simulasie.

Vir toekomstige navorsing word aanbeveel dat additionele eksperimentele data, van 'n trektoets, gebruik word tesame met dié van die inflasie toets vir 'n meer akkurate beskrywing vir die kornea materiaal. Daar moet ook opgelet word dat wanneer GVT gemodelleer word, dat die keuse van limbus randvoorwaardes, inflasie toetsdata vir kalibrasie en aannames ten opsigte van materiaal koëffisiënte belangrik is. Die modellerings aannames, of keuses, kan die finale resultate beïnvloed en dus ook die studie gevolgtrekkings.

ACKNOWLEDGEMENTS

As I reach the end of both an exciting and frustrating adventure, one that was filled with not only times of euphoria but of depression as well, I think it's only fitting to pay tribute to those who guided and supported me on this adventure.

First off, I just want to give a sense of how it feels to undertake an extensive study, not knowing where to start or where you will end up, just to finally obtain that coveted piece of paper - the one which validates your intelligence, ability to think and academic existence. I think this experience is perfectly captured in an anecdote titled "A lesson from a Mad Hatter":

> *One of the first steps to accomplishing great things in your life is to cease dwelling on the negative things in your past. Carefully assess your present strengths, successes, and achievements. Dwell on those positive events in your life, and quit limiting your potential by constantly thinking about what you have done poorly. Alice and the Mad Hatter in Wonderland had a conversation that illustrates this concept:*
>
> ALICE: *Where I come from, people study what they are not good at in order to be able to do what they are good at.*
>
> MAD HATTER: *We only go around in circles in Wonderland, but we always end up where we started. Would you mind explaining yourself?*
>
> ALICE: *Well, grown-ups tell us to find out what we did wrong, and never do it again.*
>
> MAD HATTER: *That's odd! It seems to me that in order to find out about something, you have to study it. And when you study it, you should become better at it. Why should you want to become better at something and then never do it again? But please continue.*
>
> ALICE: *Nobody ever tells us to study the right things we do. We're only supposed to learn from the wrong things. But we are permitted to study*

the right things other people do. And sometimes we're even told to copy them.

MAD HATTER: *That's cheating!*

ALICE: *You're quite right, Mr. Hatter. I do live in a topsy-turvy world. It seems like I have to do something wrong first, in order to learn from what not to do. And then, by not doing what I'm not supposed to do, perhaps I'll be right. But I'd rather be right the first time, wouldn't you?*

Undertaking a research study is not trivial, it requires a lot of blood, sweat and tears, with little return. There are times when you start to doubt your ability to do the work, which inherently leads to doubts about your intelligence. You question whether it was the right decision and whether you should have rather gone into some monotonous work environment. It was times like these where moral and emotional support was much needed. I cannot fully express the level of gratitude I have for the continued support and motivational talks, but I can definitely say, without it I would not have been able to finish at all.

- My partner, you were the rock I needed to help ground me when things were spiralling out of control. You were my personal motivational coach, always picking up the shattered pieces of my self worth and putting it back piece by piece. I owe you a lot and I cannot thank you enough for your continued support and encouragement.
- My parents, including my stepmother, you were always supportive and never wavered in your belief of me. You brought me up in a loving environment and gave me the necessary tools to take on life. Without that support and love I would not be the person I am today. There are not enough words to express my gratitude.
- My friends, even though you might not always have understood exactly what I was going through, you were always there cheering me on from the sidelines, quietly listening when I needed to vent, but never judged. I thank you for always being around when it mattered most.

I can only describe a research study as a roller-coaster ride, there are highs and lows. One day you might feel a lot of self doubt and regret, but there are just as many days where you feel empowered and thrilled to be on the academic ride. These are the days when everything goes according to plan, your code is working, there are no curve balls in the simulations and the results even look great. You start to realise that you have the necessary skills to complete a research study. You slowly start building your intellectual confidence and before you know it you have learnt and gained a great deal more than just knowledge, you have learnt more about yourself. I would like to thank all those who have in some way contributed to my overall development, you have certainly given me the skills and confidence to be great.

- Prof. Schalk Kok and Ms. Helen Inglis, you were the best supervisors a student can ask for. You not only did a superb job in advising and guiding me through the study, but you also contributed significantly to my continued development as a person and a researcher.

- Dr. Kobie Smit and Mr. Gert Wessels, I consider you both to be wonderful mentors. You were always around when I needed some advice, be it about the way academia works or about life. I have learned a great deal from your experiences and will always value your opinion.
- Dr. Onno Ubbink, my manager who has continually supported me and the work done in this study. I want to especially say thank you for taking a chance on me and giving me the opportunity to work on this project.

Finally I just want to specifically give thanks to the Advanced Mathematical Modelling competency area within the Modelling and Digital Sciences unit at the Council for Science and Industrial Research. Thank you for giving me the necessary financial backing and support to complete this research project.

All I can say is that this truly was a wonderful experience, one I hope to undergo again one day as I attempt a PhD, and I truly wish that the experience will be as fulfilling as this one. Fortunately I love roller-coaster rides and looking back, I have gained a lot more than just knowledge. I would like to leave you with one final thought:

"All growth is a leap in the dark, a spontaneous unpremeditated act without the benefit of experience."

- Henry Miller (1891-1980)

CONTENTS

GLOSSARY OF TERMINOLOGIES

Anatomy and Physiology

Anterior	In anatomy, it refers to the front part, i.e. closer to the head
Anterior Chamber	The smallest chamber located between the cornea and iris filled with aqueous humor liquid
Apex	The upper point in the centre of the cornea
Aqueous Humor	A watery liquid found in the anterior chamber
Avascular	Not containing any blood vessels
Cell Detritus	Cells are lost due to the disintegration of tissue
Collagen	Family of structural proteins formed in elongated fibres
Cross-linking	Bundling of groups of lamellae which increases rigidity
Desquamation	Shedding of a surface layer
Extracellular	Located or taking place outside a cell
Glycoconjugates	General classification of carbohydrates linked with other chemicals
Ground Substance	Also known as elastin, a structural protein which contains amino acids
Keratocyte	Fibroblasts (cells which synthesize the extracellular matrix and collagen) which reside in the corneal stroma
Lamella	A thin plate like structure, plural lamellae
Limbus	A transitional zone where the cornea and sclera merge, also referred to as the cornea-scleral connection
Lipid	Generally used to describe oils, fats and waxes in living tissues

Meniscus	A crescent-shaped liquid
Mucoproteins	Proteins which consist of carbohydrate side-chains
Mucous	A slimy fluid which is secreted by the mucous glands
Osmosis	To equalize the concentrations of two solutions, a solvent is diffused through a semi-permeable membrane into a more concentrated solution
Posterior	In anatomy, it refers to the rear part, i.e. further away from the head
Sclera	The opaque outer coat of the human eye
Synthesis	Creating a compound aided by enzymes
Waxy Esters	A carbonyl-ether compound of a fatty acid and a fatty alcohol

Diseases, Diagnosis and Testing

Astigmatism	The refracting surfaces of the eye have different curvatures preventing the light to focus on a common point on the retina
Cataract	The lens is opaque due to degenerative changes
Corneal Edema	Accumulation of fluid in tissue spaces
Corneal Swelling	Enlargement of the corneal stroma due to an accumulation of fluid
Cyano-acrylate	Adhesive with a low viscosity
Dextran	A substance with a high molecular weight that is used to cover a corneal specimen as it is able to maintain corneal thickness within the physiological range
Enucleated Eyes	Whole eyes, with the ocular muscles intact, which were removed post-mortem
Extensometry	A technique to measure dimensional changes of a material during tensile testing
Ex vivo	Experimental or measurement process occurring outside a living organism or cell in an artificial environment
Fluorescein Dye	Chemical with a red colour and green fluorescence used during Goldmann Applanation Tonometry
Glaucoma	Condition where a rise in intraocular pressure damages the optic nerve fibres resulting in permanent blindness
In vivo	Biological processes occuring within a living organism or cell

Keratoconous	A cone shaped cornea due to a weakness or thinning of the centre
Myopia	A condition in which parallel light rays focus in front of the retina, leading to short-sightedness
Optisol	A medium in which corneal specimens are stored to keep them hydrated
Pachymeter	Device used to measure the corneal thickness
Palpation	Crude examination to estimate the intraocular pressure by touching the eye, with the eyelid closed
Porcine	Term used when referring to organs obtained from pigs
Refractive Surgery	A surgery used to improve the refractive state of the eye, to help decrease or eliminate the need for glasses
Riboflavin-ultraviolet-A	Treatment used to induce corneal cross-linking between fibres
Tonometry	A method used to measure the hydrostatic pressure within the eye

Engineering and Mathematics

Aspherical	A lens surface which varies from a spherical surface, i.e. parabolic or elliptical
Azimuth	An angle between the vertical plane containing a line and the plane of the meridian
Conicoid	Describes a quadratic surface, such as an ellipsoid, paraboloid or hyperboloid
Creep	The tendency of a solid material to move slowly or deform permanently under the influence of stresses
Equator	Line dividing the eye into its anterior and posterior parts, referred to as the x-axis
Error	Denotes the absolute error
Flat Cornea	Refers to a cornea with a large anterior radius of curvature, resulting in a flatter shape
Invariant	A characteristic of a system which remains unchanged by transformations, such as coordinate transformations, from one system to another
Meridian	Lines through the eye globe defined in terms of degrees from 0° to 180°
Non-Uniform Mesh Size	Each element in the mesh is of varying size

Optical	A line which runs between the centres of curvature of the cornea and lens, referred to as the z-axis
Sagittal	Line dividing the eye into its nasal and temporal halves, referred to as the y-axis
Steep Cornea	Refers to a cornea with a smaller anterior radius of curvature, resulting in a more ellipsoidal shape
Uniform Mesh Size	Each element in the mesh is of equal size

LIST OF ACRONYMS

CCT	Central Corneal Thickness	mm
CFD	Computational Fluid Dynamics	-
DOF	Degree of Freedom	-
FE	Finite Element	-
FEA	Finite Element Analysis	-
FEM	Finite Element Method	-
GAT	Goldmann Applanation Tonometry	-
IOP	IntraOcular Pressure	mmHg
IOPC	Numerically Calibrated IntraOcular Pressure	mmHg
IOPG	IntraOcular Pressure measured by Goldmann Applanation Tonometry	mmHg
IOPT	True IntraOcular Pressure	mmHg
NC	No Convergence	-
ORA	Ocular Response Analyzer	-
ORH	Ocular Response History	-
PCT	Peripheral Corneal Thickness	mm
RMSE	Root Mean Square Error	-
RoC	Radius of Curvature	mm

NOMENCLATURE

a_i	Correction Coefficients	-
$\bar{a}$	Directional vectors	-
A	Area	mm^2
$\mathbf{A}$	Structural tensor	-
b	Corneal Rigidity Force	N
c	Constant when defining a linear line	-
$\mathbf{C}$	Cauchy-Green deformation tensor	-
$\bar{\mathbf{C}}$	Modified Cauchy-Green deformation tensor	-
C_{10}	Stress-like parameter	MPa
CF	GAT Correction Factor	-
d	Displacement	mm
D	Diameter	mm
D_1	Incompressibility Parameter	-
E	Elastic Modulus	Pa
$\mathbf{E}$	Green-Lagrange Strain Matrix	-
f	frequency	Hz
F	Force or Objective Function	N or -
$F_{x,y}$	Fibre directional vectors	-
$\mathbf{F}$	Deformation Gradient	-
$F_{x,y}$	Fibre directional vectors	-
H	Stiffness Constant	-
i	Counter or Index	-
$\hat{\imath}$, $\hat{\jmath}$, $\hat{k}$	Directional vectors	-
$\bar{I}$	Invariant	-
$\mathbf{I}$	Identity Matrix	-
J	Jacobian	-
k_1	Stress-like parameter	MPa
k_2	Dimensionless parameter	-
K	Bulk Modulus	MPa
m	Gradient	-

M	Corneal Elastic Properties	-
n	Number of samples, or points	-
$\bar{n}$	Normal vector	-
P	Pressure	Pa
Q	Surface Asphericity	-
$\bar{r}$	Directional vector	-
R	Radius of Curvature	mm
s	Surface Tension Force	N
S_0	Elastic Tangent Stiffness Matrix	MPa
t	Time	s
U	Strain Energy Density Function	J/m^3
x, y, z	Local axis system, also denotes sample sets	mm or -
X, Y, Z	Global axis system with coordinates on the equator (X), sagittal (Y) and optical (Z) axis	mm
$\mathbf{X}$	Vector containing design variables	-

Greek Symbols

α	Temperature dependent material parameter	-
β	Degree of Non-linearity	-
Δ	Change in a property	-
ϵ	Strain	-
κ	Allowance of Penetration	-
λ	Principal Stretches	-
μ	Temperature dependent material parameter	-
ν	Poisson's Ratio	-
χ	Deformed configuration	-
X	Undeformed (or reference) configuration	-

Superscripts

el	elastic volume ratio
T	Transpose

Subscripts

1, 2	Defining two points
$0 - 27$	Used to distinguish between the number of coefficients
ant	Anterior
appl	Applanation
c	Constraction
cent	Centroid

circ	Circumferential
contact	Point of contact
e	Expansion
gap	Spacing between the cornea and applanator
sur	Surface tension
i, j, k	Indicates direction, or iteration
in	Inside
mean	Mean value of a data set
mer	Meridian
new	New point for defining contact or a new value
o	Initial
out	Outside
post	Posterior
pres	Prescribed
r	Reflected
sec	Secant
tan	Tangent
vol	Volumetric

Mathematical symbols and operators

$(\dot{\bullet})$	Rate of Change
$\vec{\bullet}$	Vector
bold	Matrix
$\otimes$	Dyadic Product, or the product of two vectors ($a_i b_j$)
∇	Gradient
det	Determinant of a matrix
tr	Trace, or sum of the diagonal of a matrix (C_{ii})

Abbreviations

c.f.	Compare (abbreviation for the latin word confer)
2D	Two Dimensional
3D	Three Dimensional
Displ	Displacement
Abs	Absolute
Appl	Applanator
Nr	Number
Elems	Elements
min	Minimum

LIST OF FIGURES

LIST OF TABLES

CHAPTER 1

INTRODUCTION

1.1 BACKGROUND

"Biomechanics is the mechanics applied to biology"
- Y.C. Fung, founder of modern biomechanics (1919-)

As stated by Fung (cited in Ateshian and Friedman, 2009) in the above quote, biomechanics is the field in which mechanics applied to biological tissues and systems is studied. This field has progressed significantly from its early stages during the 1960s and 1970s, where rigorous engineering methods were used to study biological tissues and systems (Ateshian and Friedman, 2009).

Ateshian and Friedman (2009) stated that in earlier studies of biomechanics "one of the most pressing needs was to characterize the mechanical properties of various tissues in relation to their structure, to better understand their function". This question is still one of the more important questions for which there are not always answers. This is especially true when considering corneal tissue (De Moraes *et al.*, 2008; Hamilton and Pye, 2008; Franco and Lira, 2009), the main refracting component in the human eye.

Several experimental studies have been conducted to estimate corneal material properties *ex vivo* using porcine (Hollman *et al.*, 2002; Wollensak *et al.*, 2003; Dupps *et al.*, 2007; Elsheikh *et al.*, 2009, 2008b) and human corneas (Hoeltzel *et al.*, 1992; Bryant and McDonnell, 1996; Hjortdal, 1996; Wang *et al.*, 1996; Wollensak *et al.*, 2003; Dupps *et al.*, 2007; Elsheikh *et al.*, 2007a,b; Franco and Lira, 2009). However, there is no consensus on the results of these studies, which leads to a large range of proposed material properties to describe the cornea. In recent years, analytical (Orssengo and Pye, 1999; Liu and Roberts, 2005) and numerical (Elsheikh *et al.*, 2006; Kwon *et al.*, 2008) models of the cornea have been employed to simulate Goldmann Applanation Tonometry (GAT) in an attempt to understand the effect of material properties on the corneal behaviour, as well as to explain the discrepancies encountered in experimental observations.

GAT is the most common method used to estimate the IntraOcular Pressure (IOP) by measuring the indentation resistance of the cornea. The measured IOP is then utilized not only for glaucoma screening (Williams, 2007) but to determine the course of treatment during pre- and post operative care as well. However, the effects of corneal biomechanics (such as geometry, thickness and material properties) on the measured IOP are not fully understood (De Moraes *et al.*, 2008; Hamilton and Pye, 2008; Franco and Lira, 2009).

Numerical modelling methods have been employed in corneal biomechanics to investigate the corneal response to various diseases, surgeries, diagnosis techniques and treatments. Figure 1.1 illustrates the importance of the use of corneal biomechanics to aid clinicians, surgeons and experimentalists. The topics which are encircled with a red oval are investigated and discussed in this dissertation.

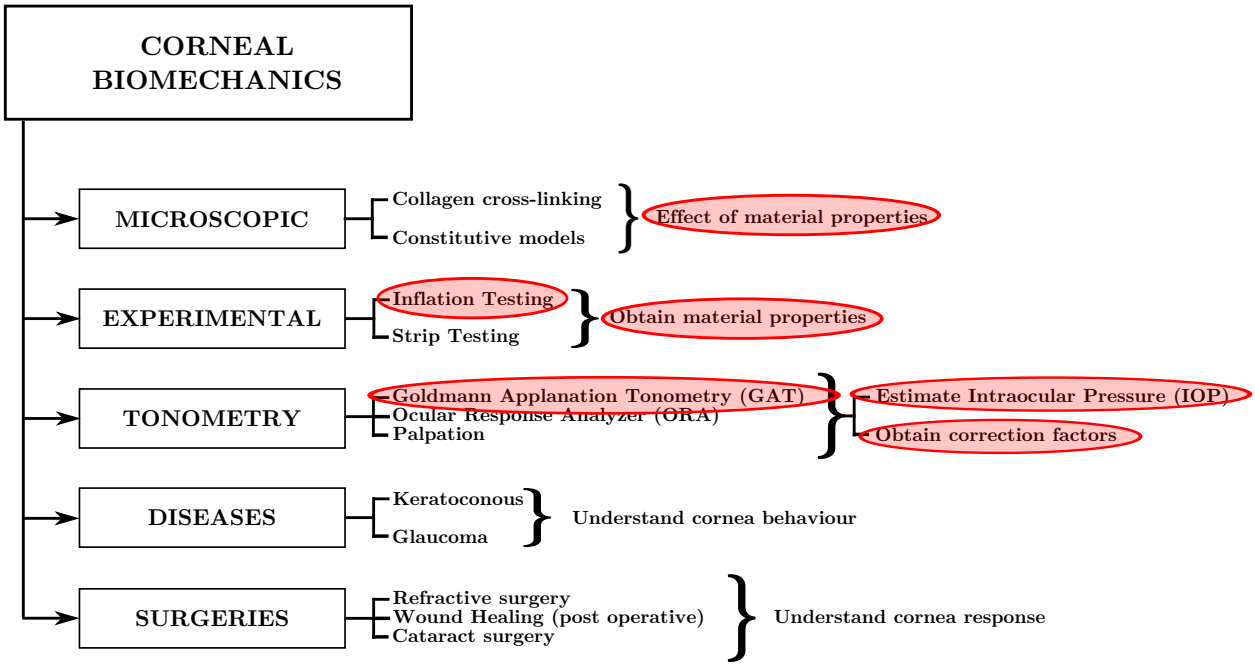

Figure 1.1: Diagram illustrating the importance of numerical modelling in corneal biomechanics for the clinician, surgeon and experimentalist. The topics encircled in red are part of the focus of this dissertation.

1.2 PROBLEM STATEMENT

The effects of Central Corneal Thickness (CCT) and corneal Radius of Curvature (RoC) on the IntraOcular Pressure (IOP) measured using Goldmann Applanation Tonometry (GAT) (IOPG) have been investigated extensively, both numerically and clinically (Brandt *et al.*, 2009). However far less is known about the influence of corneal material properties, especially in a clinical setting (De Moraes *et al.*, 2008; Hamilton and Pye, 2008). Several numerical studies (Orssengo and Pye, 1999; Liu and Roberts, 2005; Elsheikh *et al.*, 2006; Kwon *et al.*, 2008) have been conducted to quantify the influence of corneal material properties on the IOPG, but even though all these studies agree that the material properties do in fact influence the IOPG measurement, there is no consensus as to the level of influence. These observations also contradict the initial premise on which Goldmann and Schmidt (1957) developed the

device, which was that corneal material properties do not influence the estimated IOP.

Current correction equations only account for the variation in IOPG due to CCT and RoC, which is known to influence the obtained GAT readings. However, if the corneal material properties also influence the readings as Liu and Roberts (2005), Kwon *et al.* (2008) and Elsheikh *et al.* (2006) claim, then future proposed correction equations need to account for corneal material properties as well.

One possibility for the wide range of proposed corneal material properties, and correction equations, could be due to the variety of modelling assumptions made. Numerical studies (i) use a variety of experimental inflation test data with which to calibrate the constitutive models and (ii) also apply different boundary conditions to describe the experimental setup, as well as *in vivo* conditions during GAT, at the limbus. Each of these assumptions could consequently have an effect on the estimated IOP, and therefore explain the variety of proposed material properties.

This work will therefore investigate the effect that each of the mentioned numerical modelling assumptions have on the estimated IOPG. The observations, and conclusions, in this study will be used to validate the following statement:

The assumptions made by numerical modellers about material coefficients in constitutive models, calibration methods and boundary conditions, for corneal modelling, could ultimately influence the overall conclusions in numerical GAT studies.

1.3 RESEARCH QUESTIONS

The following research questions arise:

- Do the assumptions made for material coefficients in constitutive models influence the GAT results?
- What methods of model calibration are commonly used and which experimental data sets are used?
- Do the modelling choices, or assumptions, have an influence on the estimated IOP from GAT?
- Do the geometric and material properties have an influence on the estimated IOP?
- Can a multi parameter correction equation be suggested which accounts for the geometric and material property influences?
- To what extent could the overall conclusions be influenced by the modelling choices made?

1.4 RESEARCH OBJECTIVES

From the research questions the research objectives can be formulated so as to complete individual aspects of the overall thesis statement. The research objectives are:

- Develop a numerical model of the cornea, choosing a suitable constitutive model to represent the corneal structure.
- Calibrate this numerical model using two different sets of experimental inflation test data, as well as two different limbal boundary conditions.
- Evaluate the choice of calibration data and boundary conditions by simulating GAT to estimate the IOP.
- Establish the influence of corneal geometric and material properties on the estimated IOP from GAT.
- Develop a correction equation, which can correct the estimated IOP from GAT for the cases considered in this study.

1.5 SCOPE OF WORK

To answer the proposed research objectives with clarity it is necessary to define the scope of work, that is define the assumptions made in this study and clearly state any limitations. This will also help to narrow the broader scope of corneal biomechanics by only focussing on certain aspects.

1.5.1 Software

Only open-source software will be used to conduct this study:

- Python (Python Software Foundation, 2011) is used as the programming language in which the pre- and postprocessing is done.
- CalculiX (Dhondt, 2011a), a linear and non-linear Finite Element (FE) solver, is used for the Finite Element Analysis (FEA).

1.5.2 Assumptions

The following assumptions are made with regards to the corneal model:

- The cornea is assumed to be normal, with no asymmetries such as astigmatism or myopia, no swelling and no cross-linking of collagen fibres.

- The cornea is also assumed to not have diseases that could influence the structural architecture, such as keratoconous, edema or any scarring, for example.
- The cornea is assumed to be homogeneous, that is each individual layer (including the components within) is not taken into account; the entire tissue is modelled as a single tissue.
- The cornea is assumed to be dry and any effects due to the tear film or anaesthesia are not accounted for.
- The cornea is assumed to be incompressible as it mostly consists of water.

1.5.3 Limitations

This study is limited to only using the following:

- **Experimental data sets:** Only *ex vivo* experimental inflation test data, which were obtained using human corneas, are used to calibrate the constitutive models.
- **IOP measurement methods:** The only method considered to measure the IOP numerically, similar to a clinical environment, is GAT.
- **Constitutive models:** Only constitutive models which are readily available in CalculiX (Dhondt, 2011a) are considered for this study.

1.6 OVERVIEW OF CHAPTERS

This dissertation is divided into six chapters. The current chapter serves as an introduction to the problem at hand as well as discussing the objectives of this study. The other five chapters include:

Chapter 2: Corneal Biomechanics and Goldmann Applanation Tonometry

Chapter 2 provides a literature review together with a discussion on some key biological concepts. Chapter 2 starts with a discussion of the corneal anatomy and physiology to introduce the reader to the important biological terminologies used. A discussion on the corneal biomechanics follows which introduces key concepts such as IOP, stromal mechanics, corneal stiffness and the mechanical testing of corneas.

The most popular *ex vivo* method of corneal testing is inflation testing, which is discussed in depth with a review of two popular experimental studies. As the influence of certain geometric and material properties on the IOP will be investigated, a discussion on the mechanics and concerns of GAT are given as well.

The chapter ends with an in depth discussion of a few numerical studies which have quantified the corneal material properties using a variety of modelling assumptions. This discussion is included to illustrate that with a variety of modelling assumptions there is a lack of consensus on quantifying the corneal material properties.

Chapter 3: Finite Element Model of the Human Cornea

Chapter 3 discusses the development of the FE model used to conduct this study. A mathematical approach is used to develop the cornea model by assuming that it is a rotationally symmetric conicoid. Geometric properties are obtained from literature and the two limbal boundary conditions considered in this study are defined. The constitutive model under consideration is a fibre reinforced elastic model, which is available in the open-source FE solver, CalculiX (Dhondt, 2011a).

The required loads and boundaries for each simulation, that is inflation test and GAT, are discussed and studies are conducted to determine what the suitable mesh size, mesh type (uniform or non-uniform) and number of time steps are to obtain a converged solution. Several concerns, such as element types and the contact definition, are also discussed. The chapter ends with an explanation of how to obtain the Ocular Response History (ORH), which is a graph depicting the force required to applanate the cornea against the applanation diameter.

Chapter 4: Calibration of Material Coefficients with Experimental Inflation Data

In Chapter 4 the chosen constitutive model is calibrated for both limbal boundary condition cases using two different sets of experimental inflation test data. The Nelder-Mead Simplex optimization routine is used to minimize for the Root Mean Square Error (RMSE) between experimental and numerical data. Two separate cases are considered, each of which has a different set of assumptions with regards to the material coefficients. The influence of these assumptions are also investigated.

Chapter 5: Simulating Goldmann Applanation Tonometry

GAT is simulated in Chapter 5 to investigate the effect of the various modelling assumptions considered in this study. The effects of each of the two modelling assumptions, (i) calibration data and (ii) boundary condition, on the IOPG are investigated. Additionally the effects due to geometric and material properties on the estimated IOPG are also investigated. Lastly, a correction equation is proposed using the numerical GAT data for a range of corneas.

Chapter 6: Conclusions

Chapter 6 contains a summary of all the major findings, including some of the core conclusions from each of the previous chapters. Additionally, recommendations for further research are made.

CHAPTER 2

CORNEAL BIOMECHANICS AND GOLDMANN APPLANATION TONOMETRY

2.1 INTRODUCTION

The human eye (c.f. Figure 2.1) is one of the most fascinating and complex physiological organs in the human body. It senses and reacts to light in such a way that we are able to form visual images, which allow us to experience the beauty of the world we live in. However, the beauty of the world is sometimes blurred when the eye is affected by various diseases affecting eye tissues, such as corneal edema, glaucoma, cataracts, astigmatism and myopia to name a few. These diseases tend to affect geometric and material properties of the affected tissues, thus influencing ophthalmological procedures used to either quantify or treat these diseases. Over the years numerical modelling techniques have been used to quantify the predicted response of various ophthalmological properties to diseases, diagnosis and treatment procedures.

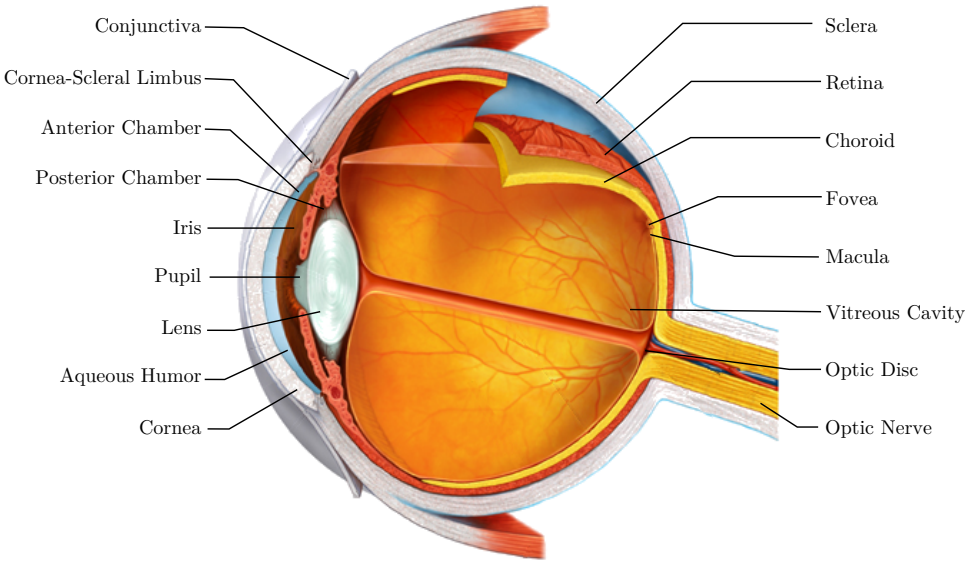

Figure 2.1: Anatomy of the human eye. [Taken from http://www.virtualmedicalcentre.com/]

From a modelling point of view the cornea is considered one of the more important tissues of the eye, as it is easily accessible for tonometry and surgical procedures (Kniestedt *et al.*, 2008). For this reason it is important to understand the corneal biomechanics which govern its response to these procedures.

As tonometry, more specifically Goldmann Applanation Tonometry (GAT), is central to disease diagnosis, as well as pre- and post surgical care, the mechanics behind this technique also need to be well established. This is especially important to understand the impact of corneal biomechanics, such as structural architecture, on the IntraOcular Pressure (IOP) measurement (De Moraes *et al.*, 2008; Franco and Lira, 2009). Corneal geometric properties, such as Central Corneal Thickness (CCT) and Radius of Curvature (RoC) are known to influence the IOP measurement during GAT, however not much is known about the influence of the corneal material properties as there is no means of determining it *in vivo*.

2.2 CORNEA ANATOMY

The information used in this section to discuss the corneal anatomy was obtained from the following sources: Jakobiec and Ozanics (1982), Rodrigues *et al.* (1982), Newell (1992) and Batterbury and Bowling (2005).

The cornea contributes approximately two thirds of the eye's refractive power and, along with the sclera, protects the eye against microorganisms (Jakobiec and Ozanics, 1982; Newell, 1992; Dupps Jr. and Wilson, 2006; Ruberti *et al.*, 2011). It is described as a transparent and avascular structure, which is sensitive to touch. On a microstructural level, it is a very complex tissue consisting of a total of five distinct layers, as well as the tear film which covers it anteriorly. The six layers that comprise the cornea are illustrated in Figure 2.2.

2.2.1 Tear Film

The tear film is located on the anterior surface of the cornea at the eye-air interface. It is approximately $6.3 - 7.6$ μm thick and is composed of three layers:

- An **outer lipid layer**, which is approximately 0.1 μm thick. This layer consists mainly of lipids and waxy esters, which form a fluid at body temperature (37°C in an average human). This layer reduces the evaporation of water, which dehydrates the cornea.
- A **central aqueous layer**, which is approximately $6 - 7$ μm thick and contains various dissolved inorganic salts and proteins. The aqueous layer lubricates the eye lids to ease the blinking process.
- An **inner mucous layer**, which is approximately $0.2 - 0.5$ μm thick and composed mainly of hydrated mucoproteins.

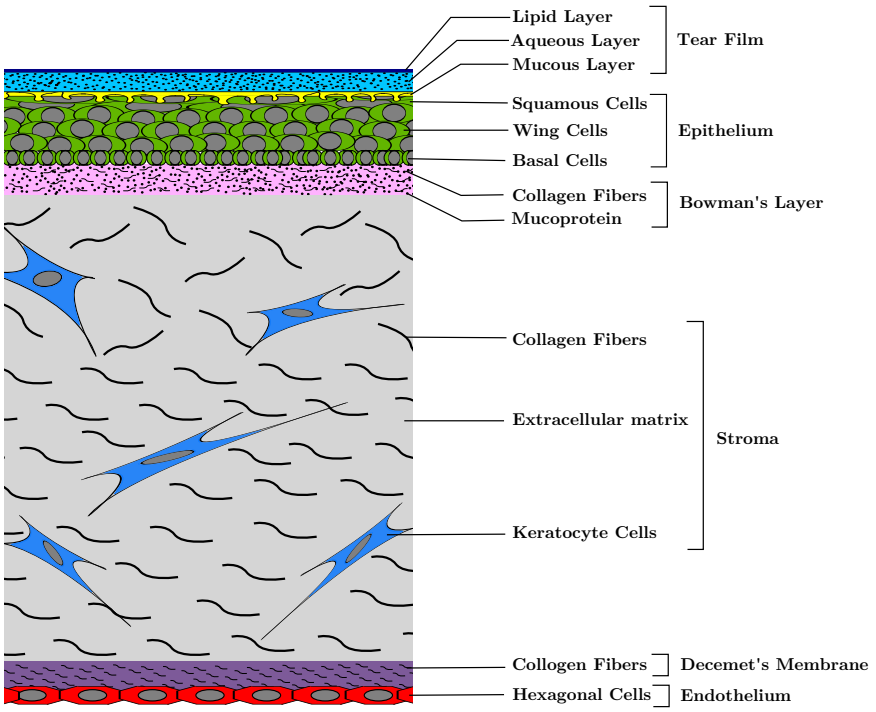

Figure 2.2: Cross section of the human cornea showing the five distinct layers of the cornea, including the tear film, as well as the composition of each layer. [Adapted from Secker and Daniels (2009)]

The tear film functions as a lubricant and coats the corneal surface to aid in blinking by maintaining a distortion free surface. It also plays a role in the corneal wound healing process and corneal desquamation by removing cell detritus.

2.2.2 Epithelium

The epithelium is the first layer encountered in the complex corneal structure, which covers the stroma anteriorly. It is approximately $50 - 60$ μm thick and is composed of about five to six layers of cells:

- Two layers of **squamous cells**, which are elongated thin cells, on the outer layer.
- Two to three layers of **wing cells**, which are oval elongated cells.
- One layer of **basal cells**, which are tall oval cells.

These cell layers are in a regular aligned pattern to ensure that cells are replaced when surface cells are desquamated.

2.2.3 Bowman's Layer

Bowman's layer is a collagenous layer which is approximately $8 - 10$ μm thick and devoid of cells. The collagen fibres are randomly orientated in a ground substance which contains mucoprotein. This composition is advantageous as the layer is able to assist in the deformation resistance, trauma and prevention of infections of the corneal tissue.

2.2.4 Stroma

The stroma, which constitutes 90% of the overall thickness of the cornea, is approximately $439 - 477$ μm thick. It is composed mainly of:

- An **extracellular matrix** which consists of collagen and other glycoconjugates to form the ground substance.
- Approximately $200 - 250$ **collagen lamellae** containing collagen fibres, which are uniform in size and spacing. The lamellae in the anterior third of the stroma are orientated at different inclines and the lamellae in the remaining two thirds of the posterior stroma are more organized. The collagen fibres within a lamella are parallel to one another and the corneal surface, but are orthogonal to fibres in adjacent lamellae (Boote *et al.*, 2003). These collagen fibres prefer a more circumferential orientation when moving towards the corneal limbus. Collagen fibres provide the corneal strength and stiffness by reinforcing the tissue (Boote *et al.*, 2006).
- **Keratocyte cells**, which are scattered through the stroma and occasionally extend into lamellae. These cells are long and flat and play a major role in wound healing and corneal transparency.

The architecture of the stroma is believed to have a considerable influence on the corneal mechanical strength, which from a clinical point of view is important to estimate the cornea's response to disease, surgery and changes in IOP (Boote *et al.*, 2011). Figure 2.3b illustrates the preferred orientation of the collagen fibres which ensure maximum corneal strength. In Figure 2.3a X-ray scattering is used to illustrate that collagen fibres are more densely packed in the 0° and 90° orientations, which is the preferred orientation. In the scatter plot an orange-red color indicates a heigher intensity of collagen fibres and blue a lower intensity.

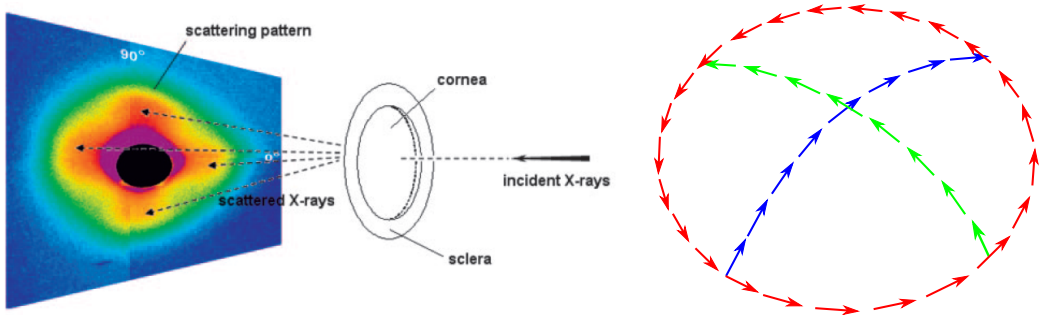

(a) X-ray scatter plot **(b)** Preferred orientation

Figure 2.3: Preferred orientations of the collagen fibres in the corneal stroma. (a) X-ray scattering is used to show a scatter plot of the collagen fibres, where the orthogonal preferred directions are illustrated in orange-red, an indication of heightened intensity [Taken from Boote *et al.* (2006)]. (b) The preferred orientation of the collagen fibres are orthogonal (blue and green) in the central corneal, bending towards the limbus (red) in a circumferential orienation [Redrawn from Boote *et al.* (2005)].

2.2.5 Decemet's Membrane

Decemet's membrane is a layer similar to Bowman's layer, except that it does not contain a ground substance. It only consists of collagen fibres which are arranged in a hexagonal pattern. This membrane, which is approximately $8 - 12$ μm thick, is able to regenerate and may form a glass membrane which extends into the anterior chamber after an injury to the cornea has occured.

2.2.6 Endothelium

The endothelium, approximately $5 - 6$ μm thick, forms the posterior surface of the cornea and consists of a single layer of flat hexagonal cells. The endothelium dehydrates the stroma, preventing swelling and loss of transparency, by removing water from the stroma into the anterior chamber through osmoses and synthesis of Decemet's membrane.

2.3 CORNEAL BIOMECHANICS

During tonometry, corneal biomechanics have an influence on the IOP measurement. It is therefore important to understand corneal biomechanics to determine its influence on the IOP measurement during tonometry. It is widely known that an increase in CCT and corneal RoC cause an over- and underestimation of the IOP measurement, respectively (Brandt *et al.*, 2009). However, not much is known about the influence of the corneal structure as there is currently no method to quantify it *in vivo* (De Moraes *et al.*, 2008; Hamilton and Pye, 2008).

2.3.1 Intraocular Pressure

IOP is the result of a dynamic balance between aqueous humor formation and drainage (Kniestedt *et al.*, 2008; Toris, 2009). When the rate of aqueous humor formation equals the outflow, a statistically normal IOP (based on population studies) of between 7 and 21 mmHg is the result (Williams, 2007; Kniestedt *et al.*, 2008; Toris, 2009).

IOP is also considered to be an important modifiable risk factor for glaucoma, even though it takes no part in the actual diagnosis, as it can be used to determine the course of treatment (Williams, 2007). Accurate and precise measurement of the IOP is therefore of great clinical importance (Kotecha *et al.*, 2009).

2.3.2 Stromal Mechanics

Mechanical properties of the cornea are known to vary regionally in the stroma due to the collagen architecture and are also directionally dependent leading to an anisotropic behaviour

(Hjortdal, 1996; Boote *et al.*, 2006). Despite the importance of the properties that characterize the corneal stroma and consequently the corneal stiffness and strength, such as the collagen fibres and ground substance, these properties have not as yet been measured *in vivo* (Boote *et al.*, 2003; Aghamohammadzadeh *et al.*, 2004).

Ground Substance

The ground substance is a matrix filled with glucose, proteins and the collagen fibres. Not much is known about its contribution to the overall corneal stiffness. The elastic modulus is estimated to be approximately 10000 times smaller than that of the collagen fibres, in the region of 40 kPa (Hjortdal, 1996).

Collagen Fibres

It is known that the collagen fibre orientation and size have an influence on not only the biomechanical, but the optical properties as well (Daxer *et al.*, 1998; Boote *et al.*, 2003, 2011). Collagen fibres contribute to the mechanical strength of the cornea to enable it to withstand the IOP on the posterior surface.

The fibres are stretched due to the IOP and when a force is applied, a reaction force from the fibres balances the applied force. This force balance, due to the collagen fibres, reinforces the cornea when in tension as the fibres are strongest axially and in directions of preferred orientation (Boote *et al.*, 2003; Aghamohammadzadeh *et al.*, 2004). The fibre elastic modulus is estimated to be in the range of $0.5 - 1.0$ GPa (Fung, 1993; Hjortdal, 1996; Boote *et al.*, 2005).

One can therefore conclude that the collagen fibres contribute more to the corneal stiffness than the ground substance. The collagen fibre orientation therefore plays a major role in the understanding of corneal biomechanics (Boote *et al.*, 2011).

2.3.3 Mechanical Testing

Corneal material properties are normally quantified by using either *ex vivo* destructive test methods (classical engineering tests) or *in vivo* non-destructive testing methods. As *in vivo* methods are less versatile than *ex vivo* methods, *ex vivo* methods are the preferred method for determining corneal biomechanical properties (Ruberti *et al.*, 2011).

In vivo

Some of the more popular *in vivo* techniques include shear wave propagation or ultrasonic techniques and the Ocular Response Analyzer (ORA).

Ultrasonic techniques have been used successfully to quantify corneal stiffness in *ex vivo* experimental studies (Wang *et al.*, 1996; Dupps *et al.*, 2007). This technique uses the relationship between wave speed and shear modulus to ultimately estimate the elastic modulus, assuming an incompressible linear elastic material.

The ORA is currently one of the few commercially available methods to estimate corneal biomechanical properties *in vivo*. This method illustrates the viscoelastic nature of the cornea by obtaining a hysteresis response when the cornea is indented using a puff of air. The ORA does not report the elastic properties of the cornea, but it has been suggested that these properties can be obtained by applying finite element models to reproduce the obtained hysteresis (Ruberti *et al.*, 2011).

Ex vivo

Some of the advantages of using destructive techniques is that various loading conditions can be explored to quantify stiffness, as well as viscoelasticity. An unfortunate disadvantage is that the collagen fibre orientation could be disrupted and if the sample is not properly hydrated, to match *in vivo* conditions, the properties obtained could be inaccurate (Ruberti *et al.*, 2011). There are currently two methods of *ex vivo* testing, namely inflation and strip extensometry tests.

During an inflation test, a whole corneal specimen (with a 2 mm scleral ring) is clamped into a pressure chamber and inflated beyond its physiological limitations. A non-linear response is obtained between the apical displacement and the applied chamber pressure, which could be used to quantify corneal biomechanical properties such as stiffness (Bryant and McDonnell, 1996; Elsheikh *et al.*, 2007a). One of the major disadvantages of this method of testing is: as the cornea is clamped onto the pressure chamber the natural load-bearing environment of the cornea might be compromised as the sclera has no active role during inflation. In *in vivo* conditions the sclera also deforms under the IOP and as it is connected to the cornea it will affect the corneal behaviour (Boote *et al.*, 2011). However, numerical studies have shown that this does not affect the corneal response or biomechanical stability (Boote *et al.*, 2011).

In a strip extensometry test a corneal strip of constant width, excised from a whole cornea, is clamped into a slow-rate tension machine. The specimen is then pulled in tension, until fracture, to obtain a stress-strain response (Hoeltzel *et al.*, 1992; Wollensak *et al.*, 2003). From this response the corneal stiffness can then be estimated.

2.3.4 Stiffness

The stiffness of the cornea is one of those properties that has not been quantified *in vivo*, whereas attempts to quantify it *ex vivo* have lead to a wide range of reported values in the literature. The results of these *ex vivo* studies are summarised in Table 2.1, where the wide range of reported values is apparent. These differences can be attributed to the various methods of testing, hydration, sample storage and preparation and even sample age (Elsheikh

et al., 2007a). A special mention should be made that the literature quantifies the stiffness of the cornea as the elastic modulus (E), but in fact it refers to the gradient of the stress-strain response at specified points, since the gradient changes continuously due to the highly non-linear behaviour.

Table 2.1: Elastic moduli of human corneas determined experimentally in several studies.

Source	Testing Method	Reported Stiffness
Hoeltzel *et al.* (1992)	Strip Stress levels equivalent to IOP $= 10 - 400$ mmHg	$E = 3.4 - 41.0$ MPa
Bryant and McDonnell (1996)	Inflation IOP $= 0.5 - 40$ mmHg	$E = 0.592 - 1.40$ MPa
Hjortdal (1996)	Inflation IOP $= 2 - 100$ mmHg	$E_{\text{sec,mer}} = 2.87 - 19.9$ MPa $E_{\text{sec,circ}} = 2.76 - 27.5$ MPa
Wang *et al.* (1996)	Ultrasonic $f = 2.25$ MHz	$E_{\text{saline}} = 4.2 - 6.4$ MPa $E_{\text{dextran}} = 10.0 - 30.0$ MPa
Wollensak *et al.* (2003)[a]	Strip $\dot{\epsilon} = 1.55$ mm/min	$E_{\text{untreated}} = 0.8 - 2.2$ MPa $E_{\text{treated}} = 3.0 - 11.8$ MPa
Elsheikh *et al.* (2007a)	Inflation IOP $= 0.0 - 75$ mmHg	$E_{\text{sec}} = 0.051 - 0.9359$ MPa $E_{\text{tan}} = 0.0139 - 2.5233$ MPa

[a] Samples were treated with riboflavin-ultraviolet-A to induce cross-linking to determine a change in elastic modulus with age.

2.4 INFLATION TEST

Inflation testing is considered to be more accurate than strip extensometry as it is more representative of the *in vivo* conditions (Elsheikh *et al.*, 2006) and has therefore been used in various numerical studies to calibrate corneal constitutive models (Bryant and McDonnell, 1996; Elsheikh *et al.*, 2006; Pandolfi and Manganiello, 2006; Kwon *et al.*, 2008).

2.4.1 Inflation Mechanics

During an inflation test, the role of the collagen fibres is important in the sense that any change in the fibre orientation could change the corneal stiffness and consequently affect the response due to IOP (Boote *et al.*, 2011). Due to the pressure on the posterior corneal surface, relaxed collagen fibres straighten to carry the imposed stresses. Boote *et al.* (2011) states that geometric properties such as CCT and corneal RoC are dominant during inflation, both of which affect the stiffness. For example, a thinner and flatter cornea will lead to a reduced stiffness and hence an increased deformation (Boote *et al.*, 2011). Conversely, a thicker and more curved cornea will experience a larger stiffness and therefore less deformation (Boote *et al.*, 2011).

2.4.2 Experimental Inflation Studies

There are two experimental inflation test studies, namely Bryant and McDonnell (1996) and Elsheikh *et al.* (2007a), which have been used most commonly to calibrate numerical models (Bryant and McDonnell, 1996; Elsheikh *et al.*, 2006; Pandolfi and Manganiello, 2006; Kwon *et al.*, 2008).

Bryant and McDonnell (1996) obtained 12 human corneas and preserved them in a corneal storage medium at 4°C, within 24 hours of a patient's death . The results for five of the tested corneas are shown in Figure 2.4, with an average CCT of 0.404 mm and anterior diameter of 11.45 mm. These corneas had a $2-3$ mm scleral ring and were tested within eight days of preservation. The corneal specimens were clamped into the inflation test rig against the scleral ring at room temperature and covered with a 15% dextran solution. Before testing, the corneal specimen was first preconditioned by cycling it between the minimum (0.5 mmHg) and maximum (40 mmHg) pressures and holding it for approximately 10 minutes at each extreme. The corneal specimen was then inflated for a range of pressures between 0.5 and 40 mmHg and allowed to creep for approximately $10-20$ minutes, before the apical displacement was measured using a fibre optic displacement probe.

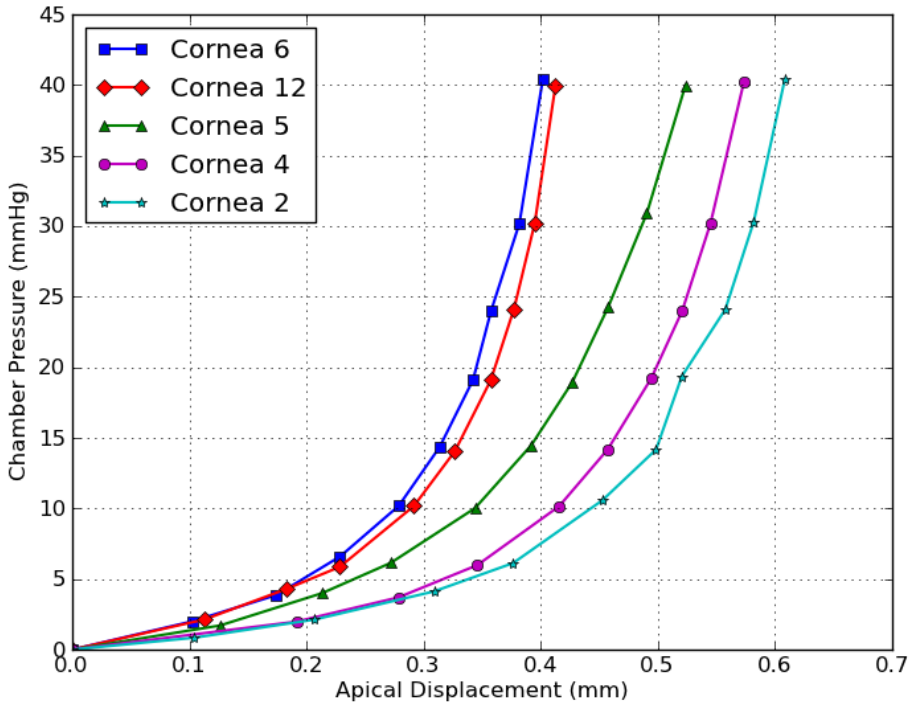

Figure 2.4: Experimental inflation test results obtained by Bryant and McDonnell (1996)

On the other hand, Elsheikh *et al.* (2007a) were able to test 13 human corneas ($50-95$ years old) in their study and each specimen was extracted while retaining a 2 mm scleral ring. The corneal specimens were preserved at 4°C in a corneal storage medium within 12 hours of a patient's death and tested within 14 days. The corneal specimens were glued, using cyanoacrylate glue, and clamped onto the pressure chamber along the scleral ring. The corneal specimens were bathed in Optisol during the test and kept at a constant temperature of 37°C,

the human body temperature. The corneal specimen was first preconditioned by applying a pressure of 0.75 mmHg for three loading and unloading cycles until its behaviour stabilized. A pressure was then applied at a rate of 3.75 mmHg/min until the corneal specimen burst, which was at pressures higher than 170 mmHg. The apical displacement was continuously monitored throughout the experiment using a laser. The obtained results are shown in Figure 2.5, with an average CCT of 0.572 mm and anterior diameter of 11.252 mm.

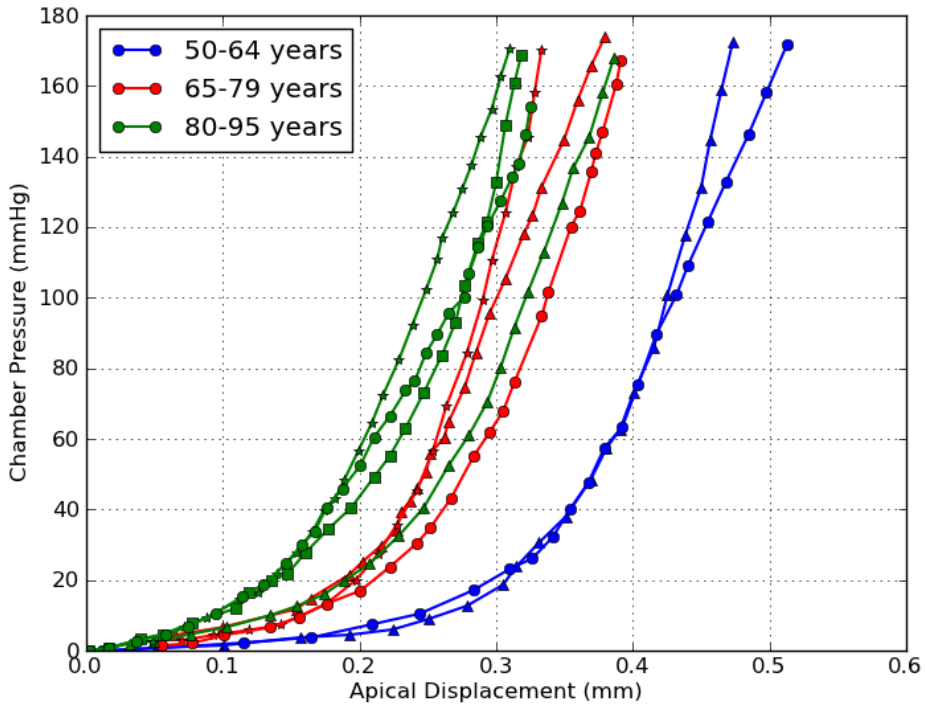

Figure 2.5: Experimental inflation test results obtained by Elsheikh *et al.* (2007a)

Superimposing the results from these two studies, as shown in Figure 2.6, it is clear that there is a wide range of data available. Even though both studies preserved and tested their corneal specimens in a similar manner, it is evident that the corneal samples from Elsheikh *et al.* (2007a) are stiffer than those tested by Bryant and McDonnell (1996). This could be either due to the age of the samples, but as Elsheikh *et al.* (2007a) tested such a wide range, from 50 to 95 years old, age is an unlikely factor. It is also not possible to compare the corneal specimen ages as the ages of the specimens used by Bryant and McDonnell (1996) were not specified. Another possible cause for the dispersion of data is that Bryant and McDonnell (1996) allowed the specimens to creep before measuring the apical displacement, whereas Elsheikh *et al.* (2007a) continuously measured the displacement, thus not allowing the sample to creep. By allowing the corneal material to creep, Bryant and McDonnell (1996) were able to capture the natural *in vivo* stress state of the cornea under a constant IOP loading.

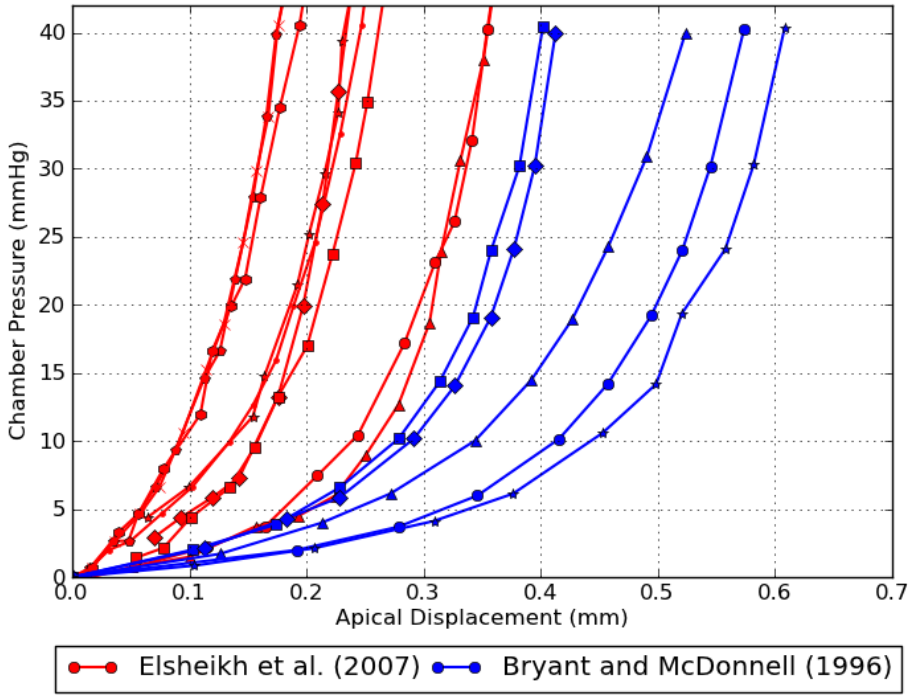

Figure 2.6: Both sets of inflation experimental data, showing the wide range of available data.

2.5 GOLDMANN APPLANATION TONOMETRY

GAT is considered to be the 'gold standard' against which all other tonometers are calibrated and judged (Kniestedt *et al.*, 2008). Along with non-contact tonometers, such as the air puff and ORA, it is the most commonly used method to estimate the IOP by measuring the resistance of the eye to some applied force.

From an opthalmological point of view, the IOP is determined by first applying a topical anaesthetic and fluorescein dye to the eye (Kniestedt *et al.*, 2008). The Goldmann applanation tonometer, which is mounted on a slit-lamp biomicroscope (Figure 2.7a), is then used to applanate the cornea. The applanator has a diameter of 3.06 mm, which Goldmann and Schmidt (1957) found to be the optimum, and is at the center of a plastic cylinder with a

(a) Applanation tonometer **(b)** Closer view of applanation **(c)** Fully applanated cornea

Figure 2.7: Goldmann Applantion Tonometry (GAT) process and results. (a) A modern GAT mounted on a slit-lamp with a (b) closer view of the applanation process and (c) corresponding results when the cornea is fully applanated (the inner edges of the semi-circles are shown with the white arrows) [Obtained from: http://www.surgitek.it and http://www.haag-streit.com].

diameter of 7.0 mm (c.f. Figure 2.7b). This cylinder is then attached to an arm which in turn is attached to a spring-loaded knob (Kniestedt *et al.*, 2008). The applied force of the applanator is then adjusted by means of this knob until the applanated area of 7.35 mm^2 is completely wet, due to the applied anaesthetic, and the inner edges of the two semi-circles touch as shown in Figure 2.7c. At this point the device gives a single measurement, the IOP due to GAT (IOPG), which is in actuality an 'estimate' of the True IntraOcular Pressure (IOPT).

In this study the internal eye pressure is referred to using several different acronyms to differentiate between the type of internal eye pressure (c.f. Figure 2.8).

- **IOP** is a general reference used when there is no need to distinguish between the different IOPs and generally refers to the true internal pressure.
- **IOPT** refers to the true internal eye pressure.
- **IOPG** refers to the measured or estimated internal eye pressure during GAT.
- **IOPC** will only be encountered in Chapter 5 and refers to the numerically estimated IOPG which is calibrated according to a numerically normal cornea.

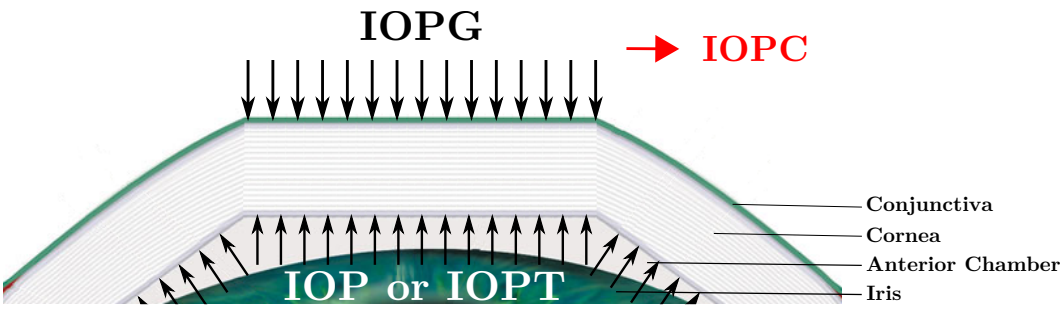

Figure 2.8: An illustration of the different types of acronyms used to reference the internal eye pressure where IOP is used to generally refer to the internal eye pressure, IOPT refers to the true internal eye pressure, IOPG is the measured or estimated internal eye pressure during GAT and IOPC is the numerically calibrated IOPG. [Adapted from http://www.angioedupro.com/ and Orssengo and Pye (1999)]

2.5.1 Applanation Mechanics

Applanation tonometry works on the principle of the Imbert-Fick law, which simply states that for a given thin walled spherical shell that the Intraocular Pressure due to GAT (IOPG), is approximated by the force (F) required to flatten a given area (A). This law is only valid if the cornea is infinitely thin, has no inherent stiffness and no other forces are acting on it (Goldmann and Schmidt, 1957).

In actuality, the cornea is a conical section of a spherical shell with a finite thickness, an associated stiffness and capillary forces develop on the corneal surface due to the anaesthetic (Goldmann and Schmidt, 1957; Ethier and Simmons, 2007). Consequently, additional forces act on the applanator during the applanation process. These additional forces, illustrated in Figure 2.9, are typically known as:

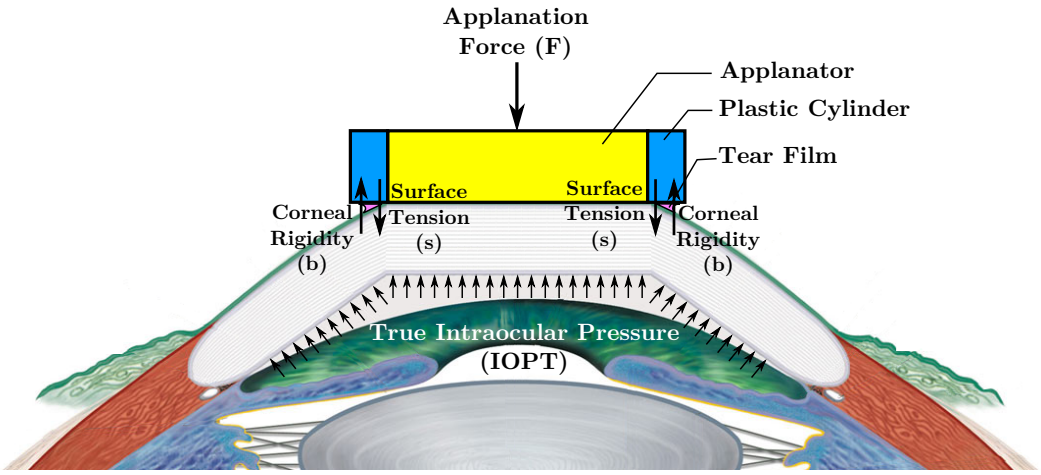

Figure 2.9: Forces acting on the applanator during applanation tonometry. The corneal rigidity (b) and surface tension (s) forces act on the applanator (yellow) which is at the center of a plastic cylinder (blue). [Redrawn from http://www.angioedupro.com/ and Ethier and Simmons (2007)]

- The **corneal rigidity or stiffness** (b in Figure 2.9), which resists deformation by essentially pushing the applanator away from the cornea.
- The **surface tension** (s in Figure 2.9) due to the presence of the anaesthetic. These surface forces tend to pull the applanator towards the cornea, forming a meniscus between the applanator and cornea during contact.

If a force balance is done considering these additional forces that act on the applanator, the Imbert-Fick law should state:

$$F + s = (\text{IOPT})(A) + b \tag{2.1}$$

However, it is difficult to determine the corneal stiffness (or rigidity) and surface tension for each patient *in vivo*, and Goldmann and Schmidt (1957) therefore decided to design the applanator in such a way that these additional forces cancel one another.

By assuming that a normal CCT is approximately 0.5 mm, Goldmann and Schmidt (1957) conducted experimental investigations with fresh enucleated eyes using applanation diameters of between 2.5 and 5.0 mm. Theoretically, a linear relationship between the applanation diameter and the difference between the pressure measured by applanation and manometery should exist. They determined that with an applanation diameter of 4.0 mm the rigidity force is larger than the surface tension force, while at a diameter of 3.0 mm the forces are approximately equal (Goldmann and Schmidt, 1957). They decided to use an applanation diameter of 3.06 mm, because at this diameter 1 gram of applied force is equivalent to 10 mmHg of the IOP (Goldmann and Schmidt, 1957; Kniestedt *et al.*, 2008). When considering 3.06 mm to be the optimum applanation diameter, Equation (2.1) reduces to a more simplistic form, such that the IOPT is estimated by:

$$\text{IOPG} \simeq \text{IOPT} = \frac{F}{A} \tag{2.2}$$

2.5.2 Associated Concerns

Over the years several clinical studies have reported errors with respect to the IOP measurement obtained using GAT, yet it still remains the 'gold standard' today.

One of the most significant causes of error in the IOP measurement is the CCT and corneal RoC (i.e. astigmatism) (Goldmann and Schmidt, 1957; Ehlers *et al.*, 1975; Kotecha, 2007; Brandt *et al.*, 2009). It is widely known that a thick, steeper cornea tends to overestimate the IOP and a thin, flatter cornea tends to underestimate the IOP (Ehlers *et al.*, 1975; Kotecha, 2007; Brandt *et al.*, 2009). When the CCT varies from the norm, the IOP measurement obtained from GAT needs to be "corrected" by $2.5 - 3.5$ mmHg for every 50 μm of thickness deviation (Ethier and Simmons, 2007). It has, for this reason, become standard practice in a clinical setting to measure the CCT (using a pachymeter) when measuring IOP (Chihara, 2008; Kniestedt *et al.*, 2008).

Not much is known about the influence of corneal stiffness on the IOP measurement. Goldmann and Schmidt (1957) said that "the instrument functions satisfactorily and that our assumption that M_o [a constant which characterizes the elastic properties of the cornea when buckled] is independent of the intraocular pressure is permissible". To the knowledge of the author there are no clinical studies to contradict this statement.

Numerical studies, however, have contradicted this statement and found that corneal stiffness does indeed influence the IOP measurement (Orssengo and Pye, 1999; Liu and Roberts, 2005; Elsheikh *et al.*, 2006; Kwon *et al.*, 2008). Researchers tend to trust these results as several studies have shown that the patient's age is indeed a factor that can influence the IOP measurement and should be accounted for in ocular tonometry (Daxer *et al.*, 1998; Elsheikh *et al.*, 2007a). Corneal stiffening is believed to be age-related, hence with an increase in age, changes in collagen fibre diameter and intermolecular spacing, as well as collagen cross-linking, contribute to changes in the corneal structure (Daxer *et al.*, 1998; Kotecha, 2007). One can therefore say, very loosely, that corneal stiffening could influence the IOP, even though this effect has not been quantified yet (Elsheikh *et al.*, 2007a).

2.6 NUMERICAL PARAMETRIC STUDIES

Due to the uncertainties related to the effect of the corneal stiffness on the measured IOP, several numerical studies have been conducted to quantify this relationship. These studies contradict the original assumption made by Goldmann and Schmidt (1957) that corneal material properties do not influence the IOP measurement. In an attempt to understand why these numerical studies have come to such a popularly accepted conclusion, the models and validation methods used in these studies are discussed here for comparison.

2.6.1 Orssengo and Pye's Linear Elastic Analytical Model

One of the first theoretical studies conducted to estimate the corneal elasticity and IOPT *in vivo* was done by Orssengo and Pye (1999). They conducted an analytical study in which they assumed the cornea to be a shell and used a linear elastic relationship between pressure and elastic modulus.

Using the approach of classical mechanics and the geometrical properties of a normal cornea (CCT = 0.52 mm and anterior RoC (R_{ant}) = 7.80 mm), they related the elastic modulus (E) to the IOPT such that:

$$E = 0.0229\text{IOPT} \tag{2.3}$$

A correction factor (CF) was also applied to correct the relationship between the IOPT and IOPG. The correction factor was calculated using the relationships obtained from the classical mechanics approach for a range of CCT and corneal RoC.

$$\text{IOPT} = \frac{\text{IOPG}}{CF} \tag{2.4}$$

To validate their analytical model (c.f. Figure 2.10a), Orssengo and Pye (1999) compared their results for IOP measurement, as influenced by CCT, to experimental and Finite Element (FE) results. They developed a 3D axisymmetric FE model using MSC/NASTRAN with R_{ant} = 7.8 mm, CCT = 0.45 mm and an applied IOPT = 30 mmHg. The corresponding elastic modulus was then determined from Equation (2.3) to be 0.69 MPa. By defining an elastic modulus and the Poisson's ratio ($\nu = 0.49$) it is implied that they used an isotropic linear elastic material model to represent the corneal structure. Orssengo and Pye (1999) were able to obtain good agreement between their theoretically predicted results and their FE results.

They concluded their study by varying the IOPT to obtain the corresponding elastic modulus, which according to Equation (2.3) has a linear relationship. Their study also concluded that Equation (2.3) may give reasonable estimates for the corneal stiffness *in vivo* within the physiological range ($7 - 21$ mmHg) for IOP.

2.6.2 Liu and Roberts' Linear Elastic Analytical Model

The work of Liu and Roberts (2005) built on the analytical model developed by Orssengo and Pye (1999), with one difference: they included the effects of surface tension due to the application of an anaesthetic (c.f. Figure 2.10b).

Like Orssengo and Pye (1999), Liu and Roberts (2005) assumed the cornea to be a thin shell with a finite thickness and also used a linear elastic material approach to relate the elastic modulus to the IOPT. They found that the surface tension effects account for a pressure of approximately 4.15 mmHg, which they subtracted from the estimated IOPG. By accounting for this surface tension, their analytical model tends to underestimate the IOPG.

By conducting a parametric study they determined the influence of each of the corneal parameters considered to have an effect on the IOPG: the CCT, corneal RoC and corneal stiffness (or elastic modulus as they refer to it). Their model accurately predicts the IOPG for the calibrated normal values ($E = 0.19$ MPa, $R_{\text{ant}} = 7.8$ mm, CCT $= 0.536$ mm), but under- and overestimates at the extremes, as found in clinical studies as well. For thin, flatter corneas the IOPG is underestimated and for thick, steeper corneas overestimated, which is to be expected.

They also showed that with an increase in elastic modulus, a linear increase in IOPG measurement is also observed, just as Orssengo and Pye (1999) found in their study. Additionally, it appears that the elastic modulus has an influence on the slope of the CCT and IOPG relationship.

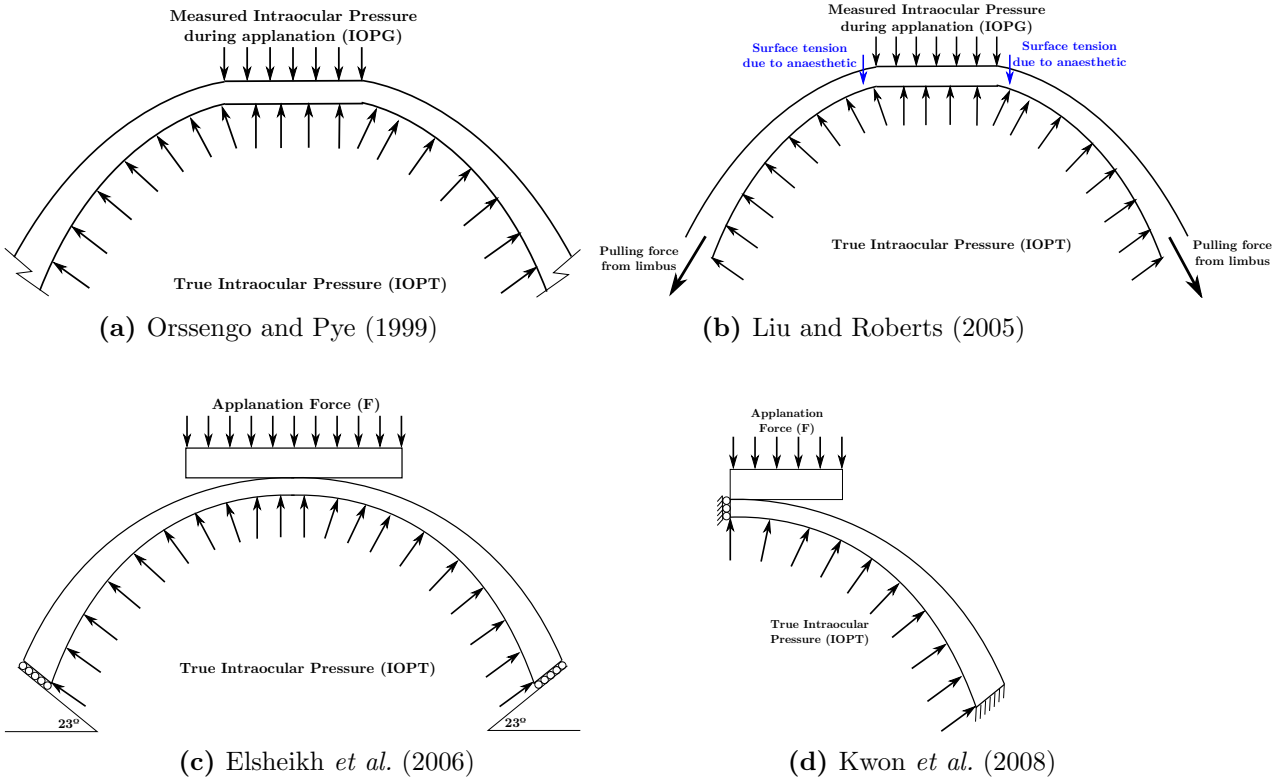

(a) Orssengo and Pye (1999) **(b)** Liu and Roberts (2005)

(c) Elsheikh *et al.* (2006) **(d)** Kwon *et al.* (2008)

Figure 2.10: Representations of the developed mathematical and numerical models used to determine the influence of material properties on the estimated IOPG. (a) and (b) are analytical models, whereas (c) and (d) are numerical FE model; with (c) a full 3D model, and (d) an axisymmetric 2D model.

2.6.3 Elsheikh's Non-Linear Numerical Model using Ogden Hyperelasticity

In their study, Elsheikh *et al.* (2006) developed a full 3D FE model (c.f. Figure 2.10c) of the human cornea to evaluate GAT.

To represent the corneal structure they decided to use a fourth order Ogden hyperelastic constitutive model, which not only adequately represents the non-linear behaviour of the

cornea, but is already available in the commercial software package, ABAQUS:

$$U = \sum_{i=1}^{4} \frac{2\mu_i}{\alpha_i^2}(\lambda_1^{\alpha i} + \lambda_2^{\alpha i} + \lambda_3^{\alpha i} - 3) + \sum_{i=1}^{4} \frac{1}{D_i}(J^{\text{el}} - 1)^{2i}, \tag{2.5}$$

where U is the strain energy function, λ_i are the principal stretches, μ_i, α_i and D_i are temperature dependent material parameters and J^{el} is the elastic volume ratio. To account for the actual connection of the cornea to the sclera at the limbal boundary, a roller support at an angle of 23° was applied. The IOPT was simulated by applying a distributed load on the posterior surface of the cornea model.

To account for the change in corneal stiffness, Elsheikh *et al.* (2006) calibrated their constitutive model against inflation test data obtained from Elsheikh and Anderson (2005), Elsheikh *et al.* (2007a) and Bryant and McDonnell (1996). The inflation test data was converted to obtain the corresponding stress-strain response and the model was calibrated only for the stress-strain responses with an initial elastic modulus of 0.08 MPa using Bryant and McDonnell (1996) and 0.30 MPa using Elsheikh and Anderson (2005). Finally their GAT simulation was calibrated using CCT = 0.52 mm and R_{ant} = 7.8 mm such that the correction factor (CF), introduced by Orssengo and Pye (1999) (c.f. Equation (2.4)), is equal to one. A correction of 0.44 mmHg, due to the surface tension of the applied anaesthetic during GAT, is applied to the IOPG.

Using this non-linear FE model, Elsheikh *et al.* (2006) analysed the effect of various corneal properties on the estimated IOPG. They found that CCT and corneal RoC do influence the estimated IOPG. Their study also concluded that with a change in corneal stiffness there is a non-linear influence on the IOPG.

2.6.4 Kwon's Axisymmetric Numerical Model using a Transverse Isotropic Fung Model

More recently, Kwon *et al.* (2008) followed a similar approach to Elsheikh *et al.* (2006) in their model construction to investigate the effect of corneal stiffness on the estimated IOPG.

Exploiting the axisymmetric nature of the cornea, Kwon *et al.* (2008) developed a 2D axisymmetric FE model (c.f. Figure 2.10d) of the cornea with a transversely isotropic extended Fung constitutive model (Fung *et al.*, 1979; Kwon *et al.*, 2008) to represent the corneal structure:

$$U = \frac{1}{2\beta}(e^{\phi} - 1), \text{ where } \phi = \beta \epsilon^T S_0 \epsilon, \tag{2.6}$$

where β represents the degree of non-linearity and it is related to the in-plane elastic modulus by means of a linear interpolation function (Kwon *et al.*, 2008) and S_0 is the initial linear elastic tangent stiffness matrix. A fixed boundary condition is assumed at the limbus and a symmetry condition is applied at the corneal apex. A distributed load was applied to the posterior surface of the model which represents the IOPT. Kwon *et al.* (2008) also accounts for the pressure drop due to the application of an anaesthetic by subtracting 4.7 mmHg from

the estimated IOPG. The constitutive model was calibrated using inflation experimental data obtained from Bryant and McDonnell (1996).

A parametric study was conducted to determine the effect of CCT and stiffness on the estimated IOPG using average values (CCT = 0.536 mm, R_{ant} = 7.77 mm, E = 0.23 MPa). From this study, Kwon *et al.* (2008) concluded that both of these properties have an influence on the estimated IOPG, with the stiffness contributing as much to the inaccurate estimation as the CCT.

2.6.5 Summary of Conclusions

Overall, all the studies in the previous sections found the CCT, RoC and stiffness to have an influence on the estimated IOPG. Table 2.2 summarises these effects on the estimated IOPG for each study mentioned in the previous sections.

Table 2.2: Summary of the main conclusions of four numerical parametric studies investigating the effect of corneal biomechanical properties on GAT.

Orssengo and Pye (1999)	**Liu and Roberts (2005)**	**Elsheikh *et al.* (2006)**	**Kwon *et al.* (2008)**
Assumed Average Properties			
CCT = 0.45 mm R_{ant} = 7.8 mm E = 0.69 MPa IOPT = 30 mmHg	CCT = 0.536 mm R_{ant} = 7.8 mm E = 0.19 MPa IOPT = 10, 15, 20 mmHg ΔP_{sur} = 4.15 mmHg	CCT = 0.520 mm R_{ant} = 7.8 mm E = 0.08, 0.30 MPa IOPT = 15 mmHg ΔP_{sur} = 0.44 mmHg	CCT = 0.536 mm R_{ant} = 7.77 mm E = 0.23 MPa IOPT = 16 mmHg ΔP_{sur} = 4.7 mmHg
Effect of central corneal thickness (CCT) on IOPG			
CCT = 0.45 − 0.59 mm	CCT = 0.44 − 0.63 mm	CCT = 0.32 − 0.72 mm	CCT = 0.35 − 0.80 mm
$\triangle$IOPG$_{\text{theory}}$ = 9 mmHg $\triangle$IOPG$_{\text{FEM}}$ = 12 mmHg	$\triangle$IOPG = 2.87 mmHg	$\triangle$IOPG$_{0.3\text{MPa}}$ = 7.03 mmHg $\triangle$IOPG$_{0.08\text{MPa}}$ = 2.35 mmHg	$\triangle$IOPG = 7.49 mmHg
Effect of corneal curvature (R_{ant}) on IOPG			
	R_{ant} = 6.99−8.61 mm	R_{ant} = 7.20−8.40 mm	
	$\triangle$IOPG = 1.76 mmHg	$\triangle$IOPG$_{0.3\text{MPa}}$ = 1.63 mmHg $\triangle$IOPG$_{0.08\text{MPa}}$ = 1.58 mmHg	
Effect of corneal stiffness (E) on IOPG			
E = 0.20 − 1.0 MPa	E = 0.10 − 0.9 MPa	E = 0.08 − 1.2 MPa	E = 0.12 − 0.3 MPa
$\triangle$IOPG$_{\text{theory}}$ = 36.5 mmHg	$\triangle$IOPG = 17.26 mmHg	$\triangle$IOPG = 17.00 mmHg	$\triangle$IOPG = 7.61 mmHg

Most notable from Table 2.2 is that the influence due to corneal stiffness is considerable in comparison to CCT and corneal RoC. It seems that Liu and Roberts (2005) and Elsheikh *et al.* (2006) are in good agreement with their overall results, despite using different techniques (analytical vs. numerical), different constitutive models (linear vs. non-linear) and different values for corneal stiffness (0.19 MPa vs. 0.08 MPa). It seems that the effect of the surface tension due to the applied anaesthetic makes a considerable difference in the IOPG due to stiffness, as this is the major difference between the models presented by Orssengo and Pye (1999) and Liu and Roberts (2005).

Not much can be deduced from the results in Table 2.2 alone and the results are therefore graphically illustrated in Figures 2.11, 2.12 and 2.13. As already mentioned the results of Liu and Roberts (2005) and Elsheikh *et al.* (2006) are in good agreement, for specific cases, especially when comparing the CCT and RoC studies.

The studies done on the effect of CCT on the estimated IOPG, Figure 2.11, show variation in the results. Liu and Roberts (2005), Elsheikh *et al.* (2006) and Kwon *et al.* (2008) are in good agreement with only slight variations in the estimated IOPG, where the corneal properties are very similar. It is seen that with a change in corneal stiffness, there is a change in the gradient of the obtained results, as shown by Orssengo and Pye (1999) (blue solid line with $E = 0.69$ MPa) with a significant change in gradient due to a higher elastic modulus; and by Elsheikh *et al.* (2006) (green solid line with $E = 0.08$ MPa and green dashed line with $E = 0.30$ MPa) with a small change in gradient as the elastic modulus increases. These results suggest that the corneal stiffness does influence the gradient of the CCT-IOPG curve.

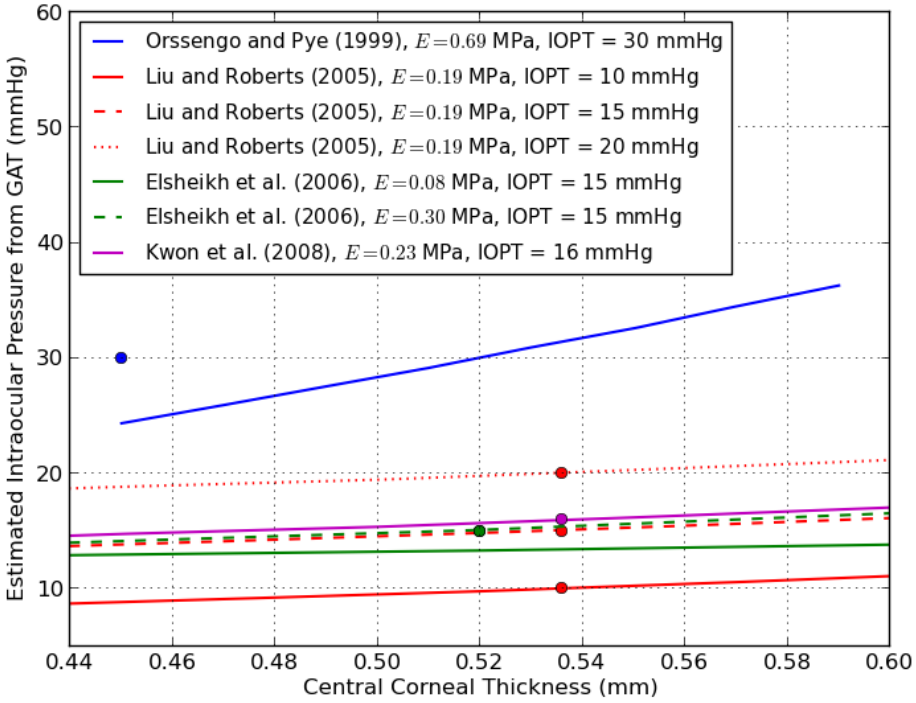

Figure 2.11: Comparison of the effect of the CCT on the IOPG for the numerical studies. All studies used a R_{ant} of 7.8 mm, except Kwon *et al.* (2008) used 7.77 mm. The colored dots show the IOPT at the assumed average properties for each study.

Figure 2.12 indicates that both studies (Liu and Roberts, 2005; Elsheikh *et al.*, 2006), despite using drastically different constitutive models (linear vs. non-linear) and methods (analytical vs. numerical), obtained similar results; especially when comparing the dashed lines, which share similar corneal properties as well. From Figure 2.12 it is also clear that even with a considerably lower stiffness ($E = 0.08$ MPa, green solid line for Elsheikh *et al.* (2006)) the results still have the same gradient but just underestimate the IOPG.

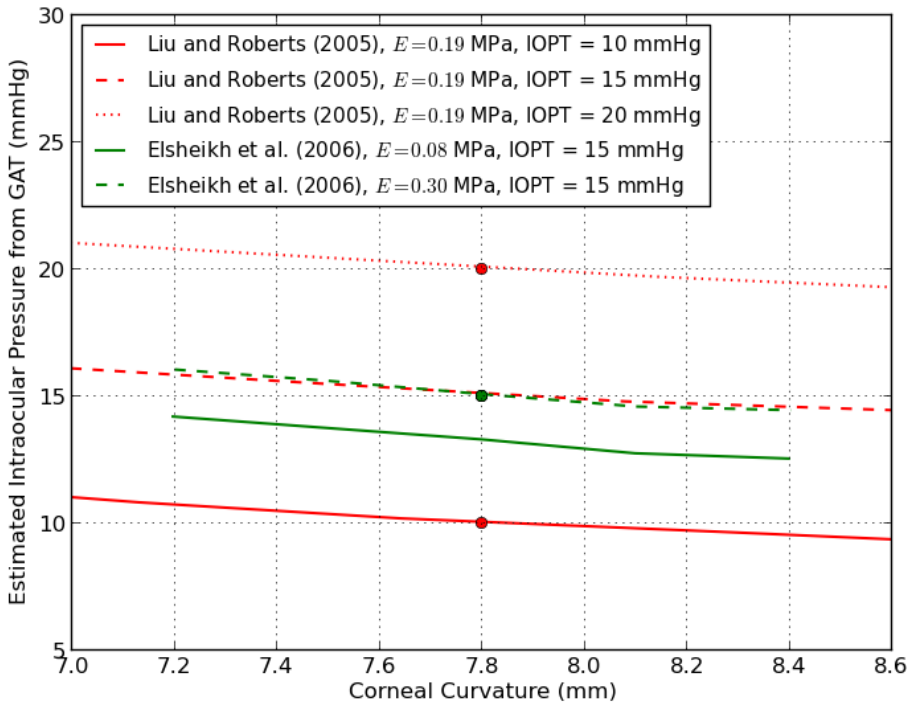

Figure 2.12: Comparison of the effect of corneal RoC on the IOPG for the numerical studiess. Liu and Roberts (2005) used a CCT of 0.536 mm and Elsheikh *et al.* (2006) used a CCT of 0.520 mm. The colored dots show the IOPT at the assumed average properties for each study.

All of these studies also investigated the influence of the corneal stiffness on the estimated IOPG, with the results summarised in Figure 2.13. There is a lot of variation in these results, which could indicate that the effect of corneal stiffness is not yet fully understood.

What is a little more disconcerning is that Orssengo and Pye (1999) and Liu and Roberts (2005) used the same model, with the only differences being that Liu and Roberts (2005) accounted for the surface tension and used a lower value for E, but yet obtained considerably different results. It is to be expected that the results between the linear and non-linear constitutive models will vary. Even though both Elsheikh *et al.* (2006) and Kwon *et al.* (2008) used experimental inflation test data (Bryant and McDonnell, 1996; Elsheikh and Anderson, 2005; Elsheikh *et al.*, 2007a) to calibrate their constitutive models, the variation in the obtained results seem to indicate that the choice of constitutive model and associated modelling assumptions (such as boundary conditions) could make a difference.

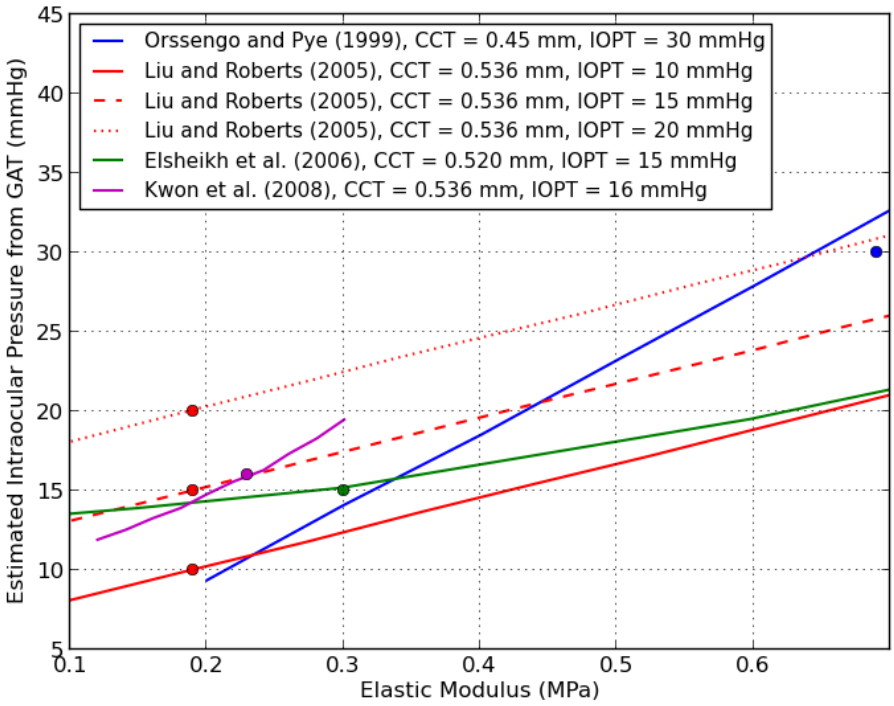

Figure 2.13: Comparison of the effect of corneal stiffness on the IOPG for the numerical studies. All studies used a R_{ant} of 7.8 mm, except Kwon *et al.* (2008) used 7.77 mm. The colored dots show the IOPT at the assumed average properties for each study.

2.7 CONCLUSION

This chapter served as an introduction to a few important concepts related to the anatomy and biomechanics of the cornea. Specific attention was paid to the corneal stiffness and its *in vivo* and *ex vivo* measurements.

Ex vivo inflation testing was found to be the most popular method of testing used to quantify corneal biomechanical properties. However, the two experimental studies most used to calibrate numerical constitutive models, have shown a wide spread in their data. One possible explanation for this spread is that one study allowed the corneal specimen to creep before measuring the apical displacement and the other did not allow for creep.

A short introduction to the mechanics of Goldmann Applanation Tonometry (GAT) was also given, along with the concerns associated with this technique in clinical practice. It was found that Central Corneal Thickness (CCT) and corneal Radius of Curvature (RoC) does influence the measured IntraOcular Pressure from GAT (IOPG). But clinically not much is known about the influence of the corneal stiffness on IOPG.

Several numerical studies found, by utilizing different techniques and constitutive models to represent the corneal structure, that the corneal stiffness influences the measured IOPG during tonometry. However, at present there are no clinical studies available to verify these numerical conclusions as there are currently no means of determining corneal material properties *in vivo*.

CHAPTER 3

FINITE ELEMENT MODEL OF THE HUMAN CORNEA

3.1 INTRODUCTION

Over the years numerical models have ranged from simple analytical models to more complex finite element models, using a variety of constitutive relations to represent the complex corneal structure (Dupps Jr. and Wilson, 2006; Ruberti *et al.*, 2011). Numerical modelling is commonly used to predict corneal response to wound healing (Dupps Jr. and Wilson, 2006), refractive surgery (Pandolfi and Manganiello, 2006; Bryant and McDonnell, 1996), Goldmann Applanation Tonometry (GAT) (Orssengo and Pye, 1999; Liu and Roberts, 2005; Elsheikh *et al.*, 2006; Elsheikh and Wang, 2007; Kwon *et al.*, 2008; Srodka, 2010), palpation (Niroomandi *et al.*, 2008), optical performance due to refractive power (Liou and Brennan, 1997) and *ex vivo* experimental studies, such as inflation (Elsheikh and Wang, 2007; Elsheikh *et al.*, 2009) and strip extensometry tests (Studer *et al.*, 2010).

The constitutive models used to represent the corneal structure in these numerical models have evolved from linear isotropic models (Orssengo and Pye, 1999; Liu and Roberts, 2005), transverse isotropic models (Kwon *et al.*, 2008; Ghaboussi *et al.*, 2009) and hyperelastic models (Elsheikh *et al.*, 2006, 2008a; Niroomandi *et al.*, 2008) to more complex anisotropic fibre reinforced models (Pandolfi and Manganiello, 2006; Pandolfi and Holzapfel, 2008; Studer *et al.*, 2010).

This chapter will discuss the development of a 3D Finite Element (FE) model of the human cornea incorporating its complex structure, which will be calibrated using experimental inflation test data in Chapter 4 and used to simulate GAT in Chapter 5. The choice of geometric properties, simulation boundary conditions and assumptions made are also discussed.

The open-source FE solver, Calculix (Dhondt, 2011a), is used in this study to conduct the Finite Element Analysis (FEA). This chapter refers to sections of the input file structure, which is more extensively discussed in Appendix A and the reader is referred to this appendix for more background.

3.2 MATHEMATICAL MODEL

3.2.1 Geometrical Properties

The cornea consists of two primary surfaces, the anterior (blue) and posterior (red) surfaces as shown in Figure 3.1. Also shown is the corneal apex, limbus, Central Corneal Thickness (CCT), anterior and posterior Radius of Curvature (RoC), Peripheral Corneal Thickness (PCT) as well as the biological and corresponding mathematical global coordinate axis.

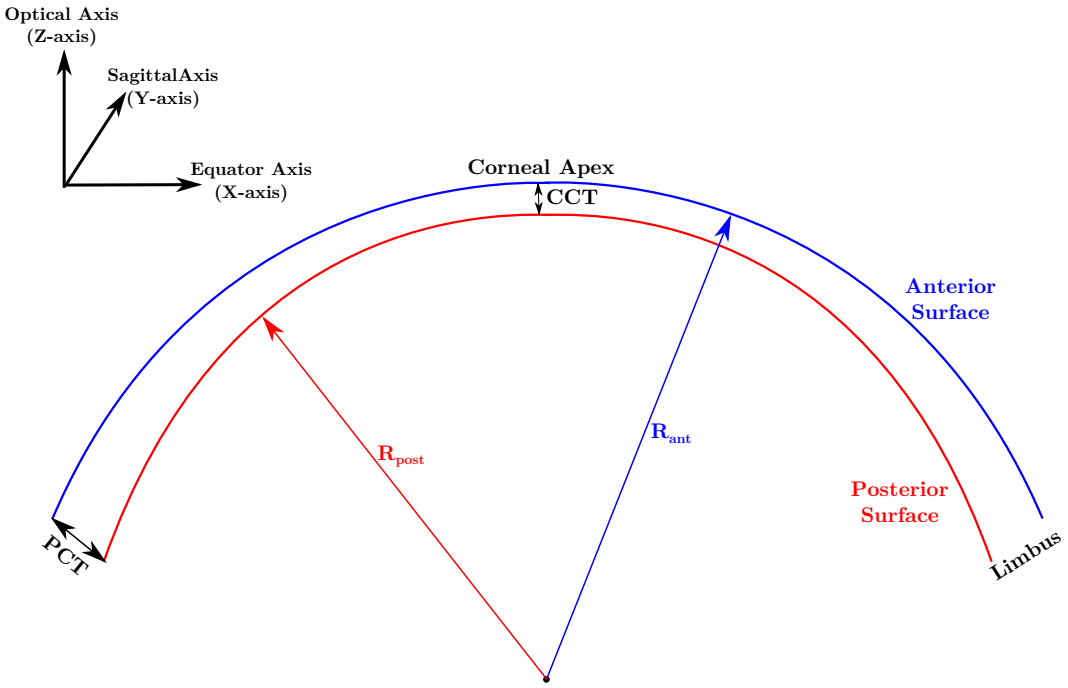

Figure 3.1: Schematic of the anterior and posterior surfaces of the cornea, where CCT is the central corneal thickness, PCT is the peripheral corneal thickness, R_{ant} is the anterior radius of curvature and R_{post} is the posterior radius of curvature in a global coordinate system.

As the cornea gradually increases in thickness from the central apex to the peripheral limbus, each surface has a different set of geometrical properties to describe its shape. These properties are obtained from various sources (Jakobiec and Ozanics, 1982; Rodrigues *et al.*, 1982; Newell, 1992; Liou and Brennan, 1997; Batterbury and Bowling, 2005) and are summarized in Table 3.1. Note for geometric properties where the literature did not correspond the average of the range of values was taken to be the properties for the average population.

Table 3.1: Corneal geometric properties as obtained from various literature sources.

Geometric Property	**Anterior Surface**	**Posterior Surface**
Radius of Curvature (RoC or R)	7.77 mm	6.20 – 6.40 mm (average: 6.30 mm)
Surface Asphericity (Q)	−0.18	−0.60
Diameter (D)	11.70 mm	-
Central Corneal Thickness (CCT)	0.50 – 0.565 mm (average: 0.53 mm)	
Peripheral Corneal Thickness (PCT)	0.52 – 1.0 mm (average: 0.76 mm)	

3.2.2 Conicoidal Equation Describing Corneal Surfaces

According to Carney *et al.* (1997) there exist several mathematical models which have been used to describe the aspherical shape of the cornea, the simplest of which is a rotationally symmetric conicoid. Liou and Brennan (1997) state that the cornea can be represented as a rotationally symmetric conicoid as it accounts for the majority of the eye's refractive power. The axis of rotation of the cornea is the optical axis (Z-axis), leading to the general equation for a 3D conicoid with the origin at (X_o, Y_o, Z_o) (Kiely *et al.*, 1982; Carney *et al.*, 1997; Smith and Atchison, 1997):

$$(X - X_o)^2 + (Y - Y_o)^2 + (1 + Q)(Z - Z_o)^2 - 2R(Z - Z_o) = 0, \tag{3.1}$$

where R is the Radius of Curvature (RoC) at the apex, Q is the surface asphericity parameter, X is the distance along the equator axis and Y the distance along the sagittal axis from the optical axis, Z. The asphericity parameter, Q, defines the type of conicoidal surface (Kiely *et al.*, 1982; Carney *et al.*, 1997; Smith and Atchison, 1997) as given in Table 3.2. The influence of the asphericity parameter on both the anterior and posterior conicoidal surfaces is illustrated in Figure 3.2.

Table 3.2: Definition of the asphericity parameter for the type of conicoid.

Asphericity	**Type of conicoid**
$Q > 0$	Oblate ellipsoidal surface with the major axis in the XY plane
$Q = 0$	Spherical surface
$-1 < Q < 0$	Prolate ellipsoidal surface with the major axis in the Z-direction
$Q = -1$	Paraboloidal surface with an axis along the Z-direction
$Q < -1$	Hyperboloidal surface

This mathematical model can however not account for some of the asymmetries found in the corneal shape, such as astigmatism, unless the RoC (R) and asphericity (Q) are described as a function of the azimuth (Kiely *et al.*, 1982; Liou and Brennan, 1997). For the purpose of this thesis, corneal asymmetries are not investigated and a normal cornea is therefore assumed such that there are no variations in RoC or asphericity.

To express Equation (3.1) explicitly in terms of the Z-coordinate, it is solved as a quadratic equation, resulting in two solutions for Z:

$$Z = \frac{[R + (1 + Q)Z_o] + \sqrt{[R + (1 + Q)Z_o]^2 - (1 + Q)[2RZ_0 + (1 + Q)Z_o^2 + (X - X_o)^2 + (Y - Y_o)^2]}}{(1 + Q)} \tag{3.2a}$$

$$Z = \frac{[R + (1 + Q)Z_o] - \sqrt{[R + (1 + Q)Z_o]^2 - (1 + Q)[2RZ_0 + (1 + Q)Z_o^2 + (X - X_o)^2 + (Y - Y_o)^2]}}{(1 + Q)} \tag{3.2b}$$

Between the two solutions given in Equations (3.2a) and (3.2b) the correct one, according to Smith and Atchison (1997), is Equation (3.2b). Using Equation (3.2b) in conjunction with the geometrical properties listed in Table 3.1, the corneal anterior and posterior surfaces

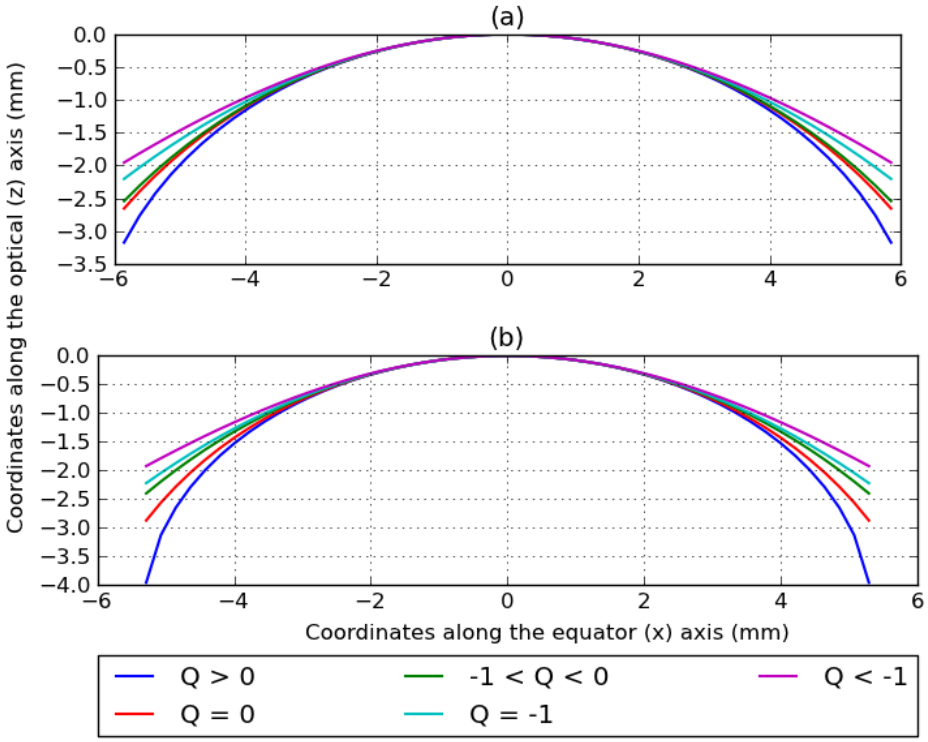

Figure 3.2: Influence of the variation in surface asphericity (Q) on the type of conicoid. A constant radius of curvature for the (a) anterior and (b) posterior corneal surfaces is assumed to be 7.77 mm and 6.3 mm, respectively (c.f. Table 3.1).

are determined to generate the corneal geometry as shown in Figure 3.3. It is seen that when using the geometric properties (c.f. Table 3.1) the PCT calculated from the generated geometry is 0.6767 mm. By either decreasing the posterior surface RoC or the asphericity parameter it is possible to obtain a PCT closer to the average value of 0.76 mm given in Table 3.1. Even though the calculated PCT is less than the average of 0.76 mm, it does still fall within the range obtained from literature and is therefore acceptable for the purposes of this study.

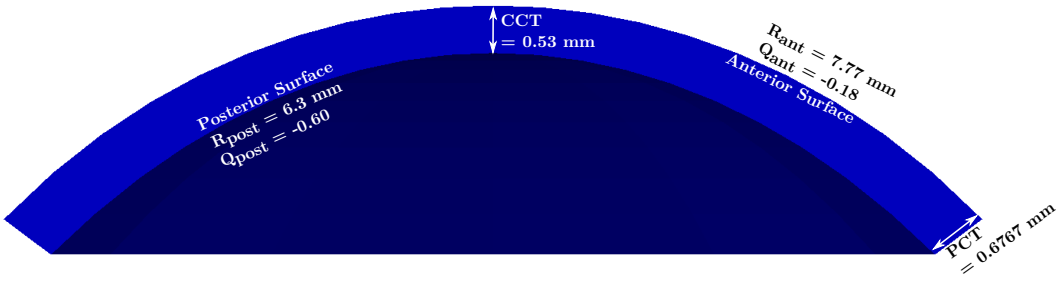

Figure 3.3: A model of the cornea using the assumed geometric properties of an average population. The PCT is calculated as 0.6767 mm, which is still within the range of $0.52 - 1.0$ mm obtained from literature.

3.2.3 Assumptions

In Section 2.2 the six structural layers of the cornea were discussed, where Bowman's membrane and the stroma are the only layers that contain collagen fibrils, which are responsible

for the tensile strength of the cornea. From a structural point of view, Dupps Jr. and Wilson (2006) found that by removing the epithelium, endothelium and Decemet's membrane little or no change is observed to the overall tensile strength of the cornea and anterior corneal RoC. On the other hand a numerical study conducted by Elsheikh *et al.* (2009) found that by modelling the individual layers of the corneal structure, the simulation results are affected, especially when the cornea is subjected to bending effects as experienced during tonometry. However, modelling the layered structure falls beyond the scope of this dissertation and the cornea is therefore assumed to be a homogenous ground material containing only collagen fibrils.

The cornea is assumed to be a nearly incompressible material as it is composed of approximately 80% water (Ruberti *et al.*, 2011).

3.3 CONSTITUTIVE MODELS

The constitutive models used to represent the complex corneal structure have ranged from simplistic linear isotropic models to more complex anisotropic models which account for the collagen fibril orientations. Some models that have been used to model the corneal structure, in a variety of simulations, include:

- **Linear isotropic model** to simulate GAT (Orssengo and Pye, 1999; Liu and Roberts, 2005) and refractive surgery (Bryant and McDonnell, 1996);
- **Transverse isotropic extended Fung model** to simulate GAT (Kwon *et al.*, 2008; Ghaboussi *et al.*, 2009);
- **Transverse linear elastic isotropic model** to simulate refractive surgery (Bryant and McDonnell, 1996);
- **Nonlinear isotropic model** to simulate refractive surgery (Bryant and McDonnell, 1996);
- **Ogden hyperelastic model** to simulate the inflation test and GAT (Elsheikh *et al.*, 2006, 2008a), refractive surgery (Bryant and McDonnell, 1996), as well as study the effects of the corneal layers on corneal biomechanics (Elsheikh *et al.*, 2009);
- **Fibre reinforced elastic model with a Mooney Rivlin base** to simulate a keratoconous cornea (Pandolfi and Manganiello, 2006) and palpation (Niroomandi *et al.*, 2008); and
- **Fibre reinforced elastic model with a Neo-Hookean base**, which includes the fibre dispersion in the 45° sectors to simulate keratoconous corneas (Pandolfi and Holzapfel, 2008).

With such a wide spread of models available, it is difficult to know which constitutive relationship actually represents the corneal structure with the most accuracy.

The choice of constitutive model is also dependent on whether the simulation requires knowledge of the corneal structure. Refractive surgery and *ex vivo* strip extensometry test simulations, for instance, specifically focus on the corneal structure and the collagen fibres will therefore need to be included in the constitutive model. On the other hand tonometry and *ex vivo* inflation tests are not reliant on the collagen fibres and one can therefore use a macroscopic constitutive model.

To account for the corneal fibres a fibre reinforced elastic model with a Neo-Hookean base is chosen (available in CalculiX (Dhondt, 2011a)), similar to the one used by Pandolfi and Holzapfel (2008), but not identical. The differences between this model and the one developed by Pandolfi and Holzapfel (2008) is that Pandolfi and Holzapfel (2008) included the fibre dispersion seen in the 45° directions and excluded the incompressibility term.

3.3.1 Fibre Reinforced Elastic Model

This model was initially developed by Holzapfel *et al.* (2000) to model arterial walls and, to the knowledge of the author, this specific formulation has not been used to represent the corneal structure. Variations of this model, however, have been shown to successfully simulate the corneal structure (Pandolfi and Manganiello, 2006; Pandolfi and Holzapfel, 2008).

The strain energy density function (U) is composed of an isotropic base material (denoting the ground substance containing no collagen) and an exponential term (denoting the collagen fibre orientations) to form an anisotropic hyperelastic model (Dhondt, 2004):

$$U = C_{10}(\bar{I}_1 - 3) + \frac{1}{D_1}(J-1)^2 + \sum_{i=4,6}^{n} \frac{k_{1i}}{2k_{2i}}[e^{k_{2i}(\bar{I}_i - 1)^2} - 1], \tag{3.3}$$

where n denotes the number of fibre families (two in this study), C_{10} and k_{1i} are stress-like parameters (MPa), k_{2i} is a dimensionless parameter and D_1 is an incompressibility constant. $\bar{I}_1$ and $\bar{I}_i$ denote the invariants of the modified Cauchy-Green deformation tensor ($\bar{\mathbf{C}}$) and J is the Jacobian (determinant of the deformation gradient).

This material model assumes that the fibres are active during tension and inactive during compression (Holzapfel *et al.*, 2000). The relevant anisotropic term (c.f. Equation (3.3)) therefore only contributes to the strain energy density function when the fibres are in tension and becomes zero when the fibres are in compression resulting in an isotropic response, that is (Holzapfel *et al.*, 2000; Dhondt, 2004):

$$\text{Tension}: \quad \bar{I}_i = \bar{I}_i \quad \text{for} \quad \bar{I}_i > 1, \tag{3.4a}$$

$$\text{Compression}: \quad \bar{I}_i = 1 \quad \text{for} \quad \bar{I}_i \leq 1. \tag{3.4b}$$

The invariants $\bar{I}_i$ ($\bar{I}_4$ and $\bar{I}_6$) are indicative of the stretch measures for the two families of collagen fibres and are defined as the squares of the stretches in the directions of the directional vectors, $\vec{a}_j$ (Holzapfel *et al.*, 2000; Dhondt, 2004):

$$\bar{I}_i = \bar{\mathbf{C}} : \mathbf{A}_j, \quad \mathbf{A}_j = \vec{a}_j \otimes \vec{a}_j, \quad i = 4, 6; \quad j = 1, 2, \tag{3.5}$$

where j refers to the number of fibre families and $\mathbf{A}_j$ denotes a structural tensor which characterises the corneal structure (or material) using the corresponding collagen fibre orientation, also known as a directional vector, $\vec{a}_j$.

The invariant $\bar{I}_1$, associated with the isotropic response, is defined as (Holzapfel *et al.*, 2000; Dhondt, 2004):

$$\bar{I}_1 = tr\bar{\mathbf{C}}, \quad \bar{\mathbf{C}} = J^{-2/3}\mathbf{C}, \quad \mathbf{C} = \mathbf{F}^T\mathbf{F}, \quad \mathbf{F} = \left(\frac{d\vec{\chi}}{d\vec{X}}\right)^T = (\nabla_o\vec{\chi})^T, \tag{3.6}$$

where $\mathbf{C}$ denotes the Cauchy-Green deformation tensor, $\mathbf{F}$ is the deformation gradient with $\vec{\chi}$ representing the deformed configuration and $\vec{X}$ is the undeformed (or reference) configuration.

Implementing Preferred Fibre Orientations

The three preferred fibre orientations, two orthogonal sets of fibres in the central cornea and one circumferential set in the limbal region, were discussed in Section 2.2. For the purpose of this study it is assumed that the fibres in the limbal region do not contribute structurally to the corneal deformation during inflation testing and GAT; and therefore only the two orthogonal fibre families in the central cornea are considered.

The orthogonal fibre directions were implemented into the numerical model by defining two vectors (F_x and F_y in the local coordinate system) which are orthogonal to one another but parallel to a plane (c.f. Figure 3.4). This was done by (1) finding a vector normal to the plane of both the wedge and brick elements, and then (2) finding two orthogonal vectors which are perpendicular to the plane's normal vector.

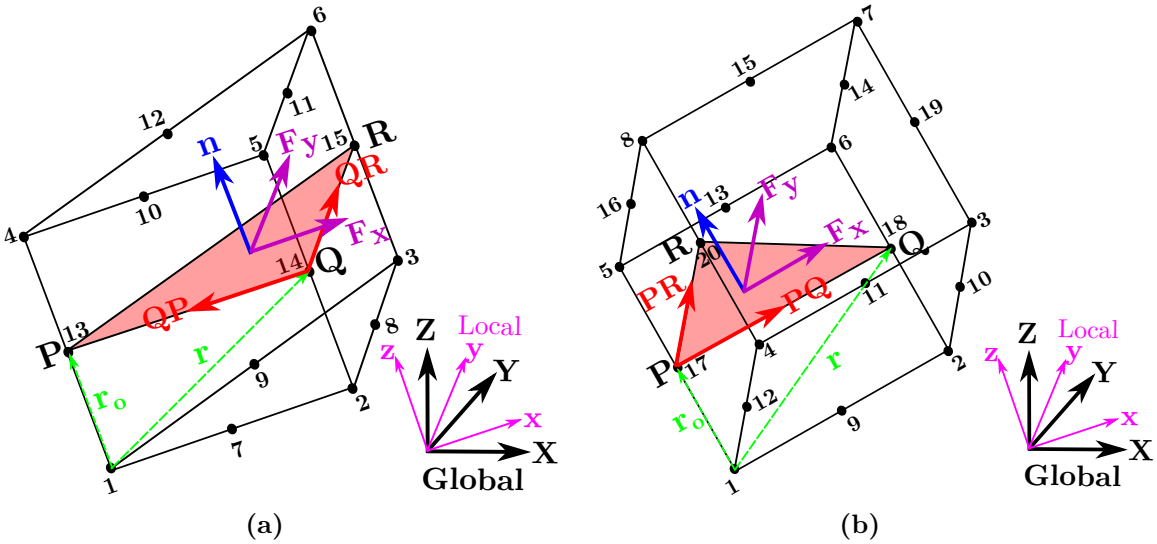

Figure 3.4: The planes used to describe the fibre orientations in a (a) wedge and (b) brick element. The vector normal to the plane is denoted by $\vec{n}$ and the vectors perpendicular to the normal vector, which indicate the fibre directions (in the local axis system), are denoted by F_x and F_y for the x and y fibre directions respectively. $\vec{r}$ and $\vec{r}_o$ indicate directional vectors from the origin to two points on the plane. The global axis system is denoted by X, Y and Z and the local axis system is denoted by x, y and z.

(1) Vector Normal to a Plane: To find the vector normal to a plane the cross product

between two vectors which lie in the plane is taken. From Figure 3.4b, two vectors in the plane PQR are defined as $\vec{PQ}$ and $\vec{PR}$ for the brick element:

$$\begin{aligned}\vec{n} &= \vec{PQ} \times \vec{PR} \\ &= \begin{bmatrix} \hat{\imath} & \hat{\jmath} & \hat{k} \\ PQ_x & PQ_y & PQ_z \\ PR_x & PR_y & PR_z \end{bmatrix} \\ &= [(PQ_yPR_z) - (PQ_zPR_y)]\hat{\imath} - [(PQ_xPR_z) - (PQ_zPR_x)]\hat{\jmath} \\ &\quad + [(PQ_xPR_y) - (PQ_yPR_x)]\hat{k}, \end{aligned} \tag{3.7}$$

where the subscripts x, y and z refer to the respective coordinate of the vector and $\hat{\imath}$, $\hat{\jmath}$ and $\hat{k}$ refer to the respective vector directions. For a wedge element the same approach as in Equation (3.7) is used, but the vectors used are $\vec{QP}$ and $\vec{QR}$.

(2) Vector Perpendicular to the Normal Vector: A vector perpendicular to the normal vector of a plane is defined as having a dot product of zero:

$$\vec{n} \cdot (\vec{r} - \vec{r}_o) = 0, \tag{3.8}$$

where $\vec{r}$ and $\vec{r}_o$ are directional vectors from the origin to a point on the plane (dashed green lines in Figure 3.4). As the x- and y-coordinates of each fibre direction is known, that is $F_x(1.0, 0.0, z_x)$ for a fibre in the equator direction and $F_y(0.0, 1.0, z_y)$ for a fibre in the sagittal direction, the only unkown is the z-coordinate, in the optical direction, for each fibre which is parallel to the defined plane in each element. By rearranging Equation (3.8) the z-coordinate, for both fibres F_x and F_y, can be determined from:

$$z_x \text{ or } z_y = \vec{r_z} - \vec{r}_{oz} = -\left[\frac{\vec{n}_x \cdot (\vec{r}_x - \vec{r}_{ox}) - \vec{n}_y \cdot (\vec{r}_y - \vec{r}_{oy})}{\vec{n}_z}\right] \tag{3.9}$$

The fibre orientations, calculated using Equations (3.7) and (3.9), are represented in the Calculix input file with the `*ORIENTATION` card to define a local axis which is applied to the material definition as follows:

```
*MATERIAL, NAME=ELASTIC_FIBRE
*USER MATERIAL, CONSTANTS=10
C1, D1, 1.0, 0.0, k11, k21, 0.0, 1.0,
k12, k22
*ORIENTATION, NAME=L1
1.0, 0.0, z_x, 0.0, 1.0, z_y
*SOLID SECTION, ELSET=E1, MATERIAL=ELASTIC_FIBRE, ORIENTATION=L1
```

The orthogonal fibre orientations, resulting from the Calculix implementation, are illustrated in Figure 3.5 with red (x-orientation) and blue (y-orientation) magnitude vectors.

To illustrate that the fibres have been implemented correctly into the constitutive model of the cornea, a Von Mises stress plot is shown in Figure 3.6 where an IOP was applied to the

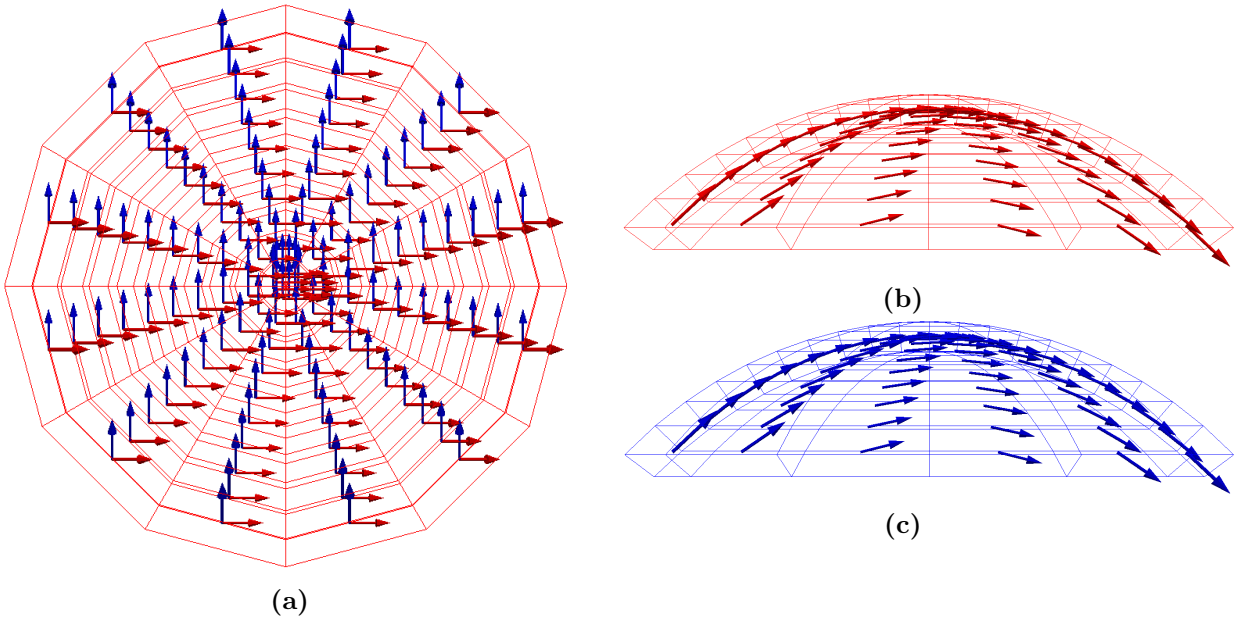

Figure 3.5: Preferred fibre orientations as implemented in Calculix, showing (a) the orthogonality of the fibres in the equator-sagittal plane as well as the fibres along (b) equator axis and (c) sagittal axis.

posterior surface of the cornea to simulate normal *in vivo* conditions (that is pre-stressing, or inflating, the cornea due to an IntraOcular Pressure (IOP) of 16 mmHg). The Von Mises stress illustrates that the fibres are dominant in the centre of the cornea, in the 0° and 90° orientations. This is a good indication that the fibre orientations have been implemented successfully.

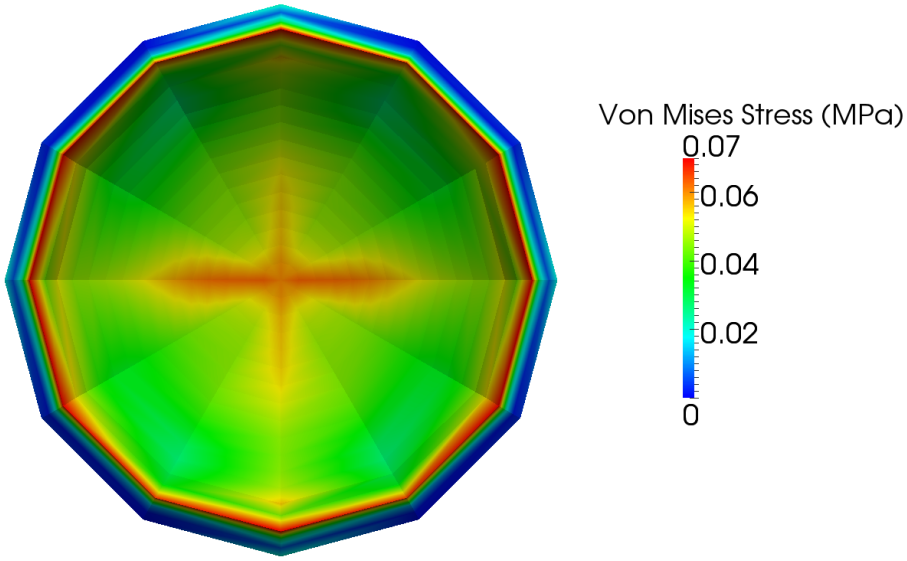

Figure 3.6: Von Mises stress plot illustrating the implementation of the fibres in the constitutive model. The dominance of the two orthogonal fibre families in the central cornea are shown by the high stress experienced in this region due to the applied intraocular pressure of 16 $mmHg$.

3.4 INFLATION SIMULATION

The inflation test that was used to calibrate the constitutive model was discussed in Section 2.4. During an inflation test a whole corneal specimen, excised with a 2 mm scleral ring, is clamped into a pressure chamber and inflated beyond its physiological capabilities.

For both the inflation test and GAT simulations, the fibre reinforced elastic constitutive model is employed using the following material coefficients: $C_{10} = 0.003871$ MPa, $D_1 = 0.4$, $k_1 = 0.035311$ MPa, $k_2 = 181.218385$. An average cornea is assumed using the values in Table 3.1 (CCT = 0.53 mm and $R_{\text{ant}} = 7.77$ mm) for all simulations conducted in this chapter.

3.4.1 Boundary Conditions

The IOP, which is applied on the posterior surface of the cornea, is simulated using a distributed load which acts normal to the surface. However, there is some uncertainty as to the boundary condition that should be applied to simulate the clamping of the corneal specimen on the pressure chamber.

Considering the experimental setup of the inflation test the logical choice for the limbal boundary condition is to completely fix it (Bryant and McDonnell, 1996; Kwon *et al.*, 2008), which will most accurately simulate the corneal specimen being glued and clamped onto the pressure chamber. On the other hand, it has been argued that as the 2 mm scleral ring is glued onto the chamber, the limbal boundary connection could still affect the corneal response. To account for this scleral connection Elsheikh *et al.* (2006) and Elsheikh and Wang (2007) demonstrated that the optimum angle for this connection is at 23°.

The boundary conditions considered for the inflation test simulation are illustrated in Figure 3.7. Both of these boundary conditions will be investigated in Chapter 4 and Chapter 5, to determine their effect on the corneal response and estimated IOP.

The fixed limbal boundary condition is simply described in the Calculix input file by using the `*BOUNDARY` card, where it is fixed from Degree Of Freedom (DOF) 1 to 3 (i.e. in the equator, sagittal and optical directions):

```
*BOUNDARY
limbus, 1,3
```

Note that the same vector calculus method described in Section 3.3.1, to implement the collagen fibre orientations, was used to define a local axis system. This local axis system was used to apply the 23° roller boundary condition. The local axis system is defined in the Calculix input file using the `*TRANSFORM` card, and the boundary is allowed to translate freely in the 3-direction (optical direction), hence only DOFs 1 and 2 (equator and sagittal directions) are fixed:

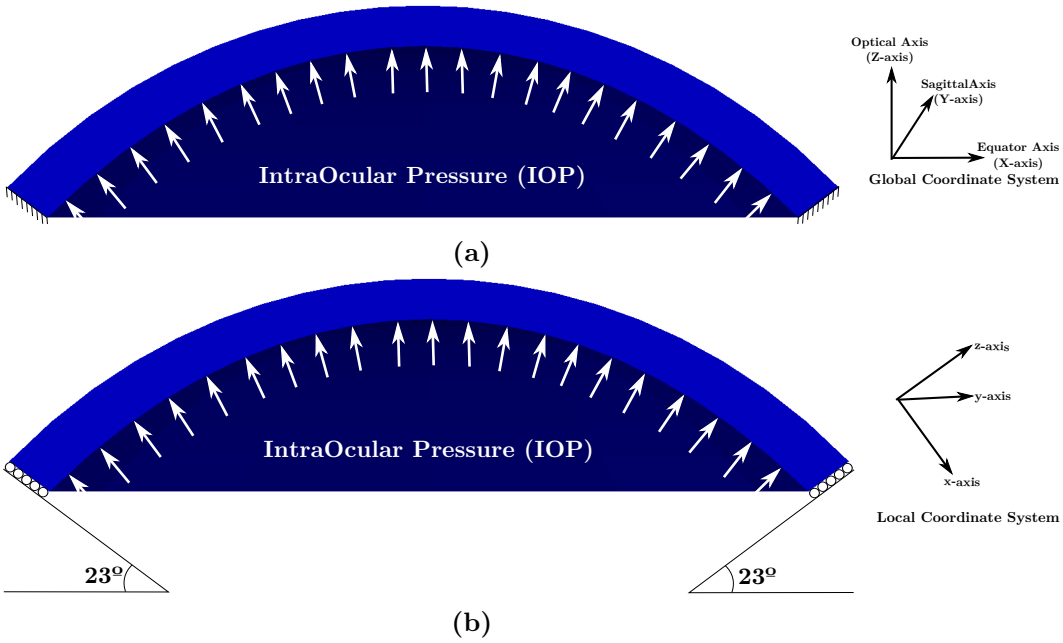

Figure 3.7: The boundary conditions used to simulate the experimental inflation test. The IOP is applied on the posterior surface with a distributed load acting perpendicular to the elements, and the two conditions for the limbal boundary are shown in (a) for a fixed boundary and (b) where the boundary is placed on a roller at an angle of 23°

```
*TRANSFORM, NSET=N15, TYPE=R
Ax, Ay, Az, Bx, By, Bz
*BOUNDARY
limbus, 1,2
```

3.4.2 Element Choice

Two element types were considered for this simulation, a linear and a quadratic brick element, both with full and reduced integration. The first set of elements, at the corneal apex, is a set of linear or quadratic wedge elements.

According to Dhondt (2011b) full integration elements are unable to capture the behaviour of incompressible materials accurately, for both linear and non-linear simulations.

Also, linear elements tend to be problematic in bending, where full integration causes elements to be too stiff and reduced integration causes them to be not stiff enough (Dhondt, 2011b). This is not directly related to the inflation simulation, which mainly undergoes tension, but it is related to the GAT simulation, where the cornea experiences some bending due to applanation. Dhondt (2011b) also states that full integration quadratic elements are problematic during bending.

These shortcomings leave only the reduced integration quadratic element, which performs well during bending according to Dhondt (2011b), but is also less computationally expensive than full integration elements as there are fewer integration points (full integration uses a $3 \times 3 \times 3$ integration scheme, whereas reduced integration uses a $2 \times 2 \times 2$ scheme).

3.4.3 Mesh Independence

The optimum mesh is determined using both limbal boundary conditions as discussed in Section 3.4.1. The mesh independence study is conducted in two parts: (1) first the number of time steps required to obtain a converged solution is determined, and (2) then an adequate mesh size is determined using this time step. The final corneal apical displacement obtained from a pressure-displacement response during an inflation test simulation is used to determine convergence.

Number of Time Steps

The effect of the number of time steps required to obtain a converged solution is investigated by using the most refined mesh considered in this study, $100 \times 40 \times 10$ (number of elements along: the equator (X), equator-sagittal (XY) plane in the circumferential orientation and optical (Z) axis).

The results are illustrated in Figure 3.8, where it is noted that a change in the number of time steps has an insignificant influence on the obtained response. This observation is also evident in Table 3.3 where the final apical displacement at a chamber pressure of 40 mmHg is summarised for each time step.

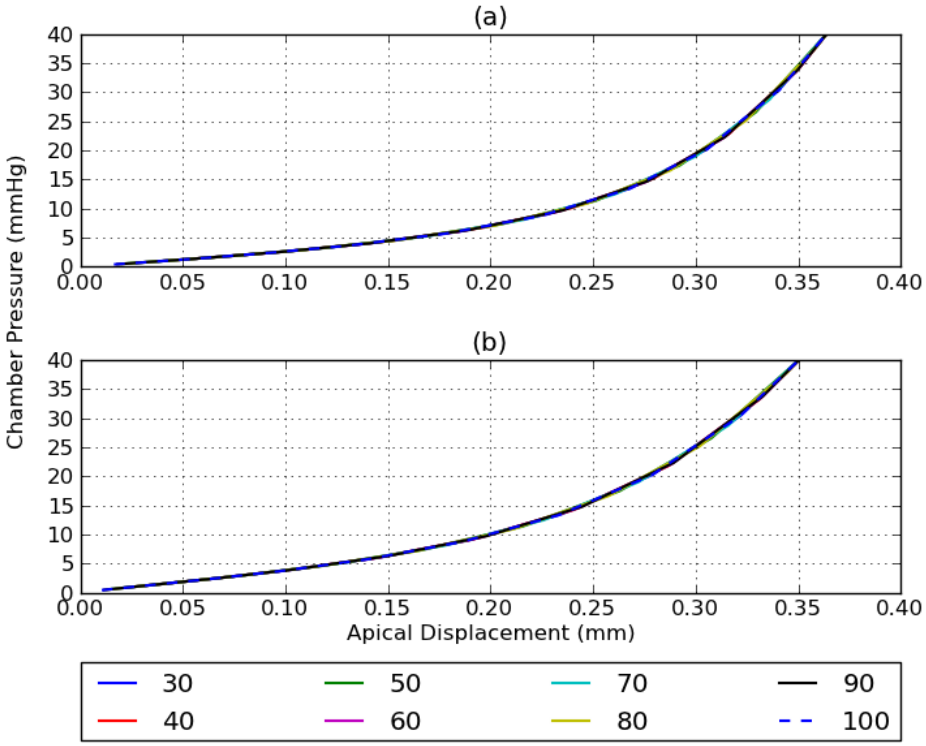

Figure 3.8: Effect of the number of time steps required to obtain a converged solution on the inflation test simulation for both limbal boundary conditions where (a) is for a fixed limbal boundary and (b) for a 23° limbal boundary.

From these results it is evident that the choice of time step does not influence the final result; and as the apical displacement converges from 30 time steps, as seen in Table 3.3, it is found

Table 3.3: Results to determine the effect of the number of time steps to obtain a converged solution for the inflation test simulation using a mesh size of $100 \times 40 \times 10$.

Nr. of Time Steps	**Fixed Boundary**		**23° Boundary**	
	Apical Displ (mm)	**Abs Error** (%)	**Apical Displ** (mm)	**Abs Error** (%)
10	No Convergence	-	No Convergence	-
20	No Convergence	-	No Convergence	-
30	0.363773	0.0	0.350406	0.0
40	0.363769	0.001010	0.350422	0.004566
50	0.363764	0.002474	0.350411	0.001427
60	0.363769	0.001010	0.35042	0.003995
70	0.363775	0.000550	0.350407	0.000285
80	0.363764	0.002474	0.350407	0.000285
90	0.363769	0.001010	0.350418	0.003425
100	0.363773	Reference	0.350406	Reference

that 30 time steps are sufficient for the inflation simulation. This number of time steps will be used for both limbal boundary conditions.

Mesh Refinement

A mesh refinement study is conducted using 30 time steps and nine different meshes of increasing refinement. The results of this study are shown in Figure 3.9 and summarised in Table 3.4 using only the final apical displacement at a chamber pressure of 40 mmHg.

Table 3.4: Results for the inflation simulation mesh convergence study using a 30 time steps.

Mesh Size	**Fixed Boundary**		**23° Boundary**	
	Apical Displ (mm)	**Abs Error** (%)	**Apical Displ** (mm)	**Abs Error** (%)
$20 \times 8 \times 2$	0.362143	0.448082	0.336576	3.946850
$30 \times 12 \times 3$	0.357788	1.645257	0.352290	0.537662
$40 \times 16 \times 4$	0.358497	1.450355	0.354836	1.264248
$50 \times 20 \times 5$	0.359762	1.102611	0.355204	1.369269
$60 \times 24 \times 6$	0.360984	0.766687	0.354976	1.304201
$70 \times 28 \times 7$	0.361966	0.496738	0.354590	1.194043
$80 \times 32 \times 8$	0.362717	0.290291	0.354148	1.067904
$90 \times 36 \times 9$	0.363308	0.127827	0.350598	0.054794
$100 \times 40 \times 10$	0.363773	Reference	0.350406	Reference

It is seen in Table 3.4 the error for both limbal boundary conditions is below 2.0% for mesh sizes from $30 \times 12 \times 3$ onwards and below 1% for a mesh size of $90 \times 36 \times 9$. As there is only a 1.0% difference between these two mesh sizes, it is decided to choose the mesh size which is computationally less expensive. A mesh size of $30 \times 12 \times 3$ is therefore deemed adequate for the purposes of this study.

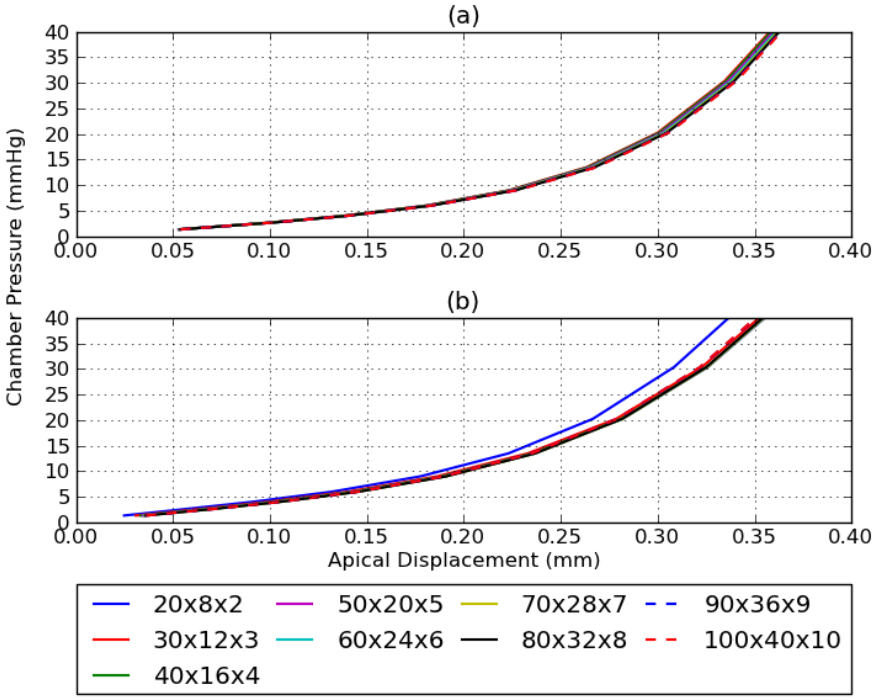

Figure 3.9: Pressure-displacement response from an inflation test mesh independence study for both limbal boundary conditions where (a) is for a fixed limbal boundary and (b) is for a 23° limbal boundary.

3.5 GOLDMANN APPLANATION TONOMETRY SIMULATION

The FE model of the human cornea developed in this chapter will be used to simulate GAT to determine what the influence of the various modelling choices (such as boundary conditions and calibration data) are on the estimated IOP obtained from the GAT simulation (IOPG). GAT was discussed in considerable detail in Section 2.5 and is numerically simulated using a contact analysis, discussed in this section.

3.5.1 Boundary Conditions

The FE model of the cornea used for the inflation test simulation, discussed in Section 3.4.1, will be used in this section with an additional rigid body definition to simulate the applanator. The cornea is first stressed by applying an IOP on the posterior surface to simulate the stress state found *in vivo*. Afterwards the applanation process is simulated by applying a prescribed displacement to the rigid body applanator. This simulation process, along with the required surface and load definitions, are illustrated in Figure 3.10. As seen in Figure 3.10, the applanator was chosen as the master surface to allow the use of a coarser mesh on the rigid body and the corneal model is therefore defined as the slave surface.

As the cornea is symmetric about the equator-optical (XZ) and sagittal-optical (YZ) planes, only a quarter model of the GAT simulation will be used, which consequently decreases

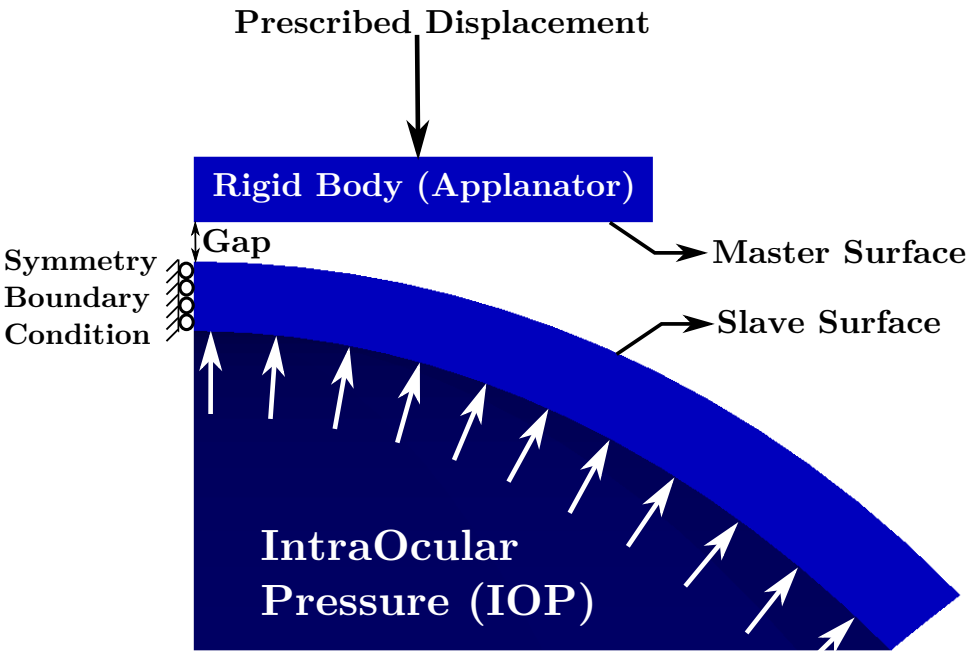

Figure 3.10: A quarter FE model of the GAT simulation defining the contact surfaces, prescribed loads and displacements.

computational time and cost. A symmetry boundary condition is defined at the corneal apex as well as the equator-optical (XZ) and sagittal-optical (YZ) planes.

As the GAT simulation aims to reproduce *in vivo* corneal behaviour, the logical choice of boundary condition is to take the scleral connection into account by allowing translation at an angle of 23°. Nevertheless, both limbal boundary conditions considered for the inflation test simulation, as discussed in Section 3.4.1 (c.f. Figure 3.7), are also considered for the GAT simulation.

3.5.2 Contact Definition

The applanator is numerically simulated as a rigid body with no inherent material properties. However, Calculix requires that a material model be assigned to each element, even if the elements belong to a rigid body. The applanator, which is made of plexiglass (Stepanik and Ossoinig, 1968; Garg, 2006), was therefore assigned a linear elastic material model with an average elastic modulus of 2880 MPa and an average Poisson's ratio of 0.402 (MatWeb Material Property Data, n.d.). It was implemented into the Calculix input file as follows:

```
*MATERIAL, NAME=LINEAR_ELASTIC
*ELASTIC, TYPE=ISO
2880.0, 0.402
*SOLID SECTION, ELSET=appl_elements, MATERIAL=LINEAR_ELASTIC
*RIGID BODY, NSET=appl_nodes, REF NODE=107, ROT NODE=106
```

Element Choice for Contact Surfaces

Quadratic reduced integration brick elements and quadratic wedge elements are used in this simulation as discussed in Section 3.4.2 . Dhondt (2011b) states that quadratic elements pose a problem with the contact analysis in Calculix as the nodal forces on the corner nodes of the element, which are equivalent to a constant pressure, are either zero or opposite in sign when compared to the mid-side nodes.

For this reason a layer of linear elements were embedded in the two contact surfaces, the anterior surface of the cornea and the posterior surface of the applanator. Consequently the material properties were divided between the two sets of elements, by grouping both linear and quadratic elements to represent the two geometries. The latest version of Calculix (v.2.5, released October 2012), not used in this study, has addressed this problem, by defining linear elements for the contact surfaces internally from the user-defined quadratic elements in the input file.

Interaction between Contact Surfaces

The contact interaction can be defined by either a linear or an exponential pressure-overclosure. A linear pressure-overclosure is used which, according to Dhondt (2011b), helps to attain convergence more easily. The linear pressure-overclosure relationship is given by (Dhondt, 2011b):

$$P(d) = Hd\left[\frac{1}{2} + \frac{1}{\pi}\tan^{-1}\left(\frac{d}{\kappa}\right)\right], \tag{3.10}$$

where P is the pressure exerted on the master surface of a contact spring element, H is a stiffness constant (the slope of the curve) which should be about 50 to 100 times the Young's modulus of the adjacent materials, κ is a tension value (the curvature of the curve) for large clearances at zero overclosure (should normally be small, default is $10/H$) and d is the overclosure (a measure of the penetration of the slave nodes into the master surface).

As a large value for H will lead to hard contact, for a first guess the stiffness of the cornea is assumed to be equivalent to the stiffness of the ground substance, 40 kPa (c.f. Section 2.3.2) which, multiplied by 50 to 100, results in $2.0 - 4.0$ MPa. An intial guess for the tension value, κ is 5.0 (using the default) when using $H = 2.0$ MPa, which is seen to be linear (c.f. Figure 3.11) indicating that κ is still too large. The tension value was then decreased by dividing it by 100, resulting in a value of 0.05 for κ. Two additional values for κ were assumed, one larger ($\kappa = 0.1$) and one smaller ($\kappa = 0.01$) than the initial assumed value.

The resulting pressure-overclosure curves, using Equation (3.10), are illustrated in Figure 3.11, where a stiffness constant of 2.0 MPa leads to a lower contact pressure than a stiffness of 4.0 MPa. Also with an increase in tension value, the corresponding contact pressure is slightly lowered. However, with such an increase, convergence problems might arise during the contact simulation. For these reasons it was decided to use a stiffness constant of 2.0 MPa, to ensure soft contact, and to use a tension value of 0.01 (which is closest to a pressure of zero) to ensure convergence.

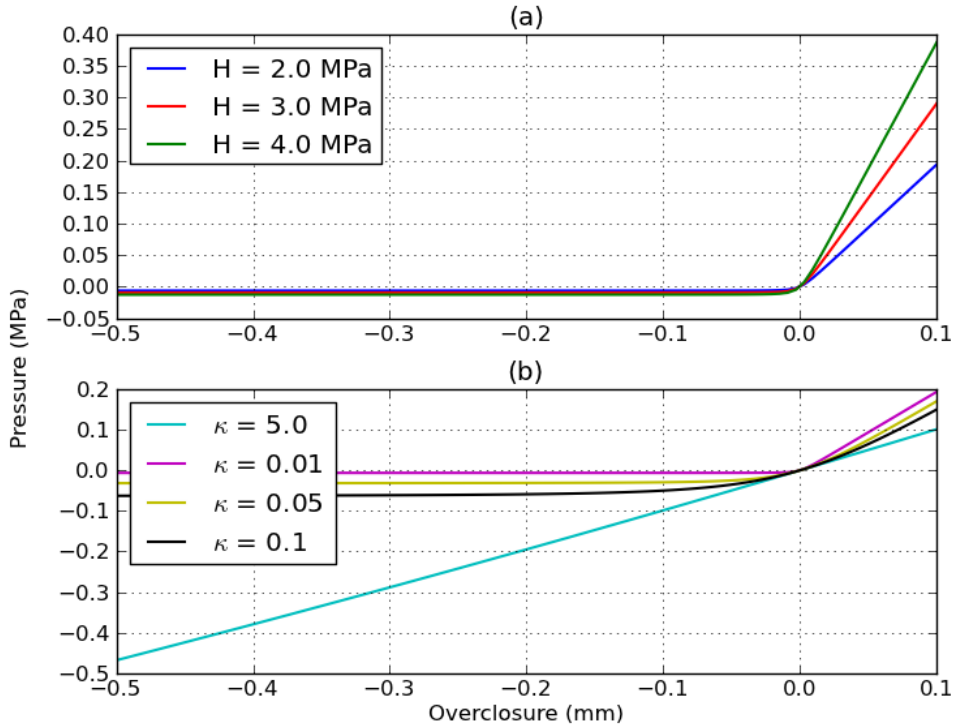

Figure 3.11: Two pressure-overclosure relationships are illustrated using (a) a stiffness constant of 2.0, 3.0 and 4.0 MPa and a tension value of 0.01; and (b) a stiffness constant of 2.0 MPa with a tension value of 0.01, 0.05, 0.1 and 5.0.

Another option when defining the contact is to choose between small and large sliding, which is a measure of the calculated contact pairing between the slave and master surfaces during the analysis. When small sliding is active the pairing between master and slave nodes is done at the start of every increment, whereas for large sliding it is done for every iteration. The small sliding option was chosen for this study as it is computationally less expensive and also converges better (Dhondt, 2011b). The contact definition in the Calculix input file is defined as follow:

```
*CONTACT PAIR, INTERACTION=ContactInteraction, SMALL SLIDING
Slave, Master
*SURFACE INTERACTION, NAME=ContactInteraction
*SURFACE BEHAVIOR, PRESSURE-OVERCLOSURE=LINEAR
2.0, 0.01
```

Associated Problems

During the GAT simulation two problems arose: (1) the number of time steps used for the inflation simulation is not enough to attain convergence during a GAT simulation, and (2) the wedge elements pose a problem during the contact analysis.

(1) Number of time steps: During the inflation test simulation it was found that 30 time steps are sufficient to attain convergence (c.f. Section 3.4.3). However, the GAT simulation

did not converge with only 30 time steps. The results of this study are illustrated in Figure 3.12 using an Ocular Response History (ORH) (c.f. Section 3.5.3) and summarised in Table 3.5.

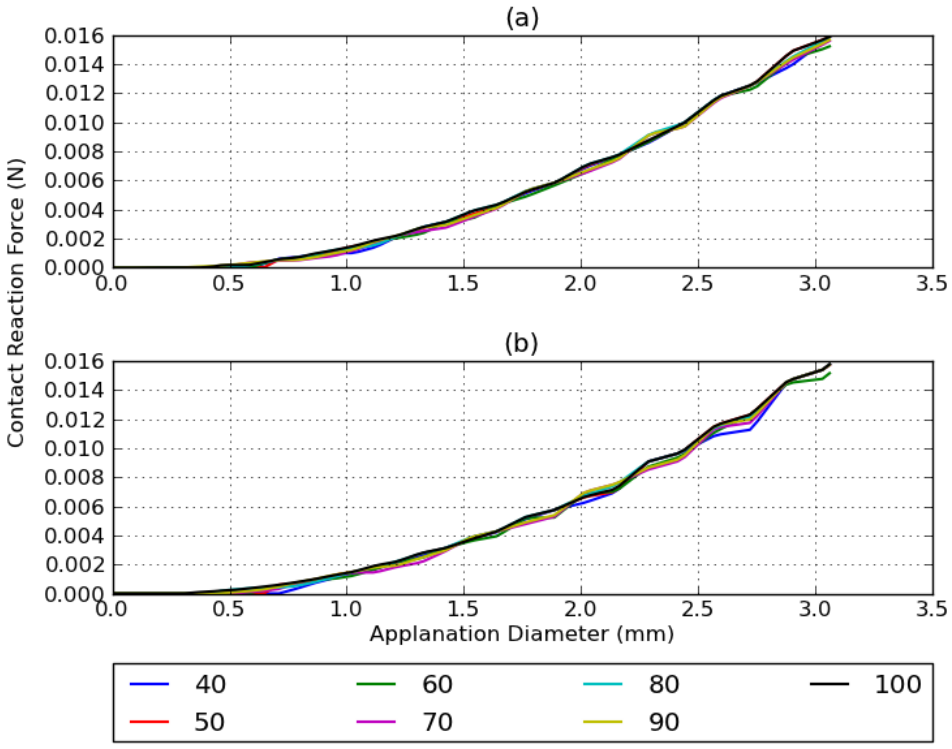

Figure 3.12: Ocular Response History (ORH) to determine the number of time steps required to attain convergence for the GAT simulation for both limbal boundary conditions where (a) is for a fixed limbal boundary and (b) is for a 23° limbal boundary.

From Figure 3.12 it is difficult to estimate the number of time steps required to obtain a converged solution. The contact force, at full applanation (an applanation diameter of 3.06 mm), is therefore shown in Table 3.5. It is noted in Table 3.5 that the error is below 1% for both limbal boundary conditions for all time steps, except when using 60 or 70 time steps. For a fixed boundary limbal condition the error is less than 2% when using 60 time steps and for a 23° limbal boundary condition the error is less than 4% when considering 70 time steps.

Table 3.5: Summary of the results to determine the influence of the number of time steps during a contact analysis considering the applanation force at an applanation diameter of 3.06 mm.

Nr. of	**Fixed Boundary**		23° **Boundary**	
Time Steps	**Appl Force** (N)	**Abs Error** (%)	**Appl Force** (N)	**Abs Error** (%)
30	No Convergence	-	No Convergence	-
40	0.015675	0.025512	0.015760	0.03805658
50	0.015679	0.0	0.015762	0.02537105
60	0.015428	1.600867	0.015736	0.19028289
70	0.015664	0.095669	0.015253	3.25383737
80	0.015673	0.038268	0.015763	0.01902829
90	0.015666	0.082914	0.015634	0.8372447
100	0.015679	Reference	0.015766	Reference

The number of time steps is therefore chosen as 80, with an error of less than 1% for both limbal boundary conditions.

(2) Wedge elements: It seems that the wedge element is very stiff during contact, illustrated in Figure 3.13a, where the applanator wedge element penetrates the corneal anterior surface. In comparison when using a finer mesh on the applanator the wedge element becomes smaller and hence does not influence the simulation as much, as illustrated in Figure 3.13b. This leaves two options:

1. Refine the applanator mesh to decrease the wedge element size, consequently increasing computational cost (c.f. Figure 3.13b), or
2. Remove the wedge elements and leave a very small hole in the corneal and applanator apexes (c.f. Figure 3.13c).

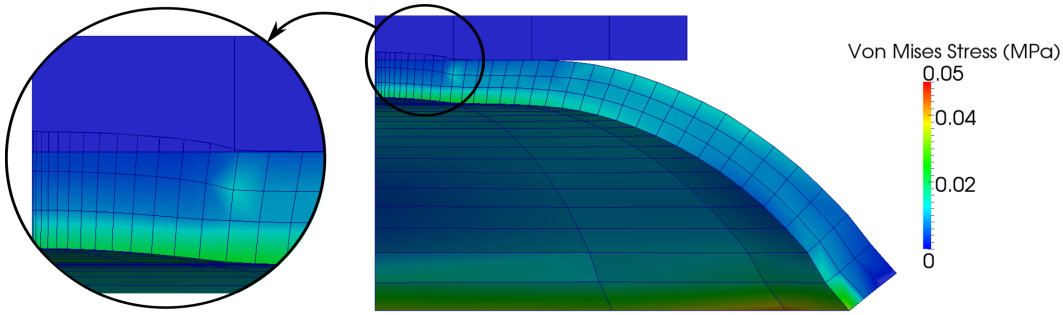

(a) Wedge elements included

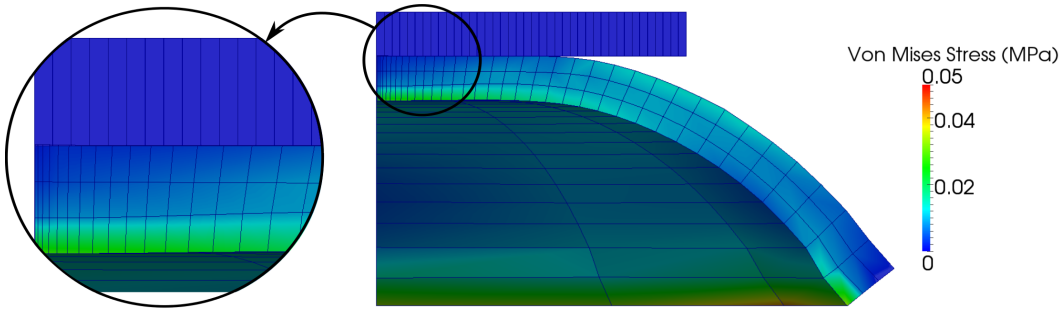

(b) Wedge elements included but with a refined mesh

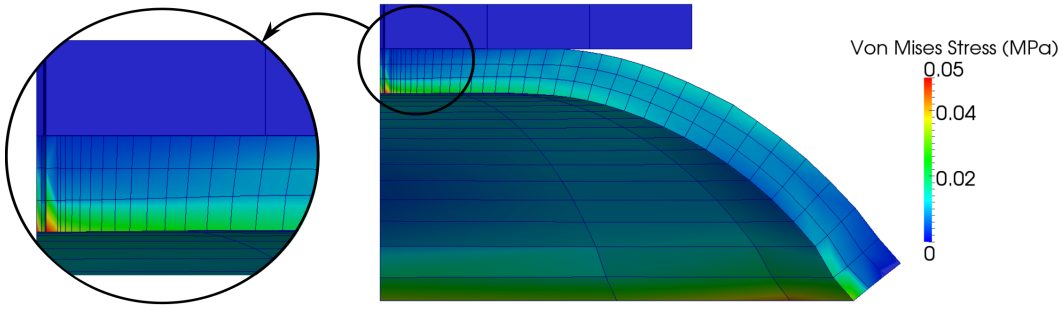

(c) Wedge elements removed

Figure 3.13: Von Mises stress plots of the GAT simulation, for a fixed limbal boundary condition, considering the influence of the wedge elements on the results. (a) and (b) contain the wedge elements, whereas (c) has no wedge elements.

The results of the three simulations shown in Figure 3.13 are summarised in Table 3.6 along with the final contact force at the point of applanation (an applanation diameter of 3.06 mm).

Table 3.6: Summary of the results to determine the influence of the wedge element during a contact analysis.

Wedge Inclusion	**Fixed Boundary**		**23° Boundary**	
	Appl Force (N)	**Abs Error** (%)	**Appl Force** (N)	**Abs Error** (%)
Wedges removed	0.015664	0.345932	0.015253	3.815109
Wedges included	0.015355	1.633568	0.015722	0.857611
Wedges included with a refined applanator mesh	0.015610	Reference	0.015858	Reference

It is clear from Figure 3.13 that to avoid mesh penetration the wedge element should either be removed (c.f. Figure 3.13b), or the applanator mesh should be refined (c.f. Figure 3.13c). From Table 3.6 it is seen that when removing the wedge elements the error is below 1% for a fixed limbal boundary condition and below 4% for a 23° limbal boundary condition. On the other hand when including the wedge elements the error is below 2% for both limbal boundary conditions. It was decided to remove the wedge elements from the simulation, creating a very small hole in the centre of the cornea and applanator (c.f. Figure 3.13c) as opposed to either increasing the computational cost by refining the mesh on the applanator or causing numerical difficulties by including the wedge elements.

3.5.3 Ocular Response History

In clinical practice, only a single IOP measurement is obtained when using GAT. This study, however, assumes that the current GAT can be modified to obtain an entire indentation response history, which will be referred to as an Ocular Response History (ORH).

The easiest way to modify the current GAT is to take additional force measurements at pre-defined applanator diameters until the point of full applanation (an applantor diameter of 3.06 mm) is reached. This would result in an ORH which contains the applanator diameter and its corresponding force. This ORH was obtained from the numerical simulation in four steps:

Step 1: The contact times are determined by obtaining the apical displacement for each time step in the simulation and comparing it to the applanator displacement.

Step 2: The applanator diameter and corresponding contact force is then obtained at the determined contact times from step one.

Step 3: The ORH is obtained from the results in step two and the resulting data is interpolated up to an applanator diameter of 3.06 mm, which is the point of interest.

Step 4: A 'smoother' curve is obtained for the ORH by refining the corneal mesh along the equator (X) axis.

In this section the inflation simulation parameters obtained in Section 3.4, as well as the assumptions made in Section 3.5.2, will be used to illustrate the process in which the ORH

is obtained. The parameters assumed in this section are summarised in Table 3.7 for ease. Note that the choice of mesh on the applanator will not influence the results as it is a rigid body.

Table 3.7: Summary of the assumed GAT simulation parameters and mesh sizes used to obtain the ORH.

Property	**Assumed Value**	**Section**
Corneal Mesh	$30 \times 12 \times 3$ (for a full model) $15 \times 3 \times 3$ (for a quarter model)	3.4.3
Applanator Mesh	$4 \times 2 \times 1$	Assumption
Number of Time Steps	80	3.5.2
Contact Interaction	$H = 2.0\ MPa$ $\kappa = 0.01$	3.5.2

Step 1: Estimate point of contact

The point of contact is estimated by first tabulating the apical displacements of each of the anterior surface nodes against the simulation time. Only the anterior surface nodes in the equator-optical (XZ) plane are considered as it is assumed that each of the corresponding surface nodes in the equator-sagittal (YZ) plane will make contact at the same time as the first set of nodes. The resulting plot is shown in Figure 3.14, where the black dashed line represents the prescribed position of the applanator (c.f. Section A.4) and the optical (Z)

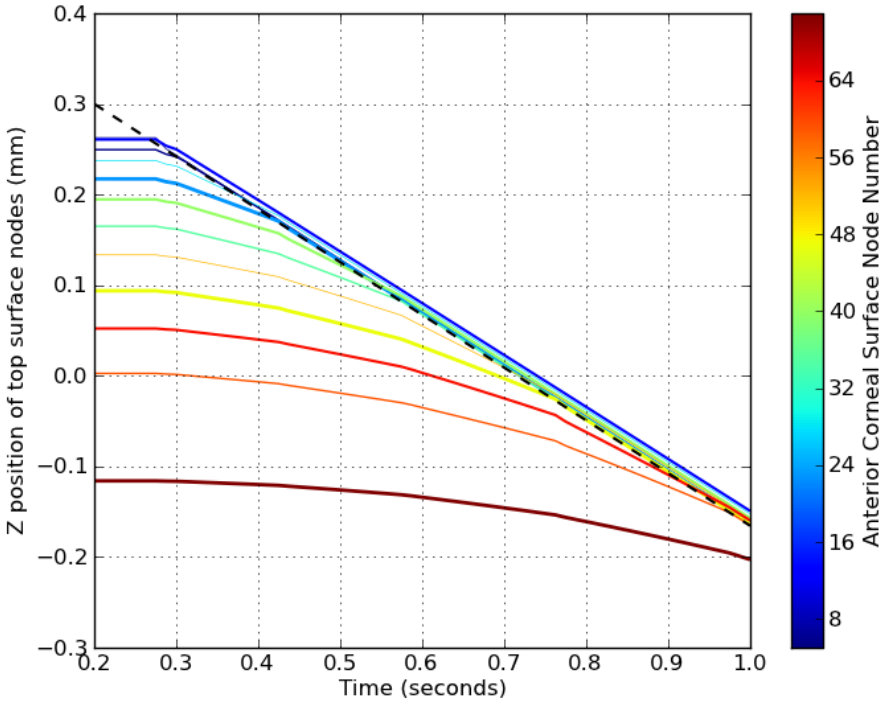

Figure 3.14: Apical displacement of the anterior corneal surface nodes during the GAT simulation used to estimate the point of contact between the applanator and corneal contact surfaces.

displacement of each node is represented by the colored lines. The offset seen in the curve is due to the allowed penetration of the applanator and corneal surfaces.

A prescribed displacement is defined on the rigid body to simulate the applanation procedure and it is ramped linearly during the applanation phase. The inflation part of the simulation only accounts for 20% of the time steps, as not many time steps are required to attain convergence. The applanation part of the simulation uses the remaining 80% of the time steps in which to perform the contact analysis. As a known prescribed displacement (d_{pres}) is applied linearly to the rigid body applanator from time 0.2 to 1.0, the applanator Z coordinate is computed as:

$$Z_{\text{new}} = mt_{\text{new}} + c, \tag{3.11a}$$

where

$$m = \frac{d_{\text{pres}}}{0.8} \quad \text{and} \quad c = d_{\text{gap}} - 0.2m \tag{3.11b}$$

Here d_{gap} is the initial starting position of the applanator, that is the gap between the cornea and applanator at time zero (c.f. Figure 3.10).

Contact between the cornea and applanator is then determined by assuming that all nodes with Z coordinates on the right side of the initial contact line (dashed black line in Figure 3.14) have made contact. The time at which each node makes contact is determined by finding the point at which the initial contact line and the linear line describing the specific nodal contact, intersects. This is illustrated in Figure 3.15 for clarity, where only one node in contact is considered as an example.

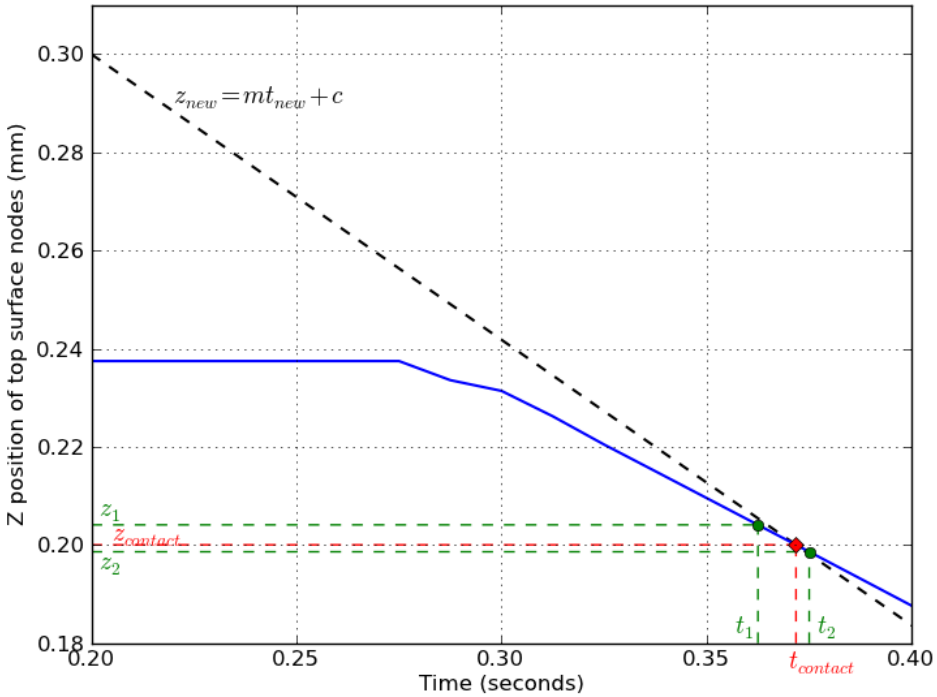

Figure 3.15: Example to estimate the time at which contact between the applanator and corneal surfaces are made using only the first node.

From Figure 3.15 the time at which contact is made, is determined by first finding the times

on either side of the initial contact line (black dashed line). Using this information a straight line for the node in contact is defined and the point at which the line intersects with the initial contact line is the assumed time at which contact is made:

$$m_1 = m \text{ (From Eq. (3.11b))}, \quad m_2 = \frac{z_2 - z_1}{t_2 - t_1}, \tag{3.12a}$$

$$c_1 = c \text{ (From Eq. (3.11b))}, \quad c_2 = z_1 - m_2 t_1, \tag{3.12b}$$

$$t_{\text{contact}} = \frac{(c_2 - c_1)}{(m_1 - m_2)} \tag{3.12c}$$

Step 2: Obtain contact time diameter and force

The applanation diameter (d) for each time, t_1 and t_2, is obtained by extracting the corresponding X-coordinate for each node in contact. The applanation diameter is then estimated using the equation for a straight line and the contact time determined in step 1:

$$d_{\text{appl}} = m_3 t_{\text{contact}} + c_3, \tag{3.13a}$$

where

$$m_3 = \frac{d_2 - d_1}{t_2 - t_1}, \tag{3.13b}$$

$$c_3 = d_1 - m_3 t_1 \tag{3.13c}$$

The obtained applanation diameter is then plotted against the contact times as shown in Figure 3.16a. The contact force plot is generated by obtaining the contact reaction force for each time step during the simulation and is shown in Figure 3.16b.

Step 3: Construct ocular response history

With the available information from step two, it is relatively simple to construct the ORH. As the applanator diameter is known for each contact time, all that is required is to obtain the corresponding contact reaction force for each of the contact time steps. This is done by interpolating between two time steps, and their corresponding forces, to obtain the contact time and hence the contact force. This result is shown in Figure 3.17, where the contact force for the corresponding applanation diameter in contact is illustrated with the black dots. Note the final contact force (y-axis) is multiplied by 4.0 (when compared to the Figure 3.16b) as the simulation was done for a quarter model, hence only a quarter of the actual force was initially observed.

As the GAT only gives a single IOP measurement, at an applanation diameter of 3.06 mm, the data is interpolated to only include the range up to the applanation diameter. Linear interpolation was used and the results are shown in Figure 3.17 where the interpolated data, using 100 points, is indicated with a solid blue line. Note that the resulting ORH is not a smooth curve. This is the result of having too few points on the cornea which are able

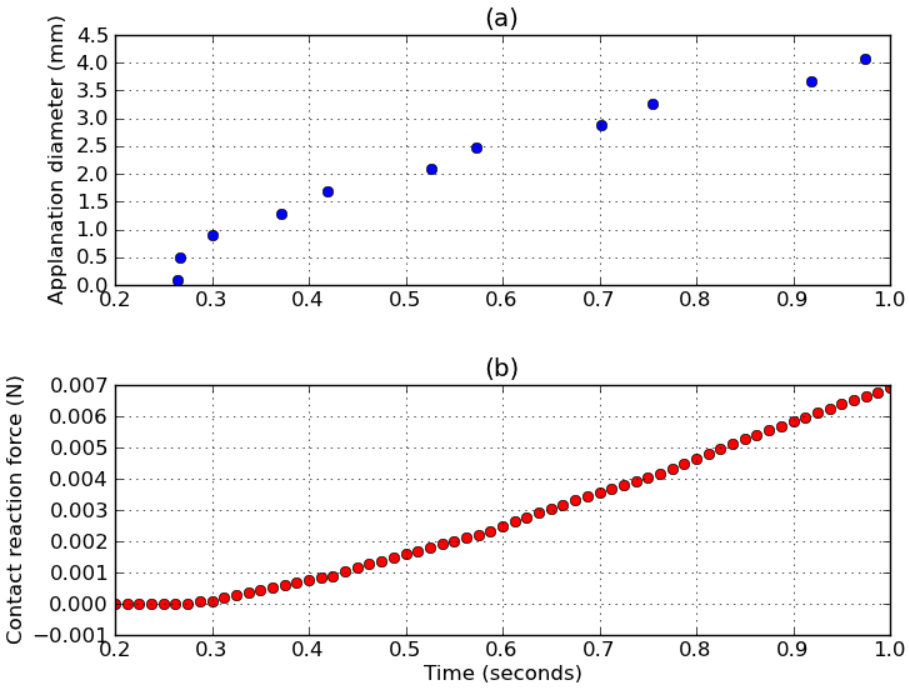

Figure 3.16: (a) The applanation diameter for each contact time along with the contact reaction force required during each time step of the simultation. (b) The contact force is a quarter of the actual force due to applanation as only a quarter model of GAT was simulated.

to make contact with the applanator, hence the corneal mesh used to simulate GAT is not refined enough.

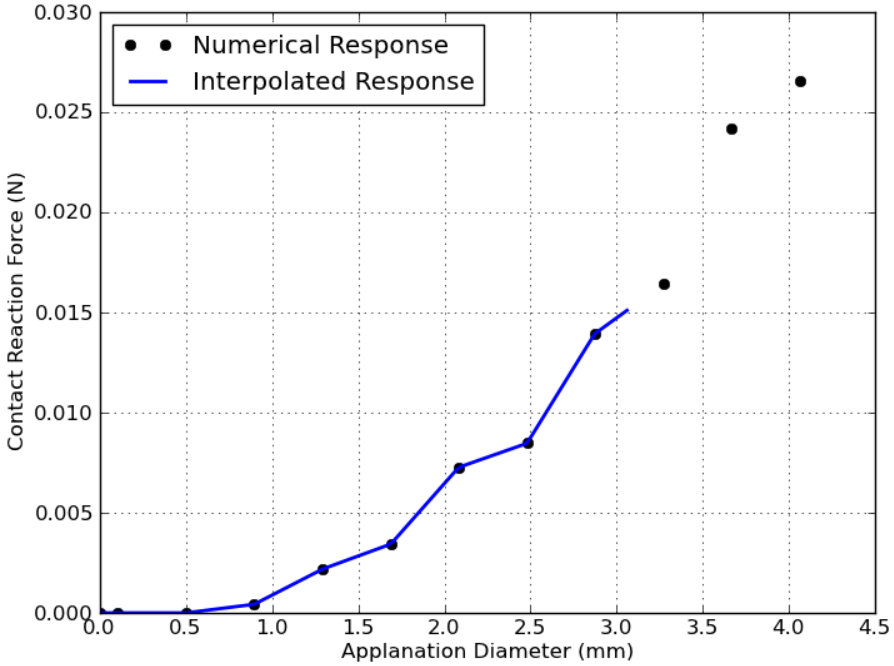

Figure 3.17: ORH of the GAT simulation, with the interpolated data (blue solid line) up to an applanating diameter of 3.06 *mm*, and the initial raw data (black circles)

Step 4: Obtain a 'smoother' response

To obtain a 'smoother' response (a curve with very few kinks or imperfections in it) it is necessary to refine the corneal mesh along the equator (X) axis, as these nodes are used to construct the ORH. The obtained ORHs for a refinement of the corneal mesh, along the equator axis, are shown in Figures 3.19 and 3.20.

Note that a mesh refined along the optical (c.f. Figure 3.18a) or circumferential (c.f. Figure 3.18b) axis will not influence the obtained ORH, as these nodes are not used to obtain the ORH, and nor will an increase in the number of time steps (c.f. Figure 3.18c).

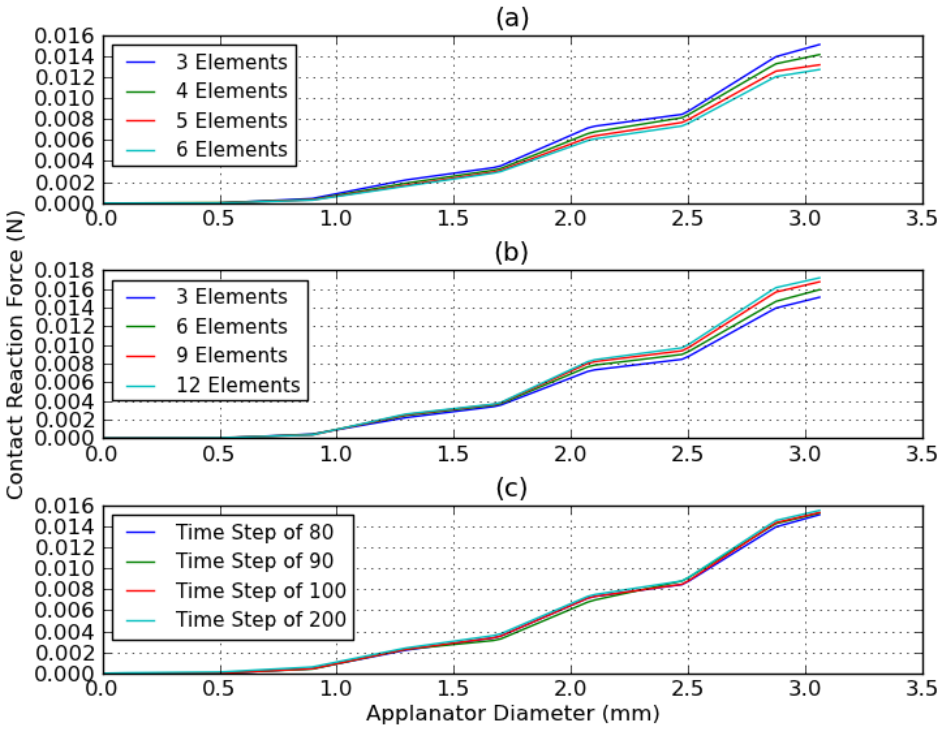

Figure 3.18: ORH for a refined mesh size along the (a) optical axis and the (b) circumferential axis, along with (c) an increasing number of time steps. Only the interpolated data is used for comparison.

Along with increasing the number of elements along the equator axis, both uniform and non-uniform meshes were employed. These results are also shown in Figures 3.19 and 3.20, with the final applanation force (at an applanation diameter of 3.06 mm) in Tables 3.8 and 3.9.

From Figures 3.19 and 3.20, it is noted that the uniform and non-uniform meshes start to produce a 'smoother' response from about 40 elements and 30 elements for the fixed and 23° limbal boundary conditions, respectively. A 'smooth' response is considered to be the response with the fewest kinks and imperfections in the curve. Comparing this observation with the results of the applanation force, at an applanating diameter of 3.06 mm, in Tables 3.8 and 3.9 it seems that the error is below 2% when using 30 and 35 elements for a fixed limbal boundary and 25 and 30 elements for a 23° limbal boundary condition.

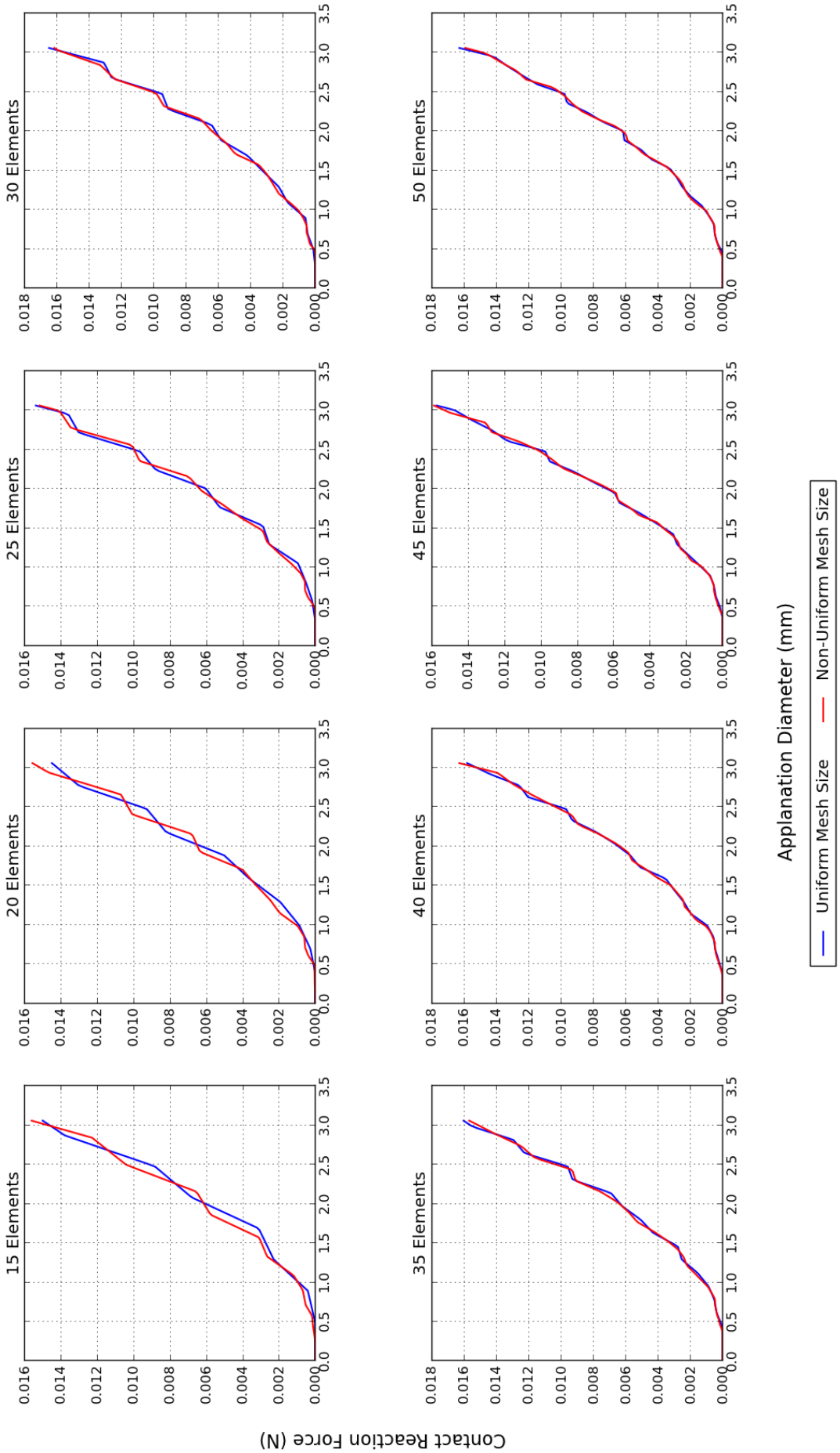

Figure 3.19: Obtaining a 'smoother' ORH by refining the corneal mesh along the equator axis using a uniform and non-uniform mesh size for a fixed limbal boundary.

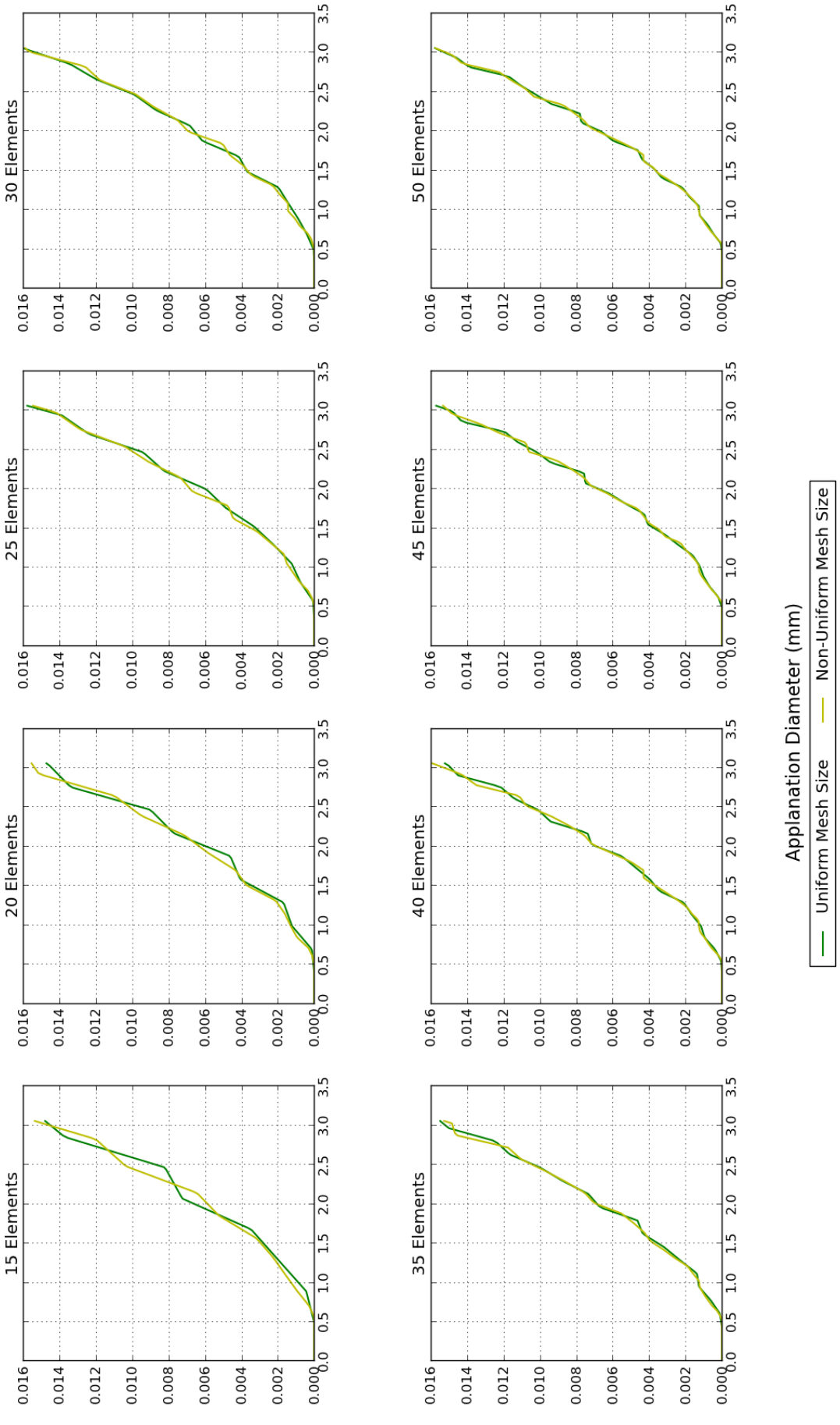

Figure 3.20: Obtaining a 'smoother' ORH by refining the corneal mesh along the equator axis using a uniform and non-uniform mesh for a limbal boundary of a 23° roller.

Table 3.8: Applanation force at an applanation diameter of 3.06 mm for uniform and non-uniform mesh sizes with mesh refinement for a fixed limbal boundary condition.

Nr of Elems	Uniform Mesh Size		Non-Uniform Mesh Size	
	Appl Force (N)	Abs Error (%)	Appl Force (N)	Abs Error (%)
15	0.014975	7.999017	0.015585	1.981132
20	0.014473	11.08312	0.015542	2.251572
25	0.015354	5.670578	0.015150	4.716981
30	0.016459	1.118142	0.016133	1.465409
35	0.016011	1.634208	0.015664	1.484277
40	0.015790	2.991952	0.016277	2.371069
45	0.015717	3.440437	0.015864	0.226415
50	0.016277	Reference	0.015900	Reference

Table 3.9: Applanation force at an applanation diameter of 3.06 mm for uniform and non-uniform mesh sizes with mesh refinement for a 23° limbal boundary condition.

Nr of Elems	Uniform Mesh Size		Non-Uniform Mesh Size	
	Appl Force (N)	Abs Error (%)	Appl Force (N)	Abs Error (%)
15	0.014782	6.211535	0.015351	2.465214
20	0.014705	6.700083	0.015523	1.372387
25	0.015764	0.019034	0.015452	1.823496
30	0.015984	1.414885	0.015864	0.794206
35	0.015479	1.789227	0.015253	3.087871
40	0.015219	3.438868	0.015903	1.041998
45	0.015700	0.387031	0.015320	2.662177
50	0.015761	Reference	0.015739	Reference

It is decided to use a refinement of 30 elements along the equator axis which yields an error of below 2% for both limbal boundary conditions. Furthermore, a non-uniform mesh size will be employed as it produces a 'smoother' response compared to a uniform mesh, which is evident in Figures 3.19 and 3.20. A $30 \times 3 \times 3$ non uniform mesh size is therefore used to simulate GAT using a quarter model, that is the number of elements along the equator-sagittal plane (3) are a quarter of those used in the full 3D model (12, c.f. Table 3.7).

3.6 CONCLUSION

The Finite Element (FE) model was developed by assuming the cornea to be a rotationally symmetric conicoid. To represent the complex corneal structure an anisotropic fibre reinforced elastic constitutive model, available in the open-source FE solver Calculix, was employed using two preferred fibre orientations in the central cornea. The cornea is also assumed to be homogenous and incompressible.

Once the FE model was constructed, the boundary conditions and mesh refinement studies were conducted for both inflation and Goldmann Applanation Tonometry (GAT) simulations.

It was found that for the inflation simulation (a full 3D model) a mesh of $30 \times 12 \times 3$ (uniform mesh size) with 30 time steps is sufficient to obtain a converged solution. For the GAT simulation (a quarter 3D model) a $30 \times 3 \times 3$ mesh (non-uniform mesh size) with 80 time steps was found to be sufficient to not only obtain a converged solution, but to also obtain a sufficiently smooth Ocular Response History (ORH).

The FE model developed in this chapter will be used to calibrate the material coefficients using experimental inflation test data in Chapter 4. This is followed by a sensitivity study in Chapter 5 to determine the effect of various numerical modelling assumptions as well as corneal geometric and material properties on the ORH obtained from GAT simulations.

CHAPTER 4

CALIBRATION OF MATERIAL COEFFICIENTS WITH EXPERIMENTAL INFLATION DATA

4.1 INTRODUCTION

The most popular method for calibrating a corneal numerical constitutive model is to use experimental inflation test data. According to Elsheikh *et al.* (2006) this method of testing is considered more accurate than strip extensometry testing as it is more representative of the *in vivo* conditions (the load application speed represents that of the applied IntraOcular Pressure (IOP)). Inflation testing was discussed in considerable detail in Section 2.4 where it was noted that there is a variation in experimental inflation test data.

In this chapter the fibre reinforced elastic constitutive model, implemented into the Finite Element (FE) model developed in Chapter 3, is calibrated by means of an inflation test simulation. The material coefficients are obtained using a simple optimization algorithm to minimize the Root Mean Square Error (RMSE) between the numerical and experimental inflation test data.

4.2 OPTIMIZATION FORMULATION

The material coefficients required to describe the corneal material are identified by solving an unconstrained optimization problem. The Nelder-Mead simplex method as implemented in the SciPy module (Scipy Community, 2011) is used to minimize the RMSE for the inflation test. The objective function is therefore defined as:

$$\min\ F(\mathbf{X}) = \text{RMSE} = \sqrt{\frac{\sum_{i=1}^{n}(\text{exp}_i - \text{num}_i)^2}{n}}, \tag{4.1}$$

where exp_i is the experimental inflation data set and num_i is the numerical inflation data set, n is the sample size and $\mathbf{X}$ is a vector containing the material coefficients. For a more detailed description of the optimization method and RMSE definition refer to Appendix B.

4.3 NUMERICAL MODEL INCOMPRESSIBILITY

For an elastic fibre reinforced constitutive model, the strain energy density function (U) is defined as (c.f. Equation (3.3), Section 3.3.1)):

$$U = C_{10}(\bar{I}_1 - 3) + \frac{1}{D_1}(J-1)^2 + \sum_{i=4,6}^{n} \frac{k_{1i}}{2k_{2i}}[e^{k_{2i}(\bar{I}_i - 1)^2} - 1], \tag{4.2}$$

where n denotes the number of fibre families (two in this study), C_{10} and k_{1i} are stress-like parameters (MPa), k_{2i} is a dimensionless parameter and D_1 is an incompressibility constant used to enforce incompressible behaviour. $\bar{I}_1$ and $\bar{I}_{4,6}$ denote the invariants of the modified Cauchy-Green deformation tensor ($\bar{\mathbf{C}}$) and J is the Jacobian (determinant of the deformation gradient) which should be equal to one for an incompressible material. The numerical model incompressibility is represented by the volumetric part:

$$U_{\text{vol}} = \frac{1}{D_1}(J-1)^2 \tag{4.3}$$

To determine the value of J, the strains obtained at each integration point are used and defined as:

$$\mathbf{E} = \frac{1}{2}\left(\mathbf{F}^T\mathbf{F} - \mathbf{I}\right), \tag{4.4}$$

where $\mathbf{E}$ is the Green-Lagrange strain and $\mathbf{I}$ is an identity matrix. An expression for J is obtained by rearranging Equation (4.4):

$$J = \det(\mathbf{F}) = \sqrt{\det(2\mathbf{E} + \mathbf{I})} \tag{4.5}$$

The values of D_1 for which the model retains its incompressible behaviour are then determined from an inflation test simulation. The results of this are shown in Figure 4.1 using the same material coefficients as in Section 3.4: $C_{10} = 0.003871$ MPa, $k_1 = 0.035311$ MPa and $k_2 = 181.218385$.

From Figure 4.1 it is noted that when $D_1 \geq 1.0$ the model incompressibility could be compromised as the value for J ($= \det(\mathbf{F})$) is larger than 1.01, which is indicative of a volume change larger than 0.5% that is, a violation of incompressibility. Also, it was found that when using values of $D_1 \leq 0.23$ numerical difficulties arise when the material properties change, even though a smaller value of D_1 ensures incompressible behaviour. For these reasons a value of $D_1 = 0.4$ is considered small enough to ensure model incompressibility while ensuring numerical stability.

A similar elastic fibre reinforced constitutive model (Pandolfi and Manganiello, 2006), as considered in this dissertation, has been shown to capture the highly non-linear behaviour exhibited by the cornea. The varying values of D_1 is compared to the incompressibility enforced by Pandolfi and Manganiello (2006) in Figure 4.2, where it is evident that a value of 0.4 compares well with their model incompressibility.

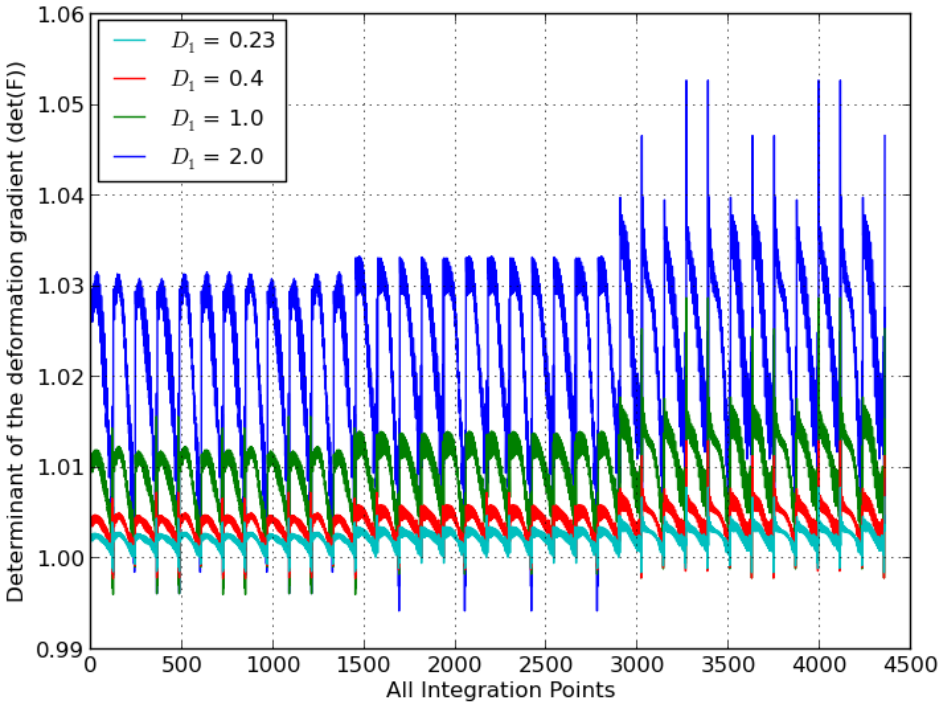

Figure 4.1: The values of the incompressibility parameter, D_1, is determined for which the cornea numerical model converges for a specific set of material properties ($C_{10} = 0.003871$ MPa, $k_1 = 0.035311$ MPa and $k_2 = 181.218385$), CCT = 0.50 mm and $R_{\text{ant}} = 7.77$ mm.

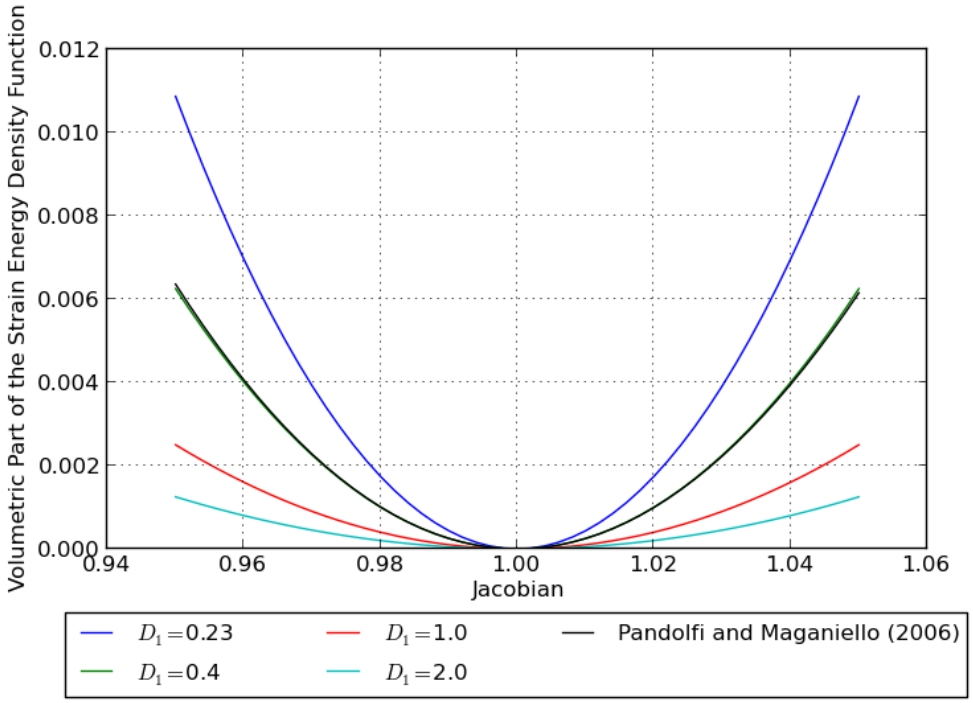

Figure 4.2: The numerical model incompressibility is illustrated using the volumetric part of the strain energy density function used in this study (dash-dot lines with crosses) as well as that defined by Pandolfi and Manganiello (2006) (dashed lines with points).

4.4 CALIBRATE ELASTIC FIBRE REINFORCED MODEL

This constitutive model requires the calibration of six material coefficients (C_{10}, D_1, k_{11}, k_{21}, k_{12}, k_{22}) when considering two families of fibres as discussed in Section 3.3.1. D_1 is considered to be a penalty parameter, used to enforce the material incompressibility, and is therefore assumed to remain constant at a value of 0.4 as discussed in the previous section. To further reduce the number of variables to optimize, it was assumed that the two orthogonal fibre families contribute equally in strength such that $k_{11} = k_{12} = k_1$ and $k_{21} = k_{22} = k_2$ (Pandolfi and Manganiello, 2006). These assumptions reduces the number of variables to optimize from six to three.

Note that both sets of experimental inflation test data, that is from Bryant and McDonnell (1996) and Elsheikh *et al.* (2007a), are used to calibrate the elastic fibre reinforced model. The data sets will be referred to as Bryant and Elsheikh inflation test data, respectively.

4.4.1 Case 1: Optimize Three Parameters

The results for optimizing the three material coefficients (C_{10}, k_1 and k_2) for this constitutive model are summarised in Tables 4.1 and 4.2 for the Bryant and Elsheikh inflation test data, respectively. The results are also graphically illustrated in Figures 4.3 and 4.4.

Bryant Inflation Data

The results in Table 4.1 indicate that there is good agreement between the experimental and numerical data with low values for the RMSE (RMSE ≤ 0.01), which is also visible in Figure 4.3.

Table 4.1: Optimization results calibrating only three material coefficients using Bryant inflation data. The incompressibility parameter, D_1, is fixed at 0.4.

Data Set	C_{10} **(MPa)**	k_1 **(MPa)**	k_2 **(-)**	**RMSE**
Fixed Boundary				
Set 1	0.004001	0.032322	173.506583	0.002031
Set 2	0.007192	0.026542	183.295523	0.002273
Set 3	0.002897	0.028653	96.120886	0.005025
Set 4	0.003935	0.015068	102.073936	0.006023
Set 5	0.005755	0.010422	104.555934	0.007411
23° **Boundary**				
Set 1	0.005113	0.016631	232.952614	0.002199
Set 2	0.007425	0.012284	241.387579	0.003185
Set 3	0.004001	0.016287	128.288432	0.005879
Set 4	0.004188	0.007985	134.617674	0.006290
Set 5	0.004029	0.006611	125.115893	0.004783

With a change in limbal boundary condition, from fixed to a 23° roller, it is seen from Table 4.1 that: (i) C_{10} mostly increases by $3.24 - 52.40\%$, although for material set 5 it seems to decrease by 29.99%, (ii) k_1 decreases by $36.57 - 53.72\%$ and (iii) k_2 increases by $19.66 - 35.87\%$.

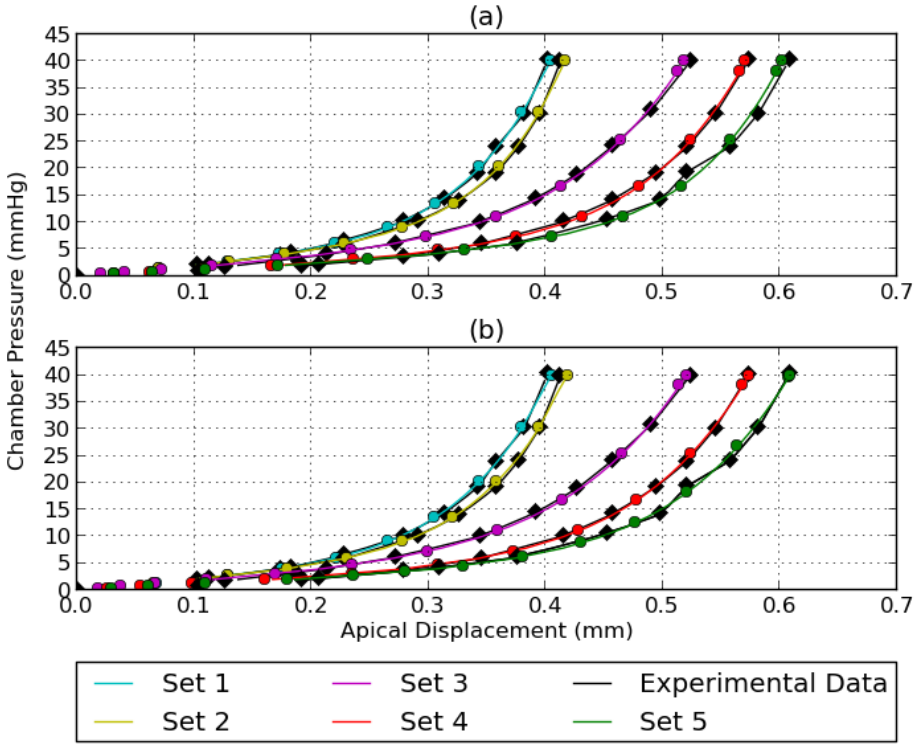

Figure 4.3: Optimization results by calibrating only three material coefficients using the Bryant inflation test data, where the incompressibility parameter, D_1, is fixed at 0.4. The results are shown for both the (a) fixed limbal boundary condition and the (b) limbal boundary on a 23° roller. The raw data is shown with the filled diamonds and circles (black indicates experimental data and other colors indicate numerical data), whereas the interpolated data are illustrated with the solid lines.

Elsheikh Inflation Data

Table 4.2: Optimization results calibrating only three material coefficients using Elsheikh inflation data. The incompressibility parameter, D_1, is fixed at 0.4.

Data Set	C_{10} **(MPa)**	k_1 **(MPa)**	k_2 **(-)**	**RMSE**
Fixed Boundary				
Set 1	0.003855	0.019626	236.874501	0.003345
Set 2	0.002459	0.027724	192.075484	0.005880
Set 3	0.025373	0.052000	521.365872	0.002976
Set 4	0.011072	0.043765	513.665028	0.001945
Set 5	0.003075	0.050982	305.819215	0.005528
Set 6	0.002775	0.077986	262.859468	0.000830
Set 7	0.005362	0.117310	498.664777	0.001935
Set 8	0.004102	0.121458	390.854989	0.003430
Set 9	0.003397	0.109116	494.976919	0.002819

Continues on the following page

Table 4.2 - *Continued from previous page*

Data Set	C_{10} (MPa)	k_1 (MPa)	k_2 (-)	RMSE
23° Boundary				
Set 1	0.005176	0.007333	357.793776	0.003521
Set 2	0.002466	0.015903	265.696728	0.005580
Set 3	0.023337	0.015789	701.965386	0.002431
Set 4	0.013090	0.013776	749.650654	0.001320
Set 5	0.002898	0.029179	418.226615	0.005298
Set 6	0.004496	0.049866	347.488225	0.000686
Set 7	0.004610	0.070691	653.095306	0.002056
Set 8	0.005098	0.077684	513.454737	0.003540
Set 9	0.004394	0.069777	664.034592	0.002781

It is evident from Table 4.2 and Figure 4.4 that there is good agreement between the experimental and numerical results (RMSE ≤ 0.01). A change in boundary condition, results in the same conclusions as with the Bryant inflation data: (i) C_{10} mostly increases by $0.29-34.27\%$, except for material sets 3, 5 and 7 which decrease by $5.76-8.02\%$, (ii) k_1 decreases by $36.04-69.64\%$ and (iii) k_2 increases by $30.97-51.05\%$.

Also note that when comparing the material properties to those in Table 4.1: (i) C_{10} on average decreases, except for material sets 3 and 4 which increase and (ii) k_1 and k_2 on average increase, with k_2 almost a factor 2 larger.

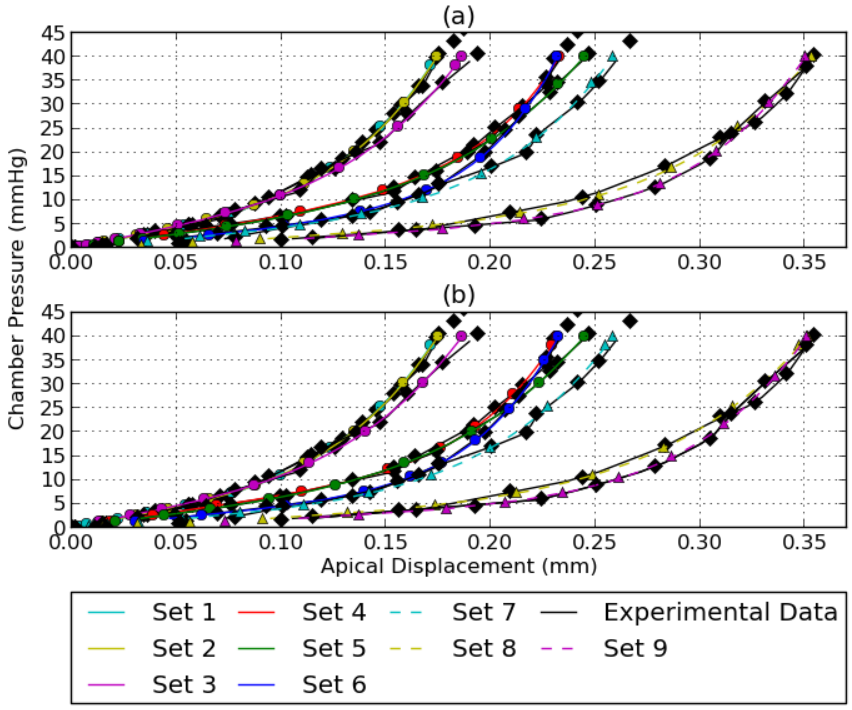

Figure 4.4: Optimization results by calibrating only three material coefficients using the Elsheikh inflation test data, where the incompressibility parameter, D_1, is fixed at 0.4. The results are shown for both the (a) fixed limbal boundary condition and the (b) limbal boundary on a 23° roller. The raw data is shown with the filled diamonds and circles (black indicates experimental data and other colors indicate numerical data), whereas the interpolated data are illustrated with the solid lines.

4.4.2 Material Coefficient Sensitivity Study

A sensitivity study is conducted to determine the sensitivity of each of the material coefficients in the model. The results of this study, using the final apical displacement, are shown in Table 4.3 where the material data sets using the Bryant inflation test data for a fixed limbal boundary condition are used. To ensure that no numerical difficulties arise the number of time steps used for the inflation test simulation are doubled resulting in the use of 60 time steps.

Table 4.3: Sensitivity study using the final apical displacement (mm) to determine the sensitivity of each material coefficient using the Bryant inflation data for a fixed limbal boundary.

Material Coefficient	+10%	+5%	**Base**	−5%	−10%
Material data set 1					
C_{10}	0.40488	0.40445	0.404	0.40355	0.40308
k_1	0.394641	0.40013	0.404	0.40804	0.41226
k_2	0.3887	0.39612	0.404	0.4124	0.42137
Material data set 2					
C_{10}	0.41769	0.4171	0.41649	0.41586	0.41521
k_1	0.40926	0.41281	0.41649	0.42034	0.42437
k_2	0.40084	0.40842	0.41649	0.42508	0.43427
Material data set 3					
C_{10}	0.5187	0.5184	0.51809	0.51779	0.51747
k_1	0.50802	0.51296	0.51809	0.52345	0.52903
k_2	0.49969	0.50862	0.51809	0.52817	0.53892
Material data set 4					
C_{10}	0.57152	0.57111	0.57069	0.57027	0.56983
k_1	0.56189	0.5662	0.57069	0.57538	0.58028
k_2	0.54973	0.5599	0.57069	0.5822	0.5945
Material data set 5					
C_{10}	0.60278	0.60225	0.6017	0.60114	0.60056
k_1	0.5934	0.59747	0.6017	0.60613	0.61076
k_2	0.57952	0.59028	0.6017	0.61388	0.6269

It is seen from Table 4.3 that a $\pm 10\%$ change in C_{10} results in a $0.06 - 0.23\%$ change in the final apical displacement from the base case. In comparison, a change in k_1 and k_2 results in a $0.70 - 2.32\%$ and $1.83 - 4.30\%$ change in the apical displacement, respectively.

These results indicate that C_{10} is the least sensitive of the three material coefficients considered, as a $\pm 10\%$ change in C_{10} results in a less than 0.3% change in apical displacement.

4.4.3 Case 2: Optimize Two Parameters

To determine the influence of the assumptions made regarding the material coefficients on both the inflation and Goldmann Applanation Tonometry (GAT) simulations, one of the material coefficients is kept constant. The previous section has shown that C_{10} is the least sensitive to a change in value and it is therefore decided to fix it. The value for C_{10} varies between 0.002459 and 0.025373 MPa considering both inflation test simulations (c.f. Tables 4.1 and 4.2). It is therefore assumed that the stiffness of the ground substance is the same for all corneas. It was shown in Section 2.3.2 that the ground substance stiffness is 40 kPa, or 0.04 MPa, but as this value is outside the range obtained for C_{10} it is decreased by a factor of 10 resulting in a value of 0.004 MPa, which is well within the range obtained from Case 1 ($0.002459 - 0.025373$ MPa).

Bryant Inflation Data

It is clear from Figure 4.5 and Table 4.4 that even with two material coefficients the experimental inflation test data is sufficiently captured (RSME < 0.01). A change in limbal boundary condition causes a decrease in k_1 of $40.93 - 55.10\%$ and an increase in k_2 of $25.96 - 42.77\%$.

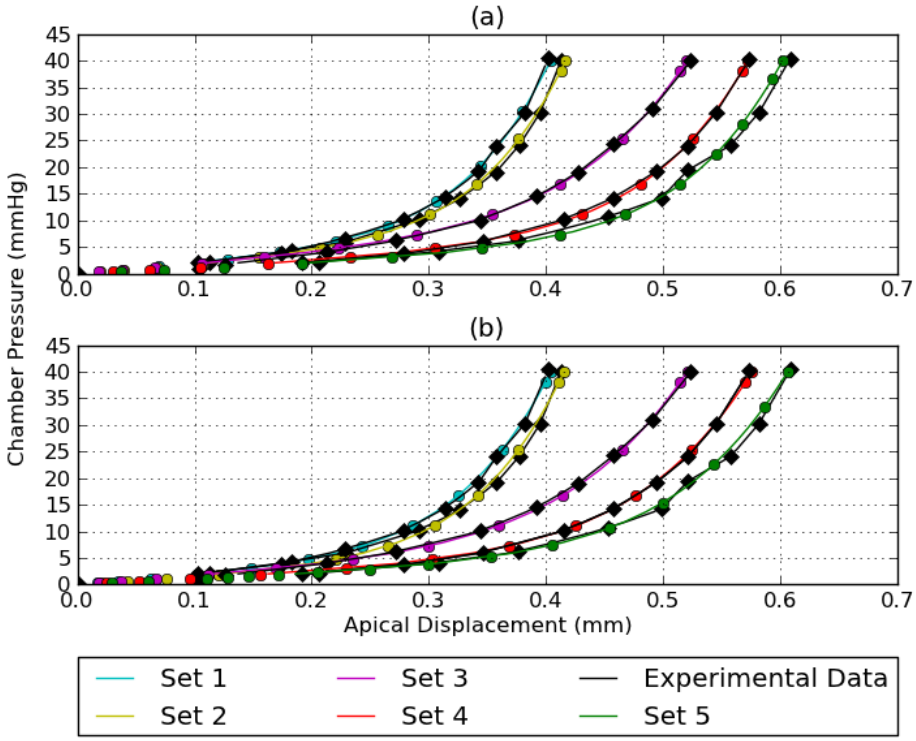

Figure 4.5: Optimization results for the calibration of only two material coefficients using the Bryant inflation test data ($C_{10} = 0.004$ MPa and $D_1 = 0.4$). The results are shown for both the (a) fixed limbal boundary condition and the (b) limbal boundary on a 23° roller. The raw data is shown with the filled diamonds and circles (black indicates experimental data and other colors indicate numerical data), whereas the interpolated data are illustrated with the solid lines.

Table 4.4: Optimization results for the calibraton of only two material coefficients using Bryant inflation data. The incompressibility parameter, D_1, is fixed at 0.4 and the ground substance stiffness, C_{10}, is fixed at 0.004 MPa.

Data Set	k_1 **(MPa)**	k_2 **(-)**	**RMSE**
Fixed Boundary			
Set 1	0.032314	173.524735	0.002031
Set 2	0.028284	171.250320	0.004699
Set 3	0.029997	93.877053	0.007337
Set 4	0.015398	100.511427	0.006451
Set 5	0.011258	100.036084	0.008182
23° **Boundary**			
Set 1	0.017431	230.184112	0.002755
Set 2	0.012699	244.499753	0.009684
Set 3	0.016282	128.187764	0.005912
Set 4	0.008900	128.445522	0.007446
Set 5	0.006650	126.000732	0.005121

When compared to Table 4.1, it is seen that by keeping C_{10} constant there is a decrease in the value of k_1 by $0.02 - 8.02\%$ and $0.59 - 11.46\%$ for a fixed and 23° limbal boundary condition, respectively. The value of k_2 also undergoes a change, either decreasing (Fixed: Set 1 and 23°: Sets 2, 5) or increasing (Fixed: Sets 2, 3, 4, 5 and 23°: Sets 1, 3, 4) for different material sets, by $0.01 - 6.57\%$ and $0.71 - 4.59\%$ for a fixed and 23° limbal boundary, respectively.

Elsheikh Inflation Data

The experimental and numerical results are in good agreement with RMSE values below 0.01 (c.f. Table 4.5 and Figure 4.6). It is also, once again, noted that with a change in limbal boundary condition that k_1 decreases by $35.38 - 61.95\%$ and k_2 increases by $29.10 - 50.17\%$.

Table 4.5: Optimization results for the calibraton of only two material coefficients using Elsheikh inflation data. The incompressibility parameter, D_1, is fixed at 0.4 and the ground substance stiffness, C_{10}, is fixed at 0.004 MPa.

Data Set	k_1 **(MPa)**	k_2 **(-)**	**RMSE**
Fixed Boundary			
Set 1	0.019478	238.828940	0.003350
Set 2	0.027157	203.283923	0.006946
Set 3	0.080369	288.909945	0.003517
Set 4	0.050330	398.274776	0.002721
Set 5	0.051998	311.296780	0.005738
Set 6	0.080452	266.891325	0.000911
Set 7	0.112656	491.468940	0.001939
Set 8	0.120654	392.926876	0.003434
Set 9	0.112066	496.112503	0.002820

Continues on the following page

Table 4.5 - *Continued from previous page*

Data Set	k_1 **(MPa)**	k_2 **(-)**	**RMSE**
		23° **Boundary**	
Set 1	0.007412	358.640556	0.005001
Set 2	0.013934	277.530562	0.006162
Set 3	0.050403	370.979069	0.003471
Set 4	0.027787	531.049667	0.003412
Set 5	0.028866	418.849262	0.005514
Set 6	0.050432	344.558315	0.000687
Set 7	0.070776	651.447913	0.002061
Set 8	0.077969	511.319119	0.003557
Set 9	0.070284	667.458985	0.002844

For a change in inflation test data used, it is noted that k_1 mostly increases and that k_2 is a factor $2-3$ larger than when using Bryant inflation test data.

When compared to Table 4.2, it is clear that by assuming a constant value for C_{10} that: (i) k_1 changes by $0.66-54.56\%$ (Sets 1, 2, 7 and 8 increase) and $0.012-219.23\%$ (Sets 2 and 5 decrease) for a fixed and 23° limbal boundary condition, respectively; and (ii) the change in k_2 is smaller than that of k_1, where k_2 changes by $0.23-44.59\%$ (Sets 3, 4 and 7 decrease) and $0.15-47.15\%$ (Sets 1, 2, 5 and 9 increase) for a fixed and 23° limbal boundary condition, respectively.

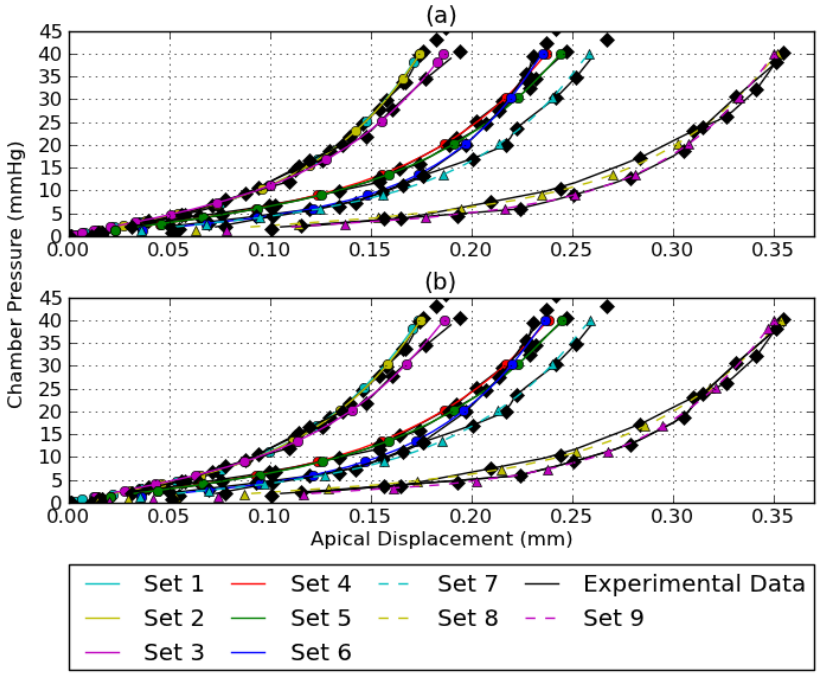

Figure 4.6: Optimization results for the calibration of only two material coefficients using the Elsheikh inflation test data ($C_{10} = 0.004$ MPa and $D_1 = 0.4$). The results are shown for both the (a) fixed limbal boundary condition and the (b) limbal boundary on a 23° roller. The raw data is shown with the filled diamonds and circles (black indicates experimental data and other colors indicate numerical data), whereas the interpolated data are illustrated with the solid lines.

4.5 CONCLUSION

This chapter dealt with the calibration of the elastic fibre reinforced constitutive model. Two sets of experimental inflation test data, Bryant and McDonnell (1996) and Elsheikh *et al.* (2007a), were used to calibrate the constitutive model. This was done by solving an unconstrained minimization problem, in which the Root Mean Square Error (RMSE) between the experimental and numerical results were minimized.

To investigate the influence of assumptions made with regards to material coefficients two cases were considered: (i) optimize three material coefficients, with an incompressibility parameter of 0.4 and (ii) assume that the ground substance is the same for all corneas, thereby only optimizing two material coefficients. For both sets of inflation test data a change in limbal boundary condition indicated that there is an increase in k_2, while k_1 decreases. It was also noted that when assuming the stiffness of the ground substance in all corneas to be the same ($C_{10} = 0.004$ MPa) k_1 and k_2 vary depending on the material data set, but still allow sufficient freedom to fit the inflation data.

Also interesting to note is that independent of the assumptions made it was possible to capture the experimental inflation test behaviour for all material data sets in all cases, with RMSE values below 0.01.

CHAPTER 5

SIMULATING GOLDMANN APPLANATION TONOMETRY

5.1 INTRODUCTION

Goldmann Applanation Tonometry (GAT) is the most common method used to estimate the Intraocular Pressure (IOP) by measuring the indentation resistance of the cornea. The estimated IOP is the primary indicator used for glaucoma screening.

There are several sources of error in the IOP estimation when using GAT of which the geometrical quantities are the most well known. These include the Central Corneal Thickness (CCT) and corneal Radius of Curvature (RoC), where a thick and steep cornea overestimates the IOP and a thin and flat cornea underestimates the IOP. To account for these measured inaccuracies several correction equations (Orssengo and Pye, 1999; Chihara, 2008; Kwon *et al.*, 2008; Elsheikh *et al.*, 2011; Guzmán *et al.*, 2013) have been proposed to correct the obtained measurement. The surface tension, due to the applied anaesthesia could also influence the IOP measurement, but only up to 1 mmHg too high (Goldmann and Schmidt, 1957). Numerical studies tend to amend their obtained IOP estimations, to account for this effect, using a value of approximately 4 mmHg (Orssengo and Pye, 1999; Kwon *et al.*, 2008), although more recently a value of 0.44 mmHg was used for this correction (Elsheikh *et al.*, 2006).

In this chapter, GAT is simulated to investigate the effect of various modelling assumptions, such as experimental inflation test data for calibration and limbal boundary conditions, as well as the effect of geometric and material properties on the estimated IOP. A correction equation is then proposed in an attempt to correct for GAT inaccuracies.

5.2 DEFINITION OF A NUMERICALLY NORMAL CORNEA

In this study it was decided to use the mean of the various data sets, used for the numerical investigations, to represent a normal cornea in the numerical environment.

The effect of geometric variables such as CCT, RoC and IOP are investigated in this chapter, which requires a range to be considered for each variable. In Section 2.3.1 it was noted that the statistically normal IOP is considered to be between 7 and 21 mmHg. For this study an IOP, or True IOP (IOPT), range of 8 to 24 mmHg is considered, which is within the physiological range and results in a mean IOP of 16 mmHg. The range of CCT considered is between 0.45 and 0.65 mm, with a mean CCT of 0.55 mm. The mean CCT is within the range of a normal cornea ($0.50 - 0.565$ mm) as was indicated in Table 3.1 (c.f. Section 3.2.1). Also from Table 3.1, the mean anterior RoC is taken as 7.77 mm, with the mean posterior RoC as 6.3 mm.

The Bryant inflation data captures the natural *in vivo* stress state of the cornea due to the IOPT better than the Elsheikh inflation data as creep is allowed (c.f. Section 16). For this reason the material coefficients obtained using the Bryant inflation test data during calibration are considered to represent the numerically normal cornea. Finally, the set of material coefficients that is considered to represent the numerically normal cornea is Set 3, which is the median as shown in Figure 2.4 (Cornea 5 represented in green).

During a GAT simulation the point of interest is the apex of the cornea and it is assumed that the chosen limbal boundary condition will not affect the estimated IOP from GAT (IOPG). The limbal boundary condition, which is considered to represent the numerically normal cornea, is therefore chosen to be fixed.

The Ocular Response History (ORH) for a numerically normal cornea is shown in Figure 5.1, where it is compared to the Imbert-Fick law on which GAT is based (c.f. Section 2.5.1):

$$\text{IOPG} = \frac{F}{A} \tag{5.1}$$

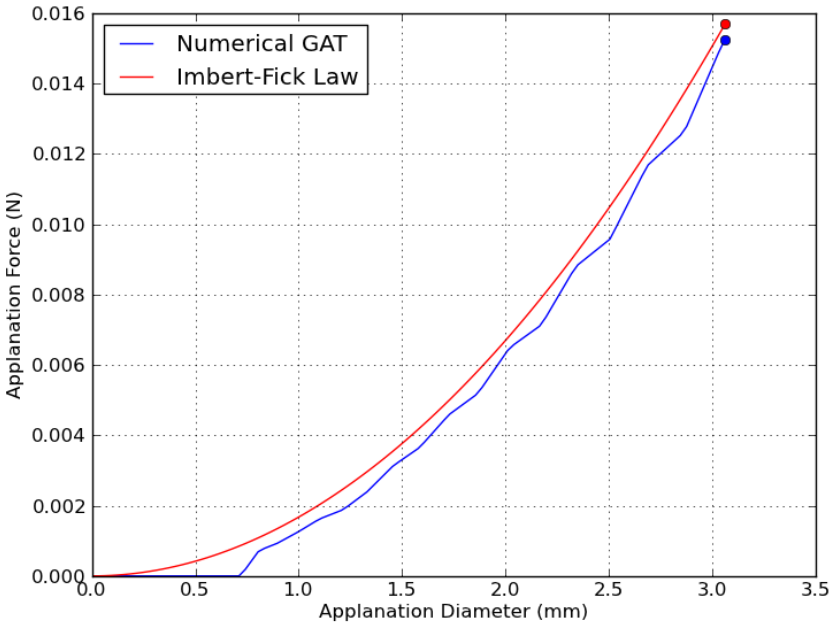

Figure 5.1: Ocular Response History (ORH) comparing the numerical GAT results for a numerically normal cornea with the Imbert-Fick law.

5.3 EFFECT OF MODELLING ASSUMPTIONS ON IOP

This section investigates the effect that various modelling assumptions might have on the estimated IOPG from the numerical GAT simulation. The assumptions investigated are:

1. **Inflation test data** used for calibrating the material coefficients of the constitutive models, i.e. Bryant inflation data vs. Elsheikh inflation data.
2. **Boundary condition** specified at the limbal region, i.e. completely fixed vs. allowed to translate on a 23° roller.

5.3.1 Calibration Methods

Two sets of experimental inflation test data are available, both of which have been used to numerically calibrate constitutive models used to represent the corneal structure in various numerical studies. As was shown in Section 2.4.2, the data obtained from both studies seem to cover a wide range of pressure-displacement responses. The question arises: which set more accurately represents the corneal response due to inflation testing?

In an attempt to answer this question the influence on the IOPG due to each inflation data set is investigated considering all four cases, that is both limbal boundary conditions paired with both sets of inflation data. The normal cornea is represented by material set 3, for the Bryant inflation test data, and material set 5, for the Elsheikh inflation test data. Material set 5 approximately represents the mean of the nine sets of material data obtained from the Elsheikh inflation test data shown in Figure 2.5 (mean is represented by the red curve with filled circles).

From Figure 5.2 it is evident, when using the data from Case 1 with a fixed limbal boundary condition, that there is a 0.87 mmHg difference between the Bryant and Elsheikh inflation test data. On the other hand, there is a 1.81 mmHg difference between the Bryant and Elsheikh inflation test data for a 23° limbal boundary condition.

When using the data from Case 2, where the ground substance stiffness (C_{10}) is constant, it is noted that the estimated IOPG is approximately $1.05 - 1.37$ mmHg higher than when using the data from Case 1, except when using the Bryant inflation test data and a 23° limbal boundary condition where it is 0.41 mmHg lower. For a fixed limbal boundary condition there is a 0.88 mmHg change with a change in inflation test data and a 0.03 mmHg change for a 23° limbal boundary condition.

5.3.2 Boundary Conditions

Two boundary conditions were considered to represent the cornea-scleral connection, (i) a completely fixed limbal boundary and (ii) a limbal boundary allowed to translate along a 23° roller. Both of these boundary conditions were applied in a numerical GAT simulation

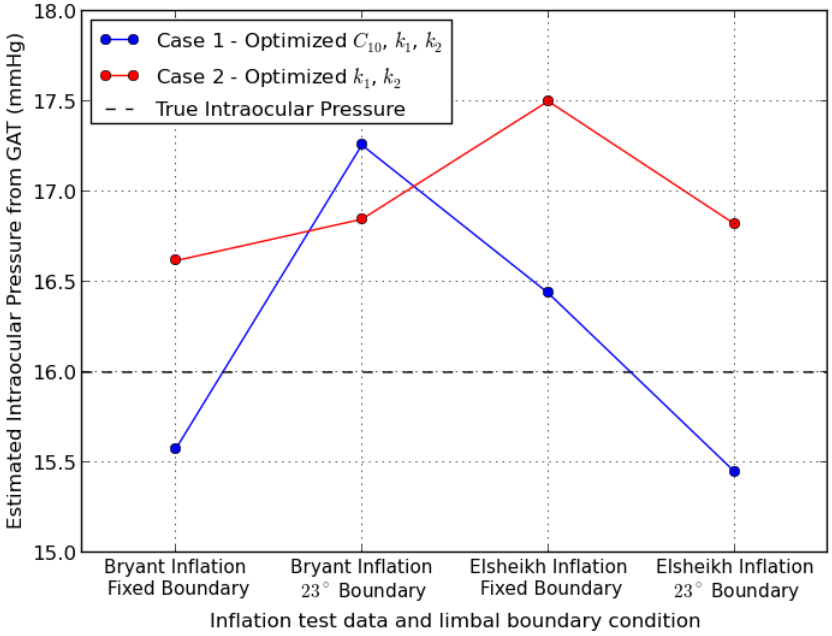

Figure 5.2: Influence of the choice of inflation test data, used during constitutive model calibration, on the estimated IOPG from a numerical GAT simulation using the properties for a normal cornea with a IOPT of 16 mmHg (black dashed line).

to estimate the IOPG considering the numerically normal corneal material properties from both sets of inflation test data, the results of which are illustrated in Figure 5.2.

It is seen from Figure 5.2 that when using the data from Case 1 there is a 1.69 mmHg difference, from a fixed to a 23° limbal boundary condition, in estimated IOPG for the Bryant inflation test data and a 0.99 mmHg difference for the Elsheikh inflation test data.

When the data from Case 2 is used there is a 0.23 mmHg difference between the two limbal boundary conditions for the Bryant inflation test data and a 0.68 mmHg difference for the Elsheikh inflation test data.

5.4 EFFECT OF GEOMETRIC AND MATERIAL PROPERTIES ON IOP

Several studies, both clinical and numerical, have been conducted to investigate the effect of RoC and CCT on the estimated IOPG. In this section the influences of RoC, CCT and material properties are investigated.

5.4.1 Central Corneal Thickness

To determine the influence of the CCT on the estimated IOPG a range of CCT between 0.45 and 0.65 mm was considered in increments of 0.05 mm. The results are illustrated

in Figure 5.3 for a numerically normal cornea, where it is evident that for a larger CCT the IOPG is overestimated and for a smaller CCT it is underestimated. This observation corresponds to the general conclusion of several clinical (Ehlers *et al.*, 1975) and numerical (Orssengo and Pye, 1999; Liu and Roberts, 2005; Elsheikh *et al.*, 2006; Kwon *et al.*, 2008) studies.

From Figure 5.3 it is seen that the estimated IOPG differs by a maximum of 1.05 mmHg and 1.12 mmHg, from the mean CCT of 0.55 mm, for the thinnest and thickest corneas considered when using the data from Case 1. When using the data from Case 2 the estimated IOPG increases by $0.76 - 1.42$ mmHg, differing by a maximum of 1.34 mmHg and 1.49 mmHg, from the mean CCT, for the thinnest and thickest corneas considered. In addition, a linear relationship between the CCT and the IOPG can be approximated, which was also observed in previous numerical studies (Orssengo and Pye, 1999; Liu and Roberts, 2005; Elsheikh *et al.*, 2006; Kwon *et al.*, 2008) (c.f. Section 2.6).

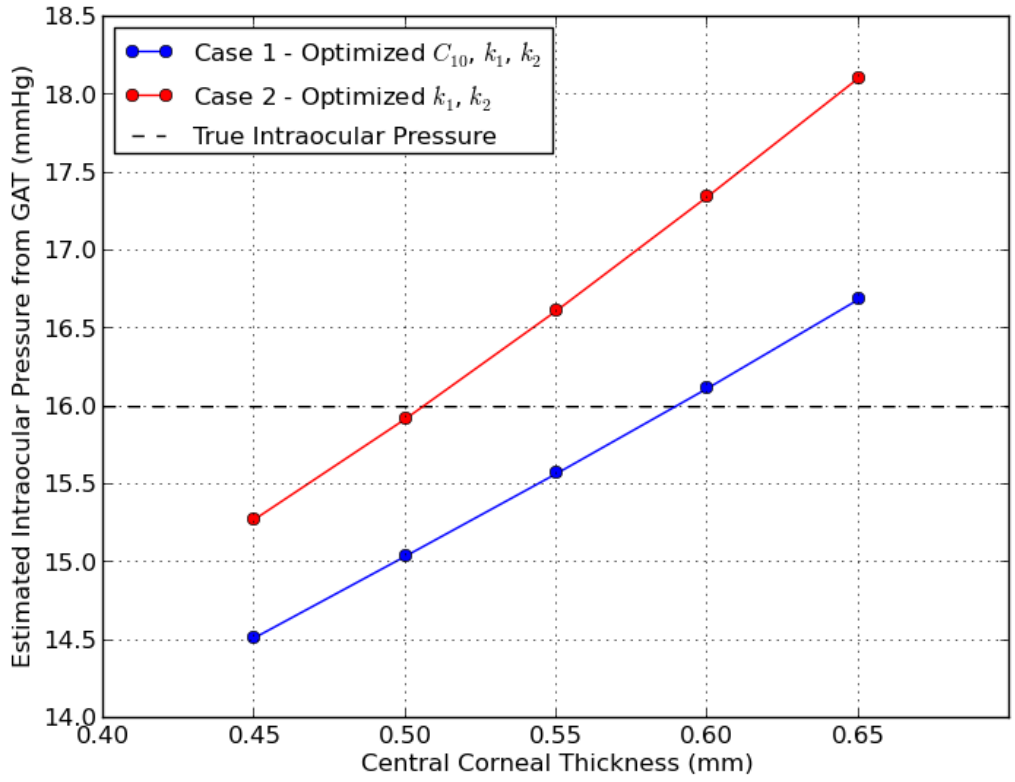

Figure 5.3: Influence of the CCT on the estimation of the IOPG for a numerically normal cornea with a IOPT of 16 mmHg (black dashed line).

5.4.2 Radius of Curvature

The second geometric property to be investigated is the influence of the anterior RoC on the estimated IOPG, shown in Figure 5.4. An anterior RoC range of between 7.0 and 8.54 mm was considered in increments of 0.385 mm. The posterior RoC was determined using the ratio of the mean anterior RoC to the mean posterior RoC (c.f. Table 3.1, Section 3.2.1):

$$\frac{R_{\text{ant,mean}}}{R_{\text{post,mean}}} = \frac{7.77\text{mm}}{6.3\text{mm}} = 1.2333 \tag{5.2a}$$

$$R_{\text{post,new}} = \frac{R_{\text{ant,new}}}{1.2333} \tag{5.2b}$$

From Figure 5.4 it is seen that the variation in IOPG due to a change in anterior RoC differs by a maximum of 0.58 mmHg and 0.47 mmHg, from a mean RoC of 7.77 mm, for a steeper and flatter cornea, using the data from Case 1. Using the data from Case 2 it is noted that the estimated IOPG increases by $0.96 - 1.15$ mmHg when compared to the results using the data from Case 1. The anterior RoC differs by a maximum of 0.67 mmHg and 0.56 mmHg, from a mean RoC, for a steeper and flatter cornea when using the data from Case 2. It is clear from these results that the IOPG is underestimated for larger values of anterior RoC (flatter) and overestimated for smaller values (steeper).

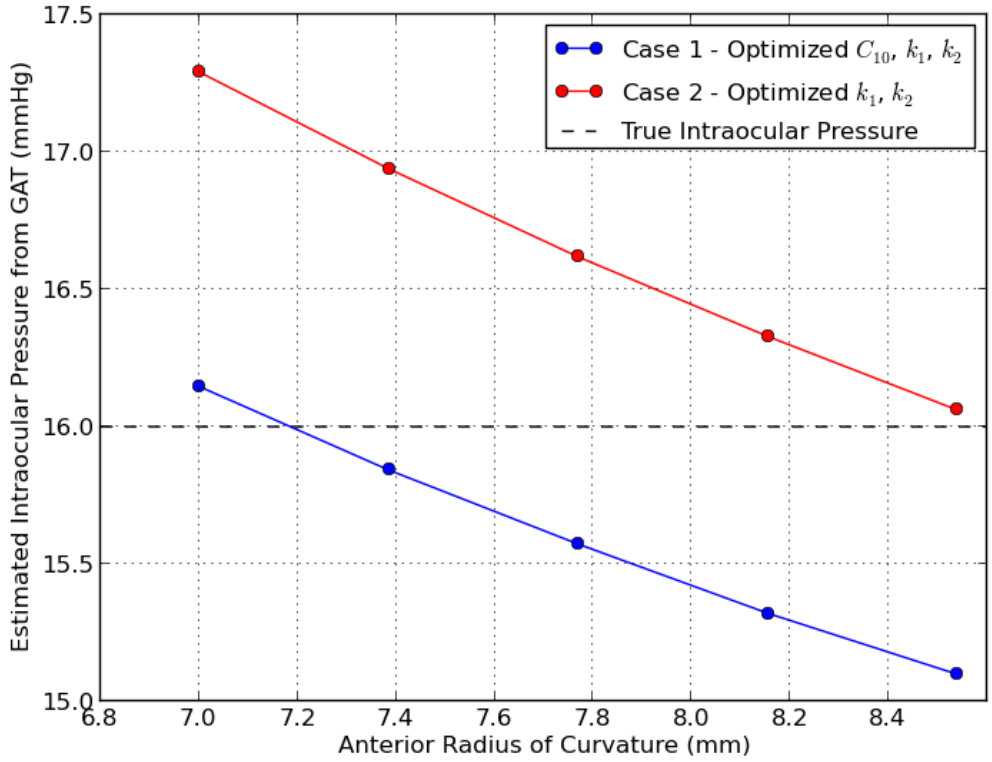

Figure 5.4: Influence of the anterior RoC on the estimation of the IOPG for a numerically normal cornea with a IOPT of 16 mmHg (black dashed line).

This conclusion, as well as the observation that the relationship between anterior RoC and IOPG can be approximated linearly, corresponds with results in various numerical studies where the influence of corneal RoC was investigated (Orssengo and Pye, 1999; Liu and Roberts, 2005; Elsheikh *et al.*, 2006; Kwon *et al.*, 2008) (c.f. Section 2.6).

5.4.3 Material Properties

The effect of the material properties are investigated by comparing the IOPG for each of the five material sets for each of the two cases considered using the fibre reinforced elastic constitutive model. The results of these cases are shown in Figure 5.5, where it is evident that the estimated IOPG using the data from Case 2 is consistently between 16.39 and 17.05 mmHg, showing only slight variations from Set 3 ($\Delta IOPG = 0.66$ mmHg from the minimum

to maximum IOPG). On the other hand, the estimated IOPG when using the data from Case 1 varies between 15.57 and 19.78 mmHg with $\Delta IOPG = 4.21$ mmHg.

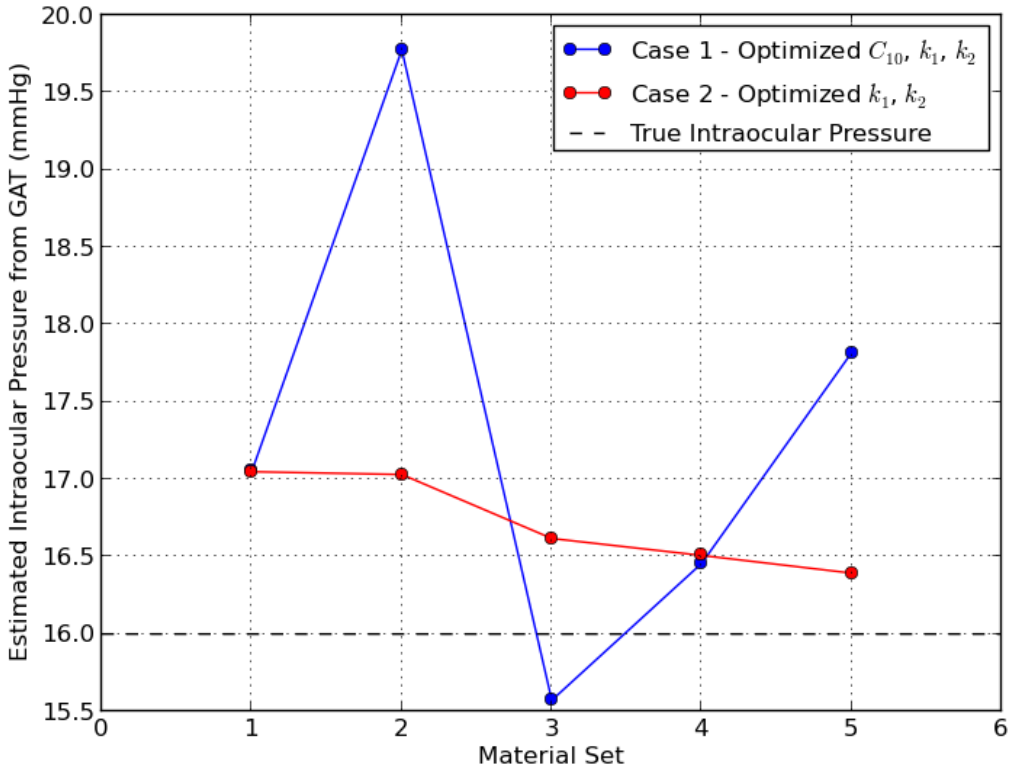

Figure 5.5: Influence of the material properties on the estimation of the IOPG, for a numerically normal cornea, considering all three cases for a fibre reinforced elastic constitutive model with a IOPT of 16 mmHg (black dashed line).

These results can be summarized with regards to the influence of material properties on the estimated IOPG:

- Case 1 indicates that material properties have an influence on the estimated IOPG, ΔIOPG = 4.21 mmHg.
- Case 2 indicates that material properties do not have a significant influence on the estimated IOPG, ΔIOPG = 0.66 mmHg.

It is also apparent that by assuming a constant stiffness for the corneal stroma ground substance (Case 2) that the estimated IOPG changes by $0.0 - 2.75$ mmHg for each material set. To investigate this effect, additional numerical GAT simulations were conducted by varying the ground substance stiffness, C_{10}, between 0.003 and 0.006 MPa. These results are shown in Figure 5.6.

The influence of the ground substance stiffness, C_{10}, is evident in Figure 5.6, where an increase in C_{10} leads to an increase in the estimated IOPG and conversely, a decrease in C_{10} decreases the estimated IOPG. This indicates that assumptions made with regards to material coefficients also have an influence on the estimated IOPG.

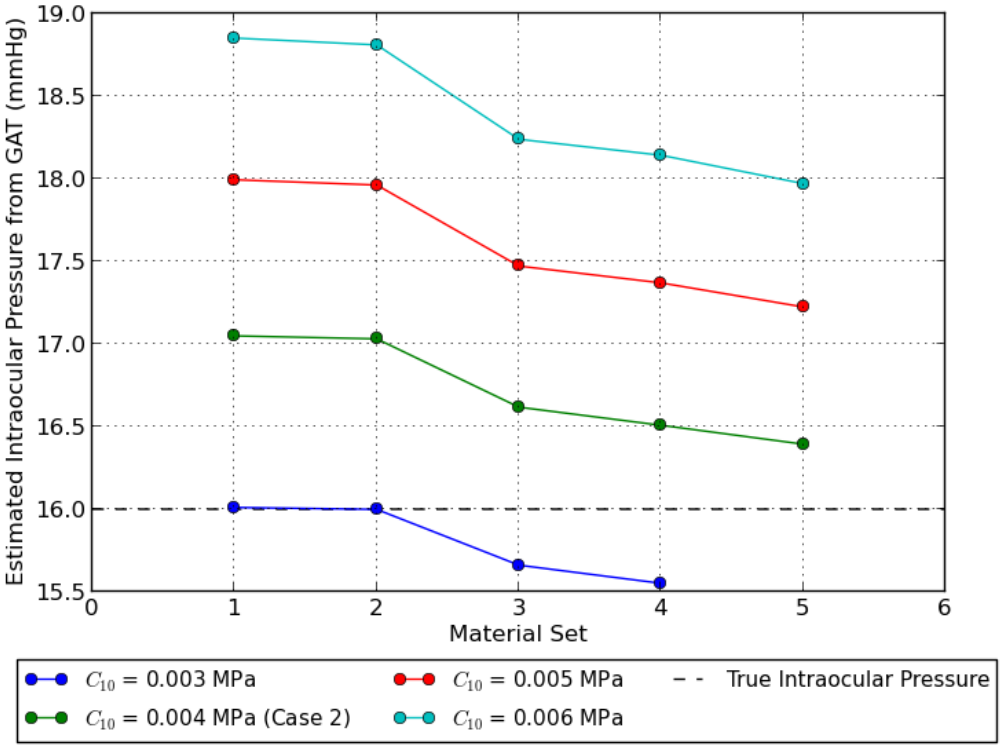

Figure 5.6: Influence of the ground substance stiffness, C_{10}, on the estimated IOPG for Case 2. The IOPT of 16 mmHg is shown with a black dashed line.

5.5 CORRECTION EQUATION

Goldmann and Schmidt (1957) calibrated the Goldmann applanation tonometer by performing manometer experiments on cadaver eyes to determine the optimum applanation diameter. To reflect the clinical calibration of the GAT a correction equation is proposed based on the numerical GAT simulations and model developed in this study.

Several correction equations have been suggested to correct for the variation in IOP due to CCT, anterior RoC and IOPG when using GAT (Orssengo and Pye, 1999; Chihara, 2008; Kwon *et al.*, 2008; Elsheikh *et al.*, 2011; Guzmán *et al.*, 2013). The relationship between the IOPT and IOPG is illustrated in Figure 5.7 for a numerically normal cornea when considering the data from both Cases 1 and 2.

From Figure 5.7 it apparent that there is a linear relationship between IOPT and IOPG and there is a need for a correction equation as the IOPT is either under- or overestimated.

5.5.1 Proposed Correction Equation

From Figures 5.3 and 5.7 it was noted that there is a linear relationship between IOPT and CCT as well as IOPT and IOPG. It was also evident from Figure 5.4 that there is a non-linear relationship between the IOPG and RoC. From Figure 5.5 there is no clear relationship between the material properties and the IOPG.

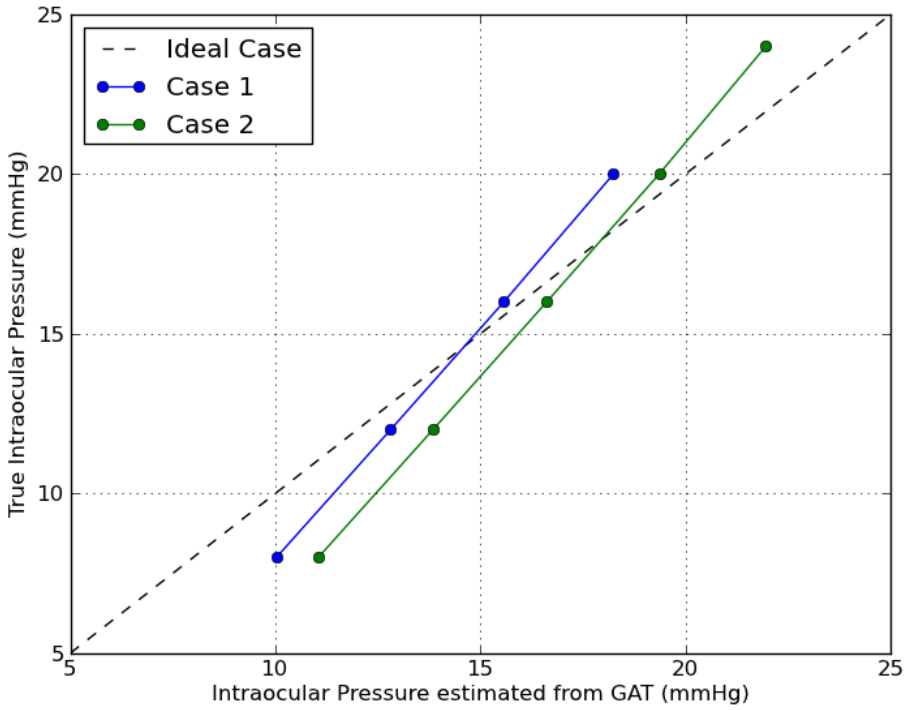

Figure 5.7: Relationship between the IOPT and IOPG for a numerically normal cornea considering both Cases 1 and 2.

For the proposed correction equation a quadratic approach is used to account for the unknown relationship between the material properties and IOPG as well as the non-linear relationship between the IOPG and RoC. The proposed correction equation is:

$$\begin{aligned}\text{IOPC} = {} & a_0 + a_1\text{IOPG} + a_2(\text{IOPG} \times R_{\text{ant}}) + a_3(\text{IOPG} \times \text{CCT}) + a_4(\text{IOPG} \times C_{10}) \\ & + a_5(\text{IOPG} \times k_1) + a_6(\text{IOPG} \times k_2) + a_7\text{IOPG}^2 + a_8 R_{\text{ant}} + a_9(R_{\text{ant}} \times \text{CCT}) \\ & + a_{10}(R_{\text{ant}} \times C_{10}) + a_{11}(R_{\text{ant}} \times k_1) + a_{12}(R_{\text{ant}} \times k_2) + a_{13}R_{\text{ant}}^2 + a_{14}\text{CCT} \\ & + a_{15}(\text{CCT} \times C_{10}) + a_{16}(\text{CCT} \times k_1) + a_{17}(\text{CCT} \times k_2) + a_{18}\text{CCT}^2 + a_{19}C_{10} \\ & + a_{20}(C_{10} \times k_1) + a_{21}(C_{10} \times k_2) + a_{22}C_{10}^2 + a_{23}k_1 + a_{24}(k_1 \times k_2) + a_{25}k_1^2 + a_{26}k_2 + a_{27}k_2^2\end{aligned} \tag{5.3}$$

where IOPC is the Calibrated IOP, IOPG is the IOP from GAT, R_{ant} is the anterior radius of curvature, CCT is the central corneal thickness and C_{10}, k_1 and k_2 represent the corneal material properties. To determine the correction coefficients in Equation (5.3) a least squares approach is used such that:

$$\mathbf{A}\vec{x} = \vec{b} \tag{5.4}$$

where $\mathbf{A}$ is a matrix of the coefficients of each of the variables (i.e. CCT, R_{ant}, IOPG, C_{10}, k_1 and k_2), $\vec{x}$ is a vector of the correction coefficients, a_i, and $\vec{b}$ is a vector of the IOPT.

A number of GAT simulations are conducted for a variety of CCTs ($0.45 - 0.60$ mm), RoCs ($7.0 - 8.54$ mm) and IOPs ($8 - 24$ mmHg) for both limbal boundary conditions utilising the material properties obtained from both sets of inflation test data. A total of 7000 simulations were conducted, using the material properties from Case 1 (3500 simulations) and Case 2

(3500 simulations), of which 331 (9.46%) and 248 (7.63%) simulations had numerical difficulties, respectively. Only half of the simulations for each considered case are used to obtain the correction coefficients in Equation (5.3) and the remaining half is used to predict the IOPC.

Correction Equation considering three material properties

Using all four data sets from Case 1, that is both sets of inflation test data with both limbal boundary conditions, the correction coefficients in Equation (5.3) are obtained. These correction coefficients are obtained by randomly sampling half of the simulations for each considered data set and are summarised in Table 5.1. The level of contribution of each term is indicated by the value of the correction coefficients. Larger values for the correction

Table 5.1: Correction coefficients obtained by randomly sampling half of the simulations for each data set using the data from Case 1.

Correction Coefficients	**Bryant Data Fixed Boundary**	**Bryant Data 23° Boundary**	**Elsheikh Data Fixed Boundary**	**Elsheikh Data 23° Boundary**
a_0	-2.78248724e+01	-9.20535668e+00	2.38009490e+02	6.39908976e+02
a_1	1.13394892e+00	1.35951221e+00	1.20228981e+00	1.35225502e+00
a_2	3.62489331e-02	4.38005496e-03	3.75154394e-02	4.05657351e-02
a_3	-7.58276994e-02	-2.40396675e-01	-1.11540457e-01	-4.08600366e-01
a_4	-4.00755811e+01	-7.12784730e+01	-1.50165947e+01	-2.55522269e+01
a_5	2.12343394e-01	-1.32807666e+00	1.67368167e+00	2.90159549e+00
a_6	-4.15196630e-04	5.23410675e-04	-4.71763408e-04	-3.44622722e-04
a_7	8.32978713e-03	1.23588366e-02	3.12061450e-03	6.38246322e-03
a_8	8.79915925e-02	3.60437229e+00	-5.22417869e-01	2.39610484e+00
a_9	3.26319085e+00	3.04811089e+00	3.23755082e+00	3.11556328e+00
a_{10}	6.18766120e+01	4.22667809e+01	3.85495393e+01	1.62915085e+01
a_{11}	5.26169510e+00	2.67458654e+01	1.77377868e+00	8.37214765e+00
a_{12}	2.25534116e-04	2.81875302e-03	3.91369821e-04	2.06155747e-04
a_{13}	-1.13804778e-01	-3.75167147e-01	-7.07747804e-02	-2.67597809e-01
a_{14}	-1.67156150e+01	-4.46054266e+00	-1.66161772e+01	-1.08675526e+01
a_{15}	-2.99412424e+03	-2.70137690e+03	-1.89576871e+03	-1.64689636e+03
a_{16}	-3.16932694e+01	-1.92020239e+01	-1.42538301e+01	-4.76505286e+01
a_{17}	-1.47175123e-02	-1.41412558e-02	-2.40578289e-02	-9.31789497e-03
a_{18}	-1.18246951e+01	-2.14575938e+01	-1.12095780e+01	-1.68299978e+01
a_{19}	9.01884226e-01	-1.92196473e-03	5.76534775e+04	-3.61116158e+04
a_{20}	-1.89677839e-02	3.20449227e-04	3.51107594e+06	1.32754806e+07
a_{21}	8.07472386e+00	4.18857828e+00	-1.00109138e+03	-1.07840003e+03
a_{22}	7.73475510e-03	1.64668094e-04	7.71494050e+06	1.62346872e+07
a_{23}	-2.02848222e+00	5.05962190e-02	5.23552324e+03	-2.73129811e+04
a_{24}	4.40896174e-01	-1.20137688e+00	-1.10392333e+02	-1.25547259e+02
a_{25}	7.03464583e-02	-1.38102591e-03	1.19026668e+05	1.59869959e+05
a_{26}	4.75957117e-01	-4.51899359e-02	-3.52807544e+00	-2.39695044e+00
a_{27}	-1.95292552e-03	6.34902921e-05	2.27965695e-02	1.54387067e-02

coefficients indicate a larger contribution to the correction equation.

The results are illustrated in Figures 5.8 through 5.15 where the data is shown before and after calibration, as well as histograms for each considered IOP to clearly show the distribution of predicted IOPC.

It is noticeable from Figures 5.8, 5.9, 5.10 and 5.11 that the proposed correction equation improves the predicted IOPC when compared to the IOPG obtained from the GAT simulation. However, it is seen that when using Elsheikh inflation test data (c.f. Figures 5.10 and 5.11) the predicted IOPC distribution is larger, varying within $0.20 - 0.90$ mmHg of the IOPT, than when using Bryant inflation test data which varies within $0.08 - 0.40$ mmHg of the IOPT (c.f. Figures 5.8 and 5.9). This is due to a wider spread in the original IOPG for Elsheikh inflation test data.

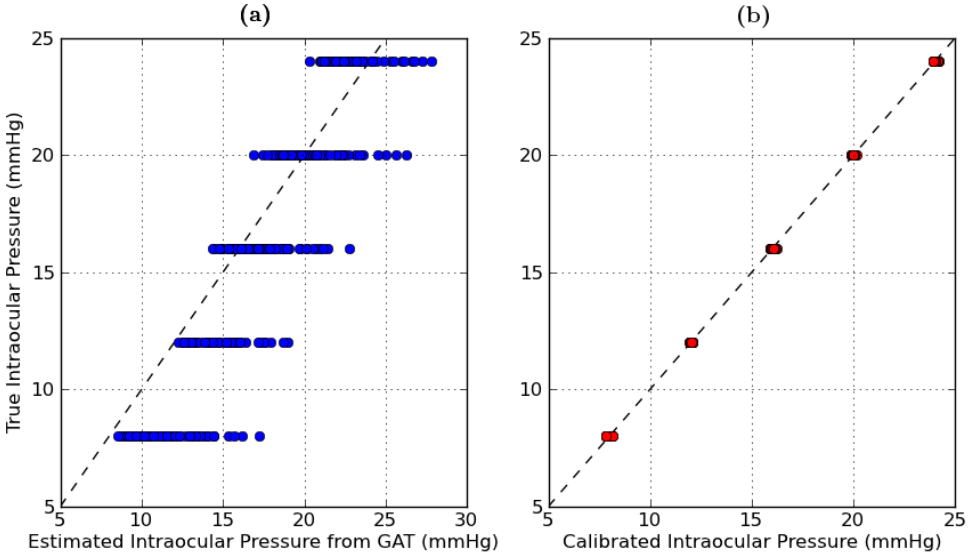

Figure 5.8: Comparison between the (a) IOPT and IOPG as well as (b) IOPT and IOPC using the Bryant inflation data and a fixed limbal boundary condition from Case 1.

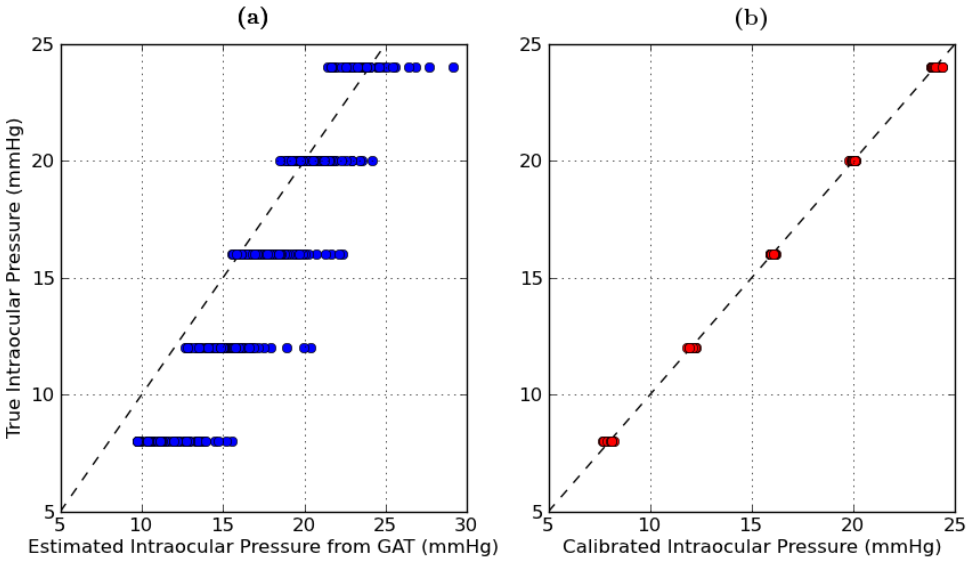

Figure 5.9: Comparison between the (a) IOPT and IOPG as well as (b) IOPT and IOPC using the Bryant inflation data and a 23° limbal boundary condition from Case 1.

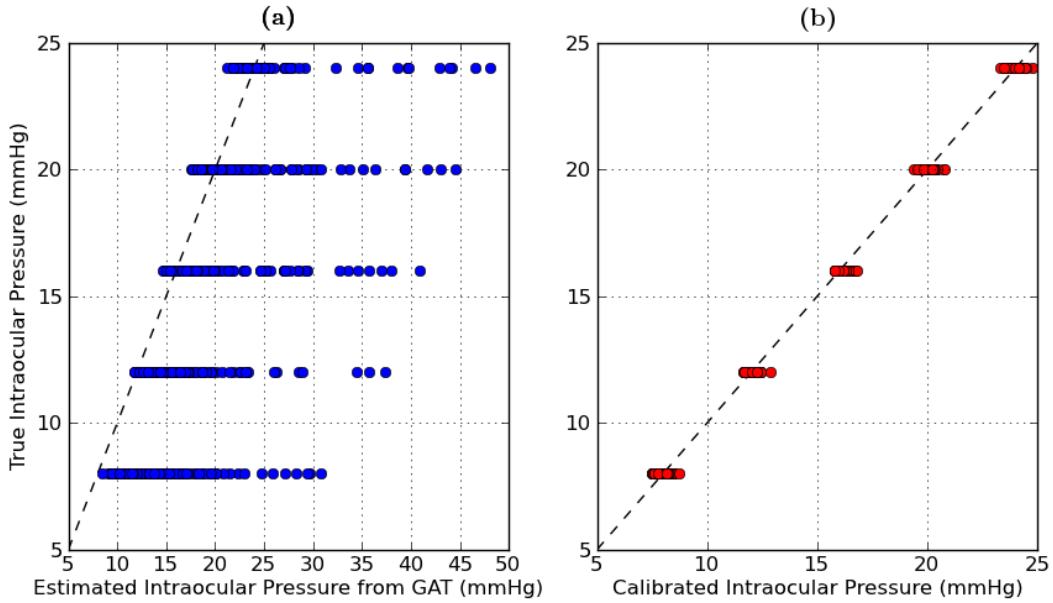

Figure 5.10: Comparison between the (a) IOPT and IOPG as well as (b) IOPT and IOPC using the Elsheikh inflation data and a fixed limbal boundary condition from Case 1.

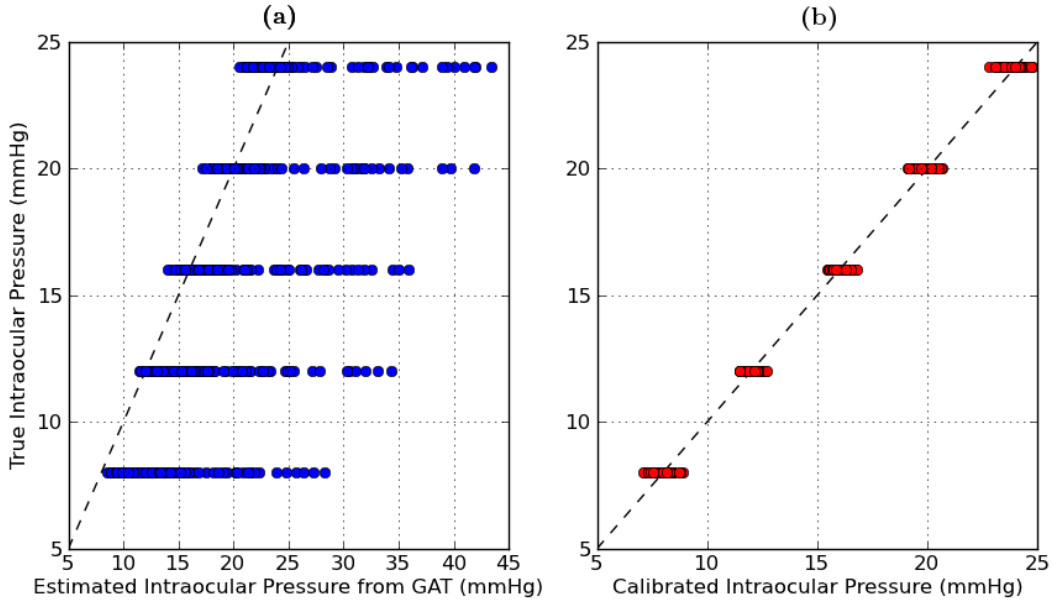

Figure 5.11: Comparison between the (a) IOPT and IOPG as well as (b) IOPT and IOPC using the Elsheikh inflation data and a 23° limbal boundary condition from Case 1.

From the histograms (c.f. Figures 5.12, 5.13, 5.14 and 5.15) it is also evident that the proposed correction equation predicts the IOPC within $0.08 - 1.30$ mmHg of the IOPT for the four data sets: Bryant inflation data with a fixed limbal boundary, Bryant inflation data with a 23° limbal boundary, Elsheikh inflation data with a fixed limbal boundary and Elsheikh inflation data with a 23° limbal boundary.

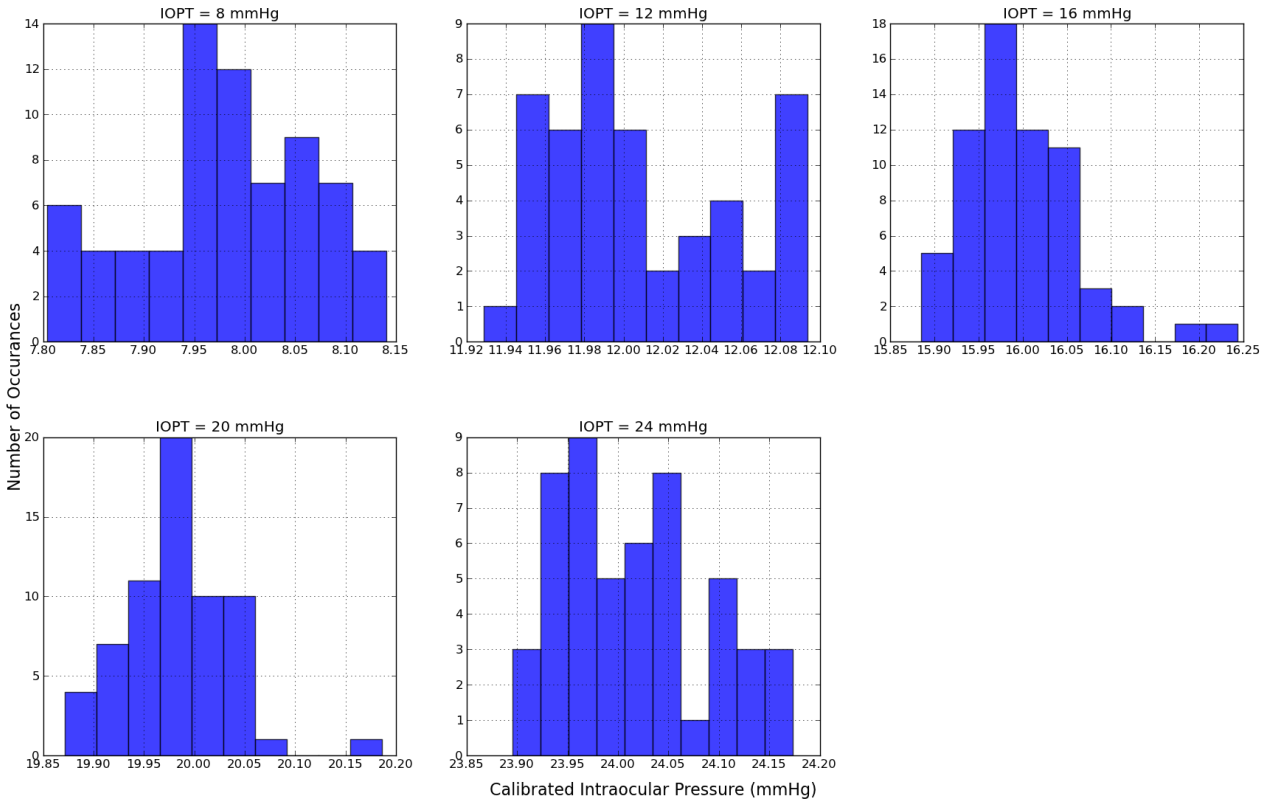

Figure 5.12: Histogram illustrating the predicted IOPC pressure distribution from IOPT when using the Bryant inflation data and a fixed limbal boundary from Case 1.

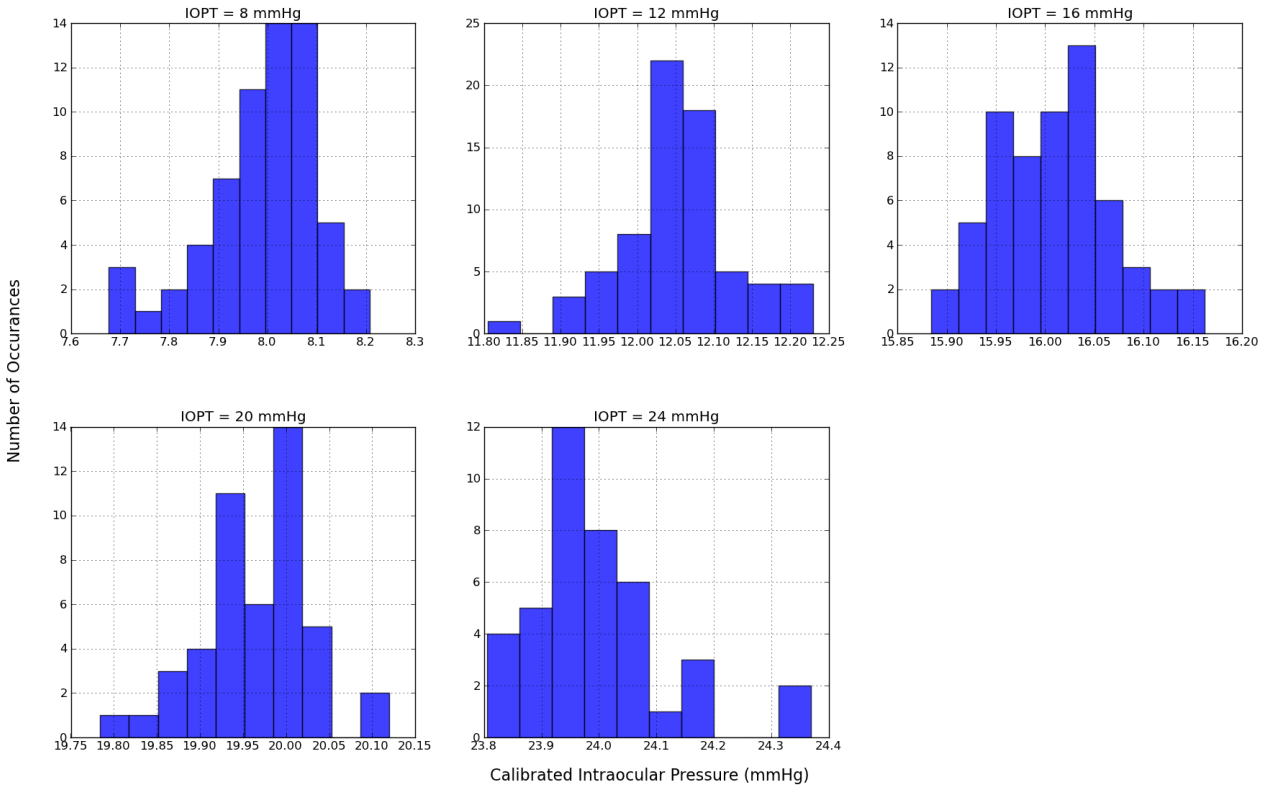

Figure 5.13: Histogram illustrating the predicted IOPC pressure distribution from IOPT when using the Bryant inflation data and a 23° limbal boundary from Case 1.

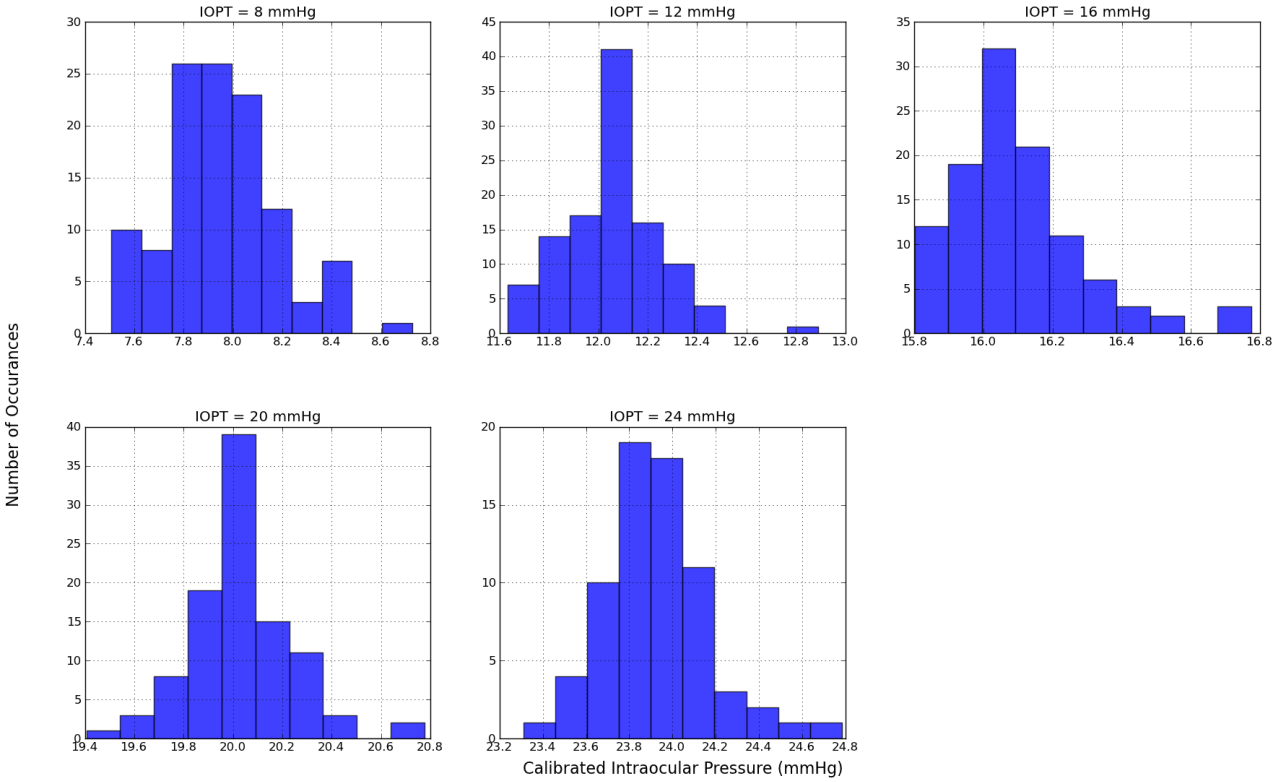

Figure 5.14: Histogram illustrating the predicted IOPC pressure distribution from IOPT when using the Elsheikh inflation data and a fixed limbal boundary from Case 1.

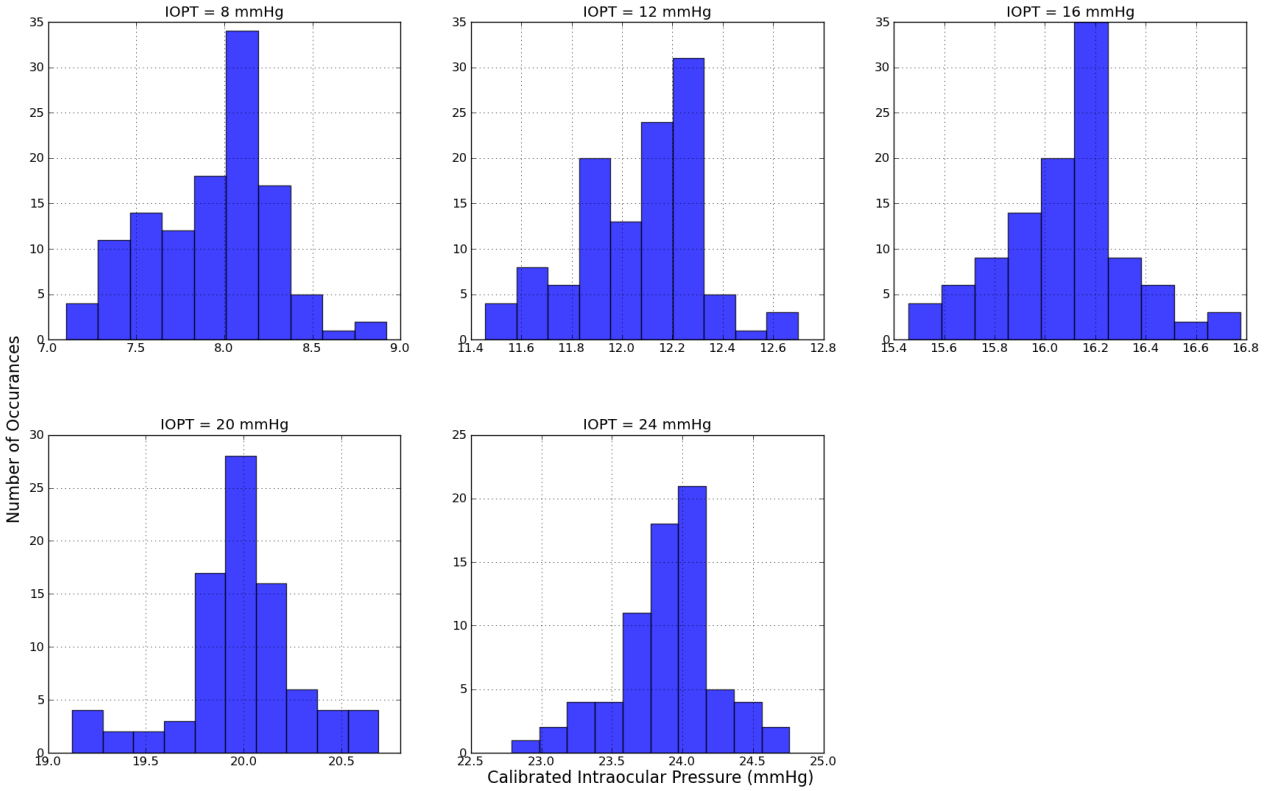

Figure 5.15: Histogram illustrating the predicted IOPC pressure distribution from IOPT when using the Elsheikh inflation data and a 23° limbal boundary from Case 1.

Correction Equation considering two material properties

In the case where only two material properties (k_1 and k_2, the stiffness related to the collagen fibres) were considered, as it was assumed that the ground substance stiffness of the cornea is the same for all corneas (C_{10} is constant), the proposed correction equation (c.f. Equation (5.3)) reduces to:

$$\begin{aligned}\text{IOPC} = a_0 &+ a_1\text{IOPG} + a_2(\text{IOPG} \times R_{\text{ant}}) + a_3(\text{IOPG} \times \text{CCT}) + a_4(\text{IOPG} \times k_1) \\ &+ a_5(\text{IOPG} \times k_2) + a_6\text{IOPG}^2 + a_7 R_{\text{ant}} + a_8(R_{\text{ant}} \times \text{CCT}) + a_9(R_{\text{ant}} \times k_1) \\ &+ a_{10}(R_{\text{ant}} \times k_2) + a_{11}R_{\text{ant}}^2 + a_{12}\text{CCT} + a_{13}(CCT \times k_1) + a_{14}(\text{CCT} \times k_2) \\ &+ a_{15}\text{CCT}^2 + a_{16}k_1 + a_{17}(k_1 \times k_2) + a_{18}k_1^2 + a_{19}k_2 + a_{20}k_2^2\end{aligned} \tag{5.5}$$

where IOPC is the Calibrated IOP, IOPG is the IOP from GAT, R_{ant} is the anterior radius of curvature, CCT is the central corneal thickness and k_1 and k_2 represent the corneal material properties. Using a least squares approach the correction coefficients are obtained for each data set considered, using the material and geometric properties from Case 2. The resulting correction coefficients are shown in Table 5.2 when using half of the randomly sampled simulations for Case 2.

Table 5.2: Correction coefficients obtained by randomly sampling half of the simulations for each data set using the data from Case 2.

Correction Coefficients	**Bryant Data Fixed Boundary**	**Bryant Data 23° Boundary**	**Elsheikh Data Fixed Boundary**	**Elsheikh Data 23° Boundary**
a_0	9.75563855e+00	-5.36115747e+00	4.97957850e+00	6.46782677e-01
a_1	9.94296107e-01	1.05344837e+00	9.00245842e-01	6.81511413e-01
a_2	3.10880315e-02	2.43854988e-03	3.87690209e-02	6.07426701e-02
a_3	8.72107634e-02	-4.88672630e-02	6.99037752e-02	-1.56114485e-01
a_4	8.24446037e-01	-4.38243542e-01	9.46113679e-01	9.35096582e-01
a_5	-5.42132015e-04	2.85012042e-04	-1.36339436e-04	8.14856649e-05
a_6	6.22255552e-03	1.08731775e-02	5.31936279e-03	1.20573027e-02
a_7	6.51583939e-01	3.66875020e+00	5.12041427e-01	1.86832752e+00
a_8	3.11734868e+00	2.77203563e+00	3.11409723e+00	2.90461185e+00
a_9	8.55801555e+00	2.16394635e+01	3.02031755e+00	5.09289095e+00
a_{10}	-5.12529077e-04	3.00075217e-03	-3.39981526e-04	7.38190761e-04
a_{11}	-1.22120473e-01	-3.55163033e-01	-1.11207223e-01	-2.48184803e-01
a_{12}	-3.03562425e+01	-2.23752673e+01	-3.20438733e+01	-2.50066977e+01
a_{13}	-1.22573088e+02	-2.21331000e+01	-5.74352364e+01	-4.15062160e+01
a_{14}	5.87727354e-03	-4.96839143e-03	1.31959768e-03	-3.38558054e-03
a_{15}	-1.22926994e+01	-1.66548676e+01	-1.19718837e+01	-1.44326725e+01
a_{16}	-5.47657790e+01	-1.61967668e+02	-1.57021705e+01	-2.46588935e+01
a_{17}	1.14836429e-01	1.31353411e-01	4.29116804e-03	-3.81484081e-03
a_{18}	-8.45907588e-01	7.36494550e-01	-7.71772716e+00	-8.91893498e+01
a_{19}	-9.07589315e-02	-3.56663053e-02	-1.31247675e-03	-4.87702101e-03
a_{20}	3.35953159e-04	2.33523311e-05	4.40600922e-06	-6.86978622e-07

The predicted IOPC, using the remaining simulations, is shown in Figures 5.16 through 5.23 where it is compared with the IOPG.

From Figures 5.16, 5.17, 5.18 and 5.19 it is clear that the predicted IOPC is an improvement over the IOPG. Also clear is that the predicted IOPC performs better, varying within $0.05 - 0.65$ mmHg of the IOPT, than when considering all three material properties as shown in the previous section (c.f. Figures 5.8-5.11). Also evident, the range of estimated IOPG, and consequently the predicted IOPC, is improved upon for the cases using the Elsheikh inflation test data when compared with Figures 5.10 and 5.11.

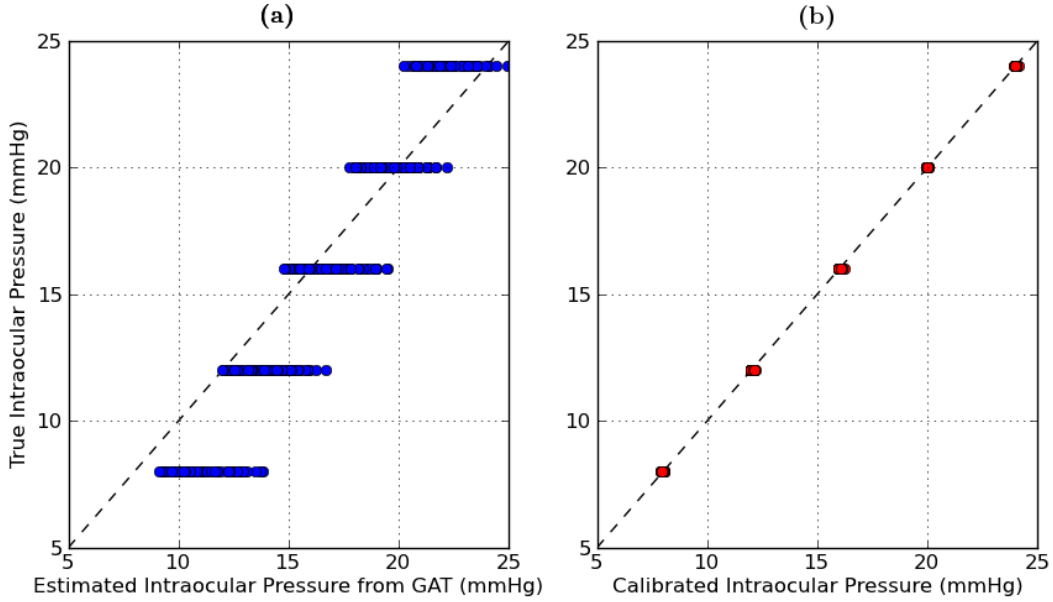

Figure 5.16: Comparison between the (a) IOPT and IOPG as well as (b) IOPT and IOPC using the Bryant inflation data and a fixed limbal boundary condition from Case 2.

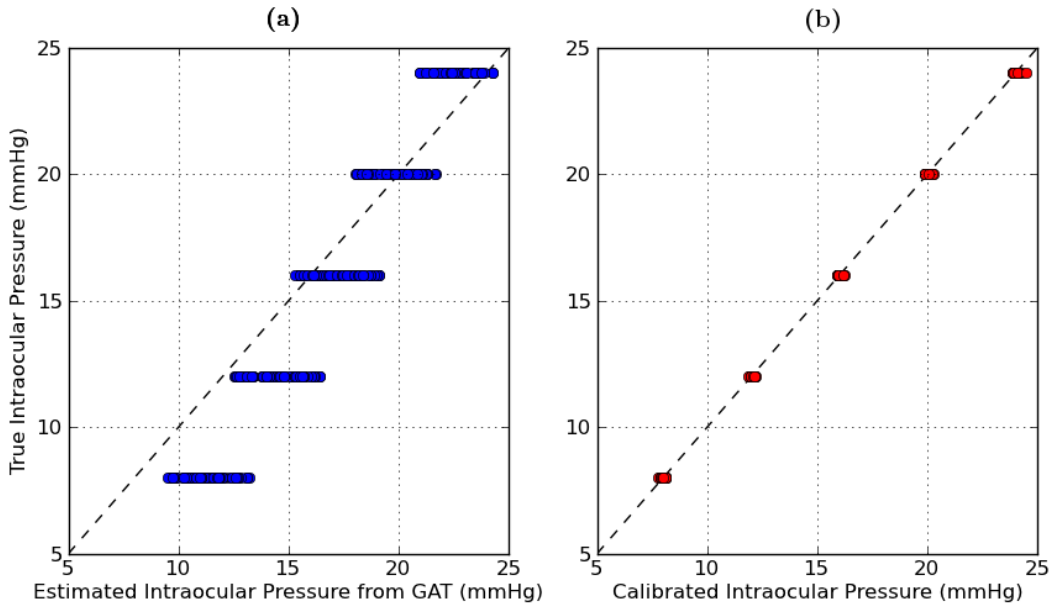

Figure 5.17: Comparison between the (a) IOPT and IOPG as well as (b) IOPT and IOPC using the Bryant inflation data and a 23° limbal boundary condition from Case 2.

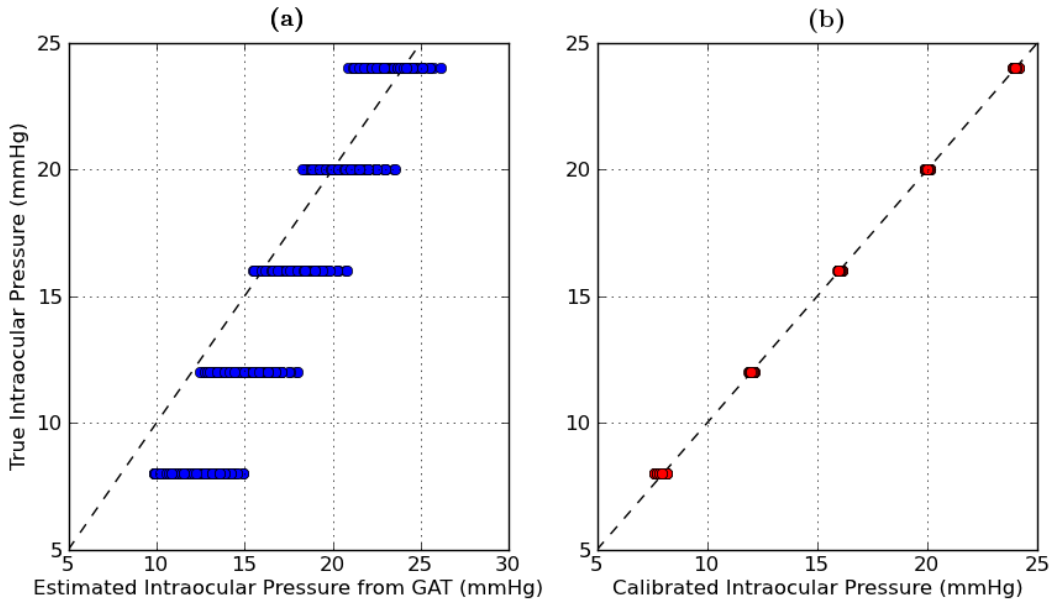

Figure 5.18: Comparison between the (a) IOPT and IOPG as well as (b) IOPT and IOPC using the Elsheikh inflation data and a fixed limbal boundary condition from Case 2.

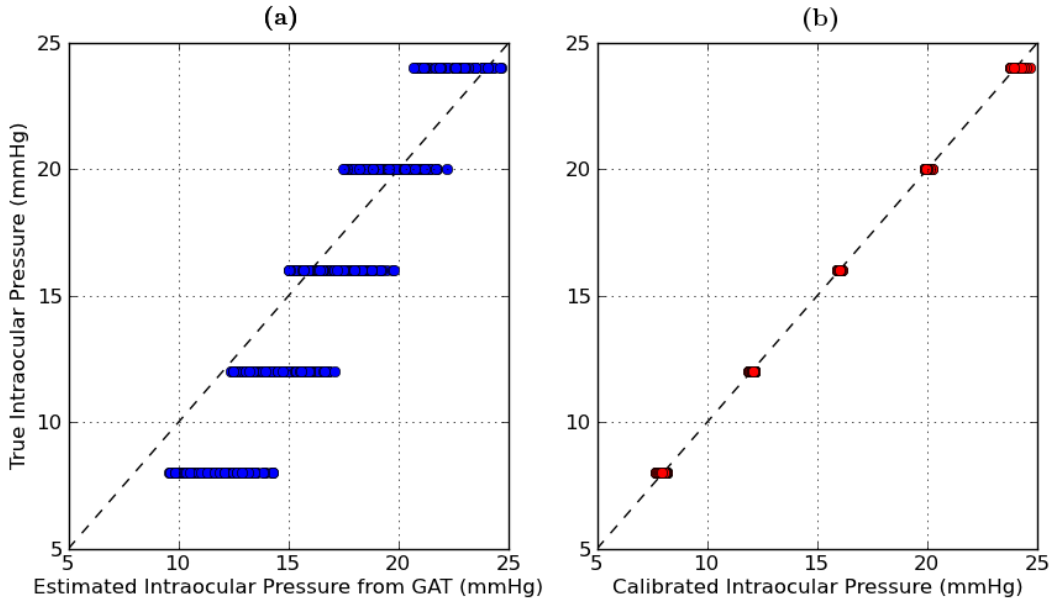

Figure 5.19: Comparison between the (a) IOPT and IOPG as well as (b) IOPT and IOPC using the Elsheikh inflation data and a 23° limbal boundary condition from Case 2.

The histograms in Figures 5.20, 5.21, 5.22 and 5.23 illustrates the distribution of the predicted IOPC for each considered IOP. From these figures, it is seen that the distribution of the predicted IOPC is less than what was observed in the previous section (c.f. Figures 5.12-5.15). For all four the considered data sets, the predicted IOPC varies within a $0.05 - 0.65$ mmHg range from the IOPT.

These results, using the data from Case 2, are a clear improvement upon those from the previous section, where the data from Case 1 was used. In both these proposed correction equations the influence of material properties were included.

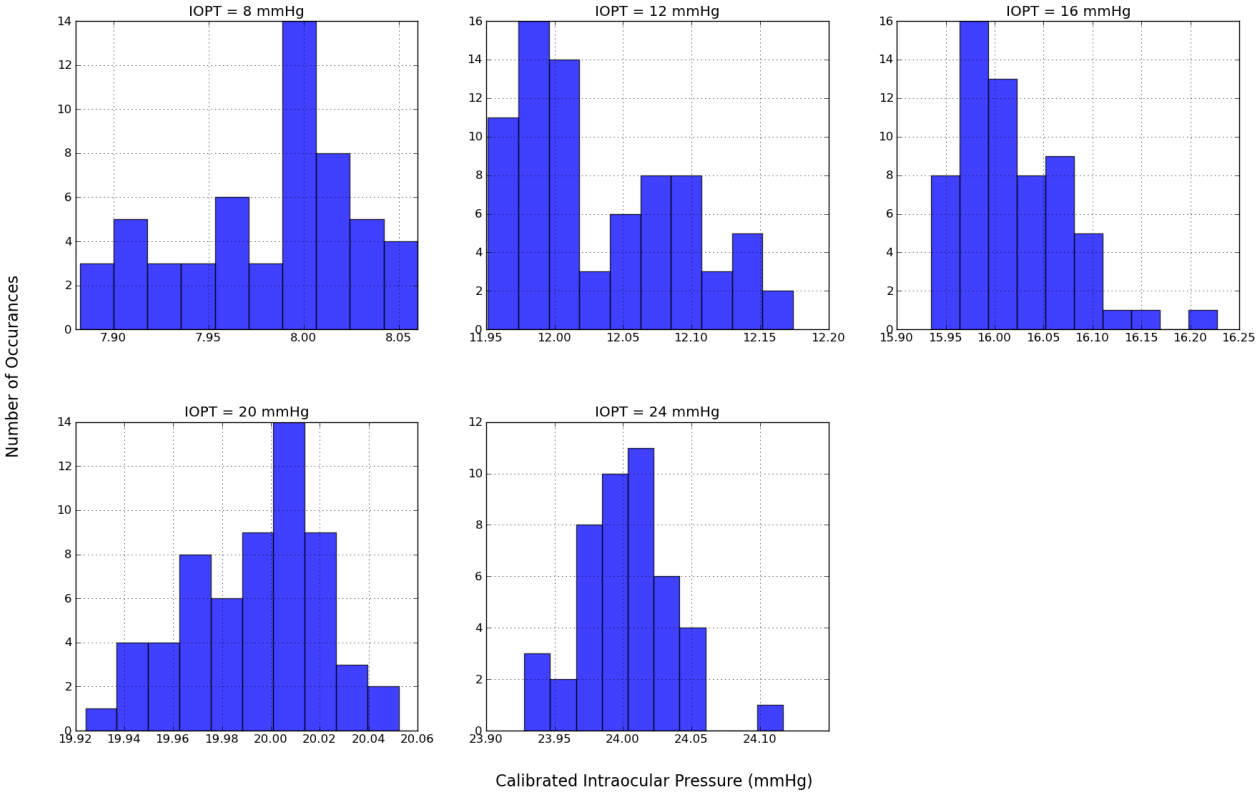

Figure 5.20: Histogram illustrating the predicted IOPC pressure distribution from IOPT when using the Bryant inflation data and a fixed limbal boundary from Case 2.

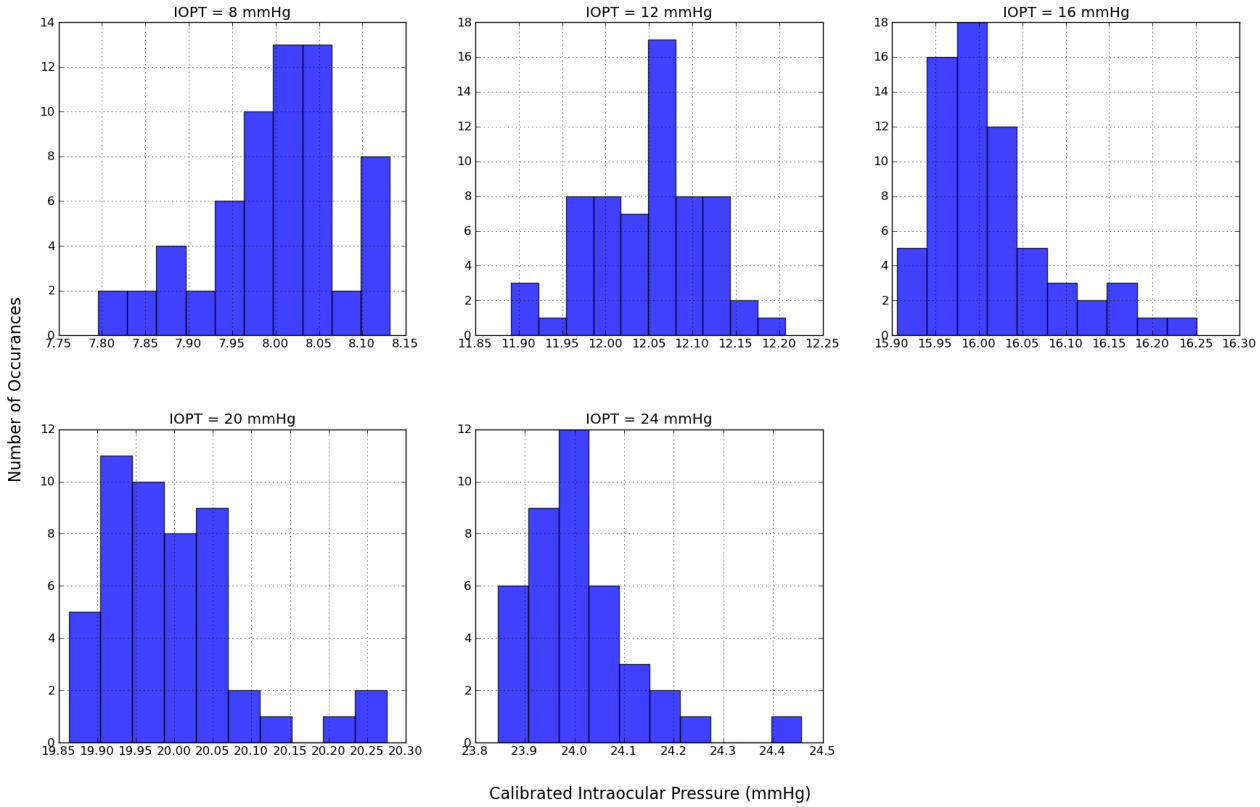

Figure 5.21: Histogram illustrating the predicted IOPC pressure distribution from IOPT when using the Bryant inflation data and a 23° limbal boundary from Case 2.

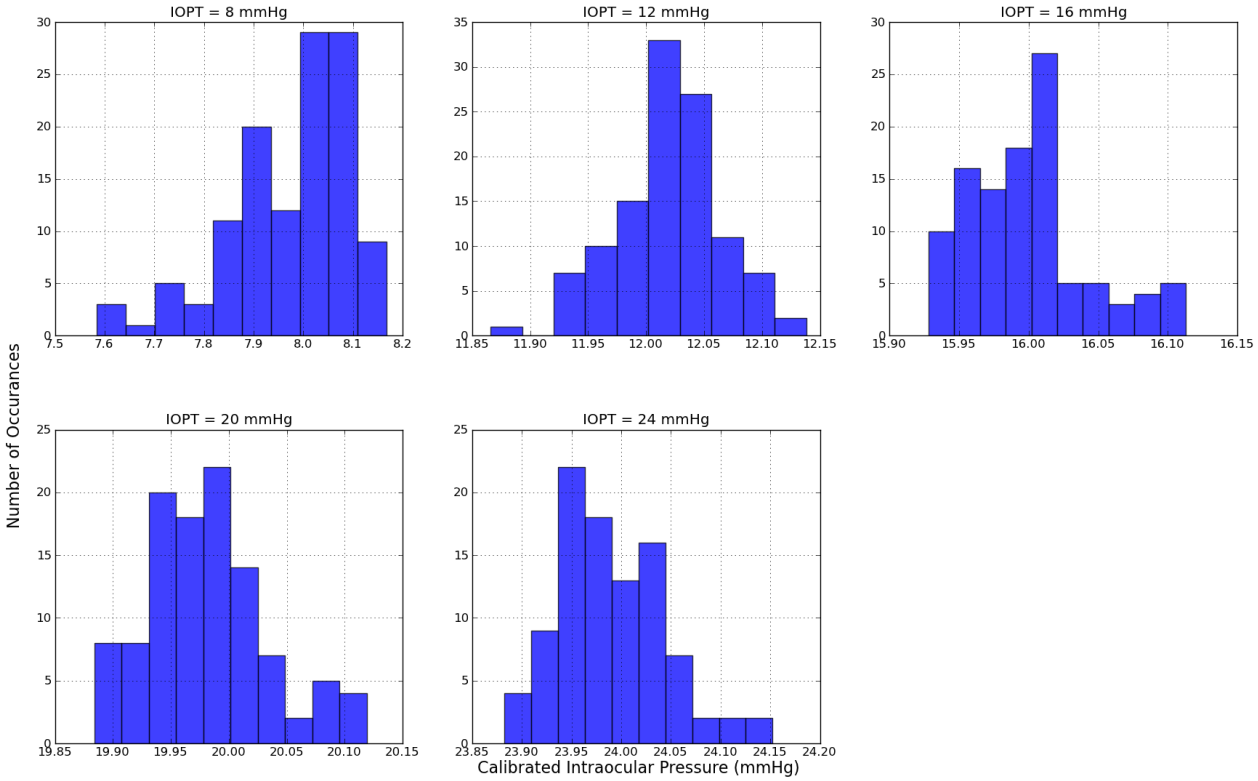

Figure 5.22: Histogram illustrating the predicted IOPC pressure distribution from IOPT when using the Elsheikh inflation data and a fixed limbal boundary from Case 2.

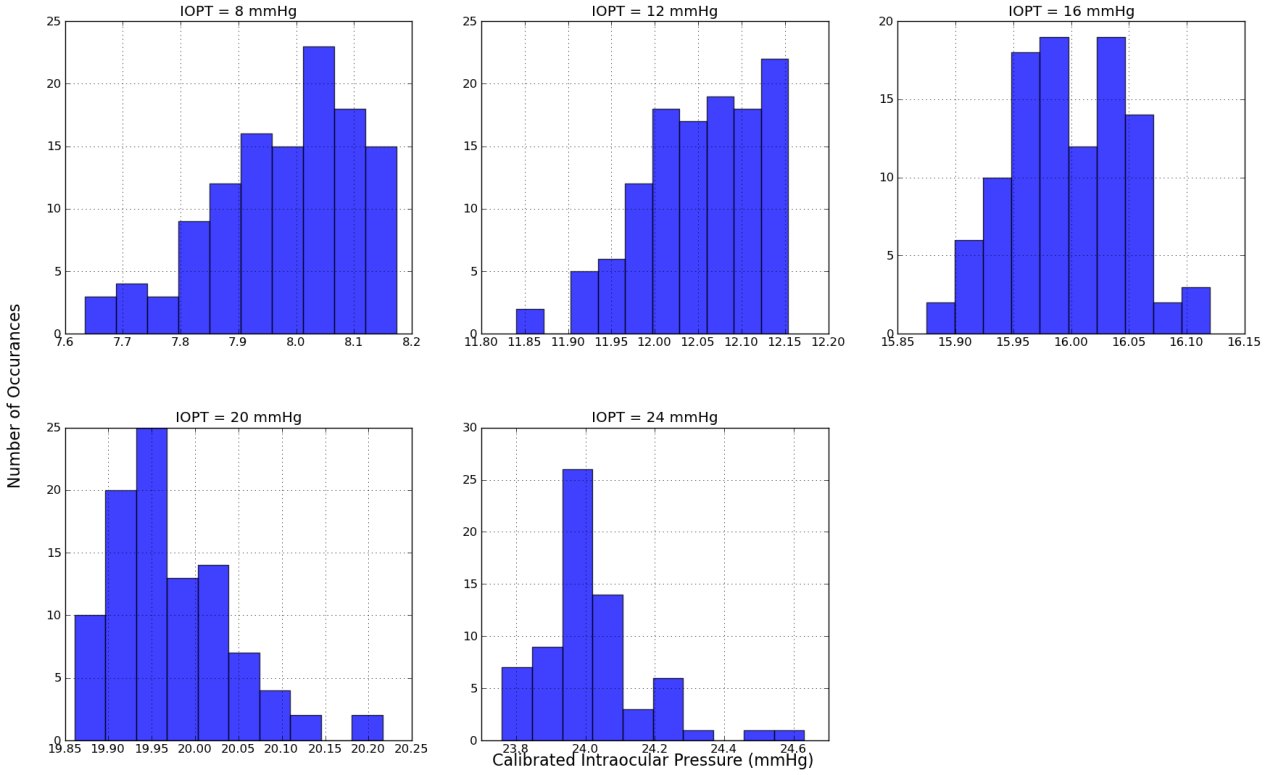

Figure 5.23: Histogram illustrating the predicted IOPC pressure distribution from IOPT when using the Elsheikh inflation data and a 23° limbal boundary from Case 2.

Correction Equation neglecting material properties

At present there are no means to estimate the corneal material properties *in vivo*. For this reason only the influences of the CCT and anterior RoC are considered in this section. When neglecting the influence of material properties (C_{10}, k_1 and k_2), Equation (5.3) reduces to:

$$\begin{aligned} \text{IOPC} = a_0 + a_1\text{IOPG} + a_2(\text{IOPG} \times R_{ant}) + a_3(\text{IOPG} \times CCT) + a_4\text{IOPG}^2 \\ + a_5 R_{\text{ant}} + a_6(R_{\text{ant}} \times \text{CCT}) + a_7 R_{\text{ant}}^2 + a_8\text{CCT} + a_9\text{CCT}^2 \end{aligned} \tag{5.6}$$

where IOPC is the Calibrated IOP, IOPG is the IOP from GAT, R_{ant} is the anterior RoC and CCT is the central corneal thickness. Using this proposed correction equation the correction coefficients are obtained using the data from both Case 1 and Case 2.

(1) Data from Case 1:
Utilizing the data from Case 1 where all three the material properties are included the correction coefficients are obtained and summarised in Table 5.3.

Table 5.3: Correction coefficients obtained by randomly sampling half of the simulations for each data set using the data from Case 1.

Correction Coefficients	**Bryant Data Fixed Boundary**	**Bryant Data 23° Boundary**	**Elsheikh Data Fixed Boundary**	**Elsheikh Data 23° Boundary**
a_0	2.99545955e+01	3.00431856e+00	-1.31192376e+01	2.58941656e+01
a_1	1.86265567e+00	1.21585207e+00	1.79956773e+00	2.50095332e+00
a_2	-2.71618565e-02	3.57061031e-02	-2.15967543e-02	-5.27518851e-02
a_3	2.10827888e-02	4.83819795e-01	1.66438819e-01	-3.21838849e-01
a_4	-1.15088059e-02	-1.46185837e-02	-2.52329469e-02	-2.90593805e-02
a_5	-3.20758287e+00	2.85368667e+00	6.89278230e+00	-6.46068295e+00
a_6	6.20237879e+00	2.59155455e+00	-4.20547537e+00	4.15828802e+00
a_7	8.69230212e-02	-2.81009480e-01	-2.43279294e-01	3.57304134e-01
a_8	-1.00001612e+02	-6.06188155e+01	-7.81893555e+01	-4.98350110e+01
a_9	2.91654801e+01	1.11322751e+01	9.09192554e+01	9.43296650e+00

The estimated IOPG and predicted IOPC along with each of the histograms, illustrating the variation in predicted IOPC from IOPT, are shown in Figures 5.24 through 5.31.

It is apparent from Figures 5.24, 5.25, 5.26 and 5.27 that the proposed correction equation does not perform well when the influence of material properties are neglected. This is evident when compared to the results from the previous sections, where the influence of material properties were included. Also noticeable is when considering Elsheikh inflation test data the variation in predicted IOPC is $1.0 - 14.1$ mmHg compared with a variation of $0.7 - 5.0$ mmHg when using Bryant inflation test data.

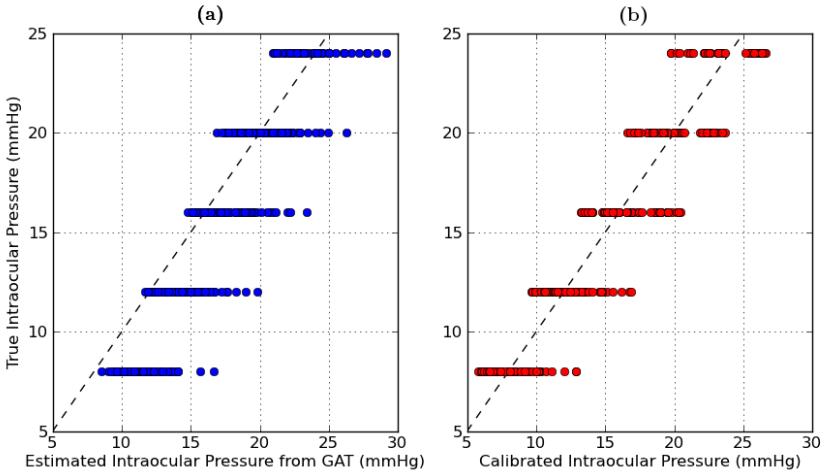

Figure 5.24: Comparison between the (a) IOPT and IOPG as well as (b) IOPT and IOPC using the Bryant inflation data and a fixed limbal boundary condition using the data from Case 1.

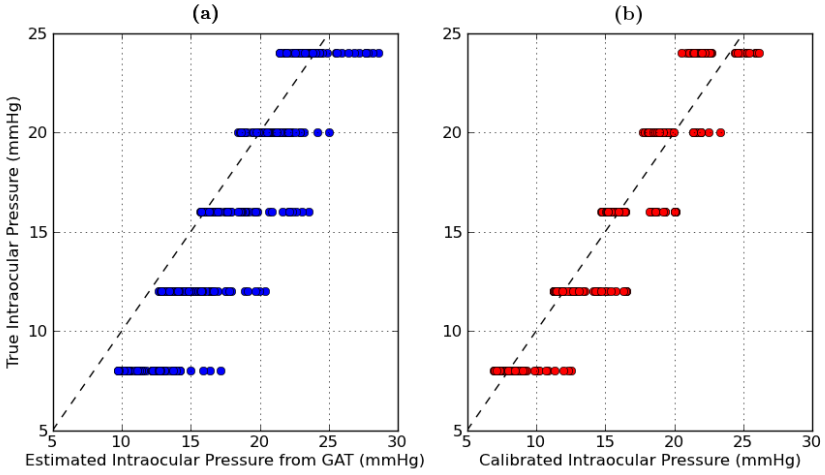

Figure 5.25: Comparison between the (a) IOPT and IOPG as well as (b) IOPT and IOPC using the Bryant inflation data and a 23° limbal boundary condition using the data from Case 1.

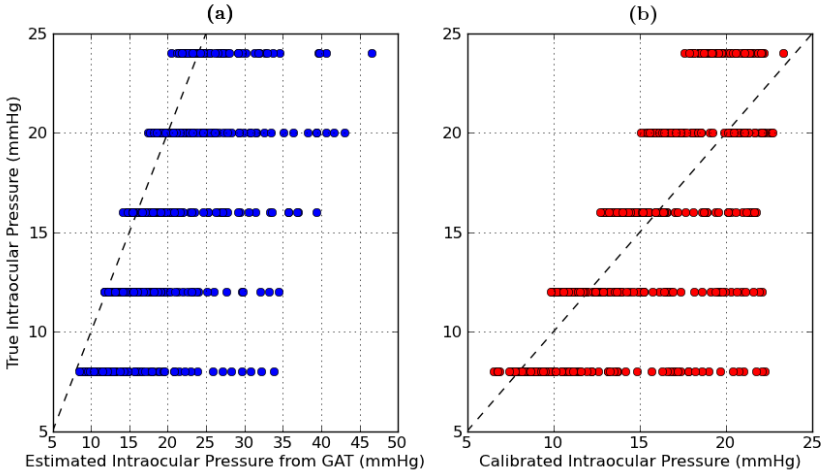

Figure 5.26: Comparison between the (a) IOPT and IOPG as well as (b) IOPT and IOPC using the Elsheikh inflation data and a fixed limbal boundary condition using the data from Case 1.

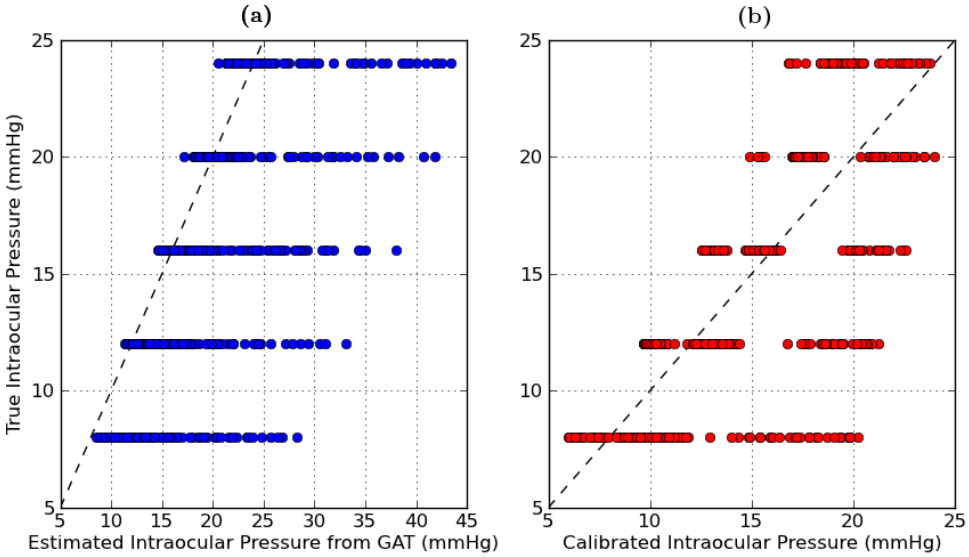

Figure 5.27: Comparison between the (a) IOPT and IOPG as well as (b) IOPT and IOPC using the Elsheikh inflation data and a 23° limbal boundary condition using the data from Case 1.

From the histograms, Figures 5.28-5.31, it is seen that the variation in predicted IOPC increases approximately by a factor $9-11$ compared to the results in a previous section where the influence of material properties was included (c.f. Figure 5.12 to 5.15). The variation in predicted IOPC is approximately $0.7-14.1$ mmHg from IOPT for all four cases considered, that is Bryant inflation data with a fixed limbal boundary condition, Bryant inflation data with a 23° boundary condition, Elsheikh inflation data with a fixed limbal boundary condition and Elsheikh inflation data with a 23° limbal boundary condition.

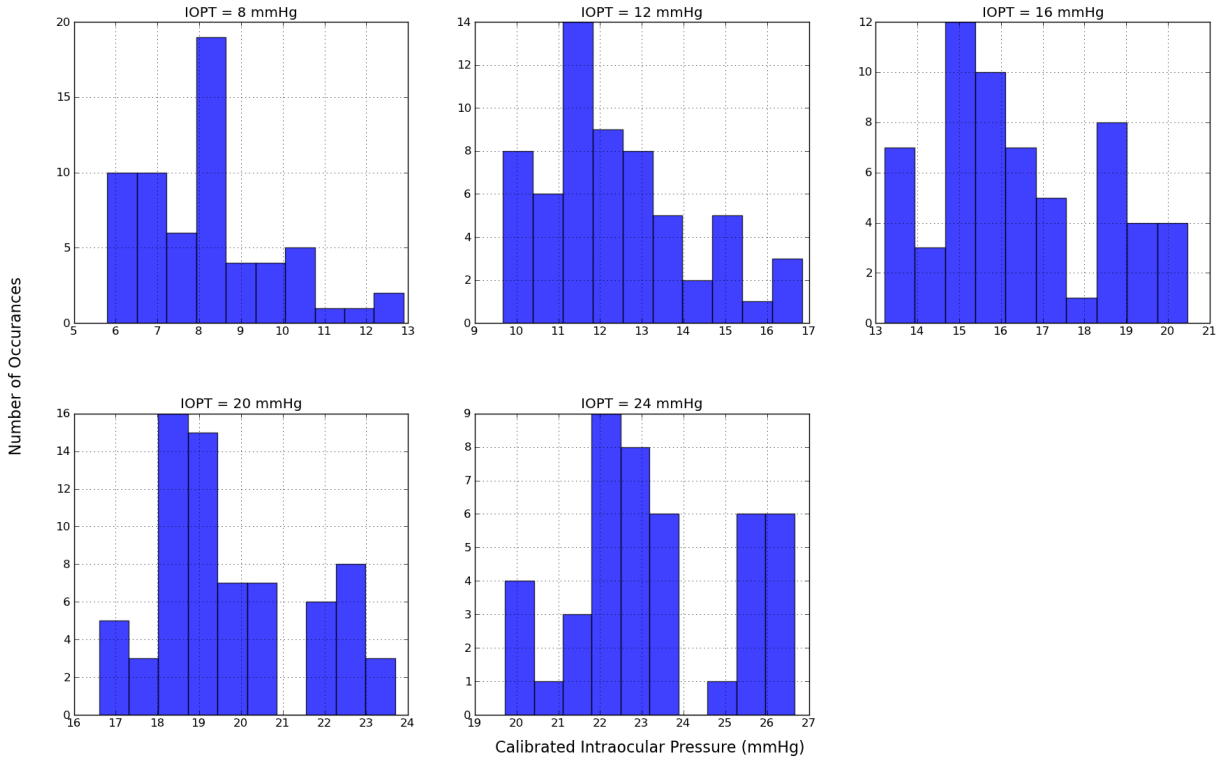

Figure 5.28: Histogram illustrating the predicted IOPC pressure distribution from IOPT when using the Bryant inflation data and a fixed limbal boundary using the data from Case 1.

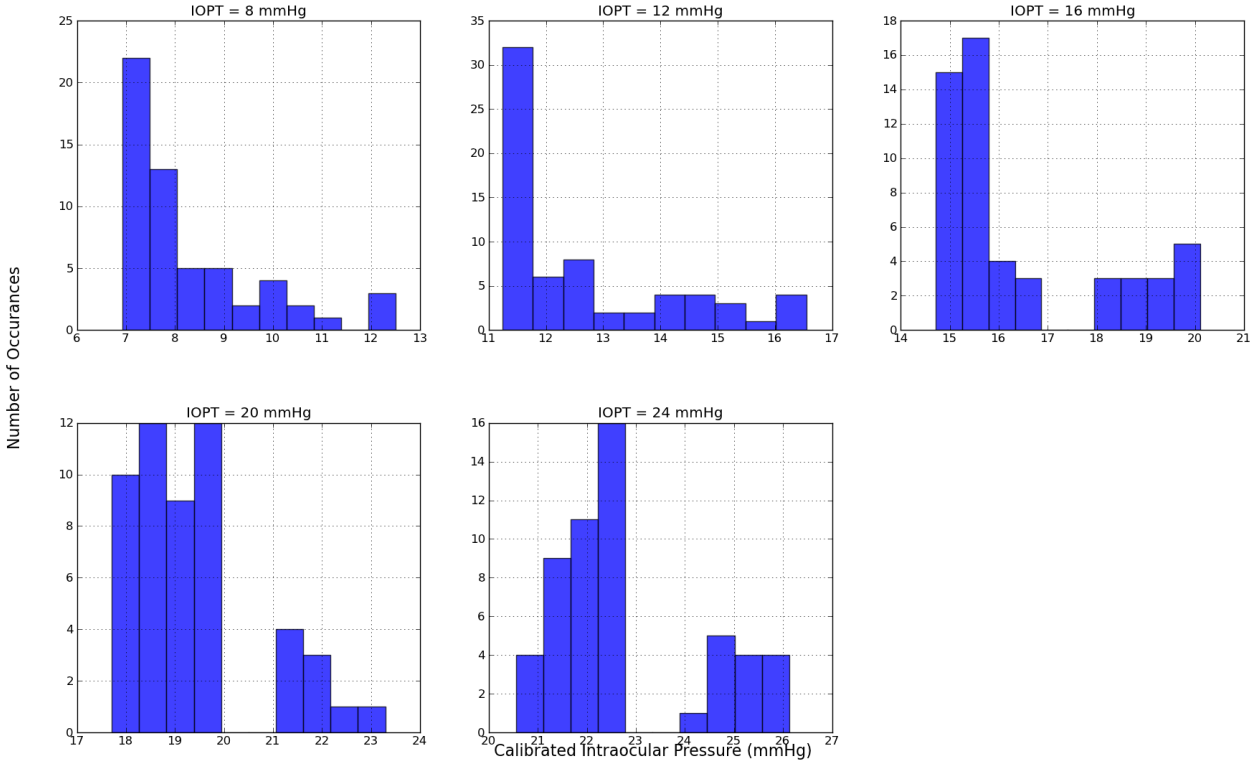

Figure 5.29: Histogram illustrating the predicted IOPC pressure distribution from IOPT when using the Bryant inflation data and a 23° limbal boundary using the data from Case 1.

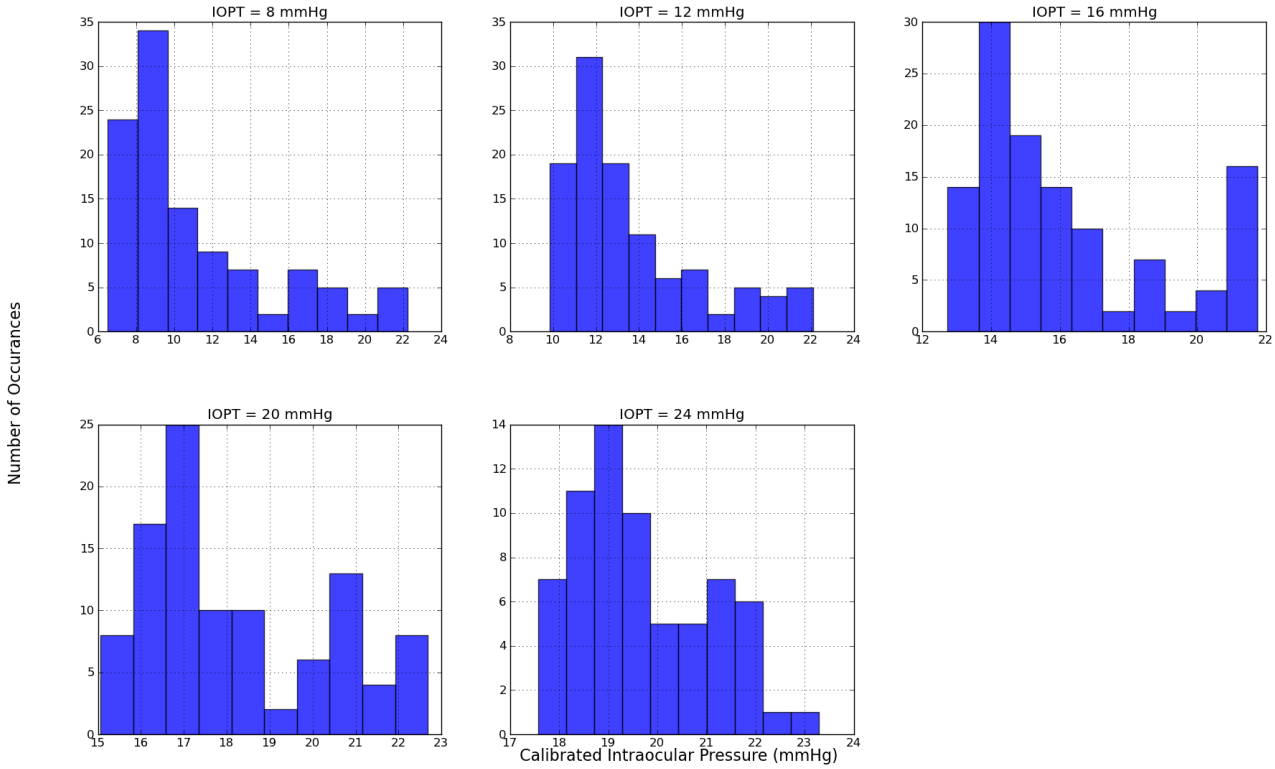

Figure 5.30: Histogram illustrating the predicted IOPC pressure distribution from IOPT when using the Elsheikh inflation data and a fixed limbal boundary using the data from Case 1.

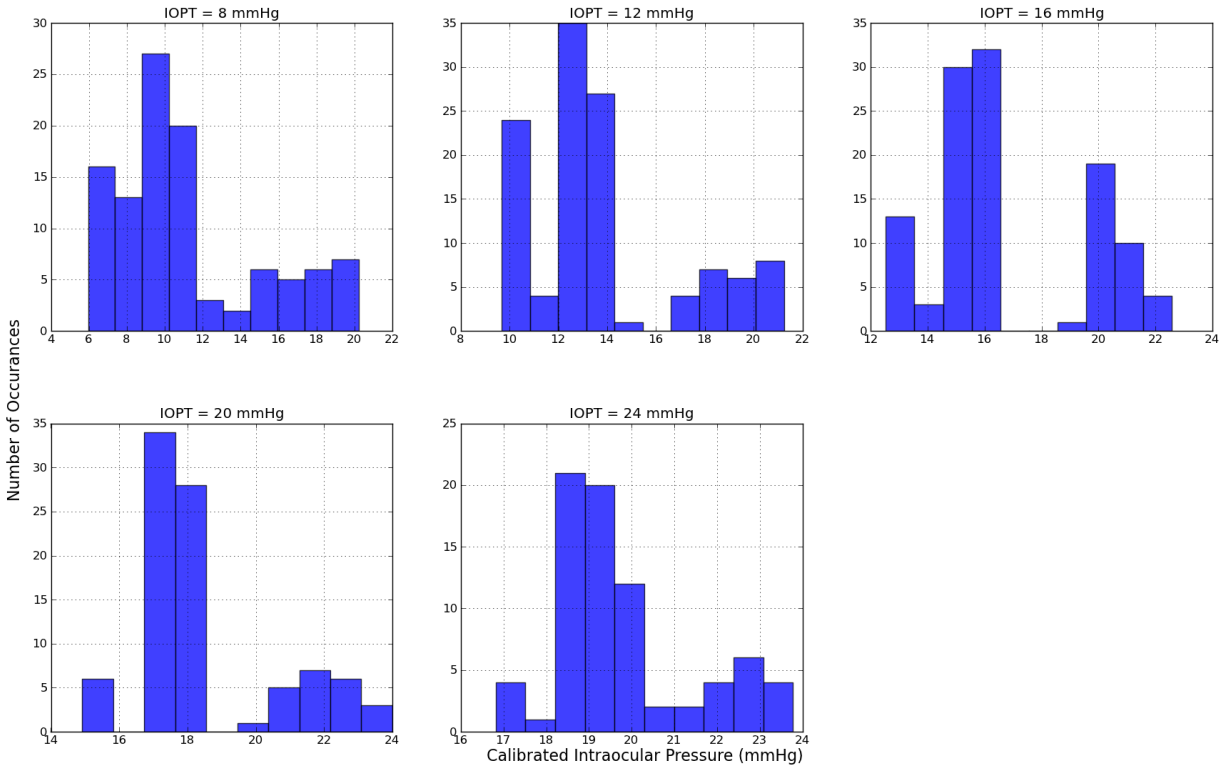

Figure 5.31: Histogram illustrating the predicted IOPC pressure distribution from IOPT when using the Elsheikh inflation data and a 23° limbal boundary using the data from Case 1.

(2) Data from Case 2:

Using the data from Case 2, where only two material properties (k_1 and k_2) were considered and the third assumed constant (C_{10}), the obtained correction coefficients are summarised in Table 5.4.

Table 5.4: Correction coefficients obtained by randomly sampling half of the simulations for each data set using the data from Case 2.

Correction Coefficients	**Bryant Data Fixed Boundary**	**Bryant Data 23° Boundary**	**Elsheikh Data Fixed Boundary**	**Elsheikh Data 23° Boundary**
a_0	2.85902600e+00	-1.46650517e+01	9.06057545e+00	-6.79895827e+00
a_1	1.10372905e+00	1.02128059e+00	9.23904613e-01	8.13570568e-01
a_2	9.74806230e-03	1.38457401e-02	4.01070267e-02	5.18472258e-02
a_3	2.21206871e-01	-1.50278873e-01	-2.20977159e-01	-1.25462179e-01
a_4	3.75396865e-03	1.23389229e-02	9.20909409e-03	1.19016195e-02
a_5	1.42911942e+00	4.45645879e+00	-1.19208392e+00	3.32495661e+00
a_6	3.93814332e+00	2.02403610e+00	2.76516397e+00	3.07836221e+00
a_7	-1.71064730e-01	-3.37424201e-01	1.26029488e-02	-3.02994671e-01
a_8	-4.49477457e+01	-1.40477080e+01	-2.78483997e+01	-2.90207583e+01
a_9	-8.42017664e+00	-1.85788359e+01	-1.19477430e+01	-1.55196859e+01

Figures 5.32 through 5.35 compare the IOPG and the IOPC with the IOPT. It is noted that the predicted IOPC is not only an improvement upon the estimated IOPG, but also upon the results when using the data from Case 1 (c.f. Figures 5.24-5.27). The results, however, are not as good as when the influence of material properties are accounted for (c.f. Figure 5.16-5.19).

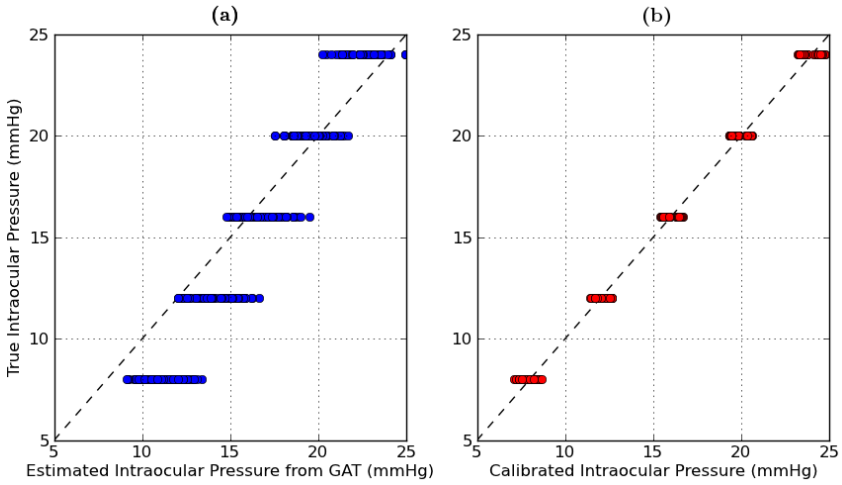

Figure 5.32: Comparison between the (a) IOPT and IOPG as well as (b) IOPT and IOPC using the Bryant inflation data and a fixed limbal boundary condition using the data from Case 2.

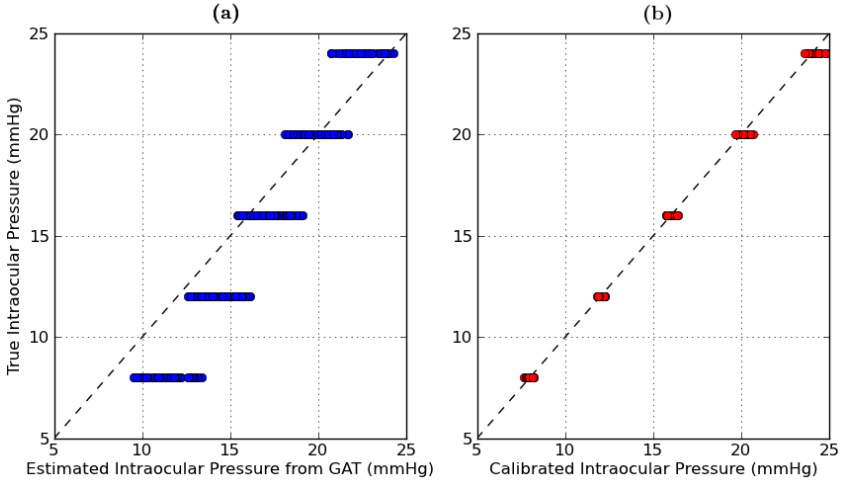

Figure 5.33: Comparison between the (a) IOPT and IOPG as well as (b) IOPT and IOPC using the Bryant inflation data and a 23° limbal boundary condition using the data from Case 2.

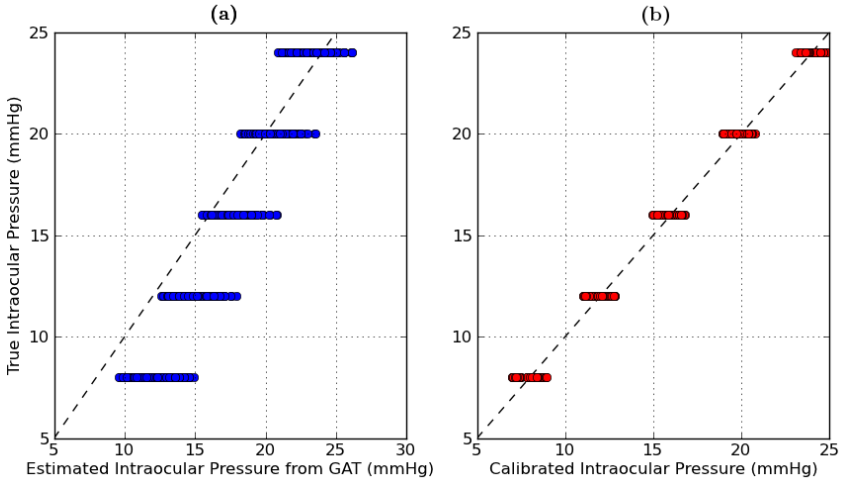

Figure 5.34: Comparison between the (a) IOPT and IOPG as well as (b) IOPT and IOPC using the Elsheikh inflation data and a fixed limbal boundary condition using the data from Case 2.

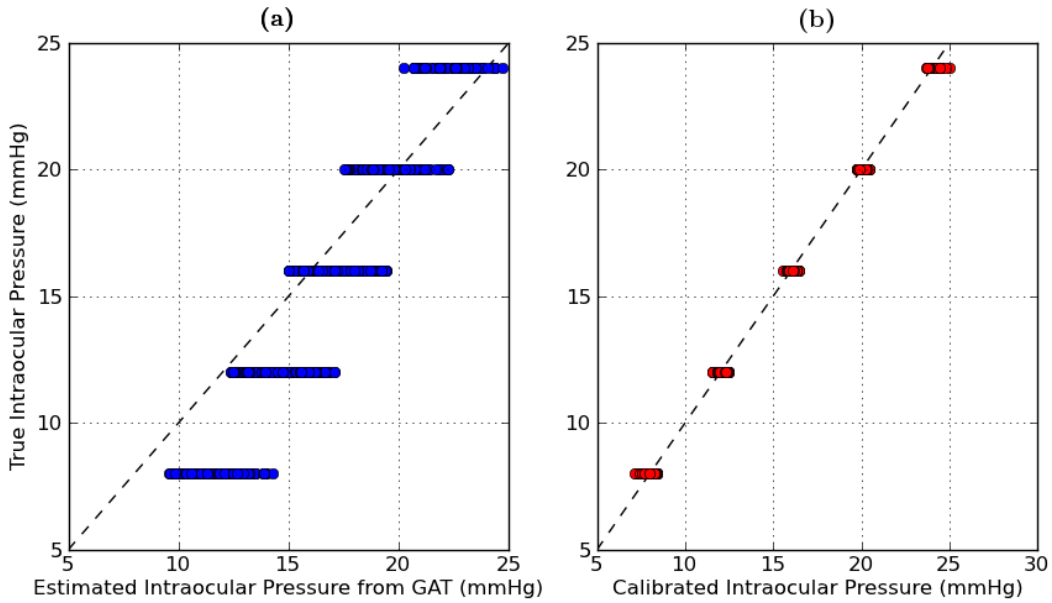

Figure 5.35: Comparison between the (a) IOPT and IOPG as well as (b) IOPT and IOPC using the Elsheikh inflation data and a 23° limbal boundary condition using the data from Case 2.

The predicted IOPC varies approximately by $0.18 - 1.10$ mmHg from the IOPT for the considered data sets, which is approximately a factor 2.0 larger than when the influence of material properties are accounted for (c.f. Figures 5.20-5.23). This result is also an improvement from using the data from Case 1 (c.f. Figures 5.28-5.31), but still not as good as when the influence of the material properties are included in the correction equation.

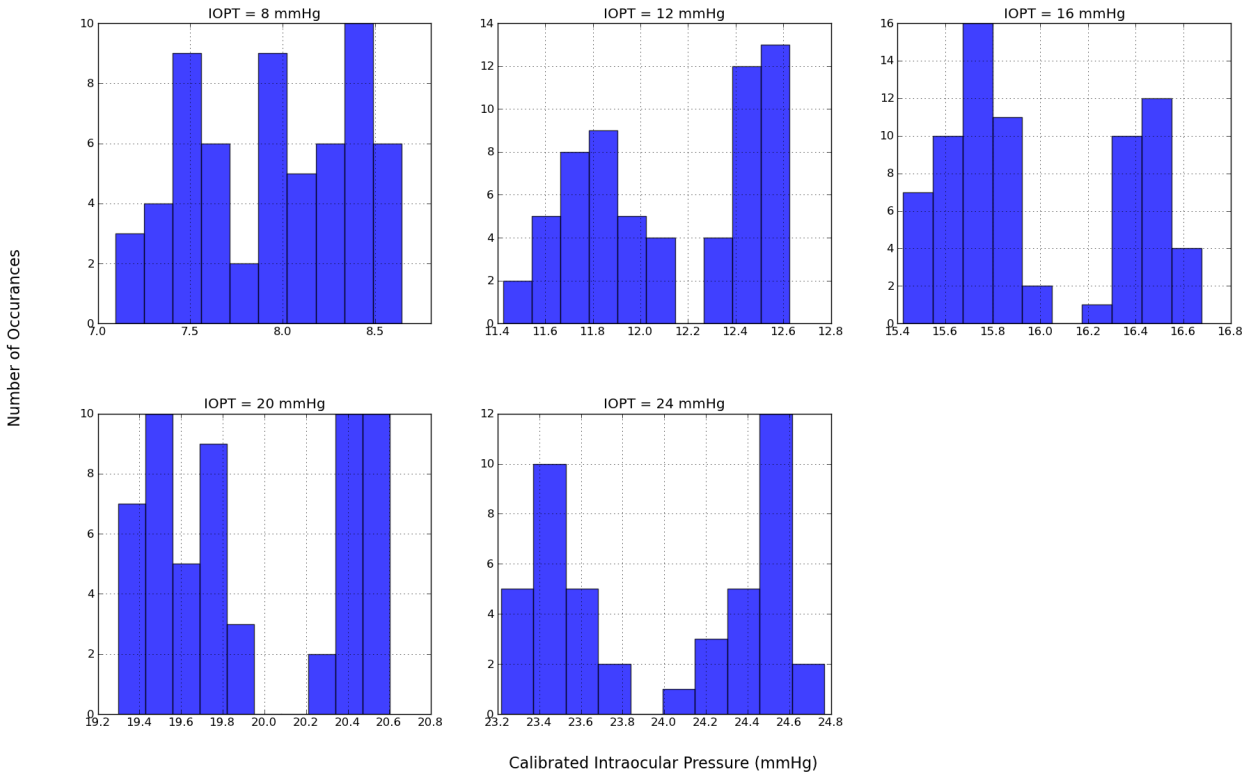

Figure 5.36: Histogram illustrating the predicted IOPC pressure distribution from IOPT when using the Bryant inflation data and a fixed limbal boundary using the data from Case 2.

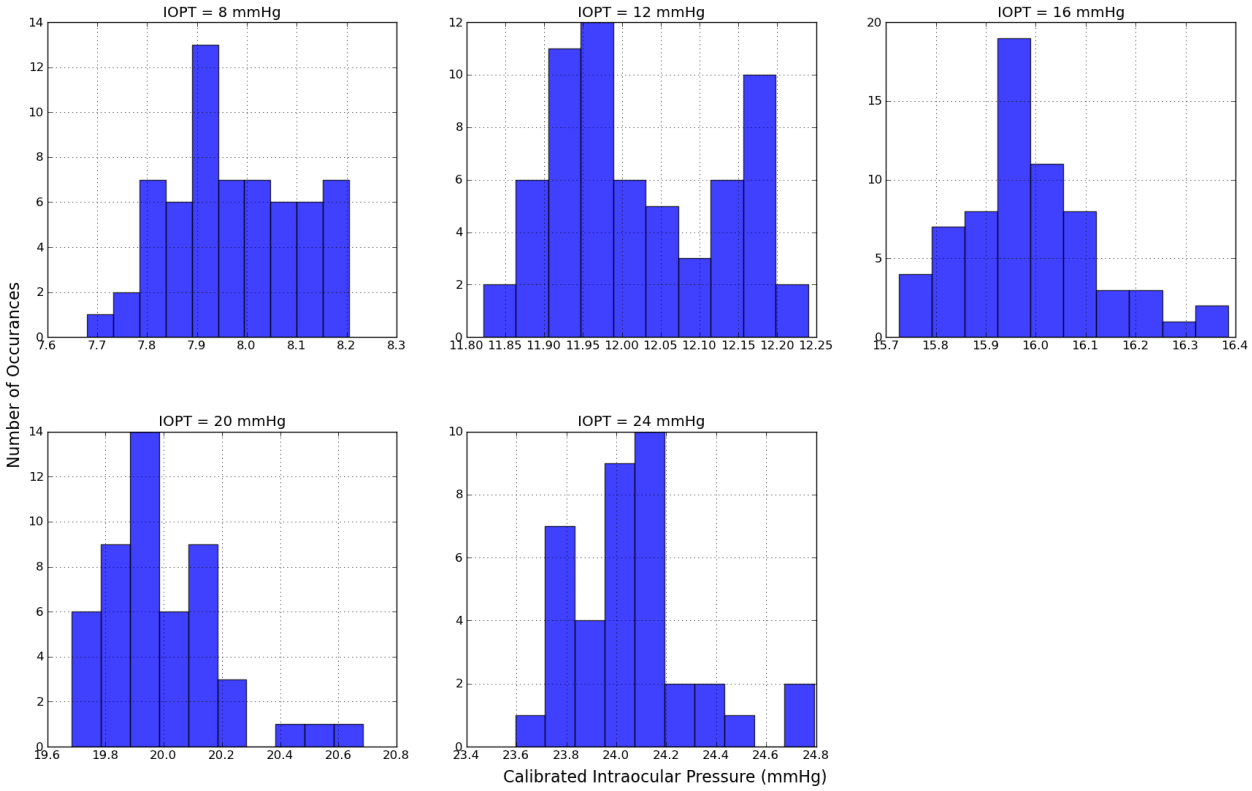

Figure 5.37: Histogram illustrating the predicted IOPC pressure distribution from IOPT when using the Bryant inflation data and a 23° limbal boundary using the data from Case 2.

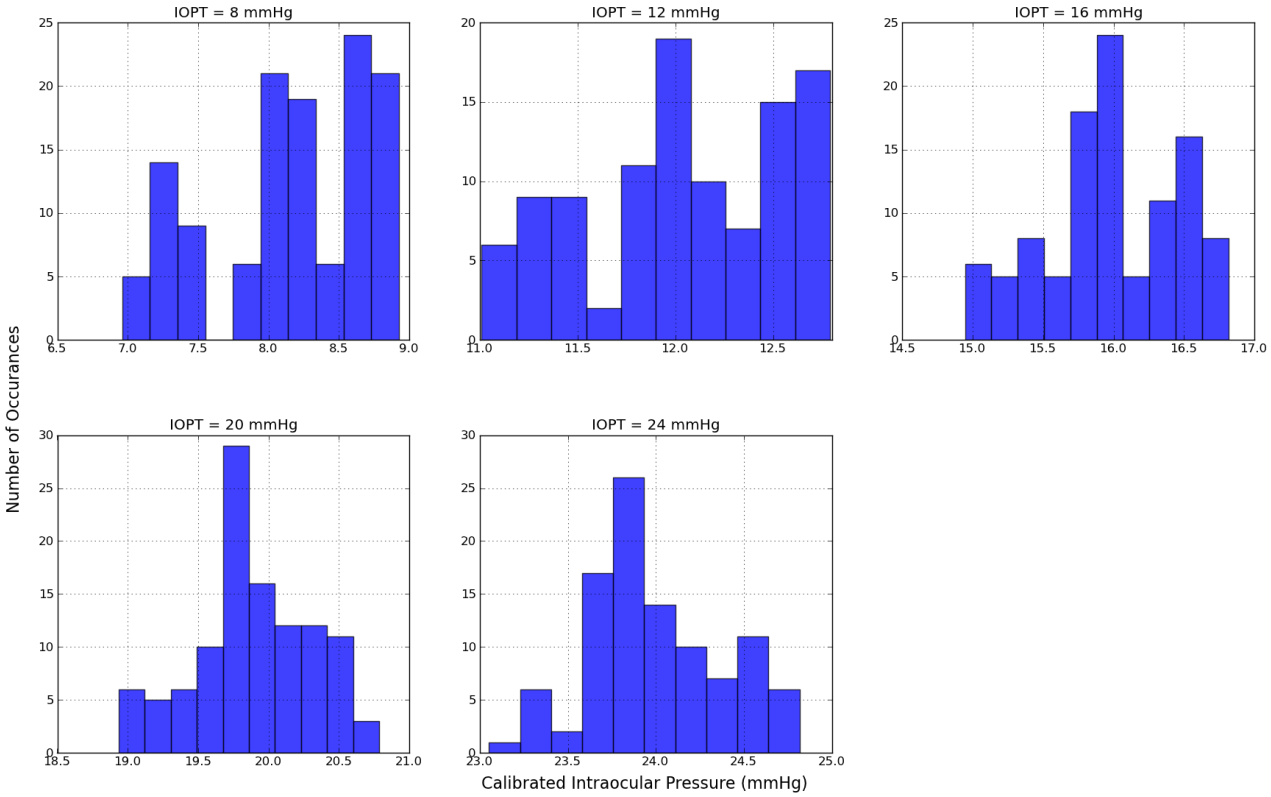

Figure 5.38: Histogram illustrating the predicted IOPC pressure distribution from IOPT when using the Elsheikh inflation data and a fixed limbal boundary using the data from Case 2.

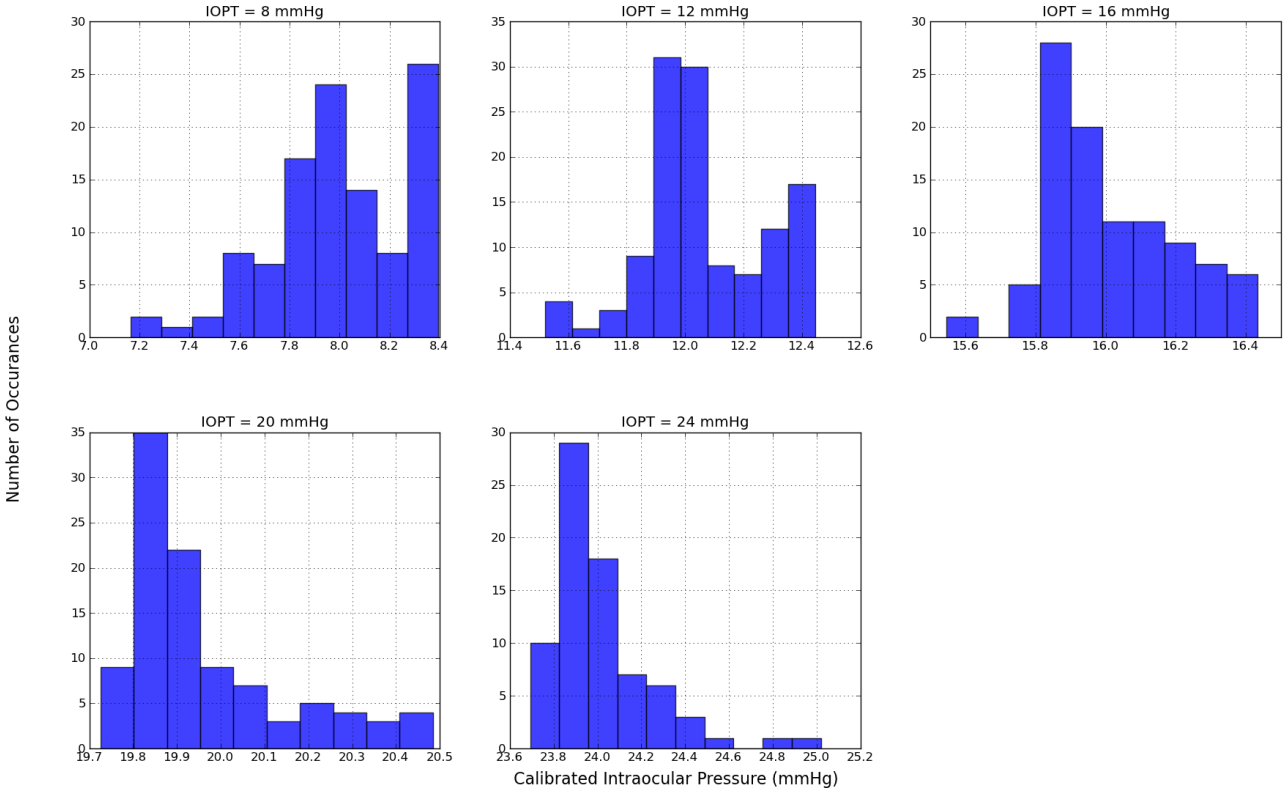

Figure 5.39: Histogram illustrating the predicted IOPC pressure distribution from IOPT when using the Elsheikh inflation data and a 23° limbal boundary using the data from Case 2.

5.5.2 Comparing Correction Equations

The proposed correction equation (c.f. Equation (5.6)), neglecting the influence of material properties and using the data from Case 1 and Case 2, is compared to several other correction equations obtained from literature (Orssengo and Pye, 1999; Chihara, 2008; Kwon *et al.*, 2008; Elsheikh *et al.*, 2011; Guzmán *et al.*, 2013) and are listed in Table 5.5.

To compare the various correction equations the values for a normal cornea are used, that is a CCT of 0.55 mm, an anterior RoC of 7.77 mm and an IOPG of 8, 12, 16, 20 and 24 mmHg. The results of this, using the data from both Cases 1 and 2, are shown in Figures 5.40 and 5.41 as well as Table 5.6.

It is evident from Figures 5.40 and 5.41 that when using the data from Case 1 to compare the correction equations the proposed correction equation performs worse than when using the data from Case 2. This is also noted with other correction equations, such as Guzmán *et al.* (2013), Kwon *et al.* (2008), Elsheikh *et al.* (2011), Shimmyo (cited in Chihara, 2008) and Chihara (2008), which differ in IOPC depending on the data used. Figure 5.41 illustrates that when using the data from Case 2 the correction equations mostly perform better than when using the data from Case 1 (c.f. Figure 5.40).

Table 5.5: Proposed correction equations as obtained from various literature sources. (CCT and R are given in mm with IOPG and IOPT in mmHg)

Source	Year	Proposed Correction Equation	Notes
Whitacre (cited in Chihara, 2008)	1993	$\text{IOPC} = \text{IOPG} + 12.28 - 0.02283\text{CCT}/10^3$	$\text{CCT} = 0.390 - 0.570$ mm
Orssengo and Pye (1999)	1999	$\text{IOPC} = \frac{\text{IOPG}}{\left(\frac{42.4(\text{CCT}/10^3)^2}{10^4 A(\mu)(1000R - \text{CCT}/(2.0\times10^3))} + \frac{3.97(10^3 R - \text{CCT}/(2.0\times10^3))\text{CCT}/10^3}{A(\mu)\times10^8}\right)}$ $A(\mu) \cong 0.433047 - 0.001859\mu - 0.228169\mu^2 + 0.237752\mu^3 - 0.135992\mu^4 + 0.032129\mu^5$ where $\mu = \frac{r_0}{\sqrt{(R - \frac{CCT}{2})CCT}} \times \sqrt[1/4]{12(1-\nu)^2}$	$A(\mu) = 0.326 - 0.342$ when $R = 7.7$ mm and $\text{CCT} = 0.45 - 0.60$ mm For $0 \leq \mu \leq 1.4$
Foster (cited in Chihara, 2008)	2000	$\text{IOPC} = 1.08\text{IOPG} + 5.5$	$\text{CCT} = 0.529 \pm 0.048$ mm
Feltigen (cited in Chihara, 2008)	2001	$\text{IOPC} = \text{IOPG} + 3.43$	$\text{CCT} = 0.580 \pm 0.054$ mm
Shimmyo (cited in Chihara, 2008)	2003	$\text{IOPC} = \text{IOPG} + \frac{(550 - \text{CCT})/10^3}{18e^{-0.005\text{IOPG}} + 0.8(R - 7.848837)}$	$\text{CCT} = 0.553 \pm 0.034$ mm
Kniestedt (cited in Chihara, 2008)	2005	$\text{IOPC} = \text{IOPG} + 3.43 \pm 1.24$	$\text{CCT} = 0.545 \pm 0.038$ mm
Kohlhaas (cited in Chihara, 2008)	2006	$\text{IOPC} = \text{IOPG} + 23.28 - 0.0423(\text{CCT}/10^3)$	$\text{CCT} = 0.569 \pm 0.044$ mm

Continues on the following page

Table 5.5 - *Continued from previous page*

Source	Year	Proposed Correction Equation	Notes
Chihara (2008)	2008	$\text{IOPC} = \frac{\text{IOPG}+4.15}{\frac{19.09(\text{CCT}/10^3)^2}{A(\mu)(R\times10^3-\text{CCT}/(2.0\times10^3))\times10^4}} + 1$	$A(\mu) = 0.326 - 0.342$ when $R =$ 7.7 mm and CCT $= 0.45 - 0.60$ mm
Kwon *et al.* (2008)	2008	$\text{IOPC} = A \cdot \text{IOPG} + B$ where $A = 0.0003(\text{CCT}/10^3) + 0.917$ $B = -0.0239(\text{CCT}/10^3) + 10.105$	CCT $= 0.436,\ 0.536,\ 0.636$ mm $E = 0.23$ MPa IOPG $= 8.8 - 25.0$ mmHg
Elsheikh *et al.* (2011)	2011	$\text{IOPC} = \text{IOPT}(A_{\text{CCT}} \times A_R \times A_{\text{Age}} \times A_{\text{IOPG}})$ where $A_{\text{CCT}} = 0.68(\text{CCT} - 0.520)^2 + 1.12(\text{CCT} - 0.520) + 1.0$ $A_R = 0.06(R - 7.8)$ $A_{\text{Age}} = 0.3 \times 10^{-6}\text{age}^3 - 88 \times 10^{-6}\text{age}^2 + 0.0085\text{age} + 0.815$ $A_{\text{IOPG}} = 1.427(\text{IOPG} + 3.373)^{-0.119}$	CCT $= 0.455 - 0.609$ mm $6.57 \leq R \leq 8.15$ Age $= 35 - 87$ years IOPG $= 14 - 42$ mmHg
Guzmán *et al.* (2013)	2013	$\text{IOPC} = 0.931R - 30.4\text{CCT} + 1.59\text{IOPG}$	$E = 0.07$ MPa CCT $= 0.5 - 0.6$ mm $R = 6.4 - 8.0$ mm IOPG $= 10 - 20$ mmHg
Current Study	2013	$\text{IOPC} = a_0 + a_1\text{IOPG} + a_2(\text{IOPG} \times R_{\text{ant}}) + a_3(\text{IOPG} \times \text{CCT}) + a_4\text{IOPG}^2 + a_5R_{\text{ant}} + a_6(R_{\text{ant}} \times \text{CCT}) + a_7R_{\text{ant}}^2 + a_8\text{CCT} + a_9\text{CCT}^2$	c.f. Table 5.3 and Table 5.4 for the correction coefficients

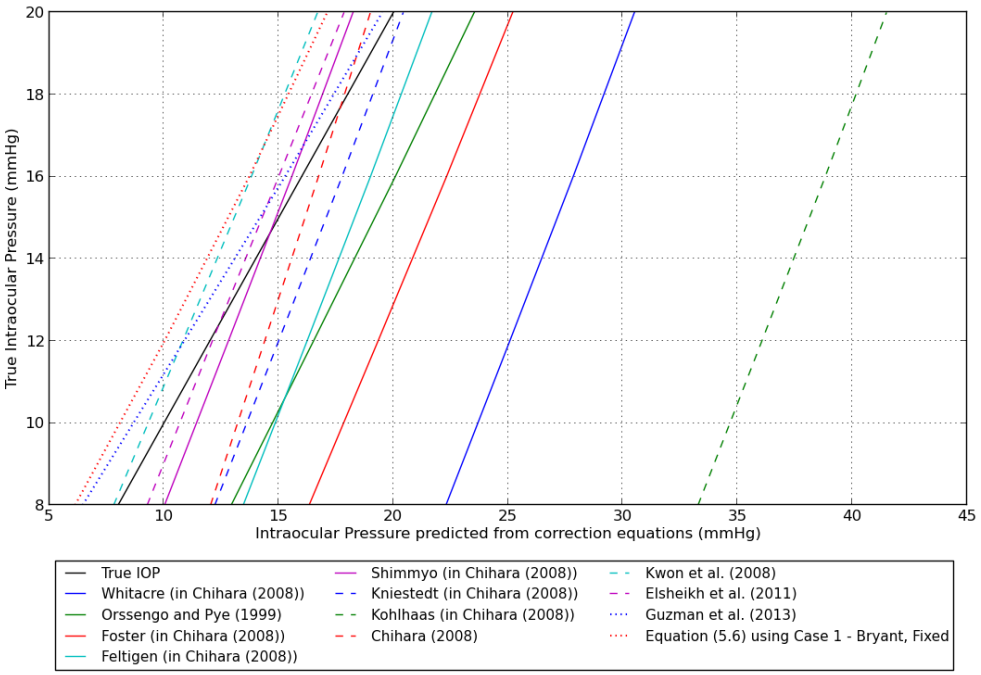

Figure 5.40: Comparison of the proposed correction equation to correction equations obtained from literature for what is considered a normal cornea in this study (CCT = 0.55 mm, R_{ant} = 7.77 mm, IOPG = 8, 12, 16, 20 and 24 mmHg) using the data from Case 1 when considering Bryant inflation data and a fixed limbal boundary condition, material data set 3.

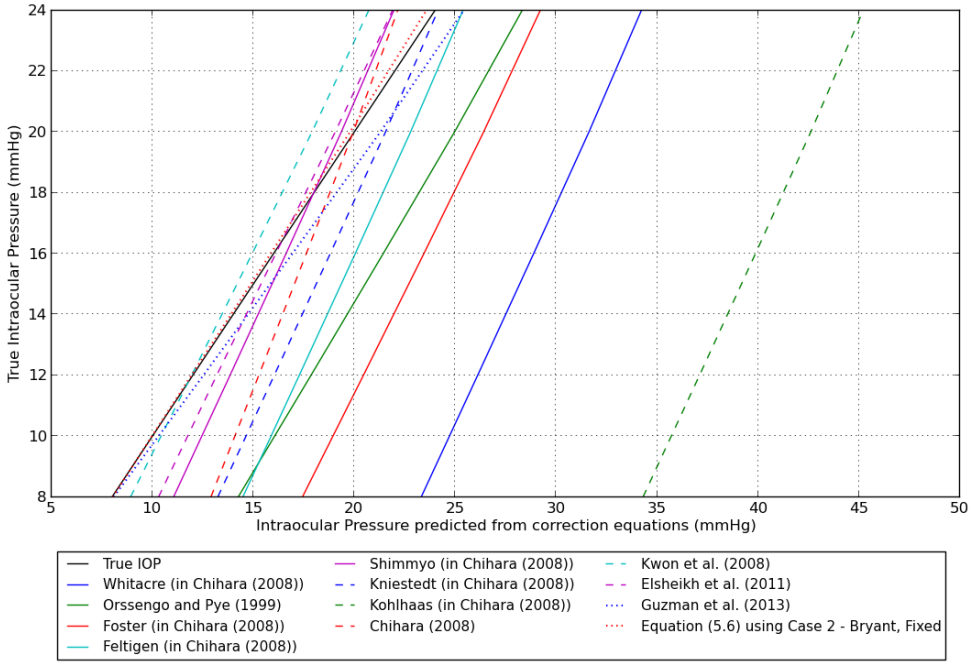

Figure 5.41: Comparison of the proposed correction equation to correction equations obtained from literature for what is considered a normal cornea in this study (CCT = 0.55 mm, R_{ant} = 7.77 mm, IOPG = 8, 12, 16, 20 and 24 mmHg) using the data from Case 2 when considering Bryant inflation data and a fixed limbal boundary condition, material data set 3.

Table 5.6: Comparison of the proposed correction equation to those from various literature sources using the data from both Case 1 and 2 for a numerically normal cornea (i.e. using Bryant inflation data, a fixed limbal boundary and material data set 3).

Source	Year	IOPC using data from Case 1					IOPC using data from Case 2				
		8 mmHg	12 mmHg	16 mmHg	20 mmHg	24 mmHg	8 mmHg	12 mmHg	16 mmHg	20 mmHg	24 mmHg
Whitacre (cited in Chihara, 2008)	1993	22.29	25.08	27.84	30.51	NC	23.32	26.11	28.89	31.62	34.22
Orssengo and Pye (1999)	1999	12.93	16.52	20.08	23.53	NC	14.25	17.86	21.43	24.97	28.32
Foster (cited in Chihara, 2008)	2000	16.33	19.34	22.32	25.20	NC	17.43	20.45	23.45	26.41	29.21
Feltigen (cited in Chihara, 2008)	2001	13.46	16.24	19.00	21.67	NC	14.48	17.27	20.05	22.79	25.39
Shimmyo (cited in Chihara, 2008)	2003	10.03	12.81	15.57	18.24	NC	11.05	13.84	16.62	19.36	21.96
Kniestedt (cited in Chihara, 2008)	2005	12.22	15.00	17.76	20.43	NC	13.24	16.03	18.81	21.55	24.15
Kohlhaas (cited in Chihara, 2008)	2006	33.28	36.07	38.83	41.50	NC	34.30	37.10	39.87	42.61	45.21
Chihara (2008)	2008	12.03	14.40	16.74	19.00	NC	12.90	15.27	17.62	19.95	22.15
Kwon *et al.* (2008)	2008	7.81	10.82	13.81	16.70	NC	8.91	11.94	14.94	17.90	20.72
Elsheikh *et al.* (2011)	2011	9.27	12.11	15.00	17.85	NC	10.30	13.19	16.11	19.06	21.90
Guzmán *et al.* (2013)	2013	6.46	10.88	15.27	19.52	NC	8.08	12.53	16.94	21.29	25.42
Current Study	2013	6.13	10.03	13.72	17.12	NC	8.03	11.93	15.86	19.79	23.58

NC - No Convergence, that is numerical difficulties arised during the GAT simulation.

It is clear from Table 5.6 that the predicted IOPC is overestimated from the IOPT with (i) more than 10.0 mmHg for Whitacre (cited in Chihara, 2008) and Kohlhaas (cited in Chihara, 2008); (ii) more than 5.0 mmHg for Foster (cited in Chihara, 2008) and (iii) less than 7.0 mmHg for Orssengo and Pye (1999), Feltigen (cited in Chihara, 2008) and Kniestedt (cited in Chihara, 2008). In contrast, the predicted IOPC is underestimated from the IOPT with (i) less than 5.0 mmHg for Shimmyo (cited in Chihara, 2008), Chihara (2008) and Kwon *et al.* (2008); (ii) less than 3.0 mmHg for Elsheikh *et al.* (2011), Guzmán *et al.* (2013) and the current study. These results also indicate that the correction equation proposed in this study compares well with the correction equations proposed by Elsheikh *et al.* (2011) and Guzmán *et al.* (2013) which varies with less than 3.0 mmHg from the IOPT.

From these results it appears that the choice of data to use, that is Case 1 or Case 2, does not influence the variation from the IOPT. However, there is a visible influence when considering the predicted IOPC from the correction equation proposed in this study. It is seen that when using the data from Case 2 that the predicted IOPC varies by less than 0.50 mmHg from the IOPT compared to the less than 3.0 mmHg variation when using the data from Case 1.

Additional results when (i) using Bryant inflation data and a 23° limbal boundary condition, (ii) Elsheikh inflation data and a fixed limbal boundary condition and (iii) Elsheikh inflation data and a 23° limbal boundary condition are shown in Appendix C for all correction equations discussed in this section.

5.6 CONCLUSION

This chapter discussed the effects of the various modelling assumptions, as well as the effects of geometric and material properties, on the estimated IntraOcular Pressure obtained from Goldmann Applanation Tonometry (GAT) (IOPG). The effects of two modelling assumptions were considered: (i) the choice of inflation data for calibration and (ii) the choice of limbal boundary condition.

By comparing the inflation test data of Bryant and Elsheikh it was noted that, for a fixed limbal boundary condition, the estimated IOPG differs by 0.87 and 0.88 mmHg when using the data from Case 1 and Case 2, respectively. Whereas when using a 23° limbal boundary condition the IOPG differs by 1.81 and 0.03 mmHg when using the data from Case 1 and Case 2, respectively. When comparing the two limbal boundary conditions for the two sets of inflation test data it was noted that the estimated IOPG differs by 1.69 (Case 1) and 0.23 (Case 2) mmHg for the Bryant inflation test data and by 0.99 (Case 1) and 0.68 (Case 2) mmHg for the Elsheikh inflation test data. The estimated IOPG difference is less than 2.0 mmHg in all considered cases when using the data from Case 1 and less than 1.0 mmHg when using the data from Case 2.

Additionally, the effects of the various geometric (Central Corneal Thickness (CCT) and anterior Radius of Curvature (RoC)) and material properties were also considered. The effect on the IOPG due to the CCT and RoC was as expected: a thick, steep cornea overestimates the IOPG and a thin, flat cornea underestimates it.

The results due to the material properties were interesting, where it was found that the assumptions made regarding material coefficients influence the estimated IOPG. When no assumptions (Case 1) are made the influence of different material data sets are apparent. However, when assuming that the corneal ground substance stiffness is constant (Case 2), the influence due to material data sets is almost neglible as the estimated IOPG is between 16.39 and 17.05 mmHg (a change of 0.66 mmHg). It appears that the ground substance stiffness plays a large role when estimating the IOPG and by either assuming it to be constant or not the influence of material properties on IOPG can be changed.

Finally, a correction equation was proposed accounting for the influence of CCT, RoC and material properties on the estimated IOPG. Three cases were investigated each considering all four data sets, that is both inflation data sets and both limbal boundary conditions:

- **Considering three material properties (Case 1):** The proposed correction equation predicted the IOPC within $0.08 - 0.90$ mmHg of the IOPT.
- **Considering two material properties (Case 2):** The predicted IOPC was within $0.05 - 0.65$ mmHg of the IOPT, an improvement from the previous case.
- **Neglecting material properties:** When using the data from Case 1 the predicted IOPC was within $0.7 - 14.1$ mmHg, whereas the IOPC was within $0.18 - 1.10$ mmHg when considering the data from Case 2.

These results clearly show that when including the material properties in the proposed correction equation a more accurate prediction of the IOPC can be obtained. It is also clear that the data used, that is either from Case 1 or Case 2, also influences the accuracy of the predicted IOPC. When only considering the geometric properties for the correction equation it is seen that the predicted IOPC is not as good as when the material properties are included in the correction equation. Also noticeable, is that the correction equation performs better when using the data from Case 2 as opposed to the data from Case 1. These results have illustrated that the assumptions made with regards to material properties do have an influence on the predicted IOPC.

When compared to correction equations from literature this proposed equation was found to within a reasonable accuracy predict the IOPT, within $1.87 - 2.88$ (Case 1) and $0.03 - 0.42$ mmHg (Case 2), for the numerically normal cornea as defined in this study. It was also seen that the correction equation performs better when using the data from Case 2 compared to when the data from Case 1 is used. After further validation of the proposed equation, by applying it to clinical data, it is possible that this equation could be used to correct the measured IOPG in a clinical setting.

CHAPTER 6

CONCLUSIONS

In this study the effects of certain numerical modelling assumptions on the estimated IntraOcular Pressure (IOPG), due to Goldmann Applanation Tonometry (GAT), were investigated. This was done by first developing a numerical Finite Element (FE) model of the human cornea. The following modelling assumptions were associated with the numerical model:

1. **Boundary conditions:** To describe the boundary at the cornea-scleral connection, or limbus, two boundary conditions were considered: (i) a fixed limbal boundary which is more representative of the experimental inflation test setup (Bryant and McDonnell, 1996) and (ii) a 23° roller boundary in which the limbal region is allowed to translate due to the applied IntraOcular Pressure (IOP). This second condition was also used to describe an alternate experimental inflation test setup, in which it is assumed that the limbus does translate due to inflation, as a 2 mm scleral ring is left on the sample (Elsheikh *et al.*, 2007a).

2. **Calibration data:** In literature two sets of experimental inflation test data are consistently used to calibrate constitutive models. These two sets of data were used in this study to calibrate the constitutive model. These data sets were referred to as Bryant (Bryant and McDonnell, 1996) and Elsheikh (Elsheikh *et al.*, 2007a) inflation test data in this study.

Using the calibrated numerical model the effects on the IOPG due to the two modelling assumptions were then investigated, as well as the effects due to corneal geometric and material properties.

6.1 SUMMARY OF FINDINGS

A short summary of the key findings, with regards to the constitutive model calibration and effects on the IOPG, is given to restate the main points of the research.

6.1.1 Constitutive Model Calibration

It was found from Chapter 4, which discussed the constitutive model calibration using inflation test data, that for a fibre reinforced elastic model considering both cases (i.e. Case 1 where three material coefficients were optimized and Case 2 where the ground substance stiffness, C_{10}, was assumed constant thereby only optimizing two material coefficients):

- A change in limbal boundary condition (from fixed to 23°) lowered the value for k_1, a measure of the collagen fibre stiffness, and increased the value for k_2, a measure of the material non-linearity. This was the case when using both sets of inflation data.
- The values for all material coefficients were much higher when using Elsheikh inflation test data than when using Bryant inflation data, for both cases of applied limbal boundary conditions.

It was also noted that the numerical inflation test results were in good agreement with the experimental results, independent of the various assumptions made. This observation coincides with Pandolfi and Manganiello (2006), where they also concluded that irrelevant of the corneal geometric or material properties used to simulate the inflation test, the obtained results compared well with experimental data from Bryant and McDonnell (1996).

6.1.2 Effects on Intraocular Pressure

Chapter 5 investigated the influence of various modelling, geometric and material property assumptions on the estimated IOPG. It was found that for:

- Modelling assumptions:
  - There was a less than 2.0 mmHg difference in the estimated IOPG for a change in inflation test data when using the data from Case 1 and a less than 1.0 mmHg difference when using the data from Case 2.
  - The same result was observed for a change in limbal boundary condition.
  - When using the data from Case 2 it was also noted that the variation in estimated IOPG, from the mean is within 0.88 mmHg for the four cases, whereas it varies within 1.81 mmHg when using the data from Case 1.
- Geometric properties:
  - The results coincided with the known influence on IOPG due to Central Corneal Thickness (CCT) and Radius of Curvature (RoC). A thin, flatter cornea tends to underestimate the IOPG whereas a thick, steeper cornea tends to overestimate the IOPG.
  - There was an increase in estimated IOPG, due to both CCT ($0.76 - 1.42$ mmHg) and RoC ($0.96 - 1.15$ mmHg), when the data from Case 2 was used compared with using the data from Case 1.

- Material properties:
  - When using the material properties obtained from Case 1 (no assumptions) it was apparent that the estimated IOPG ranged between 15.75 mmHg and 22.42 mmHg for the different sets of material data considering a True IOP (IOPT) of 16 mmHg. This result indicated that a change in material data sets (i.e. from Set 1 through to 5) tend to overestimate, as well as influence, the IOPG.
  - On the other hand, when using the material properties obtained from Case 2 (C_{10} is constant) the estimated IOPG is overestimated, but ranges between 16.39 mmHg and 17.05 mmHg. This result indicated that a change in material properties do not have a significant influence on estimated IOPG.

6.1.3 Correction Equation

A correction equation was also proposed in an attempt to account for the effects of geometric and material properties on the IOPG. Three cases were considered which utilized all the data sets from Case 1 and Case 2:

- Considering three material properties using the data from Case 1, the predicted calibrated IOP (IOPC) was within $0.08 - 1.3$ mmHg of the IOPT.
- Considering two material properties using the data from Case 2, the predicted IOPC was within $0.05 - 0.65$ mmHg.
- Considering only the geometric properties and using the data from Case 1 the predicted IOPC was within $0.7 - 14.1$ mmHg, whereas using the data from Case 2 resulted in a predicted IOPC of within $0.18 - 1.10$ mmHg of the IOPT.

These results showed that when the material properties are included in the proposed correction equation the predicted IOPC is closer to the IOPT than when the material properties are neglected from the proposed correction equation. It was also seen that the choice of which data set, either Case 1 or Case 2, also influences the accuracy of the predicted IOPC. When using the data from Case 2, when the ground substance stiffness is assumed the same for all corneas, the predicted IOPC is closer to the IOPT in both cases, that is for a correction equation when the material properties are included as well as a correction equation when neglecting the material properties.

The proposed correction equation, only considering the geometric properties, was compared with various correction equations in literature. The IOPG was estimated within a reasonable accuracy, $1.87 - 2.88$ mmHg from the IOPT for Case 1 and $0.03 - 0.42$ mmHg for Case 2, when considering a numerically normal cornea. The proposed correction equation performs better when using the data from Case 2 as opposed to the data from Case 1. However, before the proposed correction equation can be used in a clinical setting the equation should first be further refined and applied to clinical data for validation.

6.2 CONCLUSIONS

From the findings it is evident that the choice of inflation test data used for model calibration, geometric properties and assumptions with regards to material coefficients does have an influence on the estimated IOPC.

A change in inflation test data and limbal boundary condition results in an estimated IOPG difference of less than 2.0 mmHg when considering Case 1 (no assumptions to material properties) and differs by less than 1.0 mmHg when considering Case 2 (assuming a constant ground substance stiffness). This can be regarded as either an insignificant or significant change depending on the researcher conducting the study or the context of the study. Compared to the variation in clinical GAT results where errors of several mmHg can be expected when conditions differ from the norm (i.e. an abnormally thick or thin cornea) (Goldmann and Schmidt, 1957) a difference of less than 2.0 mmHg could be considered insignificant, thereby concluding that the modelling assumptions do not have a signicant influence on the estimated IOPG.

It was noted that the assumptions made with regards to material properties influenced the estimated IOPG differently depending on the case under consideration. When no assumptions are made regarding material properties the estimated IOPG varies such that it can be concluded that the material properties influences the estimated IOPG. The GAT device is therefore considered to be sensitive to a change in corneal material properties. On the other hand, when it is assumed that all corneas have the same ground substance stiffness, the material properties appear not to influence the estimated IOPG and hence the GAT device is considered to not be sensitive to a change in corneal material properties.

It is clear that each of the considered numerical cases, that is varying limbal boundary conditions, varying inflation test data and different assumptions with regards to material coefficients, were able to match the experimental inflation data closely. However, when using the obtained material properties for the different cases a wide range of estimated IOPGs were obtained with the numerical GAT simulations. This observation indicates that inflation test data alone is not sufficient for the calibration of a constitutive model. In addition to inflation test data, which only accounts for the isotropic response of the cornea, other experimental tests such as strip extensometry, which accounts for the anisotropic response, would be required to uniquely quantify material properties.

Studer *et al.* (2010) and Pandolfi and Manganiello (2006) calibrated the constitutive models, developed in their studies, using both experimental inflation and strip extensometry data. When using both sets of experimental data, both of these studies were able to capture the complex corneal behaviour in their proposed constitutive models. Pandolfi and Manganiello (2006) did however mention that their model could be further improved with additional experimental data on the geometric and material properties. Studer *et al.* (2012) also showed that when using at least two sets of data, generated artificially using a simple FE model of a tension test, the material coefficients obtained from the inverse FE method uniquely describes the corneal behaviour as opposed to only using one data set.

In conclusion, care should be taken when developing a numerical model of the cornea. It has been shown that modelling choices do affect the results obtained from GAT, thus influencing the overall conclusions drawn from a numerical study.

6.3 SUMMARY OF CONTRIBUTIONS

This study contributed towards a better understanding of the effect different modelling and corneal material assumptions could have on the overall conclusions of a study involving GAT simulations.

It was also shown that additional experimental test data is required to better understand the contribution of corneal geometric and material properties on the overall behaviour. Otherwise, a variation in numerical GAT results is observed which ultimately leads to contradictory conclusions.

Several correction equations were proposed illustrating that accurate estimations of the IOPG can be obtained by either including the material properties in the proposed correction equation or by neglecting the material properties but assuming a constant ground substance stiffness for all corneas.

6.4 RECOMMENDATIONS FOR FURTHER RESEARCH

It is recommended that future research include the use of experimental data from strip extensometry and inflation tests to calibrate constitutive models. The effect of this additional set of data on the estimated IOPG from GAT simulations could then be investigated.

Additionally, experimental studies should also be conducted to obtain further information on the corneal geometric and material properties and their influence on corneal behaviour. This will allow for more accurate constitutive model calibrations in future numerical models.

BIBLIOGRAPHY

Aghamohammadzadeh, H., Newton, R. H. and Meek, K. M. (2004). X-ray scattering used to map the preferred collagen orientation in the human cornea and limbus, *Structure* **12**(2): 249–256.

AngioEdupro Sharpoint (n.d.). anatomy_of_the_eye.png, http://www.angioedupro.com/Sharpoint/anatomy/. Retrieved 19/01/2012.

Ateshian, G. A. and Friedman, M. H. (2009). Integrative biomechanics: A paradigm for clinical applications of fundamental mechanics, *Journal of Biomechanics* **42**(10): 1444–1451.

Batterbury, M. and Bowling, B. (2005). *Ophthalmology: an illustrated colour text*, Elsevier Churchill Livingstone.

Boote, C., Dennis, S., Huang, Y., Quantock, A. J. and Meek, K. M. (2005). Lamellar orientation in human cornea in relation to mechanical properties, *Journal of Structural Biology* **149**(1): 1–6.

Boote, C., Dennis, S., Newton, R. H., Puri, H. and Meek, K. M. (2003). Collagen fibrils appear more closely packed in the prepupillary cornea: Optical and biomechanical implications, *Investigative Ophthalmology & Visual Science* **44**(7): 2941 –2948.

Boote, C., Elsheikh, A., Kassem, W., Kamma-Lorger, C. S., Hocking, P. M., White, N., Inglehearn, C. F., Ali, M. and Meek, K. M. (2011). The influence of lamellar orientation on corneal material behavior: Biomechanical and structural changes in an avian corneal disorder, *Investigative Ophthalmology & Visual Science* **52**(3): 1243–1251.

Boote, C., Hayes, S., Abahussin, M. and Meek, K. M. (2006). Mapping collagen organization in the human cornea: Left and right eyes are structurally distinct, *Investigative Ophthalmology & Visual Science* **47**(3): 901 –908.

Brandt, J., Roberts, C., Sherwood, M. and Sheets, C. (2009). The impact of central corneal thickness and corneal biomechanics on tonometry, *in* T. Shaarawy, M. B. Sherwood, J. G. Crowston and R. Hitchings (eds), *Glaucoma Volume 1: Medical Diagnosis and Therapy: Expert Consult - Online and Print*, Elsevier Health Sciences, pp. 207–212.

Bryant, M. R. and McDonnell, P. J. (1996). Constitutive laws for biomechanical modeling of refractive surgery, *Journal of Biomechanical Engineering* **118**(4): 473–481.

Carney, L. G., Mainstone, J. C. and Henderson, B. A. (1997). Corneal topography and myopia. a cross-sectional study., *Investigative Ophthalmology & Visual Science* **38**(2): 311 –320.

Chihara, E. (2008). Assessment of true intraocular pressure: The gap between theory and practical data, *Survey of Ophthalmology* **53**(3): 203–218.

Daxer, A., Misof, K., Grabner, B., Ettl, A. and Fratzl, P. (1998). Collagen fibrils in the human corneal stroma: structure and aging., *Investigative Ophthalmology & Visual Science* **39**(3): 644–648.

De Moraes, C. G. V., Prata, T. S., Liebmann, J. and Ritch, R. (2008). Modalities of tonometry and their accuracy with respect to corneal thickness and irregularities, *Journal of Optometry* **1**(2): 43–49.

Dhondt, G. D. C. (2004). *The finite element method for three-dimensional thermomechanical applications*, John Wiley and Sons.

Dhondt, G. D. C. (2011a). Calculix: A free software three-dimensional structural finite element program.

Dhondt, G. D. C. (2011b). CalculiX CrunchiX user's manual version 2.4.

Dupps Jr., W. J. and Wilson, S. E. (2006). Biomechanics and wound healing in the cornea, *Experimental Eye Research* **83**(4): 709–720.

Dupps, W. J., Netto, M. V., Herekar, S. and Krueger, R. R. (2007). Surface wave elastometry of the cornea in porcine and human donor eyes, *Journal of refractive surgery (Thorofare, N.J. : 1995)* **23**(1): 66–75.

Ehlers, N., Bramsen, T. and Sperling, S. (1975). Applanation tonometry and central corneal thickness, *Acta Ophthalmologica* **53**(1): 3443.

Elsheikh, A., Alhasso, D. and Rama, P. (2008a). Biomechanical properties of human and porcine corneas, *Experimental Eye Research* **86**(5): 783–790.

Elsheikh, A., Alhasso, D., Gunvant, P. and Garway-Heath, D. (2011). Multiparameter correction equation for goldmann applanation tonometry, *Optometry and Vision Science* **88**(1): E102–E112.

Elsheikh, A. and Anderson, K. (2005). Comparative study of corneal strip extensometry and inflation tests, *Journal of The Royal Society Interface* **2**(3): 177 –185.

Elsheikh, A. and Wang, D. (2007). Numerical modelling of corneal biomechanical behaviour, *Computer Methods in Biomechanics and Biomedical Engineering* **10**(2): 85–95.

Elsheikh, A., Brown, M., Alhasso, D., Rama, P., Campanelli, M. and Garway-Heath, D. (2008b). Experimental assessment of corneal anisotropy, *Journal of Refractive Surgery* **24**(2): 178–187.

Elsheikh, A., Ross, S., Alhasso, D. and Rama, P. (2009). Numerical study of the effect of corneal layered structure on ocular biomechanics, *Current Eye Research* **34**(1): 26–35.

Elsheikh, A., Wang, D. and Pye, D. (2007a). Determination of the modulus of elasticity of the human cornea, *Journal of Refractive Surgery (Thorofare, N.J.: 1995)* **23**(8): 808–818.

Elsheikh, A., Wang, D., Brown, M., Rama, P., Campanelli, M. and Pye, D. (2007b). Assessment of corneal biomechanical properties and their variation with age, *Current Eye Research* **32**(1): 11–19.

Elsheikh, A., Wang, D., Kotecha, A., Brown, M. and Garway-Heath, D. (2006). Evaluation of goldmann applanation tonometry using a nonlinear finite element ocular model, *Annals of Biomedical Engineering* **34**(10): 1628–1640.

Ethier, C. R. and Simmons, C. A. (2007). *Introductory biomechanics: from cells to organisms*, Cambridge University Press.

Franco, S. and Lira, M. (2009). Biomechanical properties of the cornea measured by the ocular response analyzer and their association with intraocular pressure and the central corneal curvature, *Clinical and Experimental Optometry* **92**(6): 469475.

Fung, Y. C. (1993). *Biomechanics: mechanical properties of living tissues*, Springer.

Fung, Y. C., Fronek, K. and Patitucci, P. (1979). Pseudoelasticity of arteries and the choice of its mathematical expression, *American Journal of Physiology - Heart and Circulatory Physiology* **237**(5): H620 –H631.

Garg, A. (2006). Tonometry, *in* A. Garg (ed.), *Mastering the Tech. of Glaucoma Diag. & Management*, Jaypee Brothers Publishers, pp. 65–77.

Ghaboussi, J., Kwon, T.-H., Pecknold, D. A. and Hashash, Y. M. (2009). Accurate intraocular pressure prediction from applanation response data using genetic algorithm and neural networks, *Journal of Biomechanics* **42**(14): 2301–2306.

Goldmann, H. and Schmidt, T. (1957). Über Applanationstonometrie (Applanation Tonometry), *Ophthalmologica* **134**: 221–242. quoted in Ritch, R. and Caronia, R.M. (2000), Classic Papers in Glaucoma, Kugler Publications, pp.155-162.

Guzmán, A., Arciniegas Castilla, A., Guarnieri, F. and Ramirez Rodriguez, F. (2013). Intraocular pressure: Goldmann tonometry, computational model, and calibration equation., *Journal of glaucoma* **22**(1): 10–14.

HAAG-STREIT International (n.d.a). RTEmagicC_Eye_tonometer_02.jpg.jpg, http://www.haag-streit.com/uploads/. Retrieved 06/09/2012.

HAAG-STREIT International (n.d.b). RTEmagicC_tonoView_02.jpg.jpg, http://www.haag-streit.com/uploads/. Retrieved 06/09/2012.

Hamilton, K. E. and Pye, D. C. (2008). Young's modulus in normal corneas and the effect on applanation tonometry, *Optometry and Vision Science* **85**(6): 445–450.

Hjortdal, J. . (1996). Regional elastic performance of the human cornea, *Journal of Biomechanics* **29**(7): 931–942.

Hoeltzel, D. A., Altman, P., Buzard, K. and Choe, K.-i. (1992). Strip extensiometry for comparison of the mechanical response of bovine, rabbit, and human corneas, *Journal of Biomechanical Engineering* **114**(2): 202–215.

Hollman, Kyle, W., Emelianov, S. Y., Neiss, Jason, H., Jotyan, G., Spooner, Gregory, J., Juhasz, T., Kurtz, R. and O'Donnell, M. (2002). Strain imaging of corneal tissue with an ultrasound elasticity microscope, *Cornea* **21**(1): 68–73.

Holzapfel, G. A., Gasser, T. C. and Ogden, R. A. Y. W. (2000). A new constitutive framework for arterial wall mechanics and a comparative study of material models, *Journal of Elasticity* **61**(1): 1–48.

Jakobiec, F. A. and Ozanics, V. (1982). General topographic anatomy of the eye, *in* F. Jakobiec (ed.), *Ocular anatomy, embryology, and teratology*, Harper & Row, pp. 1–9.

Kiely, P., Smith, G. and Carney, L. (1982). The mean shape of the human cornea, *Journal of Modern Optics* **29**(8): 1027–1040.

Kniestedt, C., Punjabi, O., Lin, S. and Stamper, R. L. (2008). Tonometry through the ages, *Survey of Ophthalmology* **53**(6): 568–591.

Kotecha, A. (2007). What biomechanical properties of the cornea are relevant for the clinician?, *Survey of Ophthalmology* **52**(6, Supplement 1): S109–S114.

Kotecha, A., Lim, S. and Garway-Heath, D. (2009). Tonometry and intraocular pressure fluctuation, *in* T. Shaarawy, M. B. Sherwood, J. G. Crowston and R. Hitchings (eds), *Glaucoma Volume 1: Medical Diagnosis and Therapy: Expert Consult - Online and Print*, Elsevier Health Sciences, pp. 103–113.

Kwon, T., Ghaboussi, J., Pecknold, D. and Hashash, Y. (2008). Effect of cornea material stiffness on measured intraocular pressure, *Journal of Biomechanics* **41**(8): 1707–1713.

Lagarias, J. C., Reeds, J. A., Wright, M. H. and Wright, P. E. (1998). Convergence properties of the nelder–mead simplex method in low dimensions, *SIAM Journal on Optimization* **9**(1): 112–147.

Liou, H.-L. and Brennan, N. A. (1997). Anatomically accurate, finite model eye for optical modeling, *Journal of the Optical Society of America A* **14**(8): 1684–1695.

Liu, J. and Roberts, C. J. (2005). Influence of corneal biomechanical properties on intraocular pressure measurement: Quantitative analysis, *Journal of Cataract & Refractive Surgery* **31**(1): 146–155.

MatWeb Material Property Data (n.d.). Overview of materials for acrylic, extruded.

Newell, F. W. (1992). *Ophthalmology: principles and concepts*, Mosby Year Book.

Niroomandi, S., Alfaro, I., Cueto, E. and Chinesta, F. (2008). Real-time deformable models of non-linear tissues by model reduction techniques, *Computer Methods and Programs in Biomedicine* **91**(3): 223–231.

Orssengo, G. and Pye, D. (1999). Determination of the true intraocular pressure and modulus of elasticity of the human cornea in vivo, *Bulletin of Mathematical Biology* **61**(3): 551–572.

Pandolfi, A. and Holzapfel, G. A. (2008). Three-dimensional modeling and computational analysis of the human cornea considering distributed collagen fibril orientations, *Journal of Biomechanical Engineering* **130**(6): 061006–12.

Pandolfi, A. and Manganiello, F. (2006). A model for the human cornea: constitutive formulation and numerical analysis, *Biomechanics and Modeling in Mechanobiology* **5**(4): 237–246.

Python Software Foundation (2011). Python.

Rodrigues, M., Waring III, G., Hackett, J. and Donohoo, P. (1982). Cornea, *in* F. Jakobiec (ed.), *Ocular anatomy, embryology, and teratology*, Harper & Row, pp. 153–165.

Ruberti, J. W., Sinha Roy, A. and Roberts, C. J. (2011). Corneal biomechanics and biomaterials, *Annual Review of Biomedical Engineering* **13**: 269–295. PMID: 21568714.

Scipy Community (2011). Scipy, version 0.9.0, http://docs.scipy.org/doc/.

Secker, G. and Daniels, J. (2009). Limbal epithelial stem cells of the cornea, *StemBook*. Retrieved 19/01/2012.

Smith, G. and Atchison, D. A. (1997). *The Eye and Visual Optical Instruments*, Cambridge University Press.

Spall, J. C. (2005). *Introduction to Stochastic Search and Optimization: Estimation, Simulation, and Control*, John Wiley & Sons.

Srodka, W. (2010). Goldmann applanation tonometry - not as good as gold, *Acta of Bioengineering and Biomechanics* **12**(2): 39–47.

Stepanik, J. and Ossoinig, K. (1968). Measurements of the sagittal axis of the human eye in vivo during applantation of the cornea., *The British Journal of Ophthalmology* **52**(11): 801–807.

Studer, H., Larrea, X., Riedwyl, H. and Bchler, P. (2010). Biomechanical model of human cornea based on stromal microstructure, *Journal of Biomechanics* **43**(5): 836–842.

Studer, H., Riedwyl, H. and Büchler, P. (2012). Importance of multiple loading scenarios for the identification of material coefficients of the human cornea, *Computer Methods in Biomechanics and Biomedical Engineering* **15**(1): 93–99.

Surgitek (n.d.). tonometro_goldman.jpg, http://www.surgitek.it/public/biz˙editor/Image/. Retrieved 06/09/2012.

Toris, C. (2009). Aqueous humor dynamics and intraocular pressure elevation, *in* T. Shaarawy, M. B. Sherwood, J. G. Crowston and R. Hitchings (eds), *Glaucoma Volume 1: Medical Diagnosis and Therapy: Expert Consult - Online and Print*, Elsevier Health Sciences, pp. 55–66.

Virtual Medical Centre (n.d.). 2133_eye_anatomy_label_v2_700.jpg, http://www.virtualmedicalcentre.com/uploads/VMC/DiseaseImages/. Retrieved 19/01/2012.

Wang, H., Prendiville, P. L., McDonnell, P. J. and Chang, W. V. (1996). An ultrasonic technique for the measurement of the elastic moduli of human cornea, *Journal of Biomechanics* **29**(12): 1633–1636.

Williams, S. E. I. (2007). Glaucoma, *Continuing Medical Education* **25**(10): 464–468.

Wollensak, G., Spoerl, E. and Seiler, T. (2003). Stress-strain measurements of human and porcine corneas after riboflavinultraviolet-a-induced cross-linking, *Journal of Cataract & Refractive Surgery* **29**(9): 1780–1785.

APPENDIX A

CALCULIX INPUT FILE STRUCTURE

The structure of the Calculix input file deck, with reference to the Goldmann Applanation Tonometry (GAT) simulation, is discussed here to give the reader a simple and quick explanation as to how everything is defined. The Calculix input file can be divided into three main sections, the problem definition, the model definition and the step definition.

In the problem definition section it is shown how to define the desired problem information in the input file for future reference. The model definition section explains how the geometry is described in the input file along with the required element connectivity definitions used to construct the mesh. This section also explains the definition of nodal and element sets that are used for the application of boundary conditions, along with the desired material definitions for each geometry, that is the cornea and applanator. In the step definition it is explained how to construct both the inflation and GAT simulations, with its required procedures and loading conditions, as well as how data is stored for postprocessing.

A.1 INTRODUCTION

The input file structure used to describe the cornea geometry, with the boundary conditions for both the inflation and GAT simulations, is discussed in this appendix. The basic structure for a Calculix input file is shown in Figure A.1, where the input file used for the GAT simulation is used as an example. Note that the only difference between the inflation test and GAT simulation input files is the addition of the contact definition for the GAT simulation and the corresponding prescribed displacement definition in the `*STEP` card. Apart from these two differences the input files are exactly the same.

In the following sections each part of the Calculix input file, as illustrated in Figure A.1, is discussed in more detail and accompanied by an excerpt from an example input file used to simulate GAT.

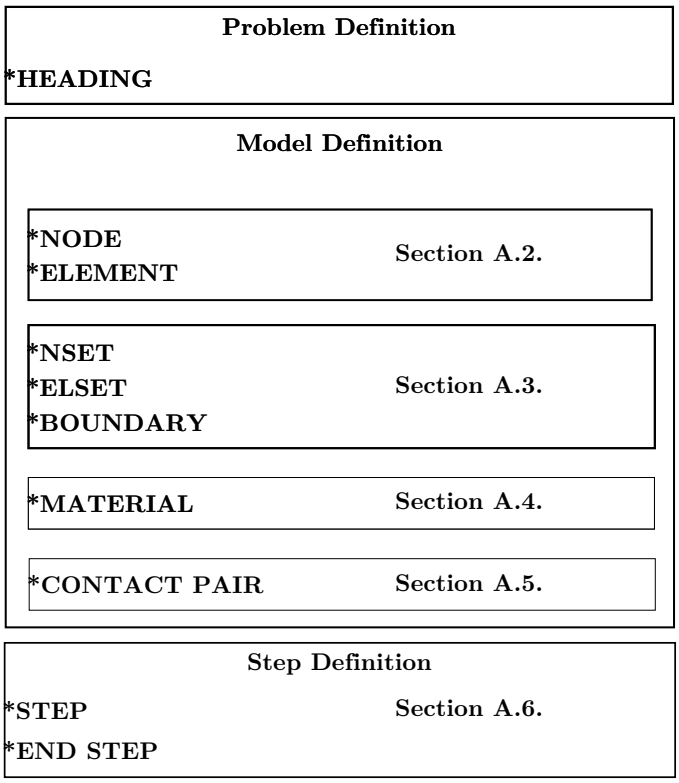

Figure A.1: A diagram illustrating the basic input structure of a Calculix input file. [Adapted from Dhondt (2011b)]

A.2 PROBLEM DEFINITION

A Calculix input file starts with a section defining the header of the input file where the problem information is stated. This section is not compulsory but is useful to identify the problem defined in an input file.

```
*HEADING
Model: GAT simulation     Date: 22 November 2012
** This input file defines the geometry (nodal coordinates and element
** connectivity), as well as boundary conditions to simulate Goldmann
** Applanation Tonometry (GAT).
** The cornea is first prestressed by applying an IntraOcular Pressure
** (IOP).
** A rigid body definition is used to simulate the applanator and a
** prescribed displacement is applied to the applanator to flatten
** the cornea.
```

A.3 MODEL DEFINITION

The model definition section is where the Finite Element (FE) model is described, that is nodal coordinates, element connectivity, boundary conditions and material descriptions. This section is broken up into subsections to describe each facet of the model definition individually.

A.3.1 Geometry Definition

The geometry definition describes the nodal coordinates and element connectivity used to define the FE model. The `*NODE` card is used to define the nodal coordinates in the form (node, x, y, z):

```
*NODE
1, 5.000000000e-02, 0.000000000e+00, -1.768383713e-01
2, 1.041917281e-01, 0.000000000e+00, -1.774122913e-01
3, 9.626060506e-02, 3.987244814e-02, -1.774122913e-01
...
4271, 1.019421161e+00, 5.124976260e+00, -2.812304318e+00
4272, 0.000000000e+00, 0.000000000e+00, 0.000000000e+00
4273, 0.000000000e+00, 0.000000000e+00, 1.000000000e+00
```

The element connectivity is defined using the `*ELEMENT` card, followed by the type of element used. The reduced integration 20-node brick element used in this study is defined by the C3D20R description, whereas the linear brick elements used for the contact definition are denoted by C3D8. An element definition takes the form (element nr, node numbers):

```
*ELEMENT, TYPE=C3D20R
1, 1, 2, 3, 4, 5, 6, 7,
  8, 9, 10, 11, 12, 13, 14, 15,
  16, 17, 18, 19, 20
2, 2, 21, 22, 3, 6, 23, 24,
  7, 25, 26, 27, 10, 28, 29, 30,
  14, 18, 31, 32, 19
...
605, 3604, 3623, 3658, 3646, 3608, 3625, 3659,
  3648, 3628, 3660, 3661, 3650, 3631, 3662, 3663,
  3653, 3620, 3633, 3664, 3656
606, 3623, 3635, 3665, 3658, 3625, 3637, 3666,
  3659, 3640, 3667, 3668, 3660, 3643, 3669, 3670,
  3662, 3633, 3645, 3671, 3664

*ELEMENT, TYPE=C3D8
607, 1, 2, 3, 4, 5, 6, 7,
  8
608, 2, 21, 22, 3, 6, 23, 24,
  7
...
748, 3604, 3623, 3658, 3646, 3608, 3625, 3659,
  3648
749, 3623, 3635, 3665, 3658, 3625, 3637, 3666,
```

```
  3659
```

Note that a set of linear elements are built into the anterior layer of the corneal geometry and the posterior layer of the applanator using the original corner nodes defined for the quadratic brick elements. This linear layer of elements is required as the contact analysis struggles with convergence when quadratic elements are used. This is due to the nodal forces on the corner nodes of the element, which are either zero or opposite in sign when compared to the midside nodes, creating a problem when contact stiffness is calculated (Dhondt, 2011b).

A.3.2 Set and Boundary Definitions

Node and element set definitions are used to define the various boundary conditions for both the inflation and GAT simulations. It is required to first define the various nodal and element sets before being able to define the required boundary conditions.

To define the IntraOcular Pressure (IOP) the posterior surface of the cornea is defined as an element set, along with the anterior surface of the cornea and the posterior surface of the applanator to define the slave and master contact surfaces. An example of how an element set is defined is given here, where the anterior surface of the cornea is defined for contact with the name of the set given as `top_surface`:

```
*ELSET, ELSET=top_surface
1, 2, 3, 4, 5, 6, 7, 8,
  ...
  188, 189, 190, 191, 192, 193, 194, 195,
  196
```

The node sets are used to define sets for the limbal boundary conditions, the symmetry boundary conditions for the GAT simulation, as well as defining the nodes for the rigid sets. An example of a node set definition is given using the limbal nodes with the name of the set given as `limbus`:

```
*NSET, NSET=limbus
597, 598, 599, 600, 602, 605, 607, 608,
    ...
  3598, 3599, 3601
```

Finally, in order to define the fibre directions in the following section, it is required to first define each element with its corresponding nodes:

```
*ELSET, ELSET=E1
1, 607
*NSET, NSET=N1
```

```
1, 2, 3, 4, 5, 6, 7,
  8, 9, 10, 11, 12, 13, 14, 15,
  16, 17, 18, 19, 20
```

Lastly, the boundary conditions are defined using the `*BOUNDARY` card with the required Degrees of Freedom (DOFs) to fix the node sets in the specific directions (1 is in the x-direction, 2 in the y-direction and 3 in the z-direction):

```
*BOUNDARY
Apex, 1,2
*BOUNDARY
sym_sagittal, 1
*BOUNDARY
sym_equator, 2
*BOUNDARY
limbus, 1,3
```

A.3.3 Material Definition

To define a material in Calculix, the `*MATERIAL` card is used along with the required nodal and element sets that define the geometry to which the material is assigned. For the inflation simulation only one material definition is required for the cornea, but for the GAT simulation two material definitions are required.

To define the fibre reinforced elastic material for the cornea with two fibre families, the element sets (as defined in the previous section) are needed to define the local axis system for the fibre orientations. A local axis system is defined by specifying two points on the new axis system (Ax, Ay, Az, Bx, By, Bz). Calculix will then calculate the orientation of this new system. The `*ORIENTATION` card is used for this. The fibre reinforced elastic material is defined using the `*USER MATERIAL` card with 10 constants (C_{10}, D_1, F_{1x}, F_{1y}, k_{11}, k_{12}, F_{2x}, F_{2y}, k_{21}, k_{22}). A material section is ended by assigning the material properties defined to a set of elements using the `*SOLID SECTION` card. The corneal material is then defined as follows:

```
*MATERIAL, NAME=ELASTIC_FIBER
*USER MATERIAL, CONSTANTS=10
0.00387103244, 0.4, 1.0, 0.0, 0.0353111404, 181.21838525, 0.0, 1.0,
  0.0353111404, 181.21838525
*ORIENTATION, NAME=L1
1.000000000e+00, 0.000000000e+00, -1.024575068e-02,
6.123233996e-17, 1.000000000e+00, -2.038006522e-03
*SOLID SECTION, ELSET=E1, MATERIAL=ELASTIC_FIBER, ORIENTATION=L1
```

For the GAT simulation, due to the addition of the applanator, it is necessary to define an additional material. The applanator is, however, defined as a rigid body using the `*RIGID`

BODY card and applying the definition to nodes associated with the applanator. Additionally a rotational and reference node is defined, the reference node is used to apply prescribed loading and displacement conditions on the applanator, and the rotational node is used to ensure that the applanator does not rotate during the simulation. As it is required to assign a material to all elements in Calculix, a simple linear elastic isotropic material definition is used to define the applanator material:

```
*MATERIAL, NAME=LINEAR_ELASTIC
*ELASTIC, TYPE=ISO
2880.0, 0.402
*SOLID SECTION, ELSET=appl_elements, MATERIAL=LINEAR_ELASTIC
*RIGID BODY, NSET=appl_nodes, REF NODE=4273, ROT NODE=4272
```

A.3.4 Contact Definition

As the GAT simulation requires a contact definition, the master and slave surfaces are first defined using the *SURFACE card and the surface definitions illustrated in Figure A.2.

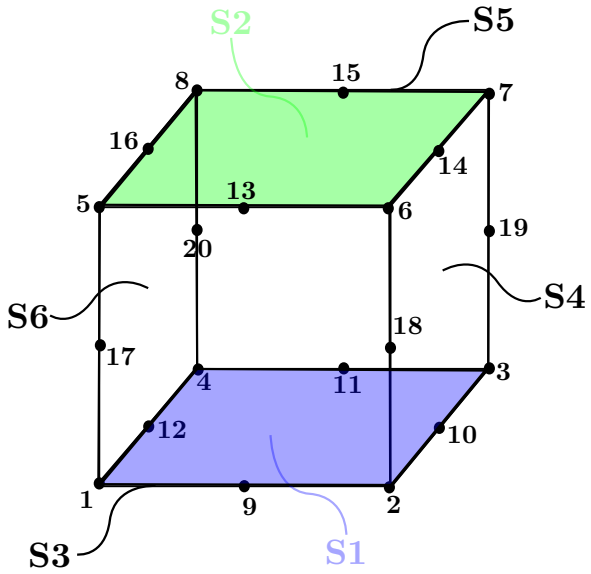

Figure A.2: Illustration of the surface definitions used in Calculix for a brick element.

After the surfaces are defined it is required to define the contact interaction with either the small and large sliding option, which is a measure of the nodal pairing between the slave and master surfaces. If small sliding is chosen, the pairing is calculated at the start of every increment, whereas large sliding calculates the pairing at every iteration. The contact is then defined using the *CONTACT PAIR card and using the small sliding option as it allows for better convergence.

The contact interaction is then defined using the pressure-overclosure parameters (stiffness constant, H and allowable penetration, κ) explained in Section 3.5.2 with the *SURFACE BEHAVIOR and defining a linear pressure-overclosure. The interaction between the contact and applanator is then initiated using the *SURFACE INTERACTION card:

```
*SURFACE, NAME=Slave, TYPE=ELEMENT
lin_top_surface, S2
*SURFACE, NAME=Master, TYPE=ELEMENT
lin_bottom_surface, S1
*CONTACT PAIR, INTERACTION=ContactInteraction, SMALL SLIDING
Slave, Master
*SURFACE INTERACTION, NAME=ContactInteraction
*SURFACE BEHAVIOR, PRESSURE-OVERCLOSURE=LINEAR
2.0, 0.01
```

A.4 STEP DEFINITIONS

The simulation conditions are defined in the *STEP card. For the inflation simulation it is only required to define the IOP loading condition using a distributed load, whereas for the GAT simulation the additional applanation definition is also required. To achieve this two loading curves are defined using the *AMPLITUDE card (time1, amplitude1, time2, amplitude2, etc.). The first defines the inflation process for the first 20% of the simulation and the second defines the applanation process for the last 80% of the simulation:

```
*AMPLITUDE, NAME=Inflate
0.0, 0.0, 0.2, 1.0
*AMPLITUDE, NAME=Contact
0.0, 0.0, 0.2, 0.0, 1.0, 1.0
```

To define the simulation conditions in the *STEP card, the optional NLGEOM needs to be specified so that the simulation can take geometrical non-linear effects into account, along with the INC option to specify the maximum number of increments. Both simulations are considered to be non-linear static, as there are no additional fluid or thermodynamic effects, and this static procedure is defined with the *STATIC card, and specifying the DIRECT option to switch off automatic incrementation. This option is removed for the inflation simulation, which converges perfectly with automatic incrementation. The time steps are indicated just below the *STATIC card (initial time increment, time period of the step, minimum time increment allowed and maximum time increment allowed):

```
*STEP, NLGEOM, INC=1000
*STATIC, DIRECT
1.000000000e-02, 1.000000000e+00, 1.000000000e-05, 1.000000000e+30
```

The loading conditions specified for the simulation are specified using the *DLOAD and *BOUNDARY cards along with the predefined loading curves. For the inflation simulation, the prescribed displacements defined under the *BOUNDARY card are neglegted. The IOP is defined using the *DLOAD card and specifying the surface to which the load should be applied similar to the

surface definitions in the previous section (c.f. Figure A.2), just replacing the `S` with a `P`. To simulate the applanation process a prescribed displacement is applied to the rigid body applanator using the `*BOUNDARY` card. The first three entries define the rotational DOFs and the last three the translational DOFs. In this case the rigid body should not be able to rotate and the only prescribed loading is a displacement along the optical axis:

```
*DLOAD, AMPLITUDE=Inflate
pressure_surface, P1, 0.00213248
*BOUNDARY, AMPLITUDE=Contact
4272, 1, 1, 0.0
4272, 2, 2, 0.0
4272, 3, 3, 0.0
4273, 1, 1, 0.0
4273, 2, 2, 0.0
4273, 3, 3, -0.449426652541
```

Lastly the required output is defined before ending the current simulation step with the `*END STEP` card. The cards ending with `PRINT` outputs all the desired data to a .dat file, whereas the cards ending with `FILE` outputs the data to a .frd file. The difference between these two output file types is that the .dat file contains the data at the integration points or whole element variables, whereas the .frd file contains data extrapolated and averaged at the nodal points. For the contact information the `CDIS` option outputs the relative contact displacements and the `CSTR` outputs the contact stresses. For nodal information `U` refers to the displacements and `RF` to the external forces, and `S` refers to stresses with `E` denoting strains for the element information. The `GLOBAL` option allows for the output of data in the global coordinate system, and the output data is defined as follow in the input file deck:

```
*CONTACT PRINT
CDIS,CSTR
*CONTACT FILE
CDIS,CSTR
*NODE PRINT, NSET=Nall, GLOBAL=YES
U, RF
*NODE FILE, GLOBAL=YES
U, RF
*EL PRINT, ELSET=Eall, GLOBAL=YES
S, E
*EL FILE, GLOBAL=YES
S, E
*END STEP
```

APPENDIX B

OPTIMIZATION AND STATISTICAL BACKROUND

A basic mathematical background is given here to understand the basic mechanisms governing the Nelder-Mead simplex optimization process, as well as what is meant by the concept of a Root Mean Square Error (RMSE). Both of these concepts are encountered in Chapter 4 where an optimization problem is defined to estimate the corneal constitutive model properties.

B.1 NELDER-MEAD SIMPLEX OPTIMIZATION

The Nelder-Mead simplex algorithm is a non-linear direct search method which uses a simplex (or triangular shape) to evaluate the objective function value (F). The Nelder-Mead method uses four methods to find the minimum value of a desired objective function, which are known as reflection, expansion, contraction and shrinking. These methods are illustrated in Figure B.1 for a 2D case. Nelder-Mead works on the premise of substituting the worst vertex point in a generated simplex with a better point to create a new simplex. The algorithm is described using the following four steps (Spall, 2005):

Step 1: Generate a simplex by creating $n+1$ points (three points for a 2D case).

Step 2: Calculate the function value (F_r) of a point reflected (x_r) from x_{n+1} (c.f. Figure B.1a), if $F_r < F_{n+1}$ then x_r is substituted for point x_{n+1} to create a new simplex.

Step 3: A new attempt is made by either stretching this point along the reflected line in an expansion process or contracting the point in a contraction process. To determine whether an expansion or contraction process should be followed F_r is compared to F_1 and F_n.

Step 3a: If $F_r < F_1$ an expansion process is followed and x_e is only substituted as the better point if F_e is less than F_r (c.f. Figure B.1b).

Step 3b: If $F_r \geq F_1$ a contraction process is followed. However, during contraction there are two possibilities, either inside or outside contraction.

Step 3b(1): If $F_n < F_r < F_{n+1}$, an outside contraction is calculated with the worst point substituted with $x_{c,out}$ only if $F_{c,out} < F_r$ (c.f. Figure B.1c).

Step 3b(2): On the other hand, if $F_r \geq F_{n+1}$ inside contraction is calculated and point $x_{c,in}$ is only accepted as the best point if $F_{c,in} < F_{n+1}$ (c.f. Figure B.1d).

Step 4: If the methods described in Step 3 fail to produce a converged solution, the shrinking method is used to obtain an improved smaller simplex (c.f. Figure B.1e). A new attempt is then made to obtain a converged solution by following Steps 2 and 3 again for the new smaller simplex.

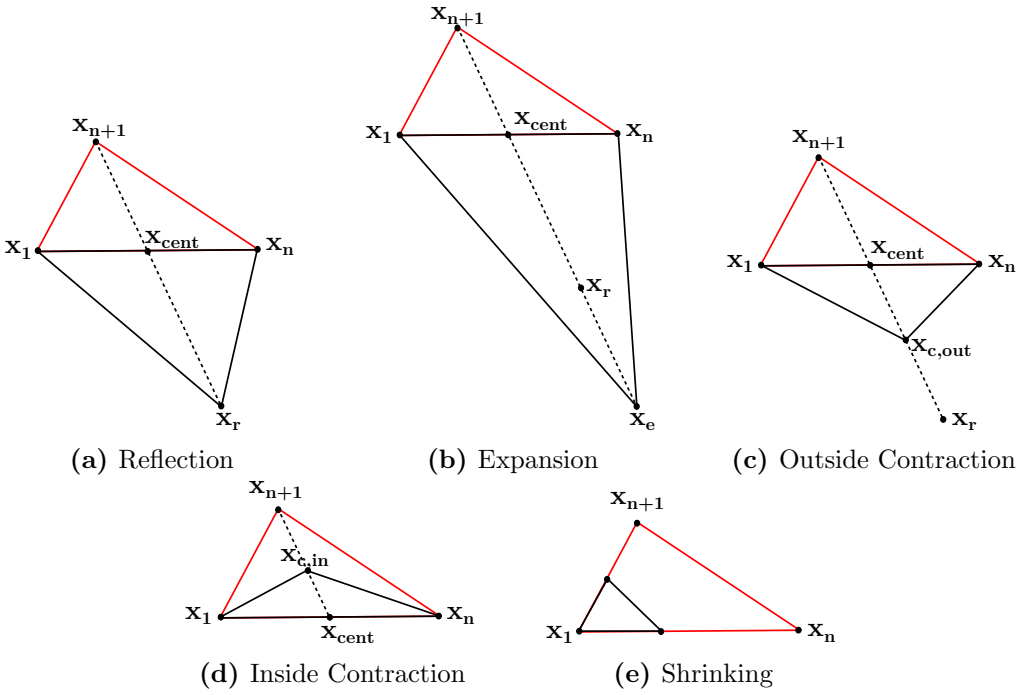

(a) Reflection **(b)** Expansion **(c)** Outside Contraction

(d) Inside Contraction **(e)** Shrinking

Figure B.1: Reflection, expansion and contraction methods used in the Nelder-Mead simplex optimization algorithm for a 2D case. The original simplex is shown as a red triangle, with the black triangle the new simplex. The dashed line represents the reflected line and x_{cent} is the centroid between the best vertex points up to x_n, therefore excluding x_{n+1}. [Redrawn from Lagarias *et al.* (1998)]

For the interested reader, a more detailed explanation on the Nelder-Mead simplex optimization can be found in Lagarias *et al.* (1998) and Spall (2005).

B.2 ROOT MEAN SQUARE ERROR

The Root Mean Square Error (RMSE) measures the difference between data from a numerical model and actual (or experimental) data, to estimate the quality of the fit. The RMSE is defined mathematically as:

$$\text{RMSE} = \sqrt{\frac{\sum_{i=1}^{n}(x_i - y_i)^2}{n}}, \tag{B.1}$$

where n is the number of observations (or sample size), x_i is the the individual values for the first sample set (i.e. numerical or predicted model) and y_i is the individual values for the second sample set (i.e. actual or experimental data).

APPENDIX C

ADDITIONAL CORRECTION EQUATION RESULTS

This appendix shows additional results when comparing correction equations and using:

1. Bryant inflation data and a 23° limbal boundary condition (c.f. Figure C.1, Figure C.2 and Table C.1).
2. Elsheikh inflation data and a fixed limbal boundary condition (c.f. Figure C.3, Figure C.4 and Table C.2).
3. Elsheikh inflation data and a 23° limbal boundary condition (c.f. Figure C.5, Figure C.6 and Table C.3).

The observations in this appendix are similar to those made in Section 5.5.2, where it was seen that the predicted Calibrated IntraOcular Pressure (IOPC) is overestimated from the True IntraOcular Pressure (IOPT) by (i) more than 5.0 mmHg for Whitacre (cited in Chihara, 2008), Kohlhaas (cited in Chihara, 2008) and Foster (cited in Chihara, 2008); and by (ii) less than 7.0 mmHg for Orssengo and Pye (1999), Feltigen (cited in Chihara, 2008) and Kniestedt (cited in Chihara, 2008). Also, the predicted IOPC is underestimated from the IOPT by less than 5.0 mmHg for Shimmyo (cited in Chihara, 2008), Chihara (2008), Kwon *et al.* (2008), Elsheikh *et al.* (2011), Guzmán *et al.* (2013) and the current study.

These results also indicate that the correction equation proposed in this study compares well with the correction equations proposed by Elsheikh *et al.* (2011) and Guzmán *et al.* (2013) which varies with less than 3.0 mmHg from the IOPT. It is also seen that when using the data from Case 2 that the predicted IOPC varies by less than 0.25 mmHg from the IOPT compared to the less than 5.0 mmHg variation when using the data from Case 1, for the proposed correction equation.

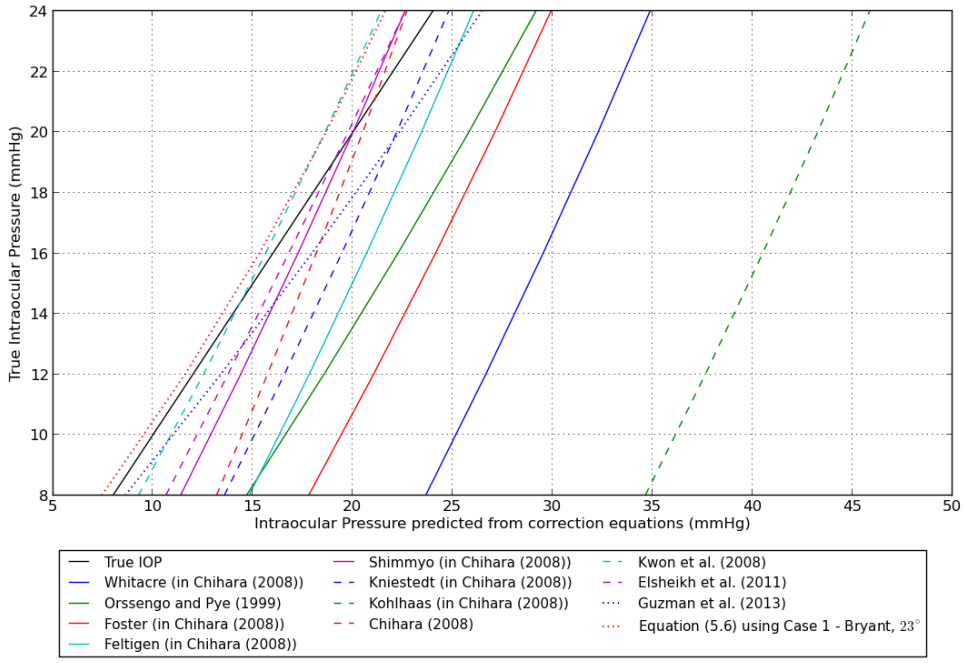

Figure C.1: Comparison of the proposed correction equation to correction equations obtained from literature for what is considered a normal cornea in this study (CCT = 0.55 mm, R_{ant} = 7.77 mm, IOPG = 8, 12, 16, 20 and 24 mmHg) using the data from Case 1 when considering Bryant inflation data and a 23° limbal boundary condition, material data set 3.

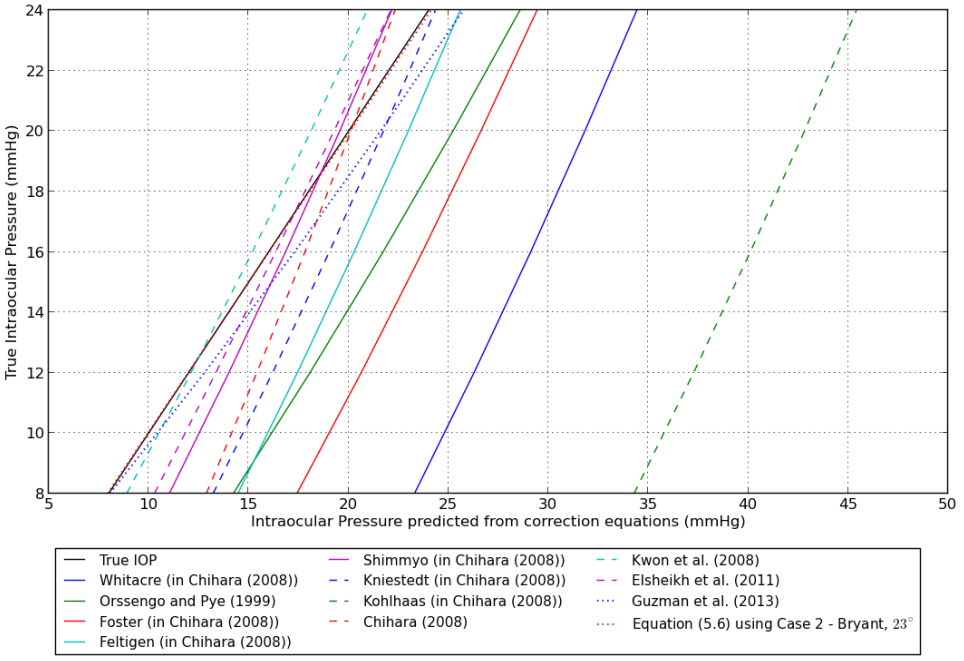

Figure C.2: Comparison of the proposed correction equation to correction equations obtained from literature for what is considered a normal cornea in this study (CCT = 0.55 mm, R_{ant} = 7.77 mm, IOPG = 8, 12, 16, 20 and 24 mmHg) using the data from Case 2 when considering Bryant inflation data and a 23° limbal boundary condition, material data set 3.

Table C.1: Comparison of the proposed correction equation to those from various literature sources using the data from both Case 1 and 2 for a numerically normal cornea and using Bryant inflation data, a 23° limbal boundary and material data set 3).

Source	**Year**	**IOPC using data from Case 1**					**IOPC using data from Case 2**				
		8 mmHg	**12 mmHg**	**16 mmHg**	**20 mmHg**	**24 mmHg**	**8 mmHg**	**12 mmHg**	**16 mmHg**	**20 mmHg**	**24 mmHg**
Whitacre (cited in Chihara, 2008)	1993	23.65	26.66	29.53	32.28	34.87	23.30	26.28	29.12	31.82	34.42
Orssengo and Pye (1999)	1999	14.68	18.56	22.26	25.81	29.16	14.23	18.07	21.73	25.22	28.57
Foster (cited in Chihara, 2008)	2000	17.79	21.04	24.14	27.11	29.91	17.42	20.63	23.70	26.62	29.43
Feltigen (cited in Chihara, 2008)	2001	14.81	17.82	20.69	23.44	26.04	14.47	17.44	20.28	22.99	25.58
Shimmyo (cited in Chihara, 2008)	2003	11.38	14.39	17.26	20.01	22.61	11.03	14.01	16.85	19.56	22.15
Kniestedt (cited in Chihara, 2008)	2005	13.57	16.58	19.45	22.20	24.80	13.23	16.20	19.04	21.75	24.34
Kohlhaas (cited in Chihara, 2008)	2006	34.64	37.65	40.52	43.26	45.86	34.29	37.27	40.10	42.81	45.41
Chihara (2008)	2008	13.18	15.73	18.17	20.50	22.71	12.89	15.41	17.82	20.12	22.32
Kwon *et al.* (2008)	2008	9.28	12.53	15.63	18.61	21.42	8.90	12.12	15.19	18.12	20.93
Elsheikh *et al.* (2011)	2011	10.64	13.76	16.80	19.76	22.61	10.29	13.36	16.36	19.27	22.11
Guzmán *et al.* (2013)	2013	8.61	13.40	17.96	22.33	26.46	8.06	12.79	17.30	21.61	25.74
Current Study	2013	7.45	11.61	15.33	18.66	21.62	7.94	11.98	16.02	20.07	24.13

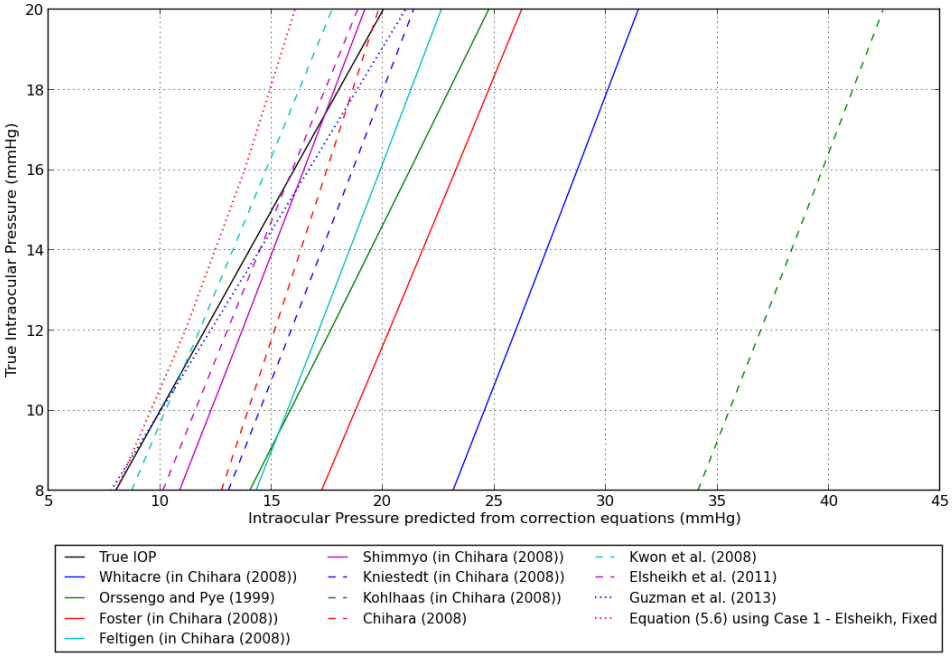

Figure C.3: Comparison of the proposed correction equation to correction equations obtained from literature for what is considered a normal cornea in this study (CCT = 0.55 mm, R_{ant} = 7.77 mm, IOPG = 8, 12, 16, 20 and 24 mmHg) using the data from Case 1 when considering Elsheikh inflation data and a fixed limbal boundary condition, material data set 3.

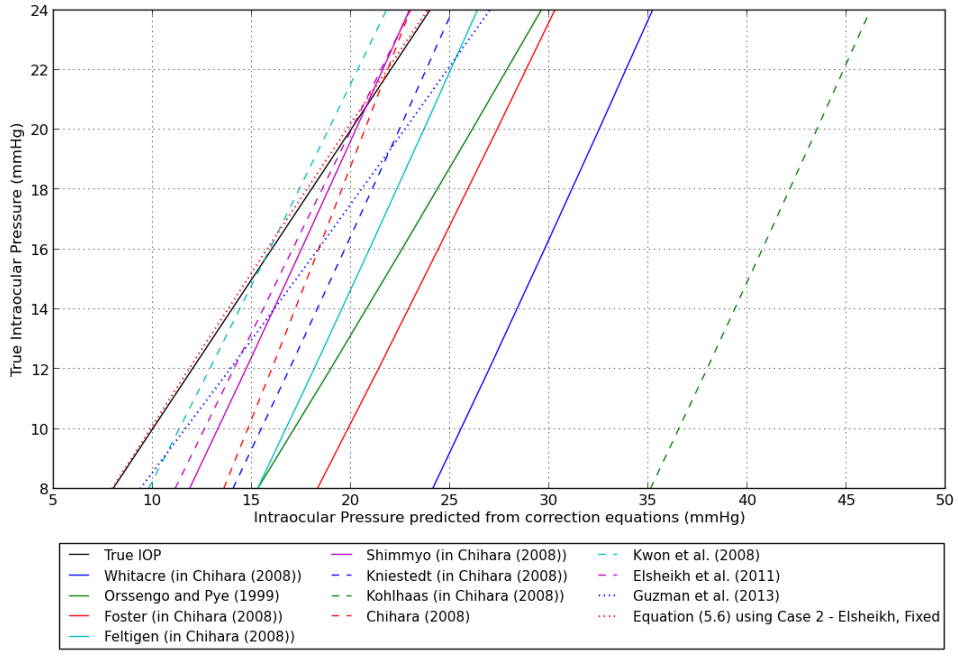

Figure C.4: Comparison of the proposed correction equation to correction equations obtained from literature for what is considered a normal cornea in this study (CCT = 0.55 mm, R_{ant} = 7.77 mm, IOPG = 8, 12, 16, 20 and 24 mmHg) using the data from Case 2 when considering Elsheikh inflation data and a fixed limbal boundary condition, material data set 3.

Table C.2: Comparison of the proposed correction equation to those from various literature sources using the data from both Case 1 and 2 for a numerically normal cornea and using Elsheikh inflation data, a fixed limbal boundary and material data set 3).

Source	Year	IOPC using data from Case 1					IOPC using data from Case 2				
		8 mmHg	12 mmHg	16 mmHg	20 mmHg	24 mmHg	8 mmHg	12 mmHg	16 mmHg	20 mmHg	24 mmHg
Whitacre (cited in Chihara, 2008)	1993	23.13	25.95	28.71	31.44	NC	24.13	26.98	29.77	32.52	35.22
Orssengo and Pye (1999)	1999	14.01	17.64	21.20	24.73	NC	15.30	18.98	22.57	26.12	29.61
Foster (cited in Chihara, 2008)	2000	17.23	20.27	23.25	26.21	NC	18.31	21.39	24.40	27.37	30.29
Feltigen (cited in Chihara, 2008)	2001	14.29	17.11	19.87	22.60	NC	15.29	18.14	20.93	23.68	26.39
Shimmyo (cited in Chihara, 2008)	2003	10.86	13.68	16.44	19.17	NC	11.86	14.71	17.50	20.25	22.96
Kniestedt (cited in Chihara, 2008)	2005	13.05	15.87	18.63	21.36	NC	14.05	16.90	19.69	22.44	25.15
Kohlhaas (cited in Chihara, 2008)	2006	34.12	36.93	39.70	42.43	NC	35.12	37.97	40.76	43.51	46.21
Chihara (2008)	2008	12.74	15.13	17.47	19.79	NC	13.59	16.01	18.37	20.71	23.00
Kwon *et al.* (2008)	2008	8.71	11.76	14.75	17.70	NC	9.79	12.88	15.90	18.87	21.80
Elsheikh *et al.* (2011)	2011	10.12	13.01	15.92	18.86	NC	11.13	14.10	17.06	20.03	23.00
Guzmán *et al.* (2013)	2013	7.79	12.26	16.65	21.00	NC	9.37	13.91	18.34	22.71	27.02
Current Study	2013	8.02	11.13	13.79	16.04	NC	7.95	11.83	15.76	19.78	23.87

NC - No Convergence, that is numerical difficulties arised during the GAT simulation.

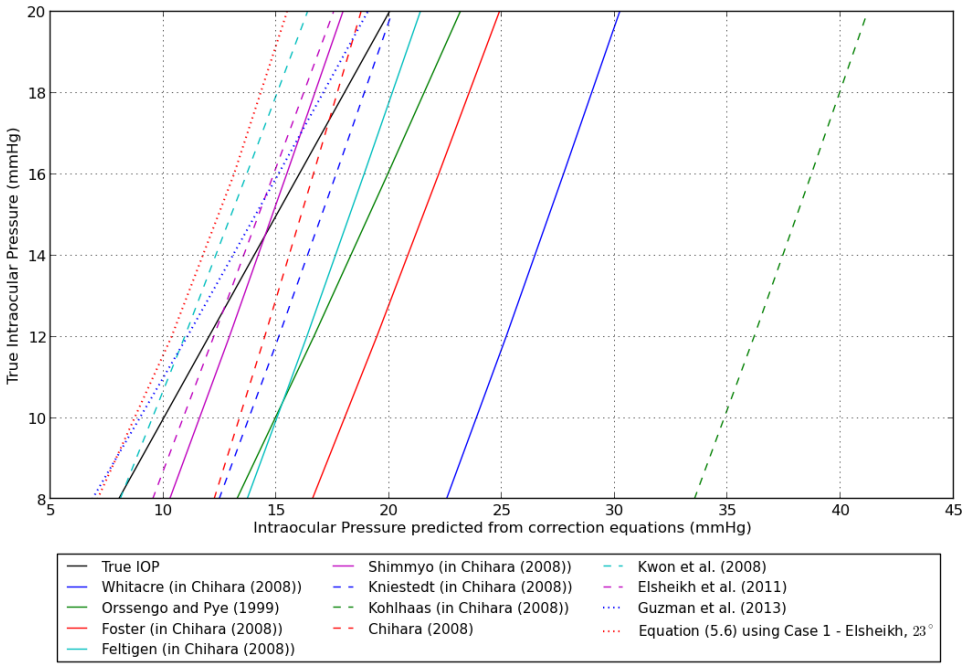

Figure C.5: Comparison of the proposed correction equation to correction equations obtained from literature for what is considered a normal cornea in this study (CCT = 0.55 mm, R_{ant} = 7.77 mm, IOPG = 8, 12, 16, 20 and 24 mmHg) using the data from Case 1 when considering Elsheikh inflation data and a 23° limbal boundary condition, material data set 3.

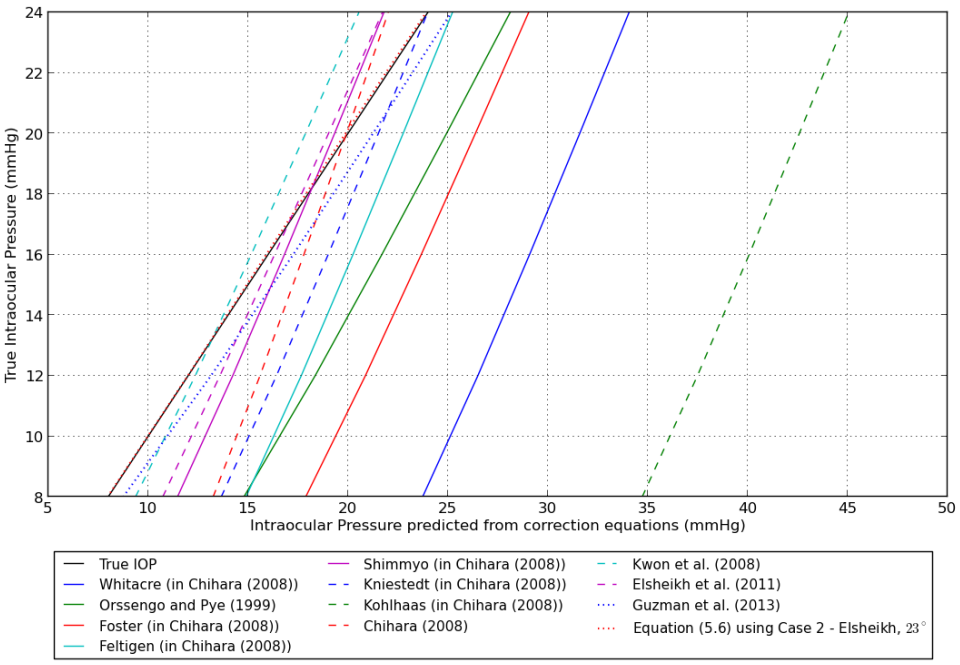

Figure C.6: Comparison of the proposed correction equation to correction equations obtained from literature for what is considered a normal cornea in this study (CCT = 0.55 mm, R_{ant} = 7.77 mm, IOPG = 8, 12, 16, 20 and 24 mmHg) using the data from Case 2 when considering Elsheikh inflation data and a 23° limbal boundary condition, material data set 3.

Table C.3: Comparison of the proposed correction equation to those from various literature sources using the data from both Case 1 and 2 for a numerically normal cornea and using Elsheikh inflation data, a 23° limbal boundary and material data set 3).

Source	Year	IOPC using data from Case 1					IOPC using data from Case 2				
		8 mmHg	12 mmHg	16 mmHg	20 mmHg	24 mmHg	8 mmHg	12 mmHg	16 mmHg	20 mmHg	24 mmHg
Whitacre (cited in Chihara, 2008)	1993	22.53	25.18	27.72	30.21	NC	23.74	26.50	29.09	31.60	34.07
Orssengo and Pye (1999)	1999	13.24	16.65	19.93	23.14	NC	14.79	18.36	21.70	24.93	28.12
Foster (cited in Chihara, 2008)	2000	16.59	19.44	22.19	24.88	NC	17.89	20.87	23.67	26.38	29.05
Feltigen (cited in Chihara, 2008)	2001	13.69	16.34	18.88	21.37	NC	14.90	17.66	20.25	22.76	25.23
Shimmyo (cited in Chihara, 2008)	2003	10.26	12.91	15.45	17.94	NC	11.47	14.23	16.82	19.33	21.80
Kniestedt (cited in Chihara, 2008)	2005	12.45	15.10	17.64	20.13	NC	13.66	16.42	19.01	21.52	23.99
Kohlhaas (cited in Chihara, 2008)	2006	33.52	36.17	38.71	41.20	NC	34.73	37.49	40.08	42.59	45.06
Chihara (2008)	2008	12.23	14.48	16.63	18.75	NC	13.25	15.60	17.80	19.93	22.02
Kwon *et al.* (2008)	2008	8.07	10.93	13.68	16.37	NC	9.37	12.36	15.16	17.88	20.55
Elsheikh *et al.* (2011)	2011	9.51	12.22	14.87	17.53	NC	10.73	13.59	16.33	19.03	21.73
Guzmán *et al.* (2013)	2013	6.83	11.04	15.08	19.04	NC	8.75	13.15	17.26	21.25	25.18
Current Study	2013	7.07	10.35	13.12	15.47	NC	7.97	11.99	15.91	19.87	23.92

NC - No Convergence, that is numerical difficulties arised during the GAT simulation.